POLITECNICO DI MILANO
DEPARTMENT OF CHEMICAL ENGINEERING
DOCTORAL PROGRAMME IN CHEMICAL ENGINEERING

Physiologically-based approach to pharmacokinetic modeling for closed-loop control of anesthesia and optimization of drug dosing in intensive care

Doctoral Dissertation of:
Adriana Savoca

Supervisor:
Prof. Davide Manca

Tutor:
Prof. Alessandra Beretta

The Chair of the Doctoral Program:
Prof. Alessio Frassoldati

2020 – Cycle XXXII

Omnia venenum sunt: nec sine veneno quicquam existit.Sola dosis facit venenum.

All things are poison, and nothing is without poison. The dosage alone determines the poison.

Paracelsus (1493/4-1541)

Abstract

Despite recent technological advances in biomedicine, the availability of model-based tools to support medical doctors in clinical decision-making is rather limited. The selection of the optimal drug dose and dosing regimen is a complex problem, which must take into account the physical characteristics of the patient and is constrained by patients' co-morbidities and therapeutic windows of drugs. This work focuses on the specific fields of anesthesia and intensive care. Anesthesia-associated risks are mostly related to medication errors, typically associated to the administration stage. In the intensive care unit (ICU), wrong dosing is reported as one of the most frequent errors. Anesthesia and intensive care share significant challenges, such as nonlinear and complex dynamics of the patients' response to drugs, uncertainty of the dose-response relation (because of high inter- and intra-individual variability), multiplicity of variables characterizing and describing the response, and operative constraints (therapeutic windows of drugs and safe clinical ranges of patients' physiological parameters). Clinical adoption of model-based tools for selection of the optimal dose can bring actual improvements in these fields, by providing a more rigorous and robust approach to inter-individual variability of the response to drugs, reducing clinicians' workload and variability in practice, and limiting potential human errors. Combination of medical doctors' experience and knowledge with such tools can guide the decision-making process and enhance patients' safety and quality of recovery.

This work can be divided into two parts. The goal of the first part is to develop and evaluate *in silico* a physiologically-based (PB) model-predictive controller for closed-loop administration of the anesthetic agent propofol and the analgesic opioid remifentanil. In clinical practice, anesthesiologists select an initial dose to induce the desired depth of anesthesia and then make adjustments basing on the monitored physiological parameters, to maintain the desired depth of anesthesia throughout the medical procedure that requires the anesthetic state (*e.g.*, surgery). For the sake of completeness, it is worth mentioning that in many parts of the world, Target-Controlled Infusion (TCI) pumps (a model-based technology) are commonly used to deliver

intravenous anesthesia. However, their performance is totally dependent on the accuracy of the embedded model and does not take into account patients' real-time data on physiological parameters. Anesthesiologists heavily rely on their experience and knowledge, setting the basis for remarkable variability of the procedure and potential human errors (related to the level of attention, stress and fatigue, and quality of communication with the rest of the operating room team). Researchers are investigating closed-loop solutions for automated anesthesia delivery. Proposed solutions differ for selected control strategy (*e.g.*, model-free or model-based), number of inputs (considered physiological parameters), and number of outputs (considered drugs). In our work, we consider both a quantitative measure of hypnotic depth and hemodynamic parameters to regulate propofol and remifentanil infusion rates, for a complete control over the anesthetic state of patients. In addition, the use of the modern physiologically-based approach to pharmacokinetic-pharmacodynamic modeling allows facing some of the most controversial challenges of anesthesia delivery, *i.e.* (i) optimal dosing in "at-risk" categories of patients (in particular, elderly, obese, and pediatric patients) and (ii) investigation and inclusion of the impact of hemodynamic changes on the patients' response and required dosing modifications, which are crucial for a smooth procedure and post-operative recovery. Special attention is also devoted to propofol-remifentanil synergistic effects on arterial pressure.

The goal of the second part of the work is to develop a multi-route PB pharmacokinetic model of melatonin for administration to critically ill patients, with the purpose of optimizing melatonin delivery for this special category. Indeed, melatonin is a well-known sleep regulator and is currently of great interest for its additional functions, *e.g.*, anti-oxidant, immunomodulatory, and anti-carcinogenic effects. Sleep disruption is a common problem in ICU and has short- and long-term adverse effects on the patients, with the risk of further compromising their recovery. Melatonin versatility to multiple routes of administration and lack of toxic effects makes it extremely appealing for application to ICU. Researchers are investigating its pharmacokinetics in both experimental and simulation studies. This work moves a step forward by showing how the proposed PBPK model can be applied to identify (i) the optimal administration route depending on the goal of the clinical treatment and (ii) the most suitable dose, dosing regimen, and time of administration according to the selected route. Although the work focuses on melatonin, the proposed approach is valid for any drug for which an ideal pharmacokinetic profile is desirable.

Contents

List of acronyms

ADME	Absorption, Distribution, Metabolism, and Elimination
AP/BP	Arterial Pressure/Blood Pressure
ASA	American Society of Anesthesiologists
AUC	Area Under the Curve
BBB	Blood-Brain Barrier
BIS	BISpectral index
BM	Body Mass
BMI	Body Mass Index
BSA	Body Surface Area
CBF	Cerebral Blood Flow
CNS	Central Nervous System
CO	Cardiac Output
CPU	Central Processing Unit
CR	Controlled Release
DCPK	Diffusion-Compartment PharmacoKinetics
DE	DErmis
DOA	Depth Of Anesthesia
DoH	Depth of Hypnosis
ECG	ElectroCardioGram
EEG	ElectroEncephaloGram
EMA	European Medicines Agency
EMG	ElectroMyography

EU	European Union
FDA	Food and Drug Administration
GICS	GastroIntestinal Circulatory System
GL	Gastric Lumen
HA	Hepatic Artery
HO	Highly perfused Organs
HR	Heart Rate
HV	Hepatic Vein
ICU	Intensive Care Unit
IEC	International Electrotechnical Commission
IQR	InterQuartile Range
IR	Infusion Rate
IV	IntraVenous
LBW	Lean Body Weight
LiDCO	Lithium Diluition Cardiac Output
LIL	Large Intestinal Lumen
LOC	Loss Of Consciousness
MAP	Mean Arterial Pressure
MBDD	Model-Based Drug Development
MeSE	Median Squared Error
MDPE	MeDian Prediction Error
MDAPE	MeDian Absolute Prediction Error
MIMO	Multiple Input Multiple Output
MO	Morbidly Obese
MPC	Model Predictive Control
NIBP	Non—Invasive Blood Pressure
NOL	NOciception Level index
OECD	Organisation for Economic Co-operation and Development

ODE	Ordinary Differential Equations
OR	Operating Room
(PB)PK	(Physiologically-Based) Pharmacokinetic(s)
PBDCPK	Physiologically-Based Diffusion-Compartment PharmacoKinetic(s)
PCLCS	Physiological Closed-Loop Controlled Systems
PD	Pharmacodynamic(s)
PDE	Partial Differential Equation
PF	Penalty Function
P(ID)	Proportional (Integral Derivative)
PO	Per Os
PONV	Post-Operative Nausea and Vomiting
PT	Poorly perfused Tissues
PV	Portal Vein
RASS	Richmond Agitation-Sedation Scale
R&D	Research & Development
RMSE	Root Mean Squared Error
ROC	Return Of Consciousness
SAP	Systolic Arterial Pressure
SC	Stratum Corneum
SD	Standard Deviation
SE	Standard Error
SIL	Small Intestinal Lumen
SISO	Single Input Single Output
SQI	Signal Quality Index
TBW	Total Body Weight
TCI	Target-Controlled Infusion
TD	TransDermal
TDD	TransDermal Device

TIVA	Total IntraVenous Anesthesia
UN	United Nations
VE	Viable Epidermis
VP	Virtual Patient
WAV_{CNS}	WAVelet-based anesthetic value for Central Nervous System monitoring index
WHO	World Health Organization
WMA	World Medical Association

CHAPTER 1

Introduction

1.1 Background and motivation

The broader scientific context of this thesis is Quantitative Pharmacology, *i.e.* "*the field of biomedical research that seeks to use computer-aided modeling and simulation to increase our understanding of the pharmacokinetics (PK) and pharmacodynamics (PD) of drugs*" (Leil and Ermakov, 2015). For the sake of clarity, pharmacokinetics is the branch of pharmacology that studies the dynamics of the processes of absorption, distribution, metabolism, and elimination (ADME) of drugs administered to living beings. It is commonly defined as "what the body does to the drug". Pharmacodynamics is rather defined as "what the drug does to the body", *i.e.* the study of drug effects along with the mechanisms leading to their manifestation.

Medicine and pharmacology have been slower compared to other fields, *e.g.*, transport and electronics, to integrate computer-aided modeling and simulation. The common belief that "*medicine is an art based on science*" (Sir William Osler, 1849-1919) is still deeply rooted in the mind of most clinicians. In fact, medicine has intrinsic empirical foundations that are still present in the methods of clinicians and approaches to education of the medical trainees. An integration of model-based tools with clinicians' expertise and knowledge is desirable to bring actual improvements in clinical practice and quality of patients' care. The pharmaceutical industry is already going down this road, with an increasing trend of model-based drug development

(MBDD) implementation throughout the phases of new drugs research and development (R&D), also supported by regulatory agencies[1]. On the contrary, the use of model-based tools for decision-support in clinical treatments is not as common in routine practice. This is true even in fields attracting considerable interest and research funding, *e.g.*, oncology (Buil-Bruna et al., 2016). The physicians' experience and mindset, the institution (*e.g.*, hospital) policies, and the regional or national context can all represent contributing factors in preventing the diffusion and adoption of innovative methodologies and tools.

For a better understanding of the objectives of this thesis, it is useful to further explore the analogy with the innovative approaches spreading in R&D of new drugs. Leil and Bertz (2014) show that since the early '60s there has been a contrasting trend between the increasing number of new drugs approved by FDA and a decrease in the productivity of pharmaceutical industry, which is defined as the number of approved drugs per USD billion of expenditures in R&D.

In brief, FDA recognized that the pharmaceutical industry was on a "Critical Path", because of a decrease of productivity related on one hand to the difficulty of finding new therapeutic targets, and on the other to the increasing costs associated with the discovery and development of new drugs (*i.e.* average cost 1.5$ billions) (Leil and Bertz, 2014). Leil and Bertz found that computer-aided modeling and simulation could be part of the solution to this problem. In fact, pre-clinical and clinical experiments constitute the most time-consuming and expensive phase of new drugs R&D. Computer-aided modeling can potentially re-create an "infinite" number of *in silico* scenarios with the goal of identifying and removing *a priori* the conditions that are responsible for decreasing the probability of success of real experiments. This approach can thus lead to the reduction in duration and costs of real experiments. In addition, models can help increase the level of understanding of drugs pharmacokinetics and pharmacodynamics, for an enriched design of pre-clinical and clinical trials and improvement of their efficacy.

This thesis argues that such advantages are easily transferable from R&D of new drugs to clinical practice. Indeed, decision-support tools based on PK-PD models of patients' dose-response relation can be used to:

- Enhance understanding and find new insights on the patients' response to

[1] European Medicines Agency (EMA, in Europe) and Food and Drug Administration (FDA, in the United States) are the main regulatory agencies.

drugs;

- Design individualized treatments, depending on the patients' characteristics (*e.g.*, demographics, presence of comorbidities, and genetics), via personalized models;
- Optimize dosing and dosing regimens, with the goal of avoiding on one hand ineffective treatments and on the other overdosing;
- Integrate and support the typically empirical approach of the teaching methods for medical trainees.

Interestingly, according to the report "Fiscal Sustainability of Health Systems" (2015) by the Organization for Economic Co-operation and Development (OECD), the "*public health spending in OECD countries has grown rapidly over most of the last half century*". Although the consequences have been positive on the population health, sustainability remains an undeniable challenge for the future years. Innovative approaches to treatments and diagnosis are required to reduce such high expenditures and at the same time ensure the progress of global health. In the long term, the introduction of new technologies in the daily routine care of patients can contribute solving the problem, although requiring transitional investment costs. PK-PD model-based tools have the potential to enhance the efficiency of patients' care and possibly reduce healthcare expenditures, by reducing medical errors and adverse outcomes, and decreasing patients' length of stays with associated costs of hospitalization. Especially, if one considers that healthcare produces a remarkable amount of data that can and should be integrated into mathematical models to improve pharmacotherapy, but is most of the times unusable, either for privacy issues, or because of unstructured formats or simply because they are discarded or locked away in databases. These data are valuable information, as they can allow a better understanding and thus mathematical description of the patients' dose-response relation.

1.2 Application to anesthesia and intensive care and objectives of the thesis

The work presented in this thesis focuses on anesthesia and the related field of

intensive care[2].

It is estimated that only in the European Union (EU), 29 million anesthetic procedures are carried out every year, of which approximately 10 millions are administered to high-risk patients (American Society of Anesthesiologists (ASA) classification[3] II or higher). About 20% are Total Intravenous Anesthesia (TIVA), which is the core of the first part of the thesis. With regard to intensive care, Rhodes et al. (2012) identified over 70 000 critical beds in Europe. These numbers are expected to grow because of progressive population aging and sizing, and increase of prevalence of chronic diseases (*e.g.*, cardiovascular diseases, obesity, and cancer).

Although anesthesia is today considered a rather safe procedure (Botney, 2008), advances in technology have not eliminated anesthesia-associated risks yet. Such risks are often related to medication errors (Schiff and Wagner, 2016). Interestingly, Cooper et al. (2009) report that most errors occur during the administration stage. Insufficient experience, poor familiarity with the medical devices, and inadequate communication with the rest of the operating room (OR) team are listed among the main contributing reasons (Cooper et al., 2009). Indeed, anesthesia-associated incidents can lead to minor and major intra- and post-operative complications. Excessively deep anesthesia has been associated with mortality and delirium, especially in high-risk patients (Kertai et al., 2010; Watson et al., 2008). Intraoperative hemodynamic fluctuations have been associated to poor outcomes of clinical procedures (Devinney et al., 2015; Reich et al., 2005). Similarly, in the intensive care unit (ICU), wrong dose is one of the most frequent errors (Kiekkas et al., 2011) and can be detrimental for critically ill patients and compromise their recovery.

Dr. David Gaba (Professor of Anesthesiology, Perioperative and Pain Medicine at Stanford University School of Medicine), a pioneer in the human factors of anesthesia, claims that the anesthesiologist has more in common with flight crews, fire chiefs, and nuclear plants operators rather than other medical doctors, except for the related field of intensive care (Reason, 2005). Reason (2005) lists a series of shared features among these fields, to support Dr. Gaba's claim. We report, rephrase, and integrate some of them, especially interesting to introduce this work:

[2] A hospital facility for provision of intensive nursing and medical care of critically ill patients, endowed with high quality and quantity of continuous nursing, medical supervision, and use of sophisticated monitoring and resuscitative equipment (https://medical-dictionary.thefreedictionary.com/intensive+care+unit).

[3] In 1963, ASA proposed a physical status classification of pre-operative patients for anesthetic risk assessment. The ASA score is a subjective evaluation of a patient's health status based on five classes (I, normal healthy patient to V, moribund patient not expected to survive without the operation) (Daabiss, 2011).

- Complex dynamics and uncertain behavior of the process (*i.e.* the patient body and the inter- and intra-individual variability of the dose-response relation);
- Multivariate process (*i.e.* several variables characterize the patient dose-effect relation);
- Intrinsic nonlinearity of the process (biological systems are nonlinear (Higgins, 2002));
- Operative constraints (*e.g.,* therapeutic window[4] of administered drugs and safe clinical ranges of physiological parameters);
- Presence of several sources of information (monitoring instruments), reliance on indirect/inferred indicators, redundant measures.

These considerations highlight the importance of the role played by human factors and the potential impact of human errors on the safety and quality of recovery of patients involved in the fields of anesthesia and intensive care. The problem is relevant not only in terms of numbers (*e.g.*, according to Kothari et al. (2010) up to 87% of anesthesia-associated incidents are related to human errors), but also in terms of costs and consumption of medical resources, because medication errors leading to adverse drug events and severe clinical consequences increase times and costs of hospitalization. Mathematical models and model-based tools for optimization of drug dosing have the potential to reduce human error and provide significant improvements in clinical practice, in terms of a more rigorous and robust approach to inter-individual variability, clinical workload reduction and decision-support, improved patient outcomes, reduced length of stays and hospitalization costs, and reduction of drugs waste. The clinical adoption of such systems would also reduce the variability in medical practice, which is strictly related to medical quality (Mackey, 2012).

Within this context, the objectives of the thesis are:

- The development and *in silico* evaluation of a physiologically-based (PB) model-predictive controller for closed-loop administration of the anesthetic agent propofol and the analgesic opioid remifentanil;
- The development of a multi-route physiologically-based pharmacokinetic

[4] The therapeutic window is the range of dosage that produces therapeutic response without causing any significant adverse effects in patients (https://medimoon.com/2014/12/therapeutic-window-and-therapeutic-index/).

(PBPK)[5] model for optimal dosing of melatonin to critically ill patients.

1.3 Thesis structure

This thesis includes two parts that are consistent with the goals stated in Section 1.2. Although each chapter is self-standing, together they constitute a progressive development towards those two specific goals. The thesis is structured as follows.

Chapter 1 Introduction

Chapter 2 Closed-loop controlled aesthesia: state of the art and challenges

Chapter 3 Model-predictive control of anesthesia with propofol and remifentanil

Chapter 4A Tackling inter-individual variability: the influence of intra-operative cardiovascular changes

Chapter 4B Tackling inter-individual variability: the influence of anatomical and physiological features

Chapter 5 Anesthetic-analgesic interactions and adequate depth of anesthesia in high-risk patients

Chapter 6 Melatonin benefits for the critically ill patient

Chapter 7 Physiologically-based pharmacokinetic modeling for transdermal delivery

Chapter 8 Physiologically-based pharmacokinetic simulations to select the optimal administration route

Chapter 9 Optimal melatonin dosing for endogenous levels in ICU patients

Chapter 10 Conclusions and future perspectives

Chapters 2 and 6 provide specific introductions to the topic of the first and second parts of the thesis, respectively, by illustrating the state of the art and clarifying the objectives of that part of the research activity.

Chapters 2 to 5 are devoted to the development of a model-based controller of TIVA administration with propofol and remifentanil. Particularly, Chapter 2 provides a short

[5] Physiologically-based pharmacokinetic (PBPK) modeling is a specific branch of pharmacokinetic modeling that combines the anatomy and physiology of the body with mathematical description of ADME processes.

introduction on the current techniques of anesthesia delivery and explains the state-of-the-art research on closed-loop methods for anesthesia induction and maintenance. Some potential ethical and practical implications of their clinical adoption are also discussed. Chapter 3 introduces the developed model-predictive controller, and its evaluation based on the modern physiologically-based approach to PK modeling. Chapters 4A and 4B propose approaches to face inter-individual variability of the response to anesthesia, by (i) using real-time hemodynamic data as input to the model to explain part of such variability and (ii) including the effects of the anatomical and physiological differences among individuals within the model, respectively. Chapter 5 presents the modifications applied to the PD models and the controller features, to account for anesthetic-analgesic synergistic interactions and induce adequate depth of anesthesia in high-risk patients.

Chapters 6 to 9 describe the development of a multi-route PBPK model to optimize melatonin dosing for critically ills. Chapter 6 introduces the features of critically ill patients and the reasons for interest in melatonin administration to this specific category. Chapter 7 focuses on the development of a PBPK model for transdermal (TD) delivery. Chapter 8 presents the identification and validation of the model for intravenous (IV) and oral (*per os*, PO) routes, and shows how PBPK simulations can be used *a priori* to select the optimal administration route, depending on the specific goal of the clinical treatment. Chapter 9 proposes a methodology for optimization of melatonin dosing for critically ill patients and discusses the results, also comparing them to dosing optimization for healthy individuals.

Finally, Chapter 10 summarizes the main innovative aspects and conclusions and offers some future perspectives of the presented work.

CHAPTER 2

Closed-loop controlled anesthesia: state of the art and challenges

2.1 Author's Note

This chapter introduces the topic of closed-loop controlled anesthesia, specifically describing the current approach to administration of IV anesthesia and the rationale and state of the art of the research on closed-loop systems for anesthesia delivery. A short discussion on the ethical problem and the impact on clinical practice deriving from routinely use of these systems concludes the chapter.

This work is part of a chapter prepared for the Elsevier book "Control applications for Biomedical Engineering Systems" edited by prof. Ahmad Taher Azar (2020).
The chapter is entitled:

Control strategies in general anesthesia administration
Adriana Savoca, Davide Manca

and provides a proper introduction to the section of the thesis concerning the research activity on closed-loop anesthesia delivery.

2.2 Anesthesia delivery today

"*The practice of medicine is an art based on science*" said the father of modern medicine Sir William Osler (1849-1919). This mindset can be partially interpreted as one of the reasons contributing to slowness by biomedicine and pharmacology to integrate computer aided modeling/simulation and control systems, compared to other fields such as transports and electronics (Leil and Bertz, 2014). Additional factors are the prejudice that biological systems are too complicated to model, and the difficulty of creating multidisciplinary teams that would work in this direction. Nonetheless, in recent years, technological advances in biomedicine and pharmacology have allowed making considerable steps forward (Leil and Bertz, 2014).

One of the most interesting emerging applications of control systems in biomedicine is automated anesthesia delivery. At present, 230 million anesthetic procedures are carried out yearly all over the world (Schiff and Wagner, 2016). Anesthesia is today considered rather safe, and its associated risks represent a small fraction of the total risk of surgical procedures. Yet, with such a high number of surgical or other painful procedures taking place every year, those risks cannot be overlooked. Although a number of studies claim an ongoing decrease in the overall global anesthesia-associated mortality, an equivalent number of studies claim the opposite and highlight discrepancies and differences in the statistics (Schiff and Wagner, 2016). In any case, researchers agree that the events leading to anesthesia-related death are often associated to medication errors, which result into overdose and critical side effects, with particular impact on the respiratory and cardiovascular systems (Schiff and Wagner, 2016). Conversely, awareness episodes related to underdosing are not that rare among patients. Indeed, selection of the optimal anesthetic dose is not an easy task. In fact, both anesthetic and analgesic agents feature narrow therapeutic windows, which mean a limited range between (i) minimum concentration levels to induce desired clinical effects and (ii) maximum levels to avoid undesired dangerous ones. The optimal dose depends not only on the patient's physical characteristics, age, possible diseases, and genetics, but also on the type of surgical operation (Absalom and Struys, 2007). The aim of the anesthetist is on one hand to achieve the desired unconsciousness and pain relief levels and on the other to accomplish a proper post-anesthesia recovery.

A balanced anesthesia results from the combination of three aspects, *i.e.* three types of drugs: (i) a hypnotic agent causing unconsciousness, (ii) an analgesic agent

producing pain relief, and (frequently) (iii) a muscle relaxant, to avoid undesired reflex activity that would interfere with surgery (essential in abdominal and cardiac surgery). Today, basing on the patient's features and their own experience, the anesthetist selects an initial dose for induction of the desired depth of anesthesia (DOA). Actually, this level of unconsciousness is not uniquely defined among anesthetists, and neither standard methods nor certified technologies are available for quantitative evaluation. Thus, the anesthetist observes the patient response and manually adjusts the initial dose until the desired DOA is reached. This phase is defined as the induction of anesthesia. After surgery starts, intra-operative surgical stimuli are likely to produce disturbances of the anesthetic state. The role of the anesthetist is to maintain DOA against such disturbances, by making further adjustments based on patient's vital parameters and electroencephalographic trace monitoring (*i.e.* maintenance phase of anesthesia) (Absalom et al., 2011).

The required drugs can be either administered by means of (i) standard syringe pumps (with desired dose as input), or (ii) Target-Controlled Infusion (TCI) pumps, first proposed in 1983 (Absalom and Struys, 2007). In this case, rather than the dose, the anesthetist selects a target (*i.e.* desired) concentration either in plasma or in the drug site of action (*aka* effect-site), and the pump evaluates the corresponding infusion rate (IR) to be administered to the patient. This calculation is typically based on a three-compartment pharmacokinetic (PK) model, which correlates the drug IR to the expected concentration.

2.3 Open-loop or closed-loop anesthesia?

Despite their name, TCI pumps work rather differently than conventional control systems. Inputs to these pumps are main physical characteristics of the patients (*e.g.*, gender, body mass, height, and age), and a desired value of the drug concentration. Calculation of the corresponding dose is based on the analytical/numerical solution of a 3-equation ordinary differential system, which describes the drug concentration evolution in the body. Classical PK models have empirical foundation and their structure is not strictly related to the patient's anatomy and physiology. Mostly, the models implemented in commercial TCI pumps were identified at the end of the '90s (*e.g.*, Schnider model for propofol (Schnider et al., 1998), Minto model for remifentanil (Minto et al., 1997)) grounding on PK studies on a limited number of healthy volunteers. As a matter of fact, several authors highlighted the necessity to identify

specific three-compartment models in case of different populations, *e.g.*, obese, children, and patients with some sort of disease (Constant and Rigouzzo, 2010; Cortinez et al., 2010; Marsh et al., 1991). Thus, inter-individual variability is likely to represent a serious concern for the anesthetist used to commercial TCI pumps.

The most critical and limiting feature of TCI pumps is that they do not adjust IR after any feedback measure(s) of the patient's anesthetic state (contrary to any real feedback control system). In fact, in case of total intravenous anesthesia (TIVA), it is not possible to measure the drug concentration in real time during the surgical operation. Consequently, the anesthesiologist can never be certain that the expected target concentration is reached within the body of the patient. In this sense, TCI pumps deliver an open-loop configuration, where the anesthetist acts as a *human controller*, as they physically close the loop by personally monitoring the vital parameters of the patient and appropriately regulating the target concentration. The same occurs in case of manual syringe pumps. Only, in this case, the anesthetist directly regulates the drug IR or chooses to administer intermittent boluses, instead of modifying the target concentration. In some cases, this regulation occurs before any disturbance (*i.e.* surgical stimuli) manifestation. Indeed, before a particularly stimulating procedure, the anesthetist may decide to increase the target concentration/drug IR to avoid possible alterations of the DOA and analgesia level of the patient, relying on their experience.

It is evident that human factors play a paramount role in TIVA procedure, in terms of continuous monitoring, training and experience, communication with the operating room team, level of fatigue and stress. Because of this way of proceeding, the control action on the anesthetic state of the patient may result irregular and intermittent, characterized by rather "random" changes of the drugs IRs (Absalom et al., 2011). Automated anesthesia delivery systems are designed with the purpose of supporting medical doctors and improving their control action of the patient's state.

Indeed, to guarantee a safer and more stable induction and maintenance of anesthesia, this alternative approach was proposed for the first time by Mayo et al. (1950). Specifically, they experimented automated delivery of anesthesia with ether in patients subject to abdominal surgery, based on the electroencephalogram trace monitoring. They applied this methodology successfully to 50 patients and proved its potentiality. Since then, several studies have designed, developed, and tested closed-loop controllers of anesthesia using different control strategies, types of inputs, and anesthetic/analgesic agents (El-Nagar and El-Bardini, 2014; Gentilini et al., 2002; Liu

et al., 2011; Nascu et al., 2015; West et al., 2013; Zhusubaliyev et al., 2015). For instance, West et al. (2013) and Zhusubaliyev et al. (2015) opted for a proportional integral derivative (PID) control strategy, whereas Nascu et al. (2015) proposed several model-based strategies for anesthesia control with propofol. All of these papers rely on classical PK modeling for either evaluation of the PID controllers or model-based control. Different strategies were also proposed to address inter-individual variability issues. In a preliminary *in silico* study, Savoca and Manca (2019) proposed physiologically-based model predictive control of both analgesia and anesthesia components. To face inter-individual variability, El-Nagar and El-Bardini (2014) proposed a fuzzy neural network-based controller, which was tested over a wide range of patient parameters. A Monte Carlo approach was instead used by Soltesz et al. (2013) to individualize the patient model of the dose-response relation via system identification during induction.

The basic principle of closed-loop controlled anesthesia is to regulate the drugs IRs automatically with limited human intervention grounding on measured indexes of the patient's DOA. The main advantage is that these systems are not distractible, and their application allows the anesthetists focusing on the patient's state, by reducing their workload. Indeed, the goal of these systems is not to replace the anesthetist in their task and experience, but rather to support them and reduce human error incidence. In fact, over the years, control systems resulted in costs decrease and efficiency increase in a wide variety of applications (Dumont, 2014).

2.4 Classic feedback vs model-predictive control of anesthesia

The strategy of a controller for anesthesia can be either (i) model-based or (ii) model-free. In case the control strategy is based on a model, the difficulty of its development and the assessment of its reliability may arise concerns in medical doctors. Conversely, model-free design is simpler and may be based on clinical guidelines embedded in the controller hardware (*e.g.*, expert system), which may result in easier understanding by clinicians. However, in both cases (*i.e.* model-based or model-free), a reliable model of the patient is needed whenever one wants to assess *in silico* the controller performance and/or tune the parameters with the goal of obtaining a reasonable trade-off between robustness and responsiveness of the control action (Parvinian et al., 2018). Feedback control grounds on a model-free strategy and is the

most employed in the industry. The reason consists in the combination of simplicity and efficacy (Sha'aban et al., 2013). Feedback control does not rely on any type of model to regulate the manipulated variable(s), but only on a proportional (P), proportional integral (PI), or proportional integral and differential (PID) action respect to the error between the set point (*i.e.* desired value of the controlled variable(s)) and the measured value of the controlled variable(s). Thus, on the plus side, the performance is independent of any error or uncertainty in the modeling and the simplicity of the working principle can enhance acceptance and understanding by clinicians. However, it is less efficient in managing multivariable problems with strong interactions among controlled variables. In addition, its intrinsic nature does not allow anticipating any corrective action before a disturbance has produced its effects on the system (this is indeed due to the feedback feature).

Conversely, model predictive control (MPC) is certainly more complex than feedback control, but has been applied successfully for decades in industrial processes (Forbes et al., 2015). MPC is a model-based strategy and therefore features some uncertainty issues, which are unavoidable. Indeed, a model of the system is used to predict its future evolution and optimize the control actions. The real-time experimental measure of the process is used to correct the so-called model mismatch (between the real system and the modeled one). One of the main advantages of MPC is the ability to tackle multivariable problems (Dumont, 2014). As already discussed, general anesthesia is a delicate balance of multiple drugs administration. In addition, the anesthetists rely on different parameters and measures to assess the patient's state, thus the problem cannot be fully treated by focusing on a single aspect. In addition, MPC ability to tackle both linear and nonlinear constraints is extremely valuable. The objective function (which is at the heart of the MPC mathematical formulation and allows identifying the optimal trajectory of the manipulated variables) can be suitably designed to account for therapeutic windows of drugs and critical ranges of the physiological variables (*e.g.*, dangerous cerebral activity, hypotension, and hypertension). In addition, oscillations of the manipulated variables (*i.e.* drugs IRs) can be limited by means of an intelligent tuning of the weights that contribute to the objective function. The pure *in silico* assessment of the MPC performance and reliability (before any *in vivo* implementation and clinical application) calls for the implementation of a different model of the patient than the one embedded in the controller, for the sake of recreating the model mismatch intrinsic to real applications.

2.5 Ethical concerns and clinical outcomes of closed-loop controlled anesthesia

After considering the advantages and technological aspects of automated delivery of anesthesia, the goal of Section 2.5 is to stimulate the interested reader to consider the controversial ethical and clinical outcomes.

The introduction of any new invention in biomedicine is expected to raise ethical concerns. With respect to the implementation of new surgical technologies and techniques, the authors of Strong et al. (2014) identify six key ethical considerations that can be suitably transferred to the context of automated anesthesia delivery. We reformulate these six points into Paragraphs 2.5.1-2.5.5. Finally, Paragraph 2.5.6 discusses potential clinical impact of control systems adoption in anesthesia.

2.5.1 Guarantee of the safety of new technology and management of timing and process for implementation

Regulatory agencies are in charge of managing the guarantee of safety of new technologies. The most well-known are USA FDA and EMA (European Medicines Agency). With similar regulatory processes, their common mission is to ensure safety and efficacy of new drugs and medical devices, while guaranteeing a rapid introduction of innovative therapies (Van Norman, 2016). This task is complicated by the fact that efforts of increasing safety often result into an increase in the costs and times for approval. It is worth underlining that there are neither universal regulatory frameworks nor processes. A very clear instance in the field of anesthesia is the case of TCI pumps. The authors of Absalom et al. (2016) identified and questioned commercial companies who were actively manufacturing and distributing TCI devices between 2004 and 2013. Despite claiming that more than 40 000 devices were sold in those years, such devices are still not approved/sold in all the countries. For instance, officially, no TCI pumps have ever been sold in the USA.

A related issue is the timing and process for implementation of new technologies. In fact, there is always a conflict between different realities: (i) the national/international framework and (ii) the local institution. Although the national organizations provide guidelines on these matters, the final effective decision on the use of new technologies is prerogative of the local institution, *e.g.*, the hospital, the medical staff, the academic department head (Sachdeva and Russell, 2007).

2.5.2 Patient's informed consent

Necessary condition for human experimentation to be both legal and ethical is the patient's informed consent. According to the Declaration of Helsinki developed by the World Medical Association (WMA) as a statement of ethical principles for medical research involving human subjects, "*each potential subject must be adequately informed of the aims, methods, sources of funding, any possible conflicts of interest, institutional affiliations of the researcher, the anticipated benefits and potential risks of the study and the discomfort it may entail, post-study provisions and any other relevant aspects of the study*" (WMA Declaration of Helsinki, 2013). This means that the medical doctor must engage the patients in a discussion aimed at not only informing them but also educating, understanding, and listening to potential doubts and questions. In case of anesthesia, this is particularly important. Since the drugs involved in the procedure may have critical adverse effects and affect not only the outcome of the surgical operation, but also the post-recovery phase, the patient must be put in the condition of complete trust in the anesthetist and their capacity of judgement and use of any tools involved in the procedure.

2.5.3 Training and credentialing physicians in new technology or technique

Often neglected, training is a critical issue regarding new medical devices. In the specific case of anesthesia, an interesting example is again the case of TCI pumps. According to Absalom et al. (2016), there are no specific rules on who can or cannot use TCIs. In addition, there is no regulated training for the use of TCI systems. This delicate point is related strictly to the clinical consequences discussed in Paragraph 2.5.6 In fact, an exhaustive and appropriate training, ideally provided by multidisciplinary experts (*e.g.*, clinicians and engineers) is essential for a responsible and effective use of automated devices for anesthesia delivery. This may help avoiding on one hand excessive trust in the instrument and on the other loss of situational awareness of the anesthetist.

2.5.4 Track and assessment of new technology outcomes

During the time interval between approval and clinical adoption/application, data on the new technology are still limited. Thus, there is an ethical obligation for early adopters to track outcomes of the new technology. Once again, rules on how to manage this pharmacovigilance phase should be issued by regulatory agencies.

Indeed, it is crucial to lead to a wide acceptance of the new device. In the context of PCLC devices (*i.e.* physiological closed-loop controllers), it is especially important to establish common performance indexes for both their development and evaluation after clinical application. The authors of Parvinian et al. (2018) refer to the consensus standard IEC 60601-1-10 as working in this direction. In fact, this collateral standard specifies requirements for the development (*i.e.* not only analysis and design, but also verification and validation) of a PCLC in medical electrical equipment. Automated anesthesia delivery systems can be included within the PCLCS class.

2.5.5 Balancing responsibilities to patients and society

In relation to the cost and value of new surgical technologies, the authors of Strong et al. (2014) point out the possible conflict of responsibility of the medical doctors: *i.e.* on one side towards the patients' wellbeing and on the other towards society (*e.g.*, from the market and the industry) for potential pressure to introduce innovative solutions. They cite the American Board of Internal Medicine principle according to which the main priority must always consist of the health and benefit of patients. We agree that this principle should absolutely be extended to closed-loop control of anesthesia, as the aim is to support anesthetists and increase the safety and stability of patients' state during anesthesia.

2.5.6 Clinical impact and risks

In the current concept of automated anesthesia, the anesthetist becomes a supervisor (*i.e.* a decision maker) of the procedure and can focus on monitoring the patient's DOA status. As discussed in Parvinian et al. (2018), depending on the degree of automation, consequences can lead to loss of situational awareness, complacency, and skill degradation. Loss of situational awareness may occur because of the anesthetist that evolves from being a human manual controller to a supervisor and decision maker of the automated control action. The natural consequence is the reduction of the time and actual procedures during which the anesthetist is actively involved in the care of the patient's anesthetic state. Additionally, if the control system proves exceptionally reliable and efficient (as it hopefully should be to guarantee a safe application), the anesthetist is exposed to the risk of overtrusting the tool. A related consequence is progressive degradation of skills. With the medical doctor less and less involved in the conscious procedure about dosing, future anesthetists may exhibit skill decay, as their skills would not be used as often as in the past, in case of high degree of automation. A series of issues related to engineering aspects will have

to be carefully assessed and analyzed in the future, such as the presence of fail-safe mechanisms, modeling uncertainty, and algorithms robustness.

These considerations are common hazards introduced by the implementation of automated systems. However, the active involvement of clinicians in the development and testing of control systems for anesthesia delivery, coordinated with the introduction of adequate methods for the evaluation and standardization of training represent the key milestones to limit likely negative impacts on clinical practice.

2.6 Conclusions

This chapter provided a discussion on the application of advanced control systems in anesthesia. Firstly, we discussed the limitations of the current manual approach to anesthesia delivery, mainly related to the impact of human factors on the choice of the optimal dosing, and the limited use of data on the monitored vital parameters (*i.e.* only for subjective interpretation of the DOA level). Afterwards, we compared the main control strategies that are being studied. Finally, some ethical and clinical implications were discussed to stimulate the reader to make their own mind on the topic and propose solutions to the remaining open problems.

We find that the "engineering" challenges of control systems applications in anesthesia can be summarized into two specific points: (i) inter-individual variability of the response to drugs and surgical stimuli and (ii) the complexity of the process that involves multiple drugs, and thus several effects that manifest their mechanism of actions and interactions. For what concerns the first issue, we believe that population PK/PD models are hardly adequate. Future work should focus on efforts to develop models able to individualize the prediction. Taking into account physiological and anatomical differences in the individuals, related to age, body mass and height, presence of disease, genetics, can make the difference. In addition, use of the on-line information of cardiovascular changes can help improving the prediction of drugs disposition within the body with consequent changes in the manifestation of their effects. PBPK models use blood flows as parameters, and thus can take into account these changes. The literature reports that PD variability is higher than PK variability among individuals. Adaptive control techniques can be evaluated to face this matter, so that the predicted PD response is adapted to the specific patients undergoing anesthesia. As for the second issue, it is no mystery that anesthesia is complex and some underlying mechanisms are still unclear. With advancing knowledge on drug-

drug interactions mechanisms, and improved tools and methods to manage multivariable problems, researchers should address the issue by increasing the quantity of data that the controller can process and use, so that drug-drug interactions and several pharmacodynamic effects can be embedded into the controller problem.

Despite difficulties related to the lack of standardization and universal regulatory frameworks, nowadays TCI pumps are a mature technology (Absalom et al., 2016). This opens an encouraging perspective for control systems application in anesthesia based on real time monitored measures of the patient's anesthetic and analgesic state. Such systems have the potential to not only reduce anesthesia-associated risks, human error incidence, and anesthetist's workload for a more efficient monitoring and focus on the patient's state, but also standardize anesthesia procedure, by reducing subjectivity of the optimal dose selection. Obviously, clinical consequences must be carefully assessed and engineering aspects validated before any clinical adoption and application.

It is our opinion that the only road for successful application of control systems in anesthesia calls for engineers and clinicians working together. In fact, on one hand engineers are essential for an effective design and development of the patient's model and control system. On the other hand, clinicians must guide engineers by providing information on crucial aspects such as the key indexes for an optimal and safe assessment of the control system performance and the essential data required to quantify the DOA level. In addition, clinicians can provide useful recommendations and specifications for the optimal design of the graphical user interface of the automated delivery tool.

CHAPTER 3

Model-predictive control of anesthesia with propofol and remifentanil

3.1 Author's Note

This chapter presents the initial work on the proposed model-predictive controller of anesthesia delivery with the anesthetic agent propofol and the analgesic opioid remifentanil. Indeed, propofol-remifentanil is a widely used combination of drugs to administer TIVA. At this stage, the controller structure includes two controlled variables, *i.e.* (i) bispectral index (BIS) and (ii) mean arterial pressure (MAP), to control the patient's levels of unconsciousness and analgesia, respectively. Propofol and remifentanil infusion rates are the manipulated variables. The patient model embedded in the *in silico* closed-loop framework and used for evaluation of the controller performance is based on a PBPK-PD model. Special focus is devoted to explaining the distinction between this approach and the classical three-compartment PK modeling approach, which is mostly used in the scientific literature related to anesthetic and analgesic drugs.

This work was published in "Biomedical Signal Processing and Control" journal:

A physiologically-based approach to model-predictive control of anesthesia and analgesia

Adriana Savoca, Davide Manca

Biomedical Signal Processing and Control 53 (2019): 101553
DOI: 10.1016/j.bspc.2019.04.030

3.2 Abstract

The application of closed-loop control systems in biomedicine unlocks prospects for optimized drug delivery based on the measurement of patients' physiological variables. However, inter-individual variability and narrow therapeutic indexes are issues that must be carefully considered. We propose an *in silico* study of a model-based controller of anesthesia and analgesia with propofol and remifentanil, based on bispectral index (BIS) and mean arterial pressure (MAP) measurements. A physiologically-based pharmacokinetic (PBPK) model, combined with a suitable pharmacodynamic model, allows describing and differentiating the dose-effect dependency for the virtual patients. The controller delivers a safe and fast induction of anesthesia, with mean rise-times below 3 min and controlled variables within the clinical safe ranges. The PBPK model allows gaining complementary information about the dynamics of the drugs absorption, distribution, metabolism, and elimination in the body. Special attention is devoted to simulating realistic intraoperative surgical stimuli and noise on the controlled variables. The controller successfully rejects disturbances on BIS and MAP related to nociceptive stimuli (*e.g.*, intubation and incision) via a robust control action, and is not diverted by noise.

Keywords: model-based control; anesthesia; analgesia; pharmacokinetics; pharmacodynamics; simulation; propofol; remifentanil.

3.3 Introduction

Although general anesthesia is commonly defined as "*a reversible state of unconsciousness, during which a patient will not perceive or be responsive to noxious stimuli*" (Sebel, 2001), anesthetists lack, on one hand, a quantitative definition of the required "depth of anesthesia" (DOA), and on the other hand a specific and

standardized method for its evaluation. A balanced anesthesia results from the combination of different components that account for multiple pharmacological effects, *i.e.* (i) the hypnotic for unconsciousness, (ii) the analgesic for pain relief, and (often) (iii) the neuro-muscular blocking agent for prevention of reflex activity. These drugs usually have narrow therapeutic indexes, and this characteristic makes their titration difficult (Absalom and Struys, 2007).

In clinical practice, the anesthesiologist sets an initial dose manually to induce anesthesia, according to standardized protocols, guidelines, and experience (*e.g.*, "Roberts" infusion regime (Roberts et al., 1988)). Afterwards, a constant infusion rate is implemented to maintain the anesthetic state, and adjustments are made depending on the subjective patient's observation. Indeed, visible signs such as movement, shaking, and changes of hemodynamics and cerebral activity manifest the patient's stress and allow identifying inadequate anesthesia and analgesia levels. As an alternative to manual infusion, Target Controlled Infusion (TCI) pumps are rather widespread for induction and maintenance of anesthesia. They rely on classical three-compartment pharmacokinetic (PK) models that correlate desired target values of the drug concentration to proper infusion rates (Servin et al., 1998; Struys et al., 1998). Since blood and effect-site concentrations cannot be measured on-line, TCI pumps implement an "open-loop" approach, which does not provide any concrete certainty that the desired target concentration is achieved. In fact, they do not take into account any real-time physiological variables (*e.g.*, arterial pressure, heart rate, and quantitative electroencephalogram indices), which are direct and measurable key indicators of the patient's anesthetic state (*i.e.* the real pharmacodynamic effect on the patient's body produced by the drugs infusion). In case of TCIs, the anesthesiologist is the real controller and TCIs are merely actuators of the control action, which can thus result biased and subject to both model mismatch and human interpretation.

Automation of anesthesia delivery based on pharmacodynamics, which entails the measurement of physiological variables, would support medical expertise and allow safer and more regular control actions on the patient's anesthetic state throughout the surgical operation. The 2015 US Food and Drug Administration Workshop about the application of Physiological Closed-Loop Controlled (PCLC) medical devices in critical care shows an increasing interest in this direction, which arises from perspectives of workload reduction and the fact that automated systems are not distractible (FDA Report on PCLC medical devices, 2015). Of course, risks related to engineering and

technical aspects need to be considered and assessed (*e.g.*, fail-safe mechanisms and algorithm failures). Although application to biomedicine is still emerging, some interesting works (*e.g.*, Gentilini et al. (2002)) recommended implementing closed-loop control systems in this field since the first years of XXI century. Several authors proposed different solutions and among them, some arrived to clinical validation. For instance, West et al. (2013) and Zhusubaliyev et al. (2015) chose a proportional-integral-derivative (PID) control strategy and relied on classical PK modeling for performance assessment. However, we claim that model predictive control (MPC) proved superior in several applications in terms of overshoot, settling time, and robustness. Indeed, a well-designed model-based control allows rejecting disturbances that can alter the anesthetic state of the patient, and by suitably tuning the weights of the objective function, it is possible to reduce the chances of having abrupt changes in the manipulated variables. In case of anesthesia, this would result in dangerous overdosing with adverse effects and longer times for recovery. Nascu and co-authors (Nascu et al., 2015) investigated different MPC strategies for anesthesia with propofol, with the controller featuring a classical three-compartment PK model. In case of model-based control, one of the main challenges to be addressed is the inter- and intra-patient variability, which are manifest in both pharmacokinetic and pharmacodynamic contributions. El-Nagar and El-Bardini (2014) tackled this problem by using a fuzzy neural network tested over a wide range of patient parameters, whereas Merigo and co-authors (Merigo et al., 2018) proposed a PID approach comprising a PK/PD model of the patient to compensate uncertainties, with a Monte Carlo method to account for inter-patient variability. Soltesz and co-authors (Soltesz et al., 2013) approached the issue by individualizing the patient model of the dose-response relation via system identification during the induction phase. Although we treat the problem from a different perspective, we believe that the individualization of the dose-response prediction is the right path to follow. Within this context, physiologically-based pharmacokinetic (PBPK) modeling has great potential. Indeed, PBPK models rely on the real anatomy and physiology of human body, and describe in detail the processes of absorption, distribution to tissues and organs, metabolism, and elimination of drugs (*i.e.* ADME processes). They are effective tools for simulation and prediction of pharmacokinetics, and recently their application has spread to various fields of pharmacology and toxicology. We believe that model predictive control of anesthesia supplemented by a physiologically-based approach to modeling can lead to more robust performances and reliable predictions of inter-

individual variability. At the *in silico* level, PBPK modeling can be used to simulate ADME processes and inter-individual PK variability. During the *in vivo* surgical intervention, PBPK modeling can be implemented in anesthesia controllers for an improved prediction of the PK response of real patients. Indeed, the application of such models potentially allows using real-time hemodynamic data to adjust drug pharmacokinetics, which is affected by conditions of hypotension (*i.e.* hypoperfusion) with consequent variations of the clinical effects. To our knowledge, no authors have yet applied physiologically-based modeling to MPC of anesthesia based on monitored patient's parameters (*i.e.* pharmacodynamic response of the patient).

A main advantage of MPC is the aptitude to manage multivariable problems. While several authors focus on only one aspect of anesthesia, our work proposes an *in silico* study of the performance of a model-based controller of anesthesia with co-administration of propofol and remifentanil. Indeed, we aim at accounting for both the essential components of hypnosis and analgesia by controlling bispectral index (BIS) and mean arterial pressure (MAP). To test the controller performance, we physically close the loop by introducing a virtual patient, whose response to changes of the input variables (*i.e.* drug infusion rates) and external disturbances (*e.g.*, surgical stimuli) is simulated via a PBPK-PD model (where PD stands for pharmacodynamics). Likewise, the controller features a classical PK-PD model for the sake of creating a model mismatch (*i.e.* in line with the mismatch between the *in vivo* patient and the controller model in case of real surgical interventions). In addition, we test the controller robustness by implementing an artificially-generated noise on the monitored variables (to mimic the oscillations and so-called artifacts of experimental measures).

Section 3.4 deals with the *in silico* control loop configuration and clarifies the choice of the controlled variables along with the selected setpoints. In particular, Paragraph 3.4.1 details the modeling aspects, while Paragraph 3.4.2 describes the optimization problem. Finally, Paragraph 3.4.3 briefly comments on how we tested the effect of measurement noise. Section 3.5 presents and discusses the results on the controller performance.

3.4 Control scheme and specifications

The main elements of the model-based framework are: (i) the control objectives, (ii) the controller structure, and (iii) the virtual patient (see Figure 1).

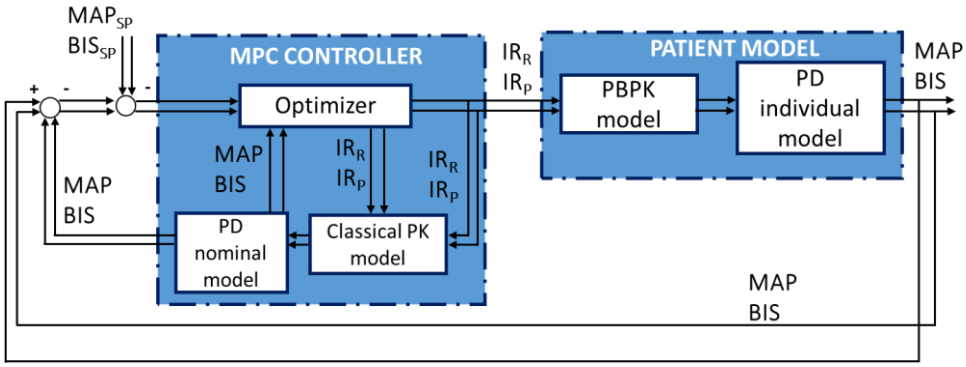

Figure 1 – Block diagram of the *in silico* control loop of anesthesia with propofol and remifentanil. The main elements are: the control objectives BIS_{SP} and MAP_{SP}; the controller block (including the optimizer and the PK three-compartment model combined with the Hill equation (PD)); the virtual patient block, *i.e.* PBPK model combined with Hill equation (PD). Outputs of the controller block are the manipulated variables IR_P and IR_R (propofol and remifentanil infusion rates, respectively). The PD models differ in terms of nominal and individual features and allow predicting the dynamics of BIS and MAP.

The controlled variables are BIS and MAP, which are respectively representative of the level of hypnosis and analgesia. The manipulated variables are the infusion rates (IRs) of propofol and remifentanil. With reference to the controller structure, the controller receives as inputs both targets (*i.e.* setpoints and lower/upper bounds) and "measured" values of BIS and MAP, and evaluates the optimal IRs of propofol and remifentanil accordingly.

In principle, the controlled variable referred to the analgesia component should quantify the pain level to assess the clinical effect of analgesic drugs. However, pain level is subjective (both from the patient and anesthetist perspectives) and thus is not particularly reliable as a controlled variable. Since opioids (especially remifentanil) suppress the hyperdynamic response of the cardiovascular system to painful stimuli, the systemic PD response can be quantified in terms of arterial pressure and heart rate (HR) changes (Song et al., 1999). We chose MAP, as controlled variable for analgesia, over HR and systolic arterial pressure (SAP) mainly because the PD model based on MAP response provides better results once validated with experimental data (see Savoca et al. (2017)). Since adequate analgesia is usually identified with MAP levels around 70 mmHg, and MAP < 60 mmHg is reported as hypotension (typically associated with hypnotics/opioids overdose), the MAP setpoint was set at 70 mmHg. Regarding the definition of the hypnosis-controlled variable, BIS is an effective quantitative index (ranging from 0 to 100 [-], *i.e.* awake patient) which is based on the EEG trace. Indeed, BIS- guided anesthesia has led to the reduction in the incidence of patient's awareness and improved recovery (Bennett et al., 2009). In addition, the scientific literature provides a number of manuscripts including experimental data that

allow validating the PD model (Flaishon et al., 1997; Liu et al., 2015; Wiczling et al., 2016). The recommended BIS range for general anesthesia in surgical interventions is set in the 40-60 [-] interval. Accordingly, we defined our target DOA to be BIS_{SP} = 50 [-].

One of the advantages of MPC over conventional feedback control (*e.g.*, PID loops) is that the concept of pairing, between manipulated and controlled variables, is overcome by the holistic approach to control exerted by the set of manipulated variables on the set of controlled ones. Indeed, this approach allows implementing not only square but also rectangular problems where the number of manipulated and controlled variables is not necessarily the same. Still, our problem features an equal number of manipulated and controlled variables and the two PBPK-PD models, used *in silico* to mimic the real patient, are focused on a direct and single interaction between the manipulated variable and the controlled one.

For the sake of clarity, we assume that propofol acts only on BIS and remifentanil on MAP (thus the two unconnected PBPK-PD models). This simplifying assumption is equivalent to considering two independent SISO (*i.e.* single-input-single-output) configurations that conceptually clash with the MPC principles of multivariable control, although the intrinsic predictive nature of model-based approach is preserved and exploited. The reason underneath this choice is that, although pharmacodynamic interactions between propofol and opioids have been widely studied, little is known of the underlying mechanism. Indeed, there is an intrinsic difficulty in highlighting and quantifying the coupled contributions of each term on the complementary one (*i.e.* the mutual effects of anesthetics vs analgesics). For instance, findings on the electroencephalogram (EEG) effects of co-administration are controversial (Kortelainen et al., 2009). Some authors (Kortelainen et al., 2009) suggest that these differences may be ascribed to a dependency of the remifentanil-induced EEG changes on the anesthesia level. In any case, the effects of remifentanil administration on the propofol concentration corresponding to loss of consciousness are not dramatic (Struys et al., 2003). Furthermore, the parameters of both our BIS and MAP models are identified with experimental data resulting from combined administration of propofol and remifentanil (Liu et al., 2015; Savoca et al., 2017), and therefore indirectly account for their interaction. Thus, we deem that our SISO approach is acceptable, although future work should focus on including such interactions within the model structure.

3.4.1 Pharmacokinetic-pharmacodynamic modeling

Since the whole anesthesia is simulated *in silico*, it is advisable to introduce a "mismatch" between (i) the model that is used for control purposes within the MPC procedure and (ii) the models that mimic the patient's response (*i.e.* the real process).

The controller model that simulates the patient's dynamic response to drug infusion consists of: (i) a PK model based on a classical three-compartment structure that is also CPU efficient, as far as the numerical solution of the optimization problem is concerned, and (ii) a PD model (*i.e.* modified Hill equation) for description and prediction of the drug pharmacological effects (Savoca et al., 2017). Indeed, empirically-based three-compartment models are the most widespread for PK description of both opioids and intravenous anesthetics. The central compartment represents plasma and is interconnected to the rapidly and slowly equilibrating compartments (that epitomize the exchange between plasma and other organs/tissues). Despite not being truly related to the anatomy/physiology of the human body, three-compartment models can suitably describe the pharmacokinetic curve of many drugs employed in anesthesia. The mathematical model consists of the material balances on the three compartments, describing the dynamics of the corresponding concentrations C_1, C_2, and C_3 (Eqs. (3.1-3)).

$$\frac{dC_1(t)}{dt} = -(k_{10} + k_{12} + k_{13})C_1(t) + k_{21}C_2(t) + k_{31}C_3(t) + \frac{IR(t)}{V_1} \tag{3.1}$$

$$\frac{dC_2(t)}{dt} = k_{12}C_1(t) - k_{21}C_2(t) \tag{3.2}$$

$$\frac{dC_3(t)}{dt} = k_{13}C_1(t) - k_{31}C_3(t) \tag{3.3}$$

Eq. (3.1) includes the input drug infusion rate $IR(t)$ and a generic elimination pathway represented by the k_{10} parameter. The compartment volumes V_1, V_2, and V_3 and their clearances CL_1, CL_2, and CL_3 are either fixed or calculated as a function of body mass, height, and age of the patient. Correlations are available in Minto et al. (1997) for remifentanil and Schnider et al. (1998) for propofol. Transfer coefficients k_{ij} implemented in the controller are calculated as ratios between clearances and volumes.

As mentioned in Section 3.3., we adopted a PBPK modeling approach to mimic the ADME processes that are undertaken by the drugs in the real patient body. The PBPK

model (Abbiati et al., 2016) is combined with a suitable PD model having the same structure as the one implemented in the controller. However, each simulated patient features different values of the PD parameters (see Eq. (3.14)) to account for inter-individual variability of the dose-response relation.

The PBPK model extensively discussed in Abbiati et al. (2016) features compartments that correspond to (possibly lumped) real tissues and organs and include physiological metabolic/elimination pathways. Indeed, the PBPK model embodies with a rather good detail both the anatomy and physiology of the patient and this facilitates the individualization of the prediction. As propofol and remifentanil are both administered intravenously, the model can be reduced to the following five compartments *i.e.* plasma, gastrointestinal circulatory system (GICS), liver, highly perfused organs (HO, *i.e.* lumping the kidneys, heart, brain, and spleen), and poorly perfused tissues (PT, *i.e.* lumping fat, muscles, bones, and skin), because the counter-diffusion to both small and large intestinal lumina is considered negligible. The mathematical expression of the model consists of Eqs. (3.4-8) that describe the drugs concentration dynamics in the body compartments, complemented by Eqs. (3.9-12), whose purpose is to describe and quantify the eliminated drug amount A^{EL} via four different pathways, *i.e.* plasma, tissues, liver metabolism, and renal excretion.

$$\begin{aligned}\frac{dC^{P}(t)}{dt} &= \frac{IR(t)}{V^{P}} + C^{PT}(t)k_{PT-P}\frac{V^{PT}}{V^{P}} + C^{L}(t)\frac{Q^{HV}}{V^{P}} + \\ &C^{HO}(t)k_{HO-P}\frac{V^{HO}}{V^{P}} - C^{P}(t)k_{EL,P}\left(1-R\right) \\ &-\frac{C^{P}(t)}{V^{P}}CL^{K} - C^{P}(t)\left(k_{P-PT}\left(1-R\right) + k_{P-HO}\left(1-R\right) + \frac{Q^{HA}}{V^{P}} + \frac{Q^{PV}}{V^{P}}\right)\end{aligned} \tag{3.4}$$

$$\frac{dC^{GICS}(t)}{dt} = -C^{GICS}(t)\frac{Q^{PV}}{V^{GICS}} + C^{P}(t)\frac{Q^{PV}}{V^{GICS}} \tag{3.5}$$

$$\frac{dC^{L}(t)}{dt} = -C^{L}(t)\left(\frac{Q^{HV}}{V^{L}} + \frac{CL^{H}}{V^{L}}\right) + C^{P}(t)\frac{Q^{HA}}{V^{L}} + C^{GICS}(t)\frac{Q^{PV}}{V^{L}} \tag{3.6}$$

$$\frac{dC^{HO}(t)}{dt} = -C^{HO}(t)k_{HO-P} + C^{P}(t)k_{P-HO}\left(1-R\right)\frac{V^{P}}{V^{HO}} \tag{3.7}$$

$$\frac{dC^{PT}(t)}{dt} = -C^{PT}(t)k_{PT-P} + C^{P}(t)k_{P-PT}\left(1-R\right)\frac{V^{P}}{V^{PT}} - C^{PT}(t)k_{EL,PT} \tag{3.8}$$

$$\frac{dA^{EL,P}(t)}{dt} = V^{P}C^{P}(t)k_{EL,P}\left(1-R\right) \tag{3.9}$$

$$\frac{dA^{EL,PT}(t)}{dt} = V^{PT}C^{PT}(t)k_{EL,PT} \tag{3.10}$$

$$\frac{dA^{EL,L}(t)}{dt} = C^{L}(t)CL^{H} \tag{3.11}$$

$$\frac{dA^{EL,K}(t)}{dt} = C^{P}(t)CL^{K} \tag{3.12}$$

Three categories of parameters can be differentiated: individualized, assigned, and adaptive (see Table A in Appendix 3.A). Individualized parameters (*i.e.* compartment volumes V^i and blood flowrates Q^i among them) are calculated via correlations available in the scientific literature (Abbiati et al., 2016). Particularly, compartment volumes are based on the organ/tissue mass fractions respect to the total body mass (depending on gender and age). Flowrates are calculated as fractions of the cardiac output that reach the organ/tissue, with cardiac output depending on the patient body surface area (BSA) (calculated as a function of patients' body mass and height). Assigned parameters depend on the drug characteristics, *e.g.*, the drug fraction R bound to plasma proteins. Finally, adaptive parameters are the ones that can be neither extrapolated from the scientific literature nor measured experimentally. Most of them are (i) drug transfer coefficients k_{i-j} representing diffusive and convective transport processes and (ii) metabolic/elimination constants $k_{EL,i}$, which are identified via a nonlinear regression of pharmacokinetic experimental data. In particular, we used adaptive parameters identified for remifentanil in Abbiati et al. (2016) with some modifications, whereas we regressed the adaptive parameters for propofol with experimental data from Schnider et al. (1998) and validated the results with Gepts et al. (1987).

Adaptive parameters related to metabolism and elimination can be appropriately modified in case of impairments such as hepatic dysfunctions and renal insufficiency. In general, the number and type of adaptive parameters depend on the properties of the drug under investigation. For instance, according to the scientific literature (see Savoca et al. (2017)), remifentanil is only metabolized via plasma and tissue esterases (related to parameters $k_{EL,P}$ and $k_{EL,T}$). In fact, the half-life of remifentanil is shorter compared to other analgesic opioids, which makes its use appealing in anesthesia. Consequently, we did not consider the hepatic and renal routes in the PBPK model of remifentanil. On the contrary, since the liver is mainly responsible for propofol metabolism, but there is also evidence of extra-hepatic elimination, the PBPK model of propofol accounts for both hepatic and extra-hepatic elimination/metabolic pathways. For a detailed mathematical description of the model, the interested reader can refer to Abbiati et al. (2016) and Abbiati and Manca (2016).

Both propofol and remifentanil exhibit a phase lag (*i.e.* delay) between the time profile of the plasma concentration and the pharmacological effect, therefore we introduced Eq. (3.13) that describes the material balance on the effect-site, *i.e.* the drug site of action (Varvel et al., 1992), where C_p and C_e are plasma and effect-site concentration, respectively.

$$\frac{dC_e(t)}{dt} = k_{e0}C_p(t) - k_{e0}C_e(t) \tag{3.13}$$

This effect-site is a virtual compartment that does not affect PK and allows accounting for the abovementioned delay. We assume that the rate constant k_{e0} for both the positive and negative terms is the same. Furthermore, since different PK inputs lead to different values of k_{e0}, we implemented in the controller values from the literature concerning three-compartment PK-PD analysis (Minto et al. (1997) and Schnider et al. (1998) for remifentanil and propofol, respectively). The patients' PBPK-PD model include k_{e0} values obtained via regression from PD experimental data. We provide further details on the procedure in Savoca et al. (2017). MAP and BIS (*i.e.* the pharmacological effects $E(t)$) are correlated to the effect-site concentrations of remifentanil and propofol respectively, by the modified Hill equation (Minto et al., 1997) as in Eq. (3.14).

$$E(t) = E_0 - (E_0 - E_{\max})\frac{C_e(t)^{\gamma}}{C_e(t)^{\gamma} + EC_{50}{}^{\gamma}} \tag{3.14}$$

where E_0 is the baseline value of the awake patient (*i.e.* before anesthesia induction), E_{max} is the maximum drug effect, EC_{50} is the concentration corresponding to 50% of the maximum effect, and Hill coefficient, γ, is a fitting parameter.

3.4.2 Optimization problem formulation and control design

The MPC optimization problem is formulated in Eq. (3.15). The controller model is called to predict the future evolution of the system over the prediction horizon h_p. This horizon is discretized into multiple time steps $k, k+1, \dots, k+h_p$ with a t_s time interval. At each time step k the controller optimizes a set of h_c optimal control actions (IR in Eq. (3.15)) based on the model predictions. Parameter h_c is called "control horizon". The first control action of this optimal set is then implemented *in silico* in the patient (*i.e.* PBPK-PD model), at the following time step $k+1$. The following control actions iterate what was carried out at time step k.

The objective function in Eq. (3.15) consists of two main terms. The first term accounts for the distance e_y between the prediction of the controlled variable y (*i.e.* MAP and BIS) and the corresponding setpoint y_{sp} (see also Eq. (3.16)). Eq. (3.17) quantifies the mismatch $\delta_y(k)$ between the model prediction and the real process, since no model can provide a perfect representation of reality. The mismatch is kept constant throughout h_p. In an in *in silico-in vivo* control loop, this term is the correction of the model prediction y respect to the real-time measured value y_r of the controlled variable. In our purely *in silico* control loop, $\delta_y(k)$ measures the distance between the PBPK-PD model (*i.e.* the *in silico* patient) and the controller model predictions. The second term of the objective function minimizes the control effort (as shown in Eq. (3.18)). As a result, the optimizer tries to find a compromise between distance from the setpoint, *i.e.* the desired DOA, and rates of change of the manipulated variables. In fact, steep changes of the drug IRs may result into dangerous overshoots of plasma concentration and oscillations that negatively affect the patient state. In Eq. (3.15) w are suitable weights, and PF are penalty functions.

$$\min_{IR(k),IR(k+1),\ldots,IR(k+h_c-1)} \left\{ \begin{array}{l} \sum_{j=k+1}^{k+h_p} \left[w_y e_y{}^2(j) + PF_y(j) + PF_{C_p}(j) \right] \\ + \sum_{i=k}^{k+h_p-1} w_{IR} \Delta IR^2(i) \end{array} \right\} \tag{3.15}$$

$$e_y(j) = \frac{\left[y(j) + \delta_y \right] - y_{sp}(j)}{y_{sp}(j)} \tag{3.16}$$

$$\delta_y(k) = y_r(k) - y(k) \tag{3.17}$$

$$\Delta IR(i) = IR(i) - IR(i-1) \tag{3.18}$$

$$PF_{C_p}(j) = w_{C_p}^{PF} \left\{ Max\left[0, \frac{C_p(j) - C_{p,\max}(j)}{C_{p,\max}(j)} \right] \right\}^2 \tag{3.19}$$

$$PF_y(j) = w_y^{PF} \left\{ \left\{ Max\left[0, \frac{y(j) - y_{\max}(j)}{y_{\max}(j)} \right] \right\}^2 + \left\{ Min\left[0, \frac{y(j) - y_{\min}(j)}{y_{\min}(j)} \right] \right\}^2 \right\} \tag{3.20}$$

We implemented penalty functions for the plasma concentration (Eq. (3.19)), and the controlled variables BIS and MAP (Eq. (3.20)). As far as plasma is concerned, the maximum value is chosen according to clinical ranges (Absalom and Struys, 2007). It is especially important in case of remifentanil IR, because of the hemodynamic stability risk pointed out by Gentilini et al. (2002). Such values should not be regarded

as fixed and rigid constraints, but more like approximate indications, because they are subject to inter-patient variability and conditions (*e.g.*, type of premedication and combination with other drugs). Similarly, minimum and maximum values for BIS and MAP are chosen according to the principle of preventing critical situations, *e.g.*, hypotension, hypertension, and dangerous cerebral activity (see Table 1).

Table 1 – Minimum and maximum values of the drugs plasma concentration and controlled variables MAP and BIS implemented in the penalty functions of the optimization problem.

Variable	**Symbol**	**Unit of measure**	**Min**	**Max**
Remifentanil plasma concentration	$C_{p,R}$	[ng/mL]	-	16
Propofol plasma concentration	$C_{p,P}$	[µg/mL]	-	14
Mean arterial pressure	MAP	[mmHg]	60	120
Bispectral index	BIS	[-]	40	60

The choice of h_p and t_s is strictly related to the process characteristic times (Gentilini et al., 2002). We assigned the time interval for control, t_s, according to a trial-and-error procedure, and finally chose t_s = 1 min as a trade-off value between aggressiveness and responsiveness of the system. However, this parameter is flexible and can be reduced in case the clinical experts find it not suitable to an effective and fast response to surgical stimuli. In clinical practice, the time for induction is within 10-15 min, thus we adopted h_p = 15 min for the analgesia loop and h_p = 20 min for the anesthesia loop. In fact, the pharmacodynamics of propofol is slower than the remifentanil one (*i.e.* slower velocity of equilibration between plasma and effect-site). The selection of the control horizon, h_c, followed a trial-and-error approach as well. In this regard, low values of h_c may result in too aggressive control actions. On the other hand, high values can jeopardize the optimization algorithm performance. We found that h_c = 4 is a suitable compromise as it limits to 8 the total number of degrees of freedom.

We tuned the weights of the objective function according to the priority of the terms. For this reason, the weights w_{BIS} and w_{MAP} are the same. The weights $w_{IR,R}$ and $w_{IR,P}$ regulate the aggressiveness of the IRs rate of change (the higher the weight the lower the aggressiveness). We improved the results by choosing different values for the induction and maintenance phases (apexes i and m in Table 2).

Table 2 – Values of the weights in the objective function. In the "Symbol" column, y represents the controlled variable, IR the manipulated variable (*i.e.* infusion rate), C_p the plasma concentration, and PF the penalty function.

Parameters	Symbol	Remifentanil (MAP)	Propofol (BIS)
Error weight	w_y	1.e6	1.e6
Input rate of change weight (induction)	w_{IR}^{i}	1.e-5	1.e-15
Input rate of change weight (maintenance)	w_{IR}^{m}	1.e-4	1.e-12
Penalty function on plasma PK weight	$w_{C_p}^{PF}$	1.e3	5.e4
Penalty function (MAP/BIS) weight	w_{y}^{PF}	1.e5	1.e5

Since the propofol dynamics is slower, we set $w_{IR,P}$<$w_{IR,R}$ to ensure acceptable rise-times for BIS and make them similar to those of MAP. We recall that in clinical practice IR_P is 3 orders of magnitude higher than IR_R (*i.e.* mg/min for propofol vs µg/min for remifentanil). Furthermore, in Eq. (3.18), the control effort term is not normalized respect to the infusion rate at the previous time step, $IR(k-1)$, to avoid any numerical errors for IR = 0. For this reason, the values of w_{IR} display a significantly different order of magnitude compared to the other weights (see Table 2 which includes also $w_{C_p}^{PF}$, w_{BIS}^{PF}, w_{MAP}^{PF}). To avoid overdosing, the penalty function terms on the controlled variables (*i.e.* feasibility/safety lower and upper bounds) have similar priority to the distance from the setpoint. A mixed language approach to programming, based on Fortran 90 and C++, merges the PK/PBPK-PD and ODE routines to the optimization classes. The unconstrained optimization procedure is based on different algorithms to ensure robustness. Simplex method is the one preferentially used by the C++ optimizer (Buzzi-Ferraris, 1993).

3.4.3 Implementation of disturbances and noise

To investigate the robustness of the controller during the maintenance phase, we implemented disturbances (*i.e.* external nociceptive stimuli) in the shape of abrupt changes in the simulated measurements of BIS and MAP. We focused on replicating clinical events and physical, feasible problems, *i.e.* intubation, incision, and episodes of arousal. Since in clinical practice, the measured physiological variables show noise and fluctuations (*aka* artifacts), we investigated the robustness towards measurement noise. Consequently, we observed and analyzed BIS of case study 4 in Absalom and Struys (2007) and MAP in Gentilini et al. (2002). We decomposed the experimental signal into two contributions: (i) a trend line and (ii) a stochastic noise. We obtained the trend line by filtering the experimental data via the Savitzky-Golay procedure

(Press et al., 1996). Afterwards, we considered the time periods with lack of stimulation, and quantified the noise contribution by analyzing the residuals between the trend and the experimental data points. We verified that these residuals are Gaussian distributed. Finally, we evaluated the mean and standard deviation, and added a Gaussian distributed noise to both BIS and MAP of the *in silico* patient, via the Box-Muller algorithm, according to Eqs. (3.21-22).

$$Noise = \mu + \sigma\sqrt{-2\log(u)}\cos(2\pi v) \tag{3.21}$$

$$y_{patient} = y_{patient} \pm Noise, \qquad y_{patient} = BIS, MAP \tag{3.22}$$

Where u and v are uniform random numbers (in the interval [0,1)), and μ and σ are the mean and standard deviation respectively.

3.5 Results and discussion

3.5.1 Induction of anesthesia

Induction of anesthesia aims at reaching the required DOA level as fast as possible, usually within 10-15 min. We simulated the behavior of the controller for nine patients with demographic characteristics reported in Table 3.

Table 3 – Demographic data of the simulated patients.

Patient #	BM [kg]	H [cm]	Gender [-]	Age [y]
1	75.5	180	M	25
2	71.3	173	F	27
3	94.5	195	M	50
4	90.3	181	F	42
5	50.5	159	F	38
6	57.7	162	F	58
7	56.7	163	M	75
8	95.1	203	M	18
9	85.2	185	M	45
Mean	75.2	177.9	5M/4F	42
SD	17.2	15.2	-	17.77

Figure 2 (top) shows the dynamics of BIS and MAP (the controlled variables), and (bottom) IRs (the manipulated variables). Control action starts at 5 min, with the change of setpoint (*i.e.* "servo problem" in engineering terms) from baseline (MAP = 80-90 mmHg and BIS = 90-100 [-]) to DOA. This pre-induction period shows consistency of the results, where a null drug concentration corresponds to the baseline value of awake patients.

For all the simulated patients, the desired DOA level is achieved with a balanced control action, which is initially steep to ensure responsivity and then decreases gradually once the setpoint is approached. The indicators of Table 4, which assess the controller performance, are: rise-time t_{rise}; time required for loss of consciousness (LOC) t_{loc}; minimum values of MAP and BIS. According to Yang et al. (2016), who studied changes in BIS as a response to LOC for young and elderly patients, we defined t_{loc} as the time required to reach BIS = 60 [-]. More specifically, they found BIS_{loc}= 57.7 (± 12.3) [-] for young patients, and BIS_{loc} = 65.4 (± 9.7) [-] for elderly patients, who are more sensitive to anesthetics effects. In addition, similar studies display BIS_{loc} values around 60 [-], hence our choice.

Individual rise-times are approximately 2-3 min for both MAP and BIS, whereas mean time to LOC is about 2 min (Table 4). The controlled variables are maintained within the recommended ranges throughout the investigated period, and the minimum values are all above the lower thresholds, *i.e.* MAP = 60 mmHg (hypotension, marked by a red dotted line in Figure 2) and BIS = 40 [-]. It is interesting to compare these results with similar works, also mentioned in Section 3.3. With respect to the control action on the hypnotic component, it is worth noticing that our rise times are comparable to those of Nascu et al. (2015) and Merigo et al. (2018), whose control strategies are model-based (in their works, the single controlled variable is BIS). It is also worth observing that our predicted infusion rates are lower than in Merigo et al. (2018). One of the reasons may be that they use the physical range of the pump flowrate as constraint on the maximum infusion rate value, whereas we implement clinical and therapeutic ranges on both controlled variables and plasma concentration, as discussed in Paragraph 3.4.2. Thus, from this point of view, our results can be considered incremental in the sense of safety and stability of the patient's anesthetic state. Conversely, our settling times are higher compared to other studies. This can be ascribed to the lower k_{e0} value in the patients' model, which depends on the data used to identify the PD parameters. By using a fuzzy neural-network-based controller, El-Nagar and El-Bardini (2014) shows rise times for MAP that are near to our results. However, for the sake of safety, we assign/accept a lower decrease of MAP from baseline, to avoid hypotension. Again, we opt for constraints that are more concerned with preventing dangerous and adverse effects. For this reason, we dedicated the last section of Paragraph 3.4.2 to a detailed discussion on weights tuning and implemented constraints. Finally, it is important to underline that for a fair and exhaustive comparison, one should compare the different control strategies, reported

in the literature, by using the same patients' models for evaluation of the performances. However, such comparison is out of the goal of this work.

The average CPU time for the simulation of one control action (with a time interval of 1 min as in Figure 2) is 0.25 to 0.45 s per patient (Intel® Core™ i7-3770 CPU @ 3.40 GHz with 8 GB RAM), which makes the proposed MPC framework viable for on-line implementation in the operation room as a decision support system for the anesthetist.

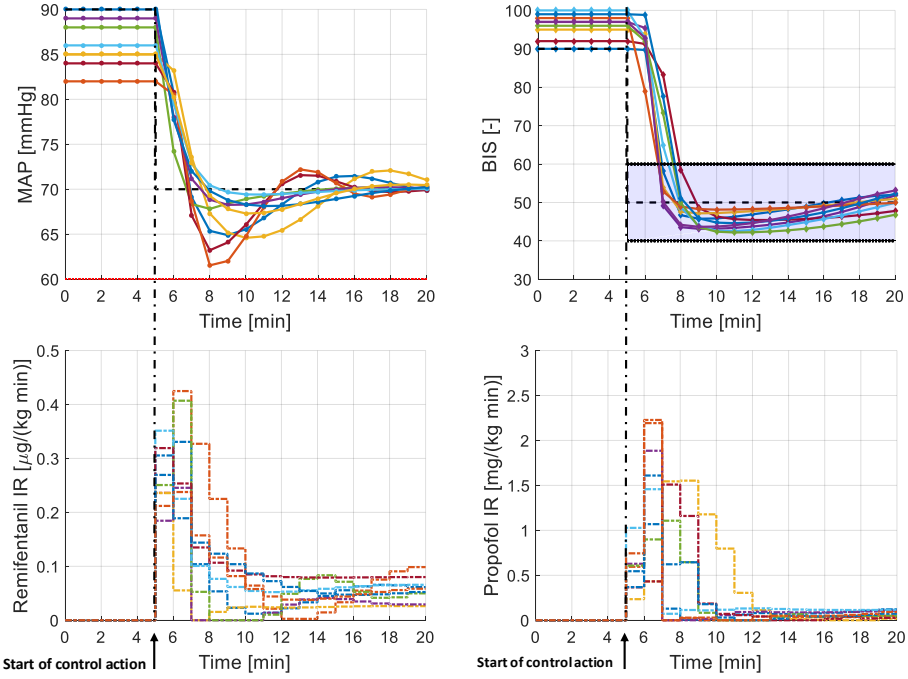

Figure 2 – Simulation of the induction phase. The black vertical dashed line marks the start of the control action (*i.e.* change of setpoint). Left panel refers to the analgesia component, right panel refers to the hypnotic component. (Top) Dynamics of controlled variables MAP and BIS. (Bottom) Dynamics of manipulated variables, *i.e.* remifentanil and propofol IRs. A straight red line corresponding to MAP = 60 mmHg marks the hypotension region. The shaded area in the BIS plot denotes the recommended clinical range, BIS = 40-60 [-].

We can assume that the *in vivo* and online application of the MPC framework is feasible because the optimal solution takes decidedly less than the control time interval of 1 min. Being the CPU time so short, it is also possible to reduce the control time interval, in case it is desirable to update the infusion rates more frequently so to reject fast-acting disturbances. It is true that in case of real surgical intervention, one should account for the instrumentation and data processing delays that can be quantified in few additional seconds. However, this would not have a significant impact on the automated model-based control of anesthesia as the on-line MPC *in vivo* application would still take a relatively short time.

Table 4 – Performance indexes for the anesthesia simulation of nine patients: rise-times, time to loss of consciousness (t_{loc} defined as time to reach BIS = 60 [-]), minimum values, and time to recovery (after the stop of control action). Last two rows list the mean and standard deviation values.

Patient #	$t_{rise,MAP}$ [min]	t_{loc} [min]	$t_{rise,BIS}$ [min]	Min_{MAP} [mmHg]	Min_{BIS} [-]	t_{rec} [min]
1	1.897	1.982	2.387	64.9	45.7	17.031
2	2.464	1.744	1.977	64.6	43.1	12.155
3	1.524	2.946	3.783	67.7	45.4	30.807
4	1.776	1.849	2.281	63.2	47.2	13.697
5	1.922	2.221	2.917	61.2	42.5	18.868
6	2.347	1.564	2.498	68.2	48.1	24.986
7	3.449	2.503	3.000	69.4	42.2	22.184
8	2.899	2.485	3.129	68.1	44.6	11.271
9	2.728	1.701	2.008	67.3	43.6	14.141
Mean	2.664	2.111	2.334	66.1	44.7	18.349
SD	0.558	0.460	0.583	2.6	1.9	6.180

Figure 3 shows that the controller maintains the setpoint with a regular and quite stable action, throughout the duration of the simulated surgical operation, in absence of disturbances. MAP dynamics settles within 15 min, whereas BIS dynamics is slower and takes around 20 min. This is not due to the trajectory of the manipulated variables, whose changes are limited for both drugs, but to the slower dynamics of propofol (compared to remifentanil), manifested in a lower k_{e0} value of the corresponding PBPK model. In fact, the smaller k_{e0}, the greater the overshoot in the peak plasma concentration to increase the plasma-effect-site gradient, *i.e.* enhance the plasma-effect-site equilibration velocity (Absalom et al., 2009). At t = 38 min the infusion stops by setting the manipulated variables to 0 (black arrow and vertical dashed line in Figure 3). Afterwards, the drugs are cleared from the virtual patient's body (by means of metabolic and excretion mechanisms), and MAP and BIS, the pharmacological effects, go back to the baseline values that characterize the awoken patient. We define t_{rec} the time to recovery that is required to exceed BIS = 90 [-] once the propofol infusion is over (see also Table 4). The mean t_{rec} value for nine patients is 18 min and 21 s, whereas the individual values exhibit a noteworthy inter-individual variability, which is consistent with reality. In the practice, time for awakening from anesthesia varies from 5 min to 1 h, depending on the administered drugs, the type of surgery, and the patient's characteristics. Indeed, in case of propofol and remifentanil, blood levels drop fast after the end of infusion and most patients are fully conscious within 15 min (Frost, 2014), but recovery time from opioids and hypnotics is subject to inter-individual variability. It is worth underlining that the controller has no part in influencing the recovery velocity once the infusion is completed. Indeed, the recovery dynamics depends on the ADME processes within the patient's body and their

pharmacodynamic variability, which are simulated by the PBPK-PD model. The recovery from anesthesia is a critical phase and in the clinical practice further quantitative and qualitative (*e.g.*, movement, response to calling) factors are usually accounted for along with BIS and MAP for a complete and reliable assessment of the awareness level. To this concern, it is important to emphasize that medical know-how is essential, and automated control of anesthesia aims at supporting the anesthesiologist's decision-making rather than replacing their role.

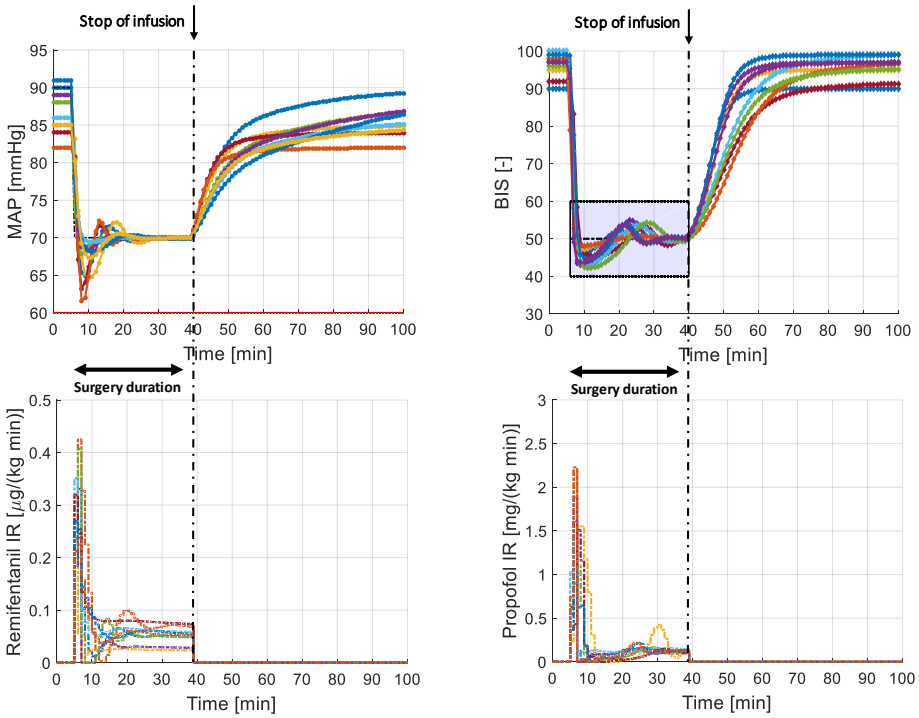

Figure 3 – Post-induction simulation in lack of disturbances. The black vertical dashed line marks the stop of control action (at t = 38 min). Left panel refers to the analgesia component; right panel refers to the hypnotic component. (Top) Dynamics of controlled variables MAP and BIS. (Bottom) Dynamics of manipulated variables, *i.e.* remifentanil and propofol IRs.

Figure 4 (for remifentanil) and Figure 5 (for propofol) portray the drug concentration time profiles in different compartments resulting from the IRs trajectories of Figure 3. We show the dynamics of the blood, effect-site, and liver concentration, and the metabolized and eliminated amounts via extra-hepatic and hepatic/renal routes. Although it is not possible to validate the PK results of the body compartments except for plasma (because measuring drug concentrations in organs and tissues is invasive and therefore unfeasible), such simulations provide useful and complementary bits of information to the anesthetist for their decision-making and situational awareness. This is especially true as the information is produced by adapting the PBPK model not only to the patient's physical characteristics, but also to the specific properties of the drug, for instance in terms of metabolic/elimination pathways.

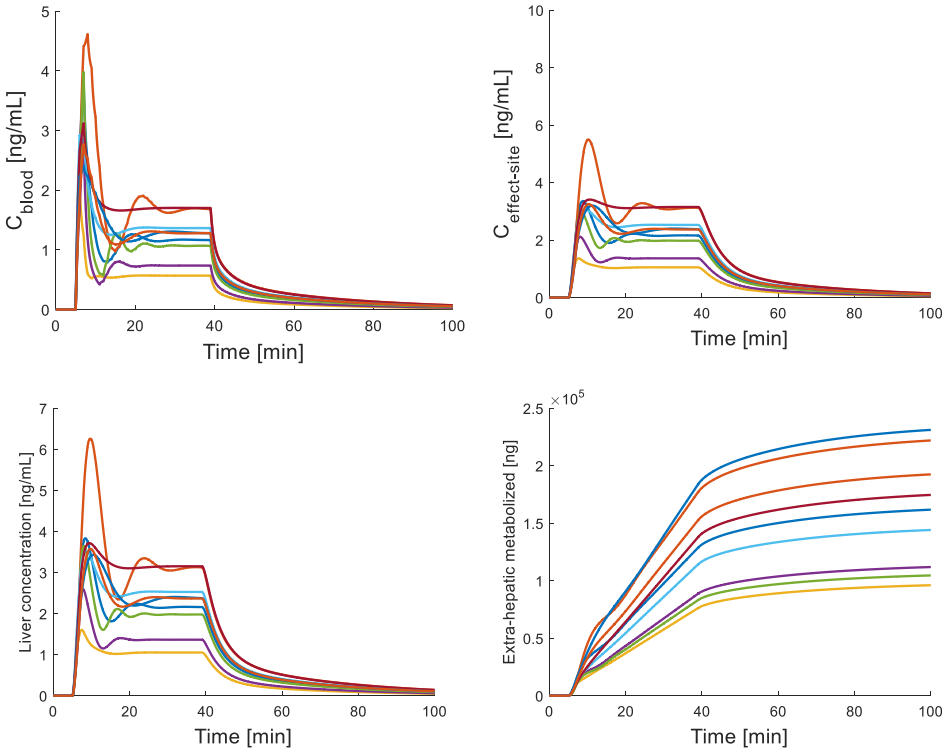

Figure 4 – Simulation of remifentanil pharmacokinetics. Top panel shows blood (left) and effect-site (right) concentrations. Bottom panel shows liver (left) and the metabolized amount via extra-hepatic route (*i.e.* plasma and tissues) (right).

It is worth observing that remifentanil blood concentration peak falls within the recommended range for induction of adequate analgesia (3-8 ng/mL, (Absalom and Struys, 2007)). For both drugs, the effect-site concentration is delayed respect to the blood concentration. For *in vivo* patients, this delay depends on age, cerebral flow, cardiac output, and PK input (Cortinez, 2014). On the modeling side, different PK models of the same drug predict different concentration profiles and therefore display different lags, which result into different k_{e0} values. For remifentanil, the controller value of k_{e0} comes from Minto et al. (1997) and depends on the patient's age (with values from 0.7 min^{-1} for a 25-year-old to 0.455 min^{-1} for a 60-year-old individual). For the *in silico* patient's model, we obtained k_{e0} = 0.33 min^{-1} (see Savoca et al. (2017) for details).

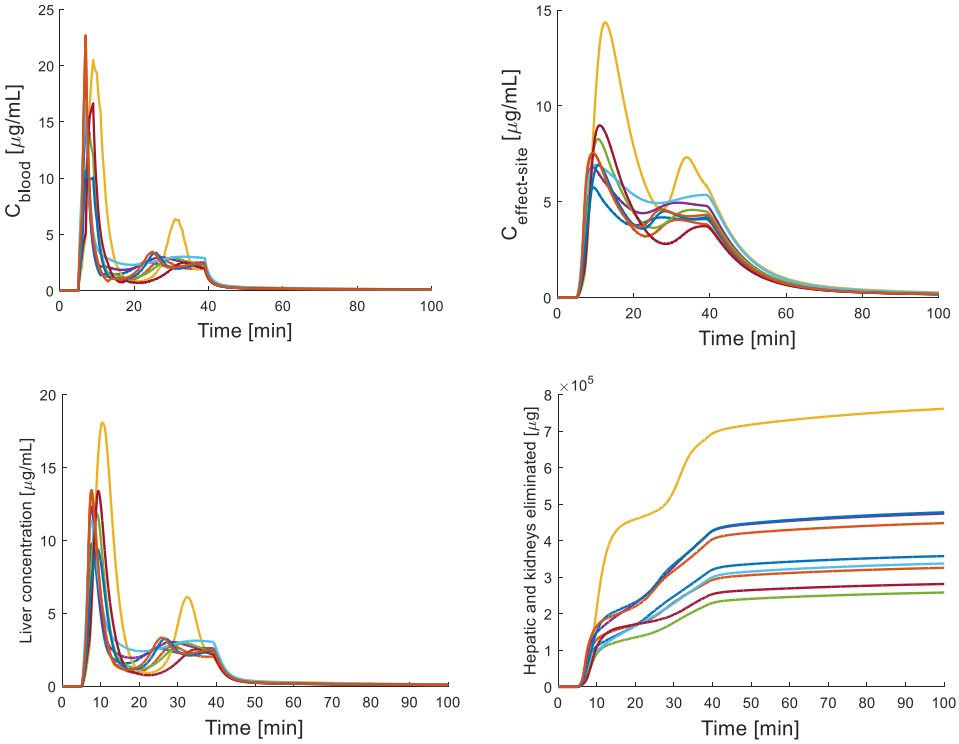

Figure 5 – Simulation of propofol pharmacokinetics. Top panel shows blood (left) and effect-site (right) concentrations. Bottom panel shows liver (left) and the eliminated amount via hepatic metabolism and renal elimination (right).

With respect to propofol, it is worth underlining that early drug distribution after bolus is not well characterized by PK classical models (*e.g.*, Schnider and Marsh models, (Cortinez, 2014)). Actually, three-compartment PK models available in the literature predict different C_{max} values and portray different curves corresponding to the early distribution phase (Cortinez, 2014). Consequently, they also feature different values of k_{e0}, *e.g.*, 0.26 min^{-1} in Marsh model and 0.456 min^{-1} in Schnider model. We believe that the physiologically-based approach leads to a more realistic description of the distribution process. Consistently with the choice of the other parameters V_i and k_{ij} of the classical PK model, we adopted Schnider's k_e0 = 0.456 min^{-1} (Schnider et al., 1998) for the propofol control loop, whilst for the *in silico* patients we evaluated k_{e0} = 0.125 min^{-1} from the experimental data of Liu et al. (2015). Indeed, this value is similar to more recent studies on propofol PD (Doufas et al., 2004). The propofol blood concentration of Figure 5 tends to a maintenance value that is consistent with medical guidelines (Absalom and Struys, 2007), *i.e.* target values of plasma concentration in between 4-5 μg/mL for unpremedicated patients and in presence of an analgesic component.

3.5.2 Response to disturbances

The maintenance phase can be addressed as a “regulator problem”. The controller must reject disturbances provoked by external events, throughout the surgical intervention, to maintain the DOA level.

Intubation is usually performed within few minutes from the beginning of induction and is an invasive procedure that stimulates the vagal nerve and provokes a sympathoadrenal reaction in the patient, which results in increased AP and HR. Higher doses of remifentanil can reduce the cardiovascular impact of intubation on the patient. There are several studies devoted to the investigation of the optimal dose for suppression of such a response (Alexander et al., 1999; Batra et al., 2004; Hall et al., 2000; O'Hare et al., 1999) to avoid dangerous situations in susceptible patients, *e.g.*, ischemia or acute heart failure (Saroj et al., 2016). Incision, among others, is a nociceptive stimulus that can cause arousal and movements of the patient and lead to significant BIS increases (Coleman et al., 2015; Yang et al., 2016). For these reasons, intubation and incision are carried out once the patient has reached the required depth of anesthesia and analgesia. In the practice, these events are currently treated by preventively increasing the target concentration of TCI pumps, to ensure a deeper level of anesthesia. It is evident that this “feed-forward” control strategy completely and only relies on the anesthetist’s experience, which is over-specified and may differ significantly among experts thus missing a universally adopted reference to good-practices and recommended procedures. From this perspective, an unbiased tool, such as the MPC framework for automated anesthesia control, can play an important role for standardization of the optimal approach to anesthesia delivery. At the same time, the anesthetist remains the supervisor as they decide and set the parameters of the intervention in terms of setpoints, thresholds, adopted drugs, administration sequence, critical times, and relative importance (*i.e.* weights) of the terms in the objective function of the control problem (see Eq. (3.15)). Other acute undesired disturbances, *i.e.* strokes, hemorrhage, and organ failure can lead to side effects such as bradycardia and hypotension. Furthermore, inter-individual variability and the intrinsic complexity of the human body can have a significant impact on the control robustness.

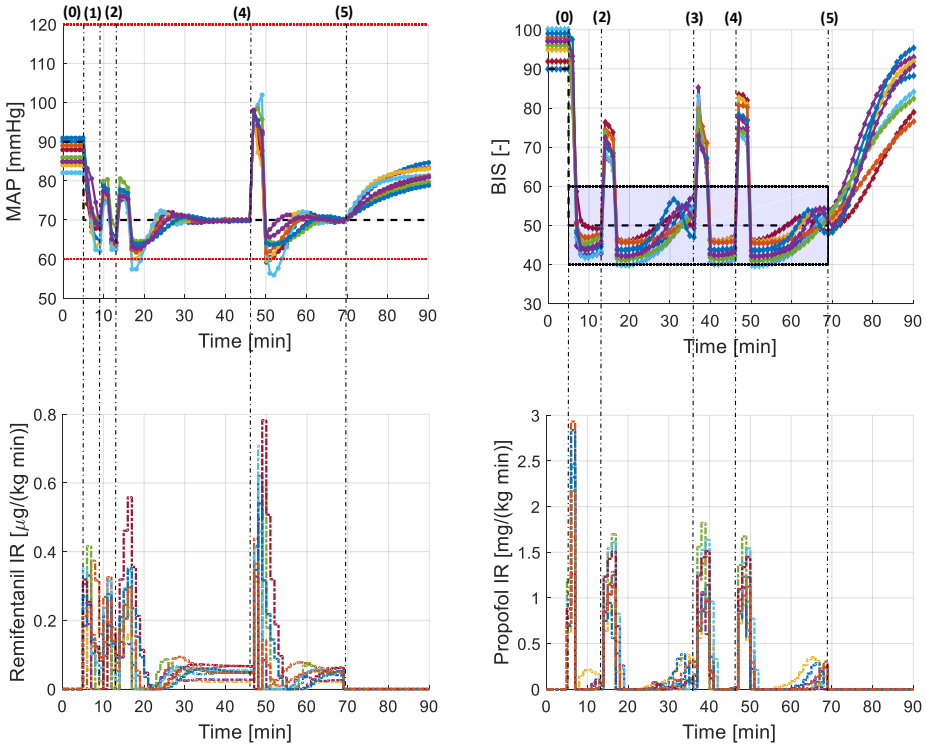

Figure 6 – Simulation of a surgical operation (total length 69 min). (Top) Dynamics of controlled variables MAP (left) and BIS (right). (Bottom) Dynamics of manipulated variables *i.e.* IRs of remifentanil (left) and propofol (right). Numbers in parentheses and black vertical dashed lines mark specific events: (0) induction of anesthesia, (1) intubation (4 min after start of induction), (2) incision, (3) and (4) arousal episodes, and (5) stop of infusion after a low-stimulation period. Red lines in the MAP diagram mark the hypo- and hypertension regions (*i.e.* MAP < 60 mmHg and MAP > 120 mmHg).

Therefore, we are interested to investigate the controller response to external stimuli, by simulating the effect of undesired events that are likely to occur in intraoperative anesthesia. The goal is to verify whether the controller is capable of re-establishing the desired anesthetic state with a rapid but safe control action. Figure 6 shows the simulation of a surgical operation with events indicated by numbers in parentheses, *i.e.* (0) induction of anesthesia, (1) intubation (performed 4 min after the start of infusion), (2) incision, (3) and (4) arousal episodes associated with an increase in BIS, and (5) end of infusion. To reproduce believable and realistic variations of the arterial pressure after intubation and incision, we referred to the scientific literature on intraoperative stimuli (Alexander et al., 1999; Batra et al., 2004; Hall et al., 2000; O'Hare et al., 1999).

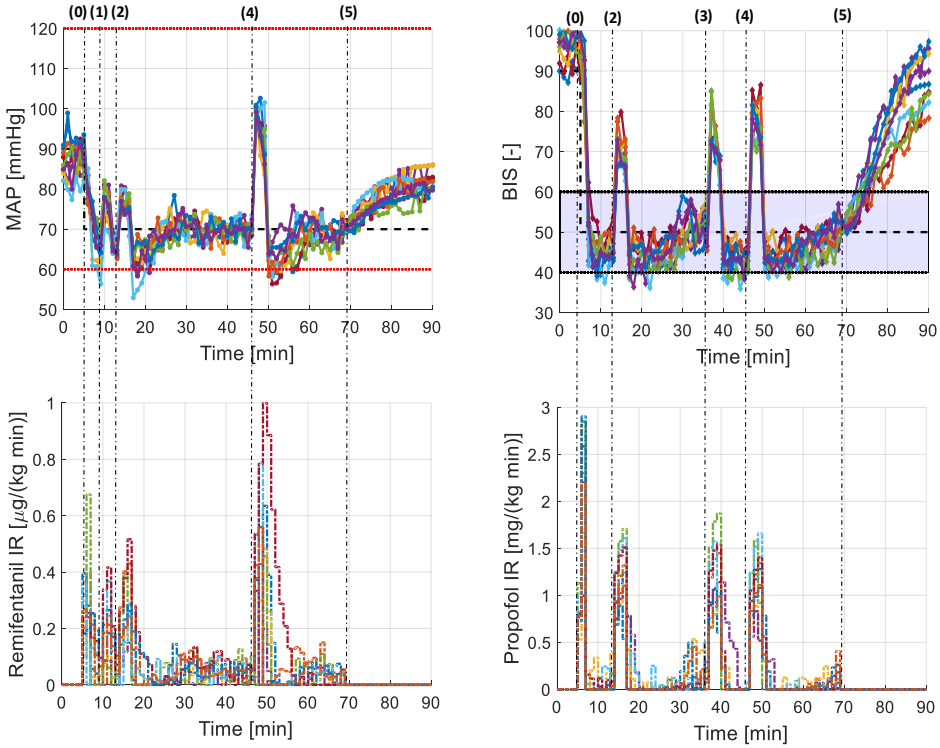

Figure 7 – Simulation of a surgical operation (duration 69 min) considering noisy controlled variables. (Top) Dynamics of controlled variables MAP (left) and BIS (right). (Bottom) Dynamics of manipulated variables *i.e.* IRs of remifentanil (left) and propofol (right). Numbers in parentheses and black vertical dashed lines mark specific events: (0) induction of anesthesia, (1) intubation (4 min after start of induction), (2) incision, (3) and (4) arousal episodes, and (5) stop of infusion after a low-stimulation period. Red lines in the MAP diagram mark the hypo- and hypertension regions (*i.e.* MAP < 60 mmHg and MAP > 120 mmHg).

We assumed that the analgesia level is sufficient to prevent peripheral noxious stimuli from reaching the brain. Consequently, we suppressed BIS reaction to intubation, because according to Nakayama et al. (2003), intubation is mediated at the subcortical level, and therefore may be unrelated to BIS, which is an indicator of cerebral cortical activity. Thus, in our simulations, only incision induces BIS changes. The controller reacts with steep but short increases of IRs (similar to small boluses in Figure 6) to avoid infringing safe boundaries. Few minutes are required to re-establish targeted depth of anesthesia and analgesia. There is only one patient that experiences a MAP value below the assigned lower bound of 60 mmHg (quantified by PF_{MAP}, in Eq. (3.20)) for a rather short time interval.

Finally, Figure 7 shows how the MPC procedure performs in case of noisy experimental measurements. In fact, the profiles of the controlled variables showed up to now are not truly realistic, as in the practice experimental measurements are subjected to noise and disturbances, especially with respect to BIS. Therefore, we repeated the simulations by adding a Gaussian-distributed noise to the patient's

model output. Figure 7 shows that the profiles of manipulated variables are moderately affected by MAP and BIS noise, however it is fair concluding that noise does not induce any instability in the control action.

The controller is capable of distinguishing between noxious stimuli and noise. Furthermore, the noise contribution is realistic because it comes from an accurate analysis of the experimental signal from clinical case-studies (see Paragraph 3.4.3 for further details).

The CPU time for the simulation of the whole surgical intervention (69 min of wall-clock time) in Figure 6 and Figure 7 (with control actions taken every minute) is 50 to 70 s for each patient on an Intel® Core™ i7-3770 CPU @ 3.40 GHz with 8 GB RAM.

3.6 Conclusions

We developed a model-predictive controller of anesthesia and tested the performance on *in silico* patients via PBPK-PD models. We considered the co-administration of propofol and remifentanil to embrace both the fundamental components of general anesthesia, *i.e.* hypnosis and analgesia. During the induction phase, the designed system is responsive, with low rise-times and settling times consistent with clinical requirements. The resulting controlled variables remain within the recommended therapeutic ranges. During the maintenance phase, the controller keeps both MAP and BIS within the safe regions, and displays robustness towards disturbances caused by simulated intraoperative stimuli and noise on measurements of the controlled variables. The intraoperative disturbances and noise were artificially generated paying attention to the reality of clinical practice. Furthermore, the time required for the controller calculations is short enough to make the on-line clinical application feasible. Indeed, the longest CPU time after several different simulations of surgical anesthesia never exceeded the control time interval. The CPU time issue is a key point that is often addressed as a disadvantage of MPC application in anesthesia compared to more recent machine learning approaches (Padmanabhan et al., 2015). However, this is not an issue for our MPC approach to total intravenous anesthesia.

In addition, the purely *in silico* controller can be used for a priori analysis of surgical operations. Current research activity is devoted to model improvement by including further factors that contribute to inter-individual variability, *e.g.*, pathologies, age changes, and pre-medication, and include other key physiological variables.

Our main future goal is clinical validation of the controller (*i.e. in vivo* implementation of the MPC procedure), which would adopt the PBPK-PD model. We think that the physiological approach could improve the predictive feature of the controller, as it would allow a more detailed description of the patient's ADME processes.

3.7 Appendix 3.A

Table A – List of physiological parameters: symbol, description, category, and units of measure.

Symbol	Description	Category	Un. of measure
$\boldsymbol{Q^{PV}}$	Blood flowrate in portal vein	Individualized	[mL/min]
$\boldsymbol{Q^{HA}}$	Blood flowrate in hepatic artery	Individualized	[mL/min]
$\boldsymbol{Q^{HV}}$	Blood flowrate in hepatic vein	Individualized	[mL/min]
$\boldsymbol{Q^{K}}$	Blood flowrate to kidneys	Individualized	[mL/min]
$\boldsymbol{V^{P}}$	Plasma compartment volume	Individualized	[mL]
$\boldsymbol{V^{L}}$	Liver compartment volume	Individualized	[mL]
$\boldsymbol{V^{GICS}}$	GICS compartment volume	Individualized	[mL]
$\boldsymbol{V^{PT}}$	Poorly perfused Tissues compartment volume	Individualized	[mL]
$\boldsymbol{V^{HO}}$	Highly perfused Organs compartment volume	Individualized	[mL]
$\boldsymbol{CL^{H}}$	Hepatic clearance, calculated as $Q^{PV}Eff_{H}$	Individualized	[mL/min]
$\boldsymbol{CL^{K}}$	Renal clearance, calculated as $Q^{K}Eff_{K}$	Individualized	[mL/min]
$\boldsymbol{R}$	Protein binding fraction	Assigned	[-]
$\boldsymbol{k_{P-PT}}$	Plasma-Poorly perfused Tissues drug transfer coefficient	Adaptive	[min^{-1}]
$\boldsymbol{k_{PT-P}}$	Poorly perfused Tissues-Plasma drug transfer coefficient	Adaptive	[min^{-1}]
$\boldsymbol{k_{P-HO}}$	Plasma-Highly perfused Organs drug transfer coefficient	Adaptive	[min^{-1}]
$\boldsymbol{k_{HO-P}}$	Highly perfused Organs-Plasma drug transfer coefficient	Adaptive	[min^{-1}]
$\boldsymbol{k_{EL,PT}}$	Tissues metabolic constant	Adaptive	[min^{-1}]
$\boldsymbol{k_{EL,P}}$	Plasma metabolic constant	Adaptive	[min^{-1}]
$\boldsymbol{Eff_{H}}$	Hepatic efficiency	Adaptive	[-]
$\boldsymbol{Eff_{K}}$	Renal efficiency	Adaptive	[-]

CHAPTER 4A

Tackling inter-individual variability: the influence of intraoperative cardiovascular changes

4A.1 Author's Note

The use of PK-PD models to describe the dose-effect relation of patients administered with anesthetic and analgesic drugs calls for the need to improve the prediction of inter-individual variability. Several factors contribute to introduce uncertainty in patients' response to anesthesia. Anesthesia is a complex multivariable process involving not only the loss of consciousness but also other concomitant body reactions, such as cardiovascular and respiratory depression. Intra-operative changes of hemodynamic parameters induce alterations of the pharmacokinetics and thus pharmacodynamics, resulting into less or more enhanced response to anesthesia. This chapter presents (i) an analysis of the extent and variability of the cardiovascular response in high-risk patients of a closed-loop anesthesia study, (ii) an application of PBPK simulations as tool to individualize the prediction basing on the patients' hemodynamic data and investigate the effects of cardiovascular changes on patients' depth of hypnosis. New correlations (from Stader et al. (2019)) were also introduced within the PBPK model presented in Chapter 3, to further improve the individualization aspect of the model prediction.

The work presented in this chapter was carried out during a research stay at Digital Health Innovation Laboratory, British Columbia Children's Hospital Research Institute (Vancouver, BC, Canada), headed by Profs Dumont and Ansermino.

This work was published in "Computer Methods and Programs in Biomedicine".

The effect of cardiac output on the pharmacokinetics and pharmacodynamics of propofol during closed-loop induction of anesthesia

Adriana Savoca, Klaske van Heusden, Davide Manca, John Mark Ansermino, Guy Albert Dumont

Computer Methods and Programs in Biomedicine (2020), 105406 (In press)
DOI: 10.1016/j.cmpb.2020.105406

4A.2 Abstract

Background and objective: Intraoperative hemodynamic stability is essential to safety and post-operative well-being of patients and should be optimized in closed-loop control of anesthesia. Cardiovascular changes inducing variations in pharmacokinetics may require dose modification. Rigorous investigational tools can strengthen current knowledge of the anesthesiologists and support clinical practice. We quantify the cardiovascular response of high-risk patients to closed-loop anesthesia and propose a new application of physiologically-based pharmacokinetic-pharmacodynamic (PBPK-PD) simulations to examine the effect of hemodynamic changes on the depth of hypnosis (DoH).

Methods: We evaluate clinical hemodynamic changes in response to anesthesia induction in high-risk patients from a study on closed-loop anesthesia. We develop and validate a PBPK-PD model to simulate the effect of changes in cardiac output (CO) on plasma levels and DoH. The wavelet-based anesthetic value for central nervous system monitoring index (WAV_{CNS}) is used as clinical end-point of propofol hypnotic effect.

Results: The median (interquartile range, IQR) changes in CO and arterial pressure (AP), 3 min after induction of anesthesia, are 22.43 (14.82-36.0) % and 26.60 (22.39-

35.33) % respectively. The decrease in heart rate (HR) is less marked, *i.e.* 8.82 (4.94-12.68) %. The cardiovascular response is comparable or less enhanced than in manual propofol induction studies. PBPK simulations show that the marked decrease in CO coincides with high predicted plasma levels and deep levels of hypnosis, *i.e.* WAV_{CNS} < 40. PD model identification is improved using the PBPK model rather than a standard three-compartment PK model. PD simulations reveal that a 30% drop in CO can cause a 30% change in WAV_{CNS}.

Conclusions: Significant CO drops produce increased predicted plasma concentrations corresponding to deeper anesthesia, which is potentially dangerous for elderly patients. PBPK-PD model simulations allow studying and quantifying these effects to improve clinical practice.

Keywords: cardiac output; hemodynamics; closed-loop anesthesia; physiologically-based pharmacokinetic modeling; propofol; high-risk patients.

4A.3 Introduction

Propofol is an intravenous (IV) hypnotic agent commonly used for induction of general anesthesia. Along with the advantages of rapid onset of unconsciousness and short duration of action, propofol has adverse effects such as cardiorespiratory depression and hypotension. These adverse effects are characterized by slower dynamics compared to the hypnotic effects (Kazama et al., 1999).

Hypotension following anesthetic drug administration in the operating room is common, including hypotension sufficiently severe to require an intervention such as vasoconstrictive drug administration to counter the hemodynamic response. Cardiovascular changes following propofol administration show high inter-individual variability and are associated with the patients' characteristics. Age over 50 y, pre-induction mean arterial pressure (MAP) values below 70 mmHg, and American Society of Anesthesiologists (ASA) classification III and IV are reported predictors of hemodynamic fluctuations (Reich et al., 2005). Although mild hypotension is considered clinically insignificant (Reich et al., 2005), association of intraoperative hemodynamic instability with mortality, stroke, and other adverse outcomes has been shown (Devinney et al., 2015; Reich et al., 2005). Currently, there is lack of evidence that commonly used target-controlled infusion (TCI) systems reduce the chances of hemodynamic fluctuations, compared to manual induction (Laso et al., 2016). One of

the goals of adoption of automated control systems in anesthesia is to increase the stability of the patients' anesthetic state, including their hemodynamics.

Induction of anesthesia is a challenging phase from the point of view of the hemodynamic response. Heart-rate (HR) and (non-invasive) blood pressure (BP) are routinely measured in clinical practice, during both induction and maintenance of anesthesia. Cardiac output (CO) monitoring on the other hand, is not as commonly used, and is generally employed at the discretion of the anesthetist in high-risk patients and/or major surgical procedures (Vincent and Fagnoul, 2012). Reports of CO changes following propofol induction of anesthesia often feature few observations (Bendel et al., 2007; Larsen et al., 1988), with limited frequency (Claeys et al., 1988; Potočnik et al., 2011), or over a short time horizon (Fairfield et al., 1991; Steib et al., 1988). Evaluation of closed-loop controllers often focus on depth-of-hypnosis (DoH) rather than the hemodynamic aspects (*e.g.*, Janda et al., 2011; Nogueira et al., 2014; Padula et al., 2017).

Hemodynamic changes are also reported to affect the pharmacokinetics of anesthetic and analgesic drugs (Adachi et al., 2001; Brodie et al., 2017; Upton et al., 1999) with consequent variations in dosing requirements. CO is reported to be a key determinant of propofol pharmacokinetics (Kurita et al., 2002; Upton et al., 1999). In particular, pharmacokinetic studies in animals show that lower cardiac outputs lead to higher plasma concentrations (Kurita et al., 2002; Upton et al., 1999). This is in line with the clinical experience according to which reduced CO leads to lower anesthetic requirements (also evident in the case of critical events, such as hemorrhage (Brodie et al., 2017)). Thus, neglecting the effect played by CO can lead to potential overdosing of propofol, which can be dangerous, especially for critically ill and/or elderly patients.

Physiologically-based pharmacokinetic (PBPK) models can account for the effect of CO changes (Upton and Ludbrook, 2005). The PBPK modeling approach is based on a simplified but nonetheless physiological description of the drug distribution and transport in the body organs and tissues, which are assimilated to homogenous compartments. Thus, the effect of CO on blood flowrates can be accounted for and the effect of CO changes on the pharmacokinetics can be studied *in silico*. When combined with a suitable pharmacodynamic (PD) model, the implications on the depth of hypnosis can also be investigated *in silico*.

The objectives of this paper are (i) to quantify CO, MAP, and HR changes observed

during closed-loop induction of propofol-remifentanil anesthesia, for a high-risk subset of the population for whom arterial blood pressure monitoring was indicated in West et al. (2018), and (ii) to investigate the influence of CO changes on pharmacokinetics and pharmacodynamics via *in silico* simulations based on PBPK-PD modelling.

4A.4 Methods

4A.4.1 Clinical data

Data were available from the clinical evaluation of closed-loop control of propofol-remifentanil anesthesia, based on the wavelet-based anesthetic value for central nervous system monitoring index (WAV_{CNS}) index provided by the NeuroSENSE NS-701 monitor (NeuroWave Systems, Cleveland Heights, OH) (West et al., 2018). Ethical approval from the Research Ethics Board (FHREB 2012-056), investigational device approval from Health Canada (206188), and patients' informed consent were previously obtained (West et al., 2018). In a subset of 15 patients, an arterial line was placed prior to induction of anesthesia, and continuous CO measurements during induction of anesthesia were available (LiDCO Rapid, LiDCO Ltd, London UK). HR was recorded using ECG (Carescape B850 multi-parameter monitor, GE Healthcare, Buckinghamshire, UK). This subset of the study population represented an "at-risk" population because of their conditions or type of surgery, for whom arterial line placement was indicated. Table 5 reports the demographics of the studied subset. Data on CO, BP, and HR were analyzed using MATLAB (MathWorks, Natick, MA).

Table 5 – Demographics of the 15 patients' cohort. Age and BMI are presented as median (interquartile range (IQR)).

N	15
Gender (F:M)	1:14
Age (y)	67 (59-73)
BMI (kg/m^2)	28.22 (25.49-30.34)

4A.4.2 Propofol physiologically-based pharmacokinetic model

In silico investigation of the effect of CO changes on pharmacokinetics is performed using a PBPK model that was developed and validated using data available in the literature, and has been applied to *in silico* simulation of closed-loop controlled anesthesia (Savoca and Manca, 2019). The structure of this model is adapted from the more complex PBPK model described in Abbiati et al. (2018) to meet propofol pharmacokinetic characteristics. The absorption, distribution, metabolism, and elimination (ADME) processes undergone by propofol within the body are described

via material balances over five compartments, corresponding to specific tissues and organs.

The number of compartments is a compromise between the mathematical complexity (along with consequent identifiability controversies) and the anatomical and physiological resemblance of the model. The following compartments are included: plasma (P), gastrointestinal circulatory system (GICS), liver (L), highly perfused organs (HO, which lump the kidneys, brain, heart, and spleen), and poorly perfused tissues (PT, which lump fat, muscles, bones, and skin). For the sake of clarity, GICS comprises the portal vein, the mesenteric artery, and the microvessels that are involved in the blood transport to and from the gastrointestinal system. The plasma compartment balance (Eq. (4A.1)) features the input infusion rate $IR(t)$, as administered by the controller in West et al. (2018). The mathematical formulation of the model consists of Eqs. (4A.1-5) that describe the dynamics of propofol concentration $C(t)$ in the body compartments, complemented by Eqs. (4A.6-7), whose purpose is to describe and quantify the eliminated drug amount via the hepatic (H) and extra-hepatic (EH) routes (for propofol case, renal and tissues pathways).

As opposed to classical three-compartment PK models, not all the parameters of the PBPK model are identified with PK data (*i.e.* measured values of blood concentration) of a specific population. There are three categories of parameters: (i) individualized, *i.e.* calculated from the demographics, (ii) assigned, *i.e.* specific values related to the drug physiochemical characteristics that are available in the literature, and (iii) regressed with PK data. Table 6 lists the model parameters and clarifies the method for their identification.

The calculation of compartment volumes V^i depends on the demographics (specifically, correlations account for patients' body surface area, height, age, and gender (Stader et al., 2019)) and allows for individualization of the pharmacokinetic prediction. The protein binding fraction, R, is assigned according to the scientific literature on propofol (Mazoit and Samii, 1999). In Eqs. (4A.1-5), Q^{HV}, Q^{PV}, and Q^{HA} are the blood flows respectively through the hepatic vein (HV), the portal vein (PV), and the hepatic artery (HA), which are calculated as a fraction of the CO. The same approach is applied to renal clearance CL^K calculated from the total blood flowrate to kidneys Q^K, which is evaluated as a fraction of CO (see Table 6). Correlations for calculation of blood flowrates depend on body surface area, height, age, gender (Stader et al., 2019).

$$\frac{dC^P(t)}{dt} = \frac{IR(t)}{V^P} + C^{PT}(t)k_{PT-P}\frac{V^{PT}}{V^P} + C^L(t)\frac{Q^{HV}}{V^P} + C^{HO}(t)k_{HO-P}\frac{V^{HO}}{V^P} - C^P(t)k_{EL,P}(1-R) - \frac{C^P(t)}{V^P}CL^K - C^P(t)\left(k_{P-PT}(1-R) + k_{P-HO}(1-R) + \frac{Q^{HA}}{V^P} + \frac{Q^{PV}}{V^P}\right) \quad (4A.1)$$

$$\frac{dC^{GICS}(t)}{dt} = -C^{GICS}(t)\frac{Q^{PV}}{V^{GICS}} + C^P(t)\frac{Q^{PV}}{V^{GICS}} - C^{GICS}(t)k_{EL,GI} \quad (4A.2)$$

$$\frac{dC^L(t)}{dt} = -C^L(t)\left(\frac{Q^{HV}}{V^L} + \frac{CL^H}{V^L}\right) + C^P(t)\frac{Q^{HA}}{V^L} + C^{GICS}(t)\frac{Q^{PV}}{V^L} \quad (4A.3)$$

$$\frac{dC^{HO}(t)}{dt} = -C^{HO}(t)k_{HO-P} + C^P(t)k_{P-HO}(1-R)\frac{V^P}{V^{HO}} \quad (4A.4)$$

$$\frac{dC^{PT}(t)}{dt} = -C^{PT}(t)k_{PT-P} + C^P(t)k_{P-PT}(1-R)\frac{V^P}{V^{PT}} \quad (4A.5)$$

$$\frac{dA^{EL,L}(t)}{dt} = C^L(t)CL^H \quad (4A.6)$$

$$\frac{dA^{EL,K}(t)}{dt} = C^P(t)CL^K + V^{GICS}C^{GICS}(t)k_{EL,GI} \quad (4A.7)$$

The remaining parameters (*i.e.* transport coefficients, *e.g.*, k_{P-PT} and metabolic constants, *e.g.*, Eff^H) are identified via nonlinear regression with pharmacokinetic data from Schnider et al. (1998). The model, with CO calculated from the demographics (as in Stader et al. (2019)) was validated using PK data from four studies in different populations (Dyck and Shafer, 1992; Gepts et al., 1987; Servin et al., 1993; Smuszkiewicz et al., 2016).

Table 6 – List of PBPK model parameters, symbols, and calculation method.

Parameter	**Symbol**	**Identification**[6]
Organ/tissue density	ρ_i	Assigned as in Valentin (2002)
Blood weight	W^B	Calculated from demographics (Stader et al., 2019)
PT weight	W^{PT}	Calculated from demographics (Stader et al., 2019)
HO weight	W^{HO}	Calculated from demographics (Stader et al., 2019)
Liver weight	W^L	Calculated from demographics (Stader et al., 2019)
Blood volume	V^B	Calculated as $\mathrm{W^B}/\rho_\mathrm{B}$
Hematocrit	h	Assigned as in Stader et al. (2019)
Plasma volume	V^P	Calculated as $\mathrm{V^B}(1-\mathrm{h})$
PT volume	V^{PT}	Calculated as $\mathrm{W^{PT}}/\rho_\mathrm{PT}$
HO volume	V^{HO}	Calculated as $\mathrm{W^{HO}}/\rho_\mathrm{HO}$

[6] Correlations from Stader et al. (2019) account for patients' body surface area, height, age, and gender.

GICS volume	V^{GICS}	Calculated as in Abbiati et al. (2018)
Liver volume	V^{L}	Calculated as $\mathrm{W^{L}}/\rho_{\mathrm{L}}$
HV blood flow	Q^{HV}	Calculated as %CO (Stader et al., 2019)
HA blood flow	Q^{HA}	Calculated as $25\%\mathrm{Q^{HV}}$
PV blood flow	Q^{PV}	Calculated as $75\%\mathrm{Q^{HV}}$
Kidneys blood flow	Q^{K}	Calculated as %CO (Stader et al., 2019)
Hepatic clearance	CL^{H}	Calculated as $\mathrm{Eff^{H}Q^{PV}}$
Renal clearance	CL^{K}	Calculated as $\mathrm{Eff^{K}Q^{K}}$
Protein binding fraction	R	Assigned as in Mazoit and Samii (1999)
PT-plasma transport coefficient	k_{PT-P}	Identified with data from Schnider et al. (1998)
Plasma-PT transport coefficient	k_{P-PT}	Identified with data from Schnider et al. (1998)
HO-plasma transport coefficient	k_{HO-P}	Identified with data from Schnider et al. (1998)
Plasma-HO transport coefficient	k_{P-HO}	Identified with data from Schnider et al. (1998)
GI tissue metabolic constant	$k_{EL,GI}$	Identified with data from Schnider et al. (1998)
Hepatic efficiency	Eff^{H}	Identified with data from Schnider et al. (1998)
Renal efficiency	Eff^{K}	Identified with data from Schnider et al. (1998)

Table 7 reports the validation results in terms of median prediction error (MDPE) and median absolute prediction error (MDAPE). MDPE and MDAPE are chosen as predictive performance indicators because they are commonly used in the scientific literature related to pharmacokinetic modeling of IV drugs employed in anesthesia and analgesia. Acceptable values are MDPE in the range within ± 20% and MDAPE 20-40% (mean values) (Eleveld et al., 2018; Hara et al., 2017). Although some values are outside these target ranges, the variability of patients' characteristics in the validation studies (*i.e.* young, elderly, healthy, critically ills, and obese) and infusion regimes (boluses and infusions) must be taken into account. Indeed, in case of critically ill patients (Smuszkiewicz et al., 2016; Gepts et al., 1987), concomitant drugs and comorbidities may influence propofol pharmacokinetics, with repercussions on the poorer predictive performance of the model. The Dyck and Shafer dataset (Dyck and Shafer (1992)) features a peculiar characteristic compared to other propofol pharmacokinetic datasets, as most blood samples were obtained up to 19 h after a 10-min IV propofol infusion. This means that most values refer to propofol sub-anesthetic concentrations. Likely, the model prediction would be superior if propofol concentrations were evaluated only during the maintenance and early elimination phases of the infusion, as in other propofol pharmacokinetic datasets. Future work should address the issue of further adapting the correlations used to identify the model parameters (see Table 2) to obese patients, as their condition involves anatomical and physiological changes that, depending on the degree of obesity, will alter propofol pharmacokinetics compared to healthy individuals. By doing so, the model prediction

of Servin's dataset (Servin et al. (1993)) would be improved.

The effect of CO on pharmacokinetics is evaluated using the propofol infusion rates as well as the measured CO data (West et al., 2018) as inputs to the PBPK model to simulate the pharmacokinetics of the patients. Hence, CO changes will affect the drug transport and final concentration within the body. Resulting PK profiles are compared to the Schnider-model predicted levels (Schnider et al., 1998).

Table 7 – Validation results of the PBPK model. First column reports the PK study (number and type of subjects involved), second and third columns list MDPE and MDAPE (mean (SD))[7].

PK study	MDPE%	MDAPE%
Servin et al. (1993) (N=8, obese)	4.05 (27.1)	40.2 (28.2)
Gepts et al. (1987) (N=16, critically ill)	-26.22 (36.96)	51.06 (31.77)
Dyck and Shafer (1992) (N=57, healthy)	-14.8 (21.2)	40.6 (16.3)
Smuszkiewicz et al. (2016) (N=1, critically ill)	-29	29

4A.4.3 Pharmacodynamic modeling and *in silico* evaluation

The phase-lag between the time course of the plasma concentration and manifestation of the pharmacological effect is accounted for by the commonly-used effect-site equation approach. The PBPK model is combined with a suitable form of the Hill equation, whose PD parameters are identified via nonlinear regression using the WAV_{CNS} data from West et al. (2018). The goodness-of-fit is evaluated via Root-Mean-Square Error (RMSE) for the PBPK-PD and Schnider three-compartment PK-PD models of the 15 patients.

The effect of different extents of CO decrease on pharmacodynamics is evaluated for a virtual patient described by a validated PBPK-PD model. The DoH is predicted for three different CO profiles, representing a 35, 50, and 70% (maximum) drop.

4A.5 Hemodynamic changes during closed-loop induction of anesthesia

Paragraph 4A.5.1 presents the hemodynamic changes observed during induction of anesthesia in the high-risk subset of the patient population in West et al. (2018). Paragraph 4A.5.2 discusses these results and compares them to reported changes

[7] Values are presented as mean (SD), except for Smuszkiewicz et al. (2016), because only average data of the study population are available in the paper. Data from other studies are available at http://opentci.org/data/propofol.

following manual induction of anesthesia with propofol in similar patients.

4A.5.1 Quantification of hemodynamic changes

Baseline values for the 15 patients in the subpopulation are median (IQR) CO 7.24 (5.57-8.02) L/min, MAP 106.6 (95-111.25) mmHg and HR 71 (58.75-78.25) b/min. 27% of the patients exhibited baseline values of CO and HR lower than 5 L/min and 60 b/min, respectively, which is not atypical considering age and ASA classes. Induction of anesthesia was performed in closed-loop. The end of induction of anesthesia was defined as the time the $WAV_{CNS} < 60$ for 30 consecutive seconds. For the 15 patients in the subpopulation, this was achieved in a median (IQR) 4.18 min (3.44-4.54 min) with a propofol dose of 1.42 (1.05-1.47) mg/kg.

Table 8 reports median (IQR) values of the drops in CO, MAP, and HR 1.5 and 3 min after induction of anesthesia. Whereas the drop in CO and MAP after 3 min is median 22.4 and 26.6%, respectively, the decrease in HR is less marked. The maximum values of the drop (*i.e.* evaluated between the start of induction and the start of the airway management) are 43.43% and 37.5% for CO and MAP, respectively (also reported in Table 8). Note that median maximum MAP drop exceeds 30%, which is typically considered clinically significant.

In some of the patients, the CO continued to decrease further after 3 min, in particular to over 50% for 1 patient and over 60% for 2 patients. However, although in some of these cases this enhanced reduction may have been caused by propofol overdosing, other factors may have contributed.

Figure 8 shows the individual trends of CO, MAP, and HR (top panel) from the start of induction until induction is completed, as defined above. The bottom panel shows median (IQR) values over the first 5 min after the start of propofol induction. The individual trends of CO, MAP, and HR drop (Figure 8) and the IQR associated to the drop (Table 8) manifest great inter-individual variability. Variability of the profiles may be partly ascribed to the differences in the patients' characteristics, diseases and physical conditions, timing of intubation, type of surgical procedure, and drug-drug interactions.

Table 8 – Median (IQR) values of CO, MAP, and HR drop 1.5 and 3 min after the start of induction. Median (IQR) values of the maximum drop are also reported (N =15).

	%ΔCO [-]	**%ΔMAP [-]**	**%ΔHR [-]**
1.5 min	7.03 (1.66-17.47)	8.93 (3.11-16.1)	5.45 (2.48-9.13)
3 min	22.43 (14.82-36.0)	26.6 (22.39-35.33)	8.82 (4.94-12.68)

max[8]	43.43 (38.57-47.74)	37.5 (32.79-52.25)	16.28 (12.99-20.36)

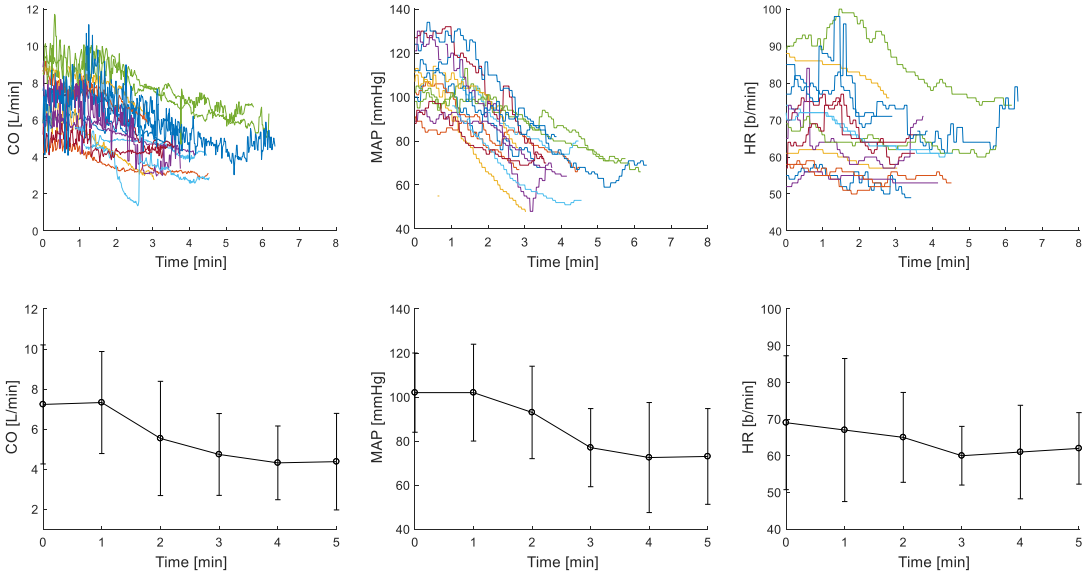

Figure 8 – (Top panel) Individual patients' trends of CO, MAP, and HR throughout the induction period (*i.e.* from the start of induction to completed induction). (Bottom panel) Median (IQR) values of CO, MAP, and HR in the first 5 min after the start of propofol induction.

4A.5.2 Hemodynamic changes after manual induction in the literature and discussion

In 15 high-risk patients scheduled for cardiac surgery, the authors in Singh et al. (2010) administered propofol 1.5 mg/kg and fentanyl 4 µg/kg. They recorded baseline and 1-min interval values of the hemodynamic variables for 3 min after induction of anesthesia. HR and MAP were recorded continuously, and CO was measured with the FloTrac-Vigileo monitor (Edwards Life Sciences, Irvine, USA), based on the analysis of the arterial pressure waveform. They found 18.7 and 17.3% decrease in CO and MAP and no statistically significant change in HR after 1 min, and mean 37.5, 34.3, and 10.5% decrease in CO, MAP, and HR after 3 min from induction.

Hemodynamic variables were continuously monitored in Vos et al. (2014) with the Nexfin monitor (Edwards LifeSciences Corporation, Irvine, CA, USA), a non-invasive pulse pressure analysis device, in 40 patients (ASA I-II-III) administered with propofol (1-3 mg/kg) and remifentanil (1 µg/kg). A decrease of mean 30, 23.8, and 26% was found in CO, MAP, and HR after induction.

In Potočnik et al. (2011), CO, MAP, and HR were recorded continuously (CO was measured using the LiDCO Plus system (LiDCO, London, UK)) during manual induction of anesthesia with 1.5-2.5 mg/kg of propofol and 0.5 µg/kg of remifentanil in

[8] Evaluated between the start of induction and the start of airway management.

24 patients (ASA II-III). Baseline values as well as the value of CO, MAP, and HR after induction (defined as 3 min after BIS < 60) and after intubation are given. They observed about 29% decrease in CO, and 22% in MAP and HR (mean values). It was noted that the open lung surgery may have contributed to the circulatory instability due to tissue hypoperfusion and thus affected these results (Potočnik et al., 2011).

In 10 elderly patients (ASA I-II) scheduled for abdominal surgery, anesthesia was induced with 1.5 mg/kg of propofol (Larsen et al., 1988). A catheter in the radial artery was inserted for continuous monitoring of arterial blood pressure, and cardiac output was measured by the thermodilution technique. Lowest values after induction were reported. There was no statistically significant change in HR, whereas a decrease of 17.5 and 33.3% in CO and MAP (mean values) was observed.

Reported HR changes are contradictory. HR is more affected by external stimuli, and differences in the study design (*e.g.*, times to intubation and to measurement of baseline values) and patients' level of anxiety are likely to produce inconsistencies. Although lowest values were not reported (except for one study), the median changes in CO and MAP observed after 1.5 and 3 min in this subpopulation of the closed-loop study in West et al. (2018) are comparable or smaller than the changes described in the literature following manual induction of anesthesia with propofol. Thus, closed-loop induction did not introduce a higher risk of hypotension and cardiovascular changes compared to manual induction. In fact, despite the age and condition of the patients, and the procedures in this subpopulation where use of an arterial line was selected, the control action provides an overall adequate compromise between hemodynamic stability and velocity of induction. Note that patients' characteristics, technology used to measure CO, drug dosing and opioid use differ among studies, and need to be taken into account in the interpretation of this comparison.

4A.6 Impact on PK and PD

This section presents the results of *in silico* evaluation of the effect of CO on pharmacokinetics and pharmacodynamics. The resulting pharmacokinetic profiles of the PBPK simulations and the commonly used three-compartment Schnider model (Schnider et al., 1998) are compared in Section 4A.6.1 for six representative cases.

Paragraph 4A.6.2 presents the results of identification of PD models for DoH using the PBPK and the Schnider PK models. *In silico* simulations of one of the PBPK-PD models are presented to evaluate the effect of different CO changes on the DoH in

Paragraph 4A.6.3.

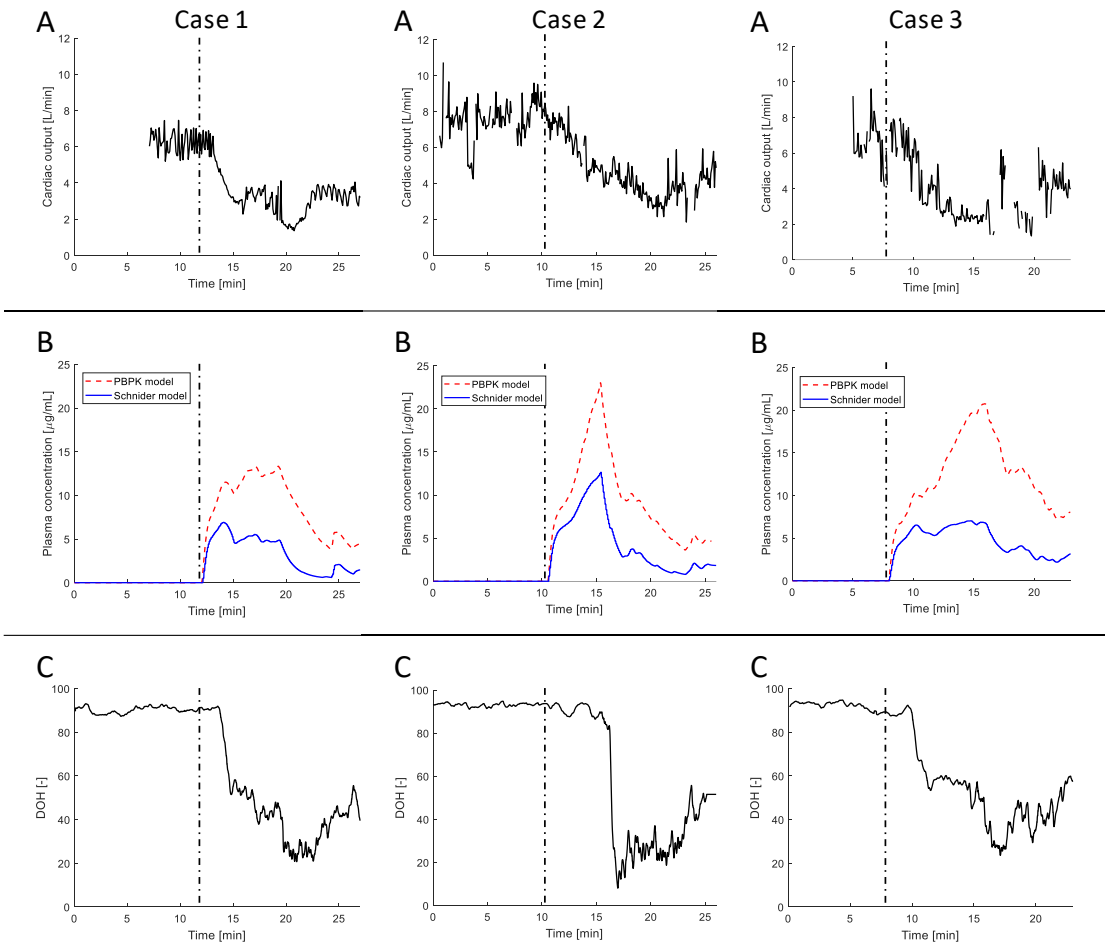

Figure 9 – Panel A shows the CO trends of the individual patients (cases 1, 2, and 3). Panel B shows the comparison between the plasma concentration dynamics predicted by our PBPK model (red dashed line) and Schnider model (blue continuous line). Panel C shows corresponding trends of the WAV_{CNS} index as DoH measure. The black dashed-dotted vertical line marks the start of propofol infusion.

4A.6.1 PBPK prediction of plasma levels

Plasma concentrations are predicted for the 15 patients described in Paragraph 4A.4.1, using the PBPK model presented in Paragraph 4A.4.2. Input to the model are demographics of those patients, infusion rate as administered by the controller, and the measured CO.

Figure 9 and Figure 10 show the measured CO (A panels), the simulated dynamics of propofol concentration (B panels), and the measured DoH (C Panels) of six representative cases, referred to as cases 1, 2, and 3 (in Figure 9), and cases 4, 5, and 6 (in Figure 10). The considered time horizon is 15 min after the start of induction of anesthesia. Missing data in the CO trends are due to either monitors disconnection or artifacts that were suitably removed in the data post-processing phase.

The PBPK-predicted plasma concentrations (red dashed line) exceed the plasma concentrations predicted by the Schnider model (blue continuous line). Discrepancies in the plasma levels prediction resulting from different PK models, are not surprising, and have been reported extensively (Coppens et al., 2011; Masui et al., 2010). It is known that early disposition propofol is not well-characterized by classical three-compartment models (Cortinez, 2014). Concentration peaks in the range between 20-30 µg/mL have been found after bolus administration (Struys et al., 2007). Higher concentrations have been found in the elderly compared to younger patients (Kirkpatrick et al., 1988). Although the Schnider model features age as covariate, studies in the elderly have shown underestimation of the Schnider PK-prediction with respect to the measured values (see positive MDPEs reported by Vuyk et al. (2001) and Cortinez et al. (2014)). Considering the patient population and the corresponding DoH overshoot and cardiovascular depression, PBPK-predicted levels are realistic.

Note that the PBPK-predicted plasma concentration shows close resemblance to the WAV_{CNS} data trend (see for instance the plasma peak (red dashed line) and the DoH drop below 40 in cases 2 and 3). In fact, cases 1, 2, and 3 (Figure 9) manifest DoH values that are below the recommended lower level of 40 for short periods, and display burst suppression behavior[9]. This behavior corresponds, with some delay, to high peaks (> 10 µg/mL) in the concentration trend as a result of the changes in CO. Instead, in cases 4, 5, and 6 (Figure 10), the CO drop is more gradual and limited ($\%\Delta CO_{max} < 45$) and the DoH trend does not indicate an overshoot and values < 40. Corresponding predicted peak plasma levels are approximately 10 µg/mL.

These results confirm that the hypnotic effects of propofol infusion may be amplified by significant CO decreases, in line with the experience from the clinical practice that adjusts drug dosing in case of patients with low CO baseline. On the other hand, PK prediction according to Schnider model prediction does not manifest abnormal levels: in fact, levels represented by the blue continuous line are comparable in most cases, except case 2.

[9] Burst suppression is an EEG pattern characterized by high-voltage, non-periodic bursts of activity alternating with an isoelectric background alternating. It is usually associated with low values of quantitative EEG monitors, such as BIS or $WAV_{CNS} < 40$.

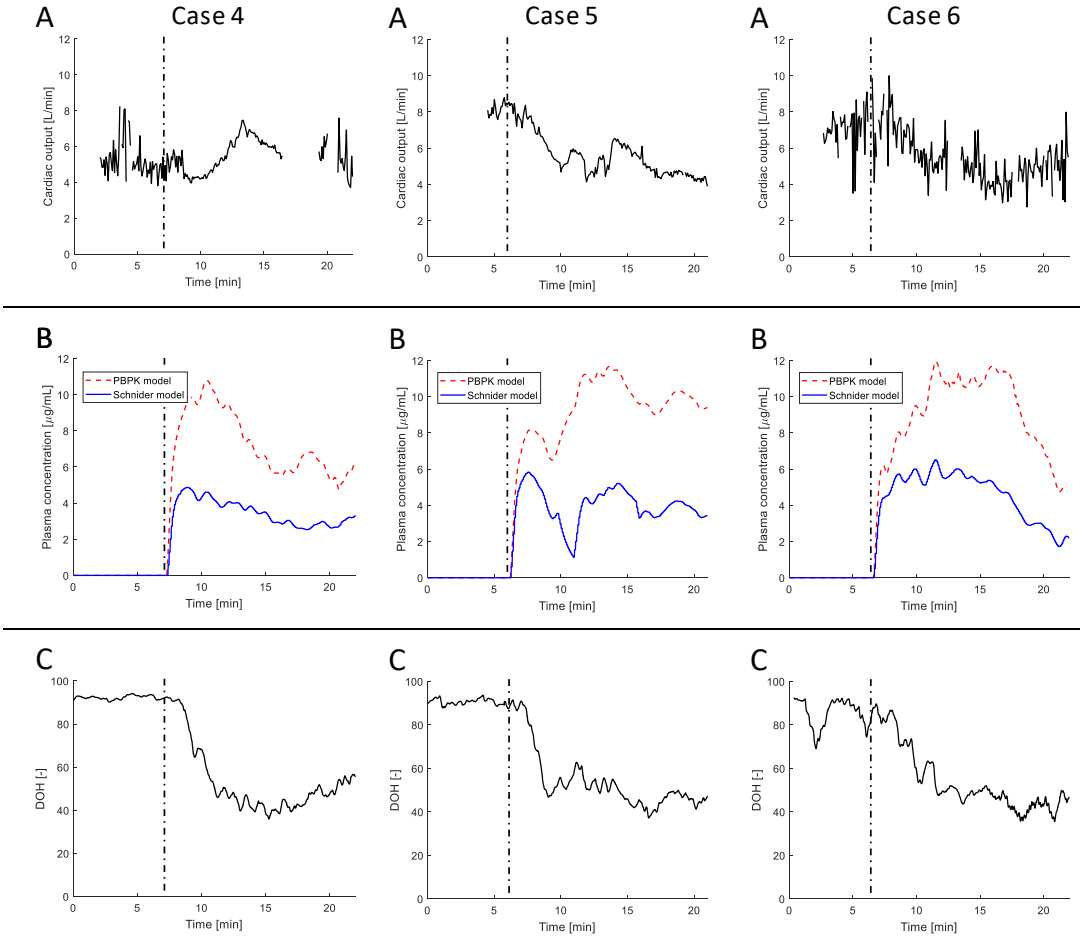

Figure 10 – Panel A shows the CO trends of the individual patients (cases 4, 5, and 6). Panel B shows the comparison between the plasma concentration dynamics predicted by our PBPK model (red dashed line) and Schnider model (blue continuous line). Panel C shows corresponding trends of the WAV_{CNS} index as DoH measure. The black dashed-dotted vertical line marks the start of propofol infusion.

The fact that deep levels of hypnosis are found in conjunction with higher predicted plasma levels (Figure 9), may also suggest that significant changes in CO are a contributing factor to the dynamics of propofol concentration in the brain with consequence of burst suppression. In addition, these trends are often observed in presence of MAP (not shown) equal to or below 70 mmHg, which is the reference lower bound for preservation of cerebral blood flow autoregulation (Drummond, 2019). Actually, low DoH values have been reported in association with both overdosing and reduced cerebral perfusion (Dahaba et al., 2010), hence in this case there may be a concomitant effect of overdosing and low cerebral perfusion resulting in burst suppression.

4A.6.2 PD model identification

Table 9 – RMSE values (median (IQR)) for the PBPK-PD and Schnider PK-PD models.

Patients	PBPK-PD RMSE [-]	Schnider PK-PD RMSE [-]
All (N = 15)	5.72 (4.67-5.99)	5.90 (5.07-6.84)
$\%\Delta CO_{max}$ > 45 (N = 6)	5.60 (5.34-5.85)	6.26 (5.54-7. 2)

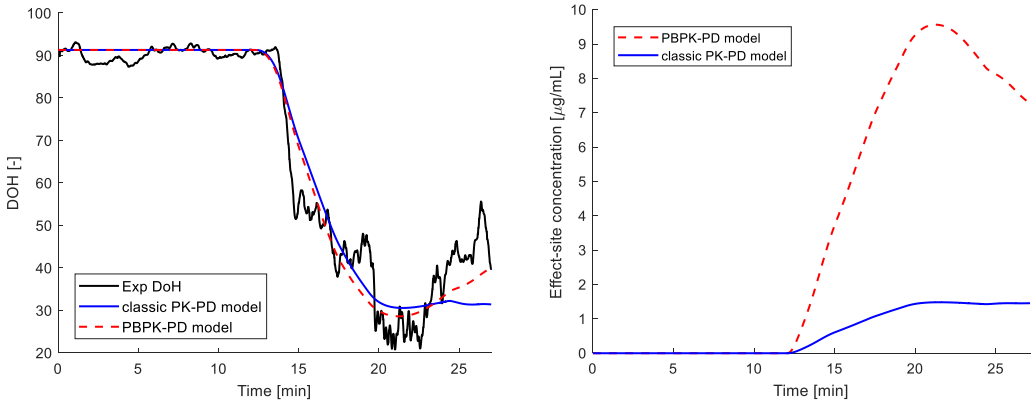

Figure 11 – Results of the PD model identification with DoH data of case 1 (black continuous line). Comparison of the DoH (left panel) and the effect-site concentration (right panel) dynamics obtained via PBPK-PD model (red dashed line) and the classical three-compartment PK-PD model (blue continuous line).

DoH data from West et al. (2018) were used to identify PD models of the 15 patients via nonlinear regression. Table 9 shows RMSE values for the PBPK-PD and the three-compartment PK-PD models. A lower value of RMSE is obtained in the cases of PBPK-PD models identified particularly with DoH data of patients subject to marked CO decreases ($\%\Delta CO_{max}$ > 45). The differences in the concentration trends discussed in Paragraph 4A.6.1 allow for improving the fit, because DoH is modeled via a modified Hill equation, as a function of propofol effect-site concentration (Savoca and Manca, 2019). Since the three-compartment PK model predicts less marked plasma concentration peaks, the slower effect-site concentration dynamics cannot describe significant DoH drops and overshoot (mostly evident in the six cases where $\%\Delta CO_{max}$ > 45, see improved RMSE shown in Table 9). As a representative case, Figure 11 shows the identified PBPK-PD and three-compartment PK-PD models of case 1, which is also used in Paragraph 4A.6.3 to simulate in silico the effect of CO on pharmacodynamics. Right panel in Figure 11 shows the effect-site concentration dynamics obtained via the two different modeling strategies to better explain such considerations. For the sake of completeness, Appendix 4A.A reports the comparison of the PBPK-PD and three-compartment PK-PD models with DoH data for the whole set of six representative cases whose predicted pharmacokinetics and DoH data were shown in Paragraph 4A.6.1.

4A.6.3 *In silico* evaluation of the effect of CO on DoH

Three different trends of CO have been used as input to the PK simulation of case 1, to evaluate the effect of different CO drops on the pharmacokinetics. The PD model identified in 4A.6.2 is now used to simulate the effect of the three CO trends on the DoH. The experimental data for this patient showed a 70% drop (maximum value) in CO (15 min following the start of induction of anesthesia), as shown in Figure 12, where the CO trend is smoothed using a moving average for a better visualization and comparison. Figure 12 shows the impact of different magnitude of CO changes on plasma PK and DoH prediction. Panel A shows three different CO trends leading to (i) 70% (continuous black line), (ii) 50% (dashed black line), and (iii) 35% drops (dashed-dotted lines). Panels B and C show the corresponding predicted plasma concentration (in red) and DoH (in blue) dynamics, respectively.

A 35% drop in CO produces a minimum predicted DoH value of 37, whereas additional CO decreases to 50% and 70% result in significant overshoots to 27 and 21, respectively. The difference between a drop of 35% and 70% leads to a 31% difference in the area under the curve (AUC, *i.e.* the area under the plasma drug concentration-time curve, reflecting the actual body exposure to drug) (see Table 10). These changes can be clinically relevant especially in “at-risk” patients. In fact, studies show that intraoperative burst suppression is associated with increased mortality (Andresen et al., 2014; Kertai et al., 2010; Watson et al., 2008) and post-operative delirium (Andresen et al., 2014; Soehle et al., 2015), with impact on lengths of stay in the intensive care unit and hospital costs.

Table 10 – AUC and minimum DoH values corresponding to the three simulated CO drop extents.

	AUC [(min mg)/mL]	DoH_{min} [-]
35% drop	110.47	34
50% drop	133.30	27
70% drop	145.58	21

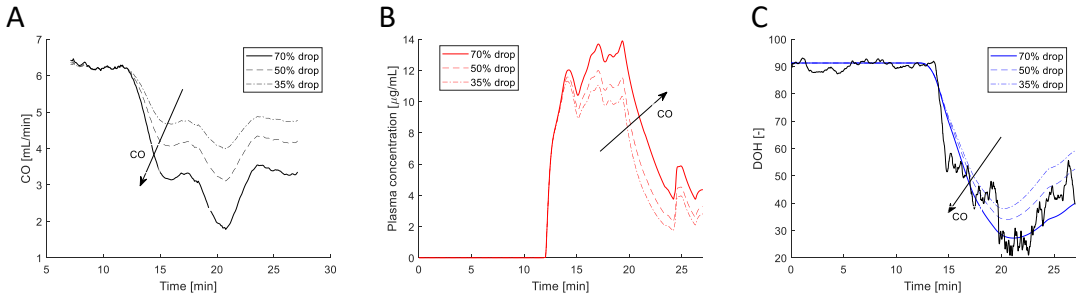

Figure 12 – Panel A shows different trends (black line) of CO corresponding to (i) 70% drop (as in case 1, continuous line), (ii) 50% drop (dashed line), (iii) 35% drop (dotted-dashed line). Panel B shows

corresponding plasma PBPK predictions (red) and Panel C DoH predictions (blue) (simulated via combined Hill function). Experimental data (black continuous line) in Panel C shows DoH trend for case 1. The black arrow points in the direction of CO decrease.

4A.7 Discussion and study limitations

Anesthesia is a complex multivariable process and some underlying mechanisms are to date not fully elucidated. The use of more mechanistic, detailed PK models, based on the anatomy and physiology of the human body, allows us to go beyond the goals of pharmacokinetic description and data fitting, typical of the empirically-based three-compartment models. Interestingly, we found PBPK simulations predicted high plasma peaks reflective of excessively deep anesthesia, as a result of marked decreases in CO. The integration of clinical data with PBPK simulations can represent a starting point for:

(i) hypotheses-making on how the cardiovascular changes affect the pharmacokinetics of anesthetic and analgesic drugs not only in plasma but also in the effect-site, and the resulting DoH;

(ii) design of experimental studies with the purpose of verifying and supplementing current knowledge on how factors such as CO variation affect propofol brain uptake and transfer across the blood-brain barrier.

Whereas we used clinical data to identify the parameters of a Hill-form equation to simulate DoH, the PBPK model was defined based on data from the literature (Schnider et al., 1998) (see Table 6). No PK data were available from West et al. (2018). This means that the PK results need to be confirmed with experimental data, and specific studies are required to better define and understand the contributions of overdosing and changes in CO on excessively deep anesthesia levels.

As previously mentioned, although it is known that changes in CO and MAP affect drugs pharmacokinetics, three-compartment PK models commonly used to analyze the pharmacokinetics of IV analgesic and anesthetic drugs are not appropriate to investigate these effects. In fact, their parameters are either fixed or only include patient demographics as covariates. As far as we know, similar points have been discussed by only two other works: Reekers (2012) and Upton and Ludbrook (2005), who both employed a recirculatory model. In case of Reekers (2012), however, the model parameters do not seem to include any covariates (*e.g.*, body mass, height, and gender). In addition, all of those parameters are identified with pharmacokinetic data, except for the venous lag time and CO. The model from Reekers (2012) aims to

describe propofol pharmacokinetics, rather than predicting and simulating virtual patients for investigation of the effects of the cardiovascular changes. In Upton and Ludbrook (2005), an interesting PBPK model is presented, in which blood flows are used to determine parameters of the final pharmacokinetic outcome. The methodology employed in our study attempts to improve the work from Upton and Ludbrook (2005) in at least two aspects. Firstly, the compartment volumes are also anatomically-based and estimated depending on the patients' characteristics. This has a direct effect on the physiological feature of the model and makes it more flexible and individualized. Secondly, assumptions on propofol metabolism and elimination pathways are based on the literature where these pathways are hepatic, renal, and tissue-based (probably gastrointestinal) (Gray et al., 1992; Hiraoka et al., 2005).

4A.8 Conclusions

This study has provided quantification of the response of high-risk patients to closed-loop induction in terms of CO, MAP, and HR. Since hemodynamics is an essential contributor to these patients' safety, evaluation of such effects is extremely valuable, especially compared to the available data on hemodynamic effects of propofol induction in the literature.

The second part of the study covered the impact of cardiovascular changes on propofol pharmacokinetics and pharmacodynamics, using a PBPK-PD modeling approach. We showed that a significant decrease in CO can lead to predicted plasma levels that cannot be calculated by three-compartment PK models. These traditional PK models, which are in routine daily use in anesthesia, may result in an amplified response in high-risk patients. This conclusion is supported by an improved prediction in the fitting of PD data with a PBPK model rather than the Schnider PK model.

Thus, the integration of CO data with PBPK simulations sheds light on the DoH outcome and offers interpretations of the inter-patient variability of the response to propofol. Although a limited number of patients were analyzed, and no pharmacokinetic data were available, these results show that PBPK-PD simulations can be employed to study and quantify the effect of the changes in CO on the DoH levels, as a rigorous investigation tool with potential applications ranging from training and education to improvement of the clinical practice through a better understanding of the impact of the hemodynamic changes on the patients DoH.

Our results may suggest that the use of PBPK model-based closed-loop systems

would allow accounting for hemodynamic effects during closed-loop control of anesthesia. Adjusting the infusion rates also based on the hemodynamic data may limit the chance of overdosing in critical patients. CO is not always monitored in every patient, thus making this feature of PBPK modeling less useful. However, the awareness of the importance of flow monitoring in high-risk populations is increasing (Green et al., 2014) and minimally invasive monitoring techniques are under development. In cases when CO is not directly monitored, correlations that infer CO from noninvasive data on either BP or perfusion can be developed and implemented

4A.9 Appendix 4A.A

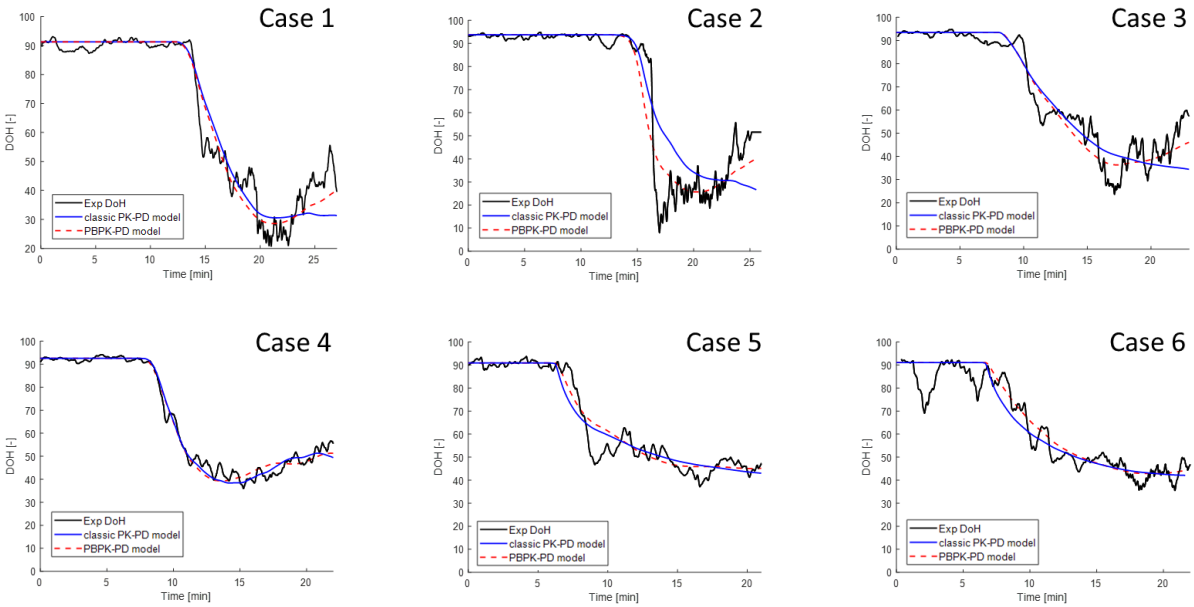

Figure A. – Results of the PD model identification with DoH data (black continuous line) for the considered six representative cases. Comparison of the PBPK-PD (red dashed line) and three-compartment PK-PD (blue continuous line) models. Cases 1, 2, and 3 feature %ΔCOmax > 45 coinciding with DoH overshoots. Cases 4, 5, and 6 feature more gradual and limited CO drops and acceptable DoH levels.

.

CHAPTER 4B

Tackling inter-individual variability: the influence of anatomical and physiological features

4B.1 Author's Note

Inter-individual variability is one of the main issues in the selection of the optimal dose. Part of this variability can be ascribed to the anatomical and physiological differences among individuals. PBPK models can be adapted to describe alterations of ADME processes associated to anatomical and physiological changes of the human body in *special* categories of patients.

This chapter proposes new correlations for the individualized parameters of the PBPK model and specific adaptive parameters to predict the pharmacokinetics and pharmacodynamics of propofol in three populations: (i) elderly, (ii) obese, and (iii) pediatric patients. These categories are frequently present in ORs and represent challenging cases from the point of view of optimal dosing because of their increased sensitivity to propofol side-effects.

In silico simulations of induction of propofol anesthesia conclude this chapter and allow assessing the performance of the model-predictive controller in those categories, also compared to manual and TCI regimens.

Part of the work presented in this chapter is from an invited paper submitted to "The Canadian Journal of Chemical Engineering" in November 2019 for the special issue of GRICU (GRuppo di Ingegneria Chimica dell'Università) 2019 conference.

Optimal dosing of anesthesia in pediatric patients: a physiologically-based model predictive control study

Adriana Savoca, Davide Manca

Under review for "The Canadian Journal of Chemical Engineering", March 2020

4B.2 Introduction

Differences in the anatomical and physiological features of individuals are among the sources of inter-individual variability manifesting in the response to drugs. Although inter-individual variability is partially produced by a "natural" variability of both anatomy and physiology of the human body, a PBPK approach to modeling has the potential of predicting at least part of the variability in PK profiles related to (i) aging, (ii) presence of specific diseases (*e.g.*, obesity), and (iii) body development stage (*i.e.* in infants, children, and adolescent patients). These factors produce anatomical, physiological, and biological changes affecting the ADME processes of drugs within the body and increase the difficulty of selecting the optimal dose. The problem is more constrained and complex in case of drugs with narrow therapeutic indexes, as is the case of propofol, an anesthetic agent, whose optimal titration is crucial to achieve a smooth intra-operative procedure and a good quality of post-operative recovery.

Although anesthesiologists are usually well-trained to manage such inter-individual variability, dosing is most of the times heavily based on their personal experience and intuition, especially in elderly and obese patients (Servin, 2017). With the aging trend of the world population (UN Report "World Population Ageing 2017", 2017), and increasing incidence of obesity in rich countries (OECD Report "Obesity Update 2017", 2017), these two categories are destined to be more and more present in ORs. Optimal propofol titration is critical in these categories, because they are more susceptible to cardiovascular and respiratory depression (Servin, 2017; Subramani et al., 2017). In pediatric patients, different levels of depth of hypnosis, *i.e.* from

conscious sedation, to deep sedation[10], to general anesthesia levels, are required for both surgery and diagnostic/therapeutic medical procedures during which it is desirable to keep the patients still, minimize their discomfort, and possibly produce amnesia (Cravero et al., 2009). Propofol use in children is quite spread (Chidambaran et al., 2015), because of clinical and practical advantages (Rigouzzo et al., 2008), although there are some concerns regarding its optimal dosing, as pediatric patients represent an "at-risk" category among the subgroups receiving anesthesia. In fact, simple allometric scaling is not always suitable to account for the effects of the growth stage on those ADME processes that generate PK and PD differences between children, adolescents, and adults.

Today TCI pumps are widely used as a tool to induce and maintain IV anesthesia. However, their optimal performance is not guaranteed in the above-mentioned populations. Indeed, the effectiveness of TCI pumps depends on the accuracy of the embedded PK model, as they are "open-loop" systems that do not consider any real-time data of the monitored physiological parameters to adjust the drug dosing. Indeed, the anesthesiologist can choose among several TCI three-compartment PK models. Since each of them was identified with data of different types and numbers of patients, there is a significant variability among their predictions. Schnider and Marsh models are the most commonly used propofol PK models for adults and are both among the embedded PK models available in most TCI pumps, but Marsh model does not include age as covariate and is therefore not recommended for use in patients older than 55 y (Servin, 2017). With respect to obese patients, some studies advice to "trick" the TCI pump by providing a reduced value of total body weight (TBW), to avoid excessive induction doses (Servin, 2017). According to Servin (2017), Schnider model is not recommended for obese patients (as it adopts James formula (James, 1976) for Lean Body Mass calculation, which performs inconsistently in case of severely obese patients (see also Absalom et al., 2009)) whereas, even with the Marsh model, it is likely that normal target concentrations will result into high induction doses. Up to now, we have limited the discussion to the two most used classical PK models for propofol, but it is evident that the availability of several PK models characterized by differences in their outputs, forces clinicians to know and remember which PK model is better for safe use of TCIs in *special* patients' categories. This may lead to ambiguity and

[10] *Deep sedation*: depression of consciousness, during which patients may require assistance to breathe and do not respond to verbal commands but only to painful stimulation; *conscious sedation*: depression of consciousness, during which patients breathe spontaneously and respond to verbal commands, either alone or accompanied by light tactile stimulation. In both states, cardiovascular functions are maintained. Definitions from Dar and Shah (2010).

confusion and adds personal interpretation based on past experience and opinion. In addition, studies have shown that the predictive performance of most classical PK models is often poor both in the elderly (Cortínez et al., 2011; Vuyk et al., 2001) and the obese (Cortinez et al., 2014).

Specific TCI PK models are available for pediatric patients and most of them have acceptable predictive performance (Hara et al., 2017; Sepulveda et al., 2011). However, in this case as well, the degree of variability among the different models' PK output is remarkable (Gaynor and Ansermino, 2016). Evidently, the presence of several available models and the issues related to their different degrees of accuracy depending on the patients' characteristics, increases the difficulty of selecting optimal dosing, rather than reducing it, especially considering that there is no official training on the use of TCI pumps (Absalom et al., 2016).

There are recent efforts of developing a "broad" model from previously published propofol PK data of different populations. Eleveld et al. (2018) published a three-compartment PK model including weight, age, height, and gender as covariates. However, we propose PBPK modeling as a more valid alternative to tackle the problem, as this approach allows accounting for changes in pharmacokinetics related to the patients' anatomical and physiological characteristics. This feature may also facilitate the understanding and thus enhance the approval by clinicians, since they are more familiar with these concepts rather than mere mathematical modeling and fitting of experimental data. In this chapter, we show how the PBPK model for propofol was adapted, identified, and validated for three categories of "challenging" patients. The adoption of this model in clinical practice would eliminate the need for discriminating and selecting among all the available PK models embedded in TCI pumps. Suitable age-dependent PD models were also identified and validated. Finally, once the PBPK-PD models were integrated into the model-predictive controller of propofol delivery, *in silico* experiments were carried out to verify the effect of aging, obesity, and growth on the control action exerted on the hypnotic effects of virtual patients. A specific *in silico* experiment, which concludes the chapter, was also designed to compare our closed-loop controlled infusion rate with those obtained via simulations of manual and TCI regimens.

4B.3 Methods: adaptation of the PBPK model

Paragraphs 4B.3.1, 4B.3.2, and 4B.3.3 discuss how the PBPK model was adapted to

predict the pharmacokinetics of (i) elderly, (ii) obese, and (iii) pediatric (*i.e.* 1-19 y) patients, respectively. The predictive performance of the adapted PBPK model is evaluated in terms of MDPE and MDAPE values, as these are the most common performance indicators employed in the literature related to PK modeling of propofol (see Eqs. (4B.1-3), in which $C_{i,p}$ and $C_{i,m}$ are the predicted and measured values of the concentration at a specific sampling time i). Specifically, MDPE is used as a measure of bias, while MDAPE as a measure of accuracy. Acceptable values are MDPE within ± 20% and MDAPE 20-40% (mean values) (Eleveld et al., 2018; Hara et al., 2017). MDPE and MDAPE values are compared to those obtained by using the most widespread classical PK models for propofol, *i.e.* Marsh and Schnider models. For the sake of clarity, in case of pediatric population, we refer to the Marsh pediatric model.

As MDPE and MDAPE are not always sufficient to evaluate the overall prediction capability of the model, we also show (i) diagnostic plots and (ii) predicted vs experimental concentration dynamics of the best, median, and worst validation cases (in terms of model accuracy).

$$PE_i = 100\frac{C_{i,m}-C_{i,p}}{C_{i,p}} \quad (4B.1)$$

$$MDPE = median(PE_i) \quad (4B.2)$$

$$MDAPE = median(|PE_i|) \quad (4B.3)$$

4B.3.1 Elderly patients

The body changes associated with aging include hypovolemia, reduction of local blood flows, and functional beta-blockade (Servin, 2017). Some of these changes can be incorporated into the evaluation of the individualized parameters of the PBPK model. Compartment volumes and blood flowrates are thus estimated via correlations developed by Stader et al. (2019), which are suitable for healthy individuals within the age range 20-99 y. In fact, their analysis included 318 studies on anthropometric parameters and provided a database purposely meant to inform PBPK models. Such correlations account for body surface area (BSA), height, gender, and age of patients.

For a better adaptation of the prediction capability of our PBPK model of propofol concentration in the considered patients, the model adaptive parameters were re-identified via a nonlinear regression with data of studies featuring elderly patients, specifically those of Schnider et al. (1998) (N = 11 patients), and additional data from

5 patients of Dyck and Shafer (1992). Remaining data of Dyck and Shafer (1992) (N = 25 patients) were used for validation of the model predictive performance. The age range of the PK data for elderly patients is (i) 62-81 y in Schnider et al. (1998) and (ii) 57-82 y in Dyck and Shafer (1992). Propofol PK data are available thanks to the "Open TCI Initiative" (see http://opentci.org/).

4B.3.2 Obese adult patients

Obese subjects feature several anatomical and physiological changes compared to healthy individuals. Blood volume, CO, and blood flowrates to organs and tissues are increased (Alexander et al., 1962; Lemmens et al., 2006). Higher weight of most organs in association with the increase of adipose tissue is also observed (Gholamzadeh et al., 2017; Mandal et al., 2012). Obesity is frequently associated with glomerular hyperfiltration (Hartmanshenn et al., 2016). This feature, in combination with increased hepatic and renal blood flowrates and higher liver weights (*i.e.* more hepatic tissue than healthy people) often lead to higher drug clearance. The heart, liver, and spleen are the main organs whose weight is affected by the fat increase (Mandal et al., 2012). Skin and fat are the main affected tissues (Fuster et al., 2016; Groenendaal et al., 2010).

Although a few correlations for estimation of CO, and organs and tissues weights in obese individuals were available in the scientific literature (*e.g.*, in Young et al. (2009)), we argue that the regressed correlations that we propose are more robust, being derived (when possible) from integrated data of different studies and/or validated with additional data.

Correlations for CO, the volumes of blood and liver, and the weights of kidneys, spleen, heart, muscles, and adipose tissue were thus estimated via a nonlinear regression with experimental data available in the scientific literature. Table 11 lists the sources of the experimental data, the individualized parameters, and the corresponding correlation. Standard errors (SEs) associated to the regressed coefficients and R-squared values are also provided in Paragraph 4B.7.1. For the sake of clarity, when data on obese patients were not available in the literature, correlations from Stader et al. (2019) were used to estimate the individualized parameters (*e.g.*, weight of bone tissue). Organs and tissues weights were converted to volumes by considering the density values associated to organs and tissues (Valentin, 2002).

Table 11 – List of studies used as data sources for identification of correlations associated to obese subjects. Last column reports the BMI or TBW range of the study group.

Individualized parameter	**Data sources**	**BMI [kg/m^2] or TBW [kg] range**
Cardiac output	Danias et al. (2003); de Divitiis et al. (1981); Hinderliter et al. (2011)	M: 18.39 – 61.15 [kg/m^2] F: 15.53 – 67.56 [kg/m^2]
Blood volume	Messerli et al. (1981); Messerli et al. (1982); Young et al. (2009)	M/F: 65.7 – 203.87 [kg]
Liver volume	Hinderliter et al. (2011)	M: 18.37 – 46.71 [kg/ m^2] F: 15.54 – 39.89 [kg/ m^2]
Kidneys weight	Young et al. (2009)	M: 102.32 – 158.79 [kg] F: 86.00 – 203.62 [kg]
Spleen weight	Young et al. (2009)	F: 39.05 – 204.51 [kg]
Heart weight	Drenick and Fisler (1992); Kumar et al. (2014)	M: 130.49 – 255.01 [kg] F: 102.70 – 226.47 [kg]
Muscles weight	Janssen et al. (2000); Young et al. (2009)	M: 101.80 – 137.53 [kg] F: 85.33 – 129.52 [kg]
Adipose tissue weight	Das et al. (2003); Geliebter et al. (2013); Hinderliter et al. (2011); Petroni et al. (2003); Boneva-Asiova and Boyanov (2008)	M: 18.33 – 55.50 [kg/m^2] F: 15.69 – 64.62 [kg/m^2]

Depending on the available data, some correlations are based on the Body Mass Index (BMI)[11], while others are based on the Total Body Weight (TBW). BMI is frequently used as a descriptor of obesity in the related scientific literature, because it is easy to calculate. According to the World Health Organization (WHO) classification, an obese individual has BMI ≥ 30 [kg/m^2] (see Table 12). It is more difficult to establish an equivalent threshold value for obesity basing solely on TBW without considering both height and body composition (*e.g.*, fat mass %). We adopted reference values from Adams et al. (2006), *i.e.* 101 kg for men and 85 kg for women. Note that, according to Servin (2017), the average BMI value of patients undergoing bariatric surgery[12] is around 50 with values over 70 being quite frequent. Unfortunately, the scientific literature lacks anatomical data associated to BMI values above 70 [kg/m^2].

We identified a specific set of adaptive parameters for propofol PK in the obese population with data of 8 patients from Servin et al. (1993) and 5 patients from Cortinez et al. (2010). Data from additional 14 patients of Cortinez et al. (2010) were used as validation cases. The BMI range of the PK data used for identification and validation of the adapted PBPK model is 33-50 [kg/m^2] (Cortinez et al., 2010; Servin et al., 1993). Propofol PK data are available thanks to the "Open TCI Initiative" (see the website http://opentci.org/).

[11] BMI is calculated as total body weight [kg]/(height [m])^2.

[12] Bariatric surgery includes several procedures performed on obese patients, with the goal of achieving weight loss, *e.g.*, removal of portions of the stomach and/or intestine (https://medical-dictionary.thefreedictionary.com/bariatric+surgery).

Table 12 – WHO BMI classification of obesity.

Range	Classification
18.5 ≤ BMI ≤ 24.9	Normal
25 ≤ BMI ≤ 29.9	Overweight
30 ≤ BMI ≤ 34.9	Moderately obese, class I
35 ≤ BMI ≤ 39.9	Severely obese, class II
BMI ≥ 40	Morbid obese, class III

4B.3.3 Pediatric patients

Experimental data associated to the pediatric population are hard to find in the scientific literature, for both ethical and practical reasons. However, it is known that "*children are not small adults*", as maturity and growth stages determine major anatomical and physiological changes and thus, dosing guidelines basing on allometric scaling (Anderson and Meakin, 2002) may not be effective enough.

CO and blood volume increase with age, along with the weights of organs and tissues (Fernandez et al., 2011). For some organs, a constant weight increase across the age range can be observed, while in other cases, adult values are reached during puberty (around 12 y). Gender-specific differences are mostly evident after puberty (see reference values of organ and tissue weights available in Valentin (2002)). Available data in the scientific literature (see Table 13) were used to derive correlations to estimate the values of cardiac output, blood volume, and most organs and tissues weights in pediatric patients via either linear or nonlinear regressions. With respect to muscles, bones, and skin weight, we used reference values (derived from data) available in Valentin (2002), while for the other variables actual data were available (see Table 13). For the sake of clarity, the organ and tissue weights in Table 13 were converted to volumes by considering the density values associated to the organs and tissues, available in Valentin (2002). When possible, we integrated data from different studies to improve the robustness of the proposed correlations. SEs associated to the regressed coefficients and R-squared values are provided in Paragraph 4B.7.1.

Table 13 – List of studies used as data sources for identification of correlations associated to pediatric subjects.

Individualized parameter	Data sources
Cardiac output	Williams (1994); Wu et al. (2016)
Blood volume	Brines et al. (1941)
Liver volume	Rylance et al. (1982)

Kidneys, spleen, heart, brain, weight	Valentin (2002)
Muscles, bones, skin weight	Valentin (2002)
Adipose tissue weight	Van der Sluis et al. (2002); Fomon et al. (1982); Schmidt et al. (2019); Marques-Vidal et al. (2008); López Sánchez et al. (2019)

Distribution of cardiac output to tissues and organs is also subject to variations with age (Fernandez et al., 2011). To account for these changes, the hepatic blood flowrate is scaled basing on the BSA of the patients (as in Johnson et al., 2005), whereas renal blood flow is 15 to 25% of cardiac output by one year of age and reaches adult values (*i.e.* about 25% of cardiac output in a healthy young adult (Stader et al., 2019)) after two years of age (Fernandez et al., 2011). As far as binding proteins concentration and hematocrit are concerned, pediatric patients show comparable values to adults after the first year of life (Anderson, 2012; Brines et al., 1941; Fernandez et al., 2011). Thus, the two related model parameters are kept unchanged compared to the PBPK model for adults.

In general, the activity of drug-metabolizing enzymes within the liver increases from birth and approaches adult values by 1–3 years of age (Lu and Rosenbaum, 2014; McLeod et al., 1992), while glomerular filtration of kidneys rapidly matures to adult levels within six months from birth (Anderson, 2012). To account for the differences associated to the drug elimination pathways and those related to the transport mechanisms, we identified the metabolic constants and drug transfer coefficients as adaptive parameters via a nonlinear regression with PK data of 16 patients from Kataria et al. (1994) (age range 3-11 y). The remaining patients of the study were used as validation cases of the identified PBPK model together with those from Marsh et al. (1991) (N = 37, age range 2-17 y).

4B.4 Methods: PD model identification

Schnider et al. (1998) showed age-dependent changes in the EEG traces of adults during anesthesia, and proved higher brain sensitivity in elderly patients, *i.e.* lower effect-site concentrations required to induce an adequate level of DoH. These results were also confirmed by other studies (Kreuer et al., 2005; Olmos et al., 2000). Indeed, the clinical practice confirms that propofol dosing requirements of elderly patients are lower than in younger patients. Age-related changes in the hypnotic effects of propofol

may be caused by the reduction of cerebral blood flow (CBF) and changes in the blood-brain barrier (BBB) permeability, which affect the two main steps of propofol transport to the site of action CNS, *i.e.* (i) convective transport via bloodstream to the brain and (ii) diffusion across BBB. Despite propofol high lipophilicity and thus its facilitated passage across BBB, PK studies in animals (Ludbrook et al., 1998) and humans (Peacock et al., 1995) investigating the velocity of equilibration of propofol concentration in plasma and jugular bulb, seem to suggest that propofol transport to brain cannot be assumed as actually blood-flow limited. Overall, the mechanism is still unclear and recent data and information on the topic lack, because of the difficulty and invasiveness of carrying out pharmacokinetic studies in the brain. For this reason, at this stage, we maintain the simplistic virtual effect-site approximation (see Chapter 3, Eq. (3.13)) to describe the pharmacokinetics of propofol in the effect-site. When more recent and mechanistic studies on propofol mechanism of transport to and within the brain are available, this section of the model will be modified according to a more physiological and individualized description of the associated transport phenomena. The dynamics of the effect as a function of the effect-site concentration is described via a modified E_{max} equation (see Chapter 3, Eq. (3.14)). However, to account for the effects of age on propofol pharmacodynamics, the EC_{50} parameter, which is the concentration that corresponds to 50% of the maximum drug effect, often used as a measure of drug potency, is reformulated as in Eq. (4B.4).

$$EC_{50} = EC_{50}{}'(-a\,age + b) \tag{4B.4}$$

By incorporating Eq. (4B.4) in the model we apply a correction factor to the EC_{50} parameter, so that the predicted brain sensitivity of the patient depends on age. Constants a and b (defined as positive values) are additional degrees of freedom in the PD model identification problem.

With respect to pediatric patients, Gregory and Andropoulos (2012) maintain that adult-children PK differences are more relevant than PD ones. However, studies show that children are more sensitive to the anesthetic effects (Jeleazcov et al., 2008; Liu et al., 2008; Munoz et al., 2004). In these studies, BIS is assumed as the clinical-endpoint to study the hypnotic effects of propofol. Main findings concern the T_{peak}, BIS_{LOC}, and BIS_{ROC} (ROC, return of consciousness) values. Specifically, Jeleazcov et al. (2008) and Munoz et al. (2004) both report lower values of T_{peak} than those of adults, whereas Liu et al. (2008) report that BIS_{LOC} and BIS_{ROC} are higher than in adults. In their TCI study, they used the same target concentrations but different PK

models for the children and adult groups. Since the EEG trace exhibits changes with age, *e.g.*, in the dominating rhythm and amplitude of the waves (this is true for both elderly (Kreuer et al., 2005) and pediatric patients (Constant, 2004)), age-related differences in BIS values of LOC and ROC are expected. For this reason, according to the findings of Jeleazcov et al. (2008) and Munoz et al. (2004), we consider Eq. (4A.5) within the effect-site compartment equation of the pediatric PBPK-PD model, to account for the influence of age on the transfer rate to the effect-site, in the range 1-19 y. In fact, the parameter k_{e0} defines the delay between the time course of plasma concentration and the manifestation of the drug effect. Constant c (defined positive) is an additional degree of freedom of the PD model identification problem associated to the considered age range. By including Eq. (4B.5) within the model, shorter time lags between the dynamics of the plasma and effect-site concentrations will be observed for younger patients. We do not include a dependence of k_{e0} on age in the adult PD model, because age was found not to influence the rate of effect change, when BIS was used as clinical end-point in adults (Kazama et al., 1999).

$$k_{e0} = k_{e0}' \exp(-c\, age) \qquad (4B.5)$$

For the sake of clarity, both the pediatric and adult models implement an assigned value of E_{max} equal to 0, which is consistent with the minimum value reached by BIS in clinical practice. Thus, E_{max} is not a degree of freedom of the identification problem.

To identify the PD models, *i.e.* for adult and pediatric patients, we used BIS data collected by Eleveld et al. (2018), who gathered them from a number of previously published studies. The sources of data, and the associated number and age range of patients are listed in Table 14. The available dataset was divided into two sub-groups of which the first was used for identification, and the second for validation purposes. Specifically, data of 5 patients from Coppens et al. (2011) were used for identification of the pediatric PD model, while data of 11 patients from Sahinovic et al. (2014) and Hannivoort et al. (2013) were used for identification of the adult PD model. RMSE, MDPE, and MDAPE values are provided for a quantitative evaluation of the model predictive performance, grounding on the BIS data of the additional patients involved in the studies.

Table 14 – Sources of the BIS data used for identification of age-dependent PD models, with associated number and age range of involved patients.

Study (# patients)	**Age [y] range**

Coppens et al. (2011), N = 28	3-11
Sahinovic et al. (2014); Hannivoort et al. (2013), N = 55	23-74

With respect to obese patients, Cortinez et al. (2014) and Van Kralingen et al. (2011) both studied the propofol PD in obese patients and did not find any significant influence of obesity on it. For this reason, the identified PD models account for neither TBW nor BMI, and we trust that the physiologically-based formulation allows describing ADME processes alterations associated to obesity and thus provides a satisfactory prediction of PK and related PD differences among healthy and obese individuals. Indeed, Eleveld et al. (2011) express the idea that PBPK modeling may be a more suitable approach to inform guidelines on propofol dosing in the obese population.

4B.5 Methods: *In silico* simulations of closed-loop controlled anesthesia

To test the controller behavior as a result of the proposed correlations and adaptive parameters, we carried out a number of *in silico* simulations of induction of anesthesia in the above-mentioned categories. At this stage, we focus on the control of the hypnotic effects, and thus only the propofol infusion rate is considered as manipulated variable. As in this chapter, BIS is the clinical endpoint of propofol hypnotic effects, the setpoint value is set at 50 [-]. For the sake of precision, this value is also appropriate for pediatric patients. In fact, firstly, although BIS is commercialized for use in adults, several studies investigated its application to pediatric patients (Coppens et al., 2011; Hsia et al., 2004; Louvet et al., 2016; Zhang et al., 2015). Secondly, despite the observed higher BIS_{LOC} values, Munoz et al. (2006) clearly state that it would be dangerous for pediatric patients to set the BIS target to values higher than 50 [-].

No substantial modifications to the formulation of the optimization problem were applied, compared to Chapter 3. Only, the iterative time interval t_s is set to 10 s, which is more suitable to guarantee a fast control action in “at-risk” categories. Both the prediction ($\mathrm{h_p}$) and control ($\mathrm{h_c}$) horizons are set via a trial and error procedure; suitable values were found to be 20 and 4 respectively. These values are multiples of the time length of control actions, t_s. The PBPK model is embedded both in the controller and in the virtual patients to describe the ADME processes undertaken by the administered

drug in the body, while the "mismatch" is maintained at the pharmacodynamic level. This choice is also justified by the fact that PD variability is more remarkable than PK variability (Levy, 1998). While the PK-PD model embedded in the MPC algorithm features the PD models identified as detailed in Section 4B.4, the patients PD models were identified via a nonlinear regression with BIS data of the individual patients that were not included in the identification dataset (Table 15 lists their demographic features). The two obese patients in Table 15 are the only exception, as they feature the same PD parameters of patient 7, but different demographic features. This approach is more useful to assess the influence of solely obesity on the control action, so that other factors (*e.g.*, age or inter-individual variability of the BIS data associated to drug-independent factors) do not affect the *in silico* simulation. Note that, since the BMI classification was developed for adults, no BMI value is provided for the listed pediatric patients in Table 15. Regardless, healthy children were considered in the simulations.

For a realistic simulation, noise is also simulated, based on clinical data analysis (the same method as the one reported in Chapter 3, Paragraph 3.4.3 was used).

Table 15 – Demographics of the simulated patients to test the effect of aging, growth, and obesity on the control action on propofol hypnotic effects.

Patient #	TBW [kg]	H [cm]	Gender [-]	Age [y]	BMI [kg/m^2]
1	16	99	F	3	-
2	20	116	M	6	-
3	29	133	M	9	-
4	41.5	149.8	F	12	-
5	56.0	170.1	M	15	-
6	79.5	165	F	25	29.2
7	66	181	F	36	20.14
8	67	157	F	60	27.18
9	72	165	M	73	26.4
10	106	181	F	52	32 (class I)
11	166	181	F	58	50.67 (class III)

4B.6 Methods: *In silico* comparison with the state-of-the-art techniques of TIVA delivery

A final *in silico* experiment concludes the chapter, and consists in comparing the closed-loop controlled infusion rates during propofol induction in a young patient (3 y old, see Table 15) with those resulting from (i) the manual infusion regimen proposed by McFarlan (McFarlan et al., 1999) (*i.e.* 2.5 mg/kg bolus followed by 250 µg/kg/min for the first 15 min, suitable for the 3-11 y age range) and Target-Controlled Infusions (TCIs) obtained with both the (ii) Paedfusor (Absalom and Kenny, 2005) and (iii)

Kataria (Kataria et al., 1994) algorithms. The goal was to compare the performances of both our closed-loop controller and the state-of-art techniques in TIVA delivery. In our comparison, TCI infusion rates were simulated with the TivaTrainer software (available at: https://www.eurosiva.eu/tivatrainer/TTweb/TTinfo.html). We implemented a target plasma concentration equal to 3 µg/mL, which is adequate to induce anesthesia in a 3-y-old patient (as in Gaynor and Ansermino (2016)).

Finally, we used the PBPK- (individual) PD model of the 3-y-old patient to simulate the resulting BIS, plasma, and effect-site concentration dynamics as a result of the infusion rates obtained via (i) closed-loop controlled, (ii) manual, and (iii) TCI induction.

4B.7 Results and discussion: PBPK-PD model changes

4B.7.1 Effect of growth stage and obesity on individualized parameters

Table 16 shows the derived equations for estimation of the individualized parameters associated to obesity. A limitation of the study is that in some cases it was not possible to base the correlations on BMI, but only on TBW because of the scarcity in experimental data (see Table 16). BMI accounts for both the height and TBW of the patient, and thus, the BMI-based equations include height as covariate, which is important to establish whether a patient falls in the classification of obese individuals. Depending on the available data, gender-specific differences were included in the derived equations.

With regard to the increase of CO, blood volume, and most organs and tissues associated to obesity, we assumed that the steepness of the increase is reduced for high values of BMI or TBW. We looked for a suitable mathematical formulation to represent this behavior. This feature also allows avoiding non-physical (*i.e.* too high, inconsistent) values in case of extrapolation to BMI > 60 [kg/m^2] and TBW > 200 [kg], for which data are limited or lacking. The mathematical formulation in Table 16 was found suitable in most cases, as the nonlinear regression procedure provided acceptable values of R-squared and low values of the parameters' SEs. However, in case of the derived correlation that evaluates the heart weight, a linear model provided a better fitting of experimental data. Rather low values of R-squared are found for computation of (i) kidneys weight (male model), (ii) spleen weight, and (iii) muscles weight (male model). Male kidneys and muscles weight data are quite sparse (Figure

15 (bottom panel)). Spleen weight data are also quite sparse, and an actual trend is difficult to detect. Actually, data show something more similar to a constant value in the range 0.2-0.4 kg. The resulting model is in fact rather flat. Nevertheless, these quantities are all lumped in the Highly perfused Organs and Poorly perfused Tissues compartment volumes, which means that the impact of spleen weight is rather low. The available equations in the literature provide similar values of R-squared for kidneys and spleen weights (Young et al., 2009). Further (less scattered) data and different mathematical formulations may improve fitting.

Table 16 – Derived correlations for estimation of the individualized parameters in obese patients (SE = standard error associated to the regressed coefficients).

Parameter [un. of measure]	**Model**	**Coefficients (SE)**	**R^2**
Cardiac output [L/min]	$a\exp\left(\frac{b}{BMI}\right) f_{age}$	$a_M = 13.55(0.50)\ a_F = 10.22(0.26)$ $b_M = -14.79(1.02)\ b_F = -16.04(0.72)$ $f_{age,M} = -0.01age + 1.3$ $f_{age,F} = -0.005age + 1.15$	M: 0.55 F: 0.76
Blood volume [L]	$a\exp\left(\frac{b}{TBW}\right)$	$a = 10.71(0.68)\ b = -56.05(7.79)$	0.56
Liver volume [L]	$a\exp\left(\frac{b}{BMI}\right)$	$a_M = 3.58(0.14)\ a_F = 2.83(0.11)$ $b_M = -21.83(1.10)\ b_F = -19.12(1.00)$	M: 0.71 F: 0.81
Kidneys weight [kg]	$a\exp\left(\frac{b}{TBW}\right)$	$a_M = 0.97(0.43)\ a_F = 0.72(0.097)$ $b_M = -83.29(53.17)\ b_F = -82.15(15.59)$	M: 0.08 F: 0.46
Spleen weight [kg]	$a\exp\left(\frac{b}{TBW}\right)$	$a = 0.28(0.045)\ b = -25.72(12.14)$	0.06
Heart weight [kg]	$a + b\,TBW$	$a_M = 0.246(0.019)\ a_F = 0.249(0.014)$ $b_M = 0.23e-2\ (0.22e-3)\ b_F = 0.15e-2(0.18e-3)$	M: 0.40 F: 0.29
Adipose tissue weight [kg]	$a\exp\left(\frac{b}{BMI}\right)$	$a_M = 438.31(25.53)\ a_F = 242.96(8.26)$ $b_M = -86.81(2.03)\ b_F = -62.88(1.30)$	M: 0.92 F: 0.96
Muscles weight [kg]	$a\exp\left(\frac{b}{TBW}\right)$	$a_M = 56.68\ (10.73)\ a_F = 46.50(7.47)$ $b_M = -45.53(21.03)\ b_F = -63.98(15.95)$	M: 0.1 F: 0.32

CO and blood volume are key determinants of drugs disposition within both the body

and the resulting PK profile. Figure 13 and Figure 14 show CO and blood volume data against proposed correlations for their estimation. In case of CO, the model was estimated basing on data of young adults (aged 30 y) from Hinderliter et al. (2011) (see Figure 13, circles in blue and pink colors referred to male and female individuals, respectively). A correction factor allows accounting for the effect of age (see Table 16) and is based on Stader et al. (2019), who report that CO decreases by 5-10% every age decade. However, it is worth mentioning that the majority of obese patients undergoing surgery are younger than 60 y (Servin, 2017).

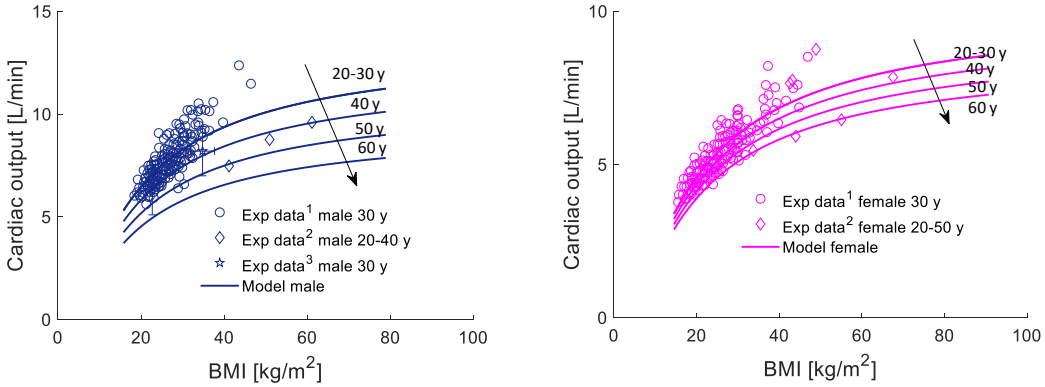

Figure 13 – Estimated (continuous line) vs measured (circles, diamonds, stars) CO as a function of BMI. Correlations and data are in blue for males and in pink for females. The black arrow points in the direction of increasing age. Different numbers in the legend refer to different data sources.

Figure 14 shows the model-predicted blood volume vs experimental values. Unfortunately, it was not possible to find gender-specific data, because a mixed group of patients was involved in the considered studies (references reported in Table 11). Nevertheless, the model provides a satisfactory goodness-of-fit.

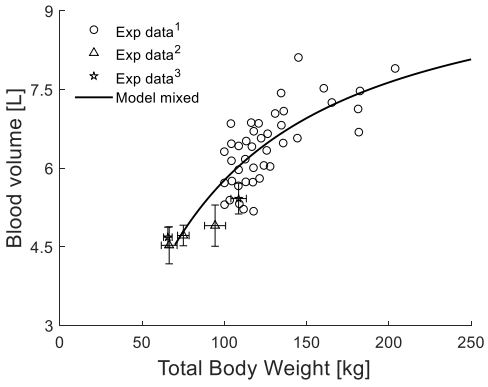

Figure 14 – Estimated (continuous line) vs measured (circles, triangles) blood volumes as a function of TBW. The correlation and data are gender-neutral. Different numbers in the legend refer to different data sources.

Some of the correlations in Table 16 are also presented in Figure 15, specifically those

for liver volume and adipose tissue weights (top panel) and kidneys and muscles weights (bottom panel). It is worth noticing that in case of adipose tissue weight, a gender-neutral correlation (black line) is proposed for BMI > 40 [kg/m^2]. In fact, on one hand, few data associated to male individuals were available for BMI > 50 [kg/m^2], and thus the derived correlation might be biased. On the other hand, we find reasonable to assume that for very high BMI values, gender differences do not affect the weight of the adipose tissue significantly.

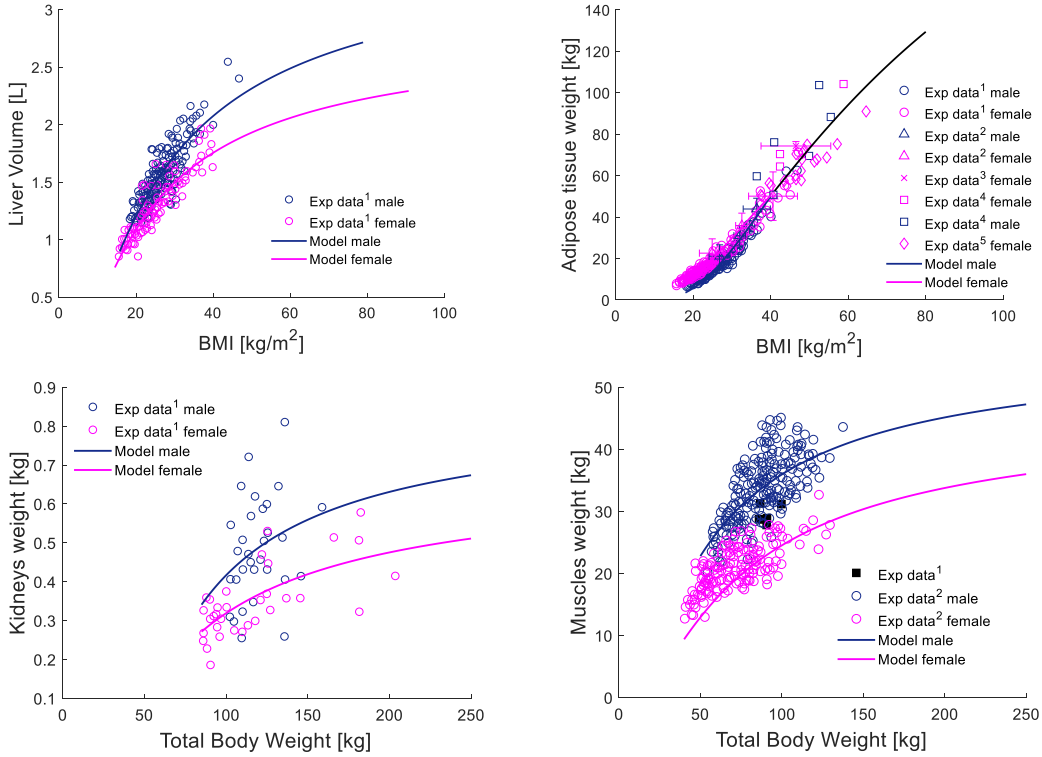

Figure 15 – Estimated (continuous line) vs measured (circles, triangles, squares, diamonds, and crosses) liver volume and adipose tissue weight (top panel) as a function of BMI and heart and kidneys weights (bottom panel) as a function of TBW. Correlations and data are in blue for males and in pink for females, while black color denotes a gender-neutral correlation. Different numbers in the legend refer to different data sources.

Table 17 shows the proposed correlations for the pediatric population. While for some parameters the data trend flattens after puberty (about 11-12 y) (*e.g.*, brain and tissues weights), in other cases, a constant increase with age can be observed (some organs weights, *e.g.*, kidneys, heart, and spleen). For this reason, different mathematical models are proposed, depending on the one that provides best data fitting. With respect to the bones, muscles, and skin weight correlations, they are suitable for age > 3 y, while in the 1-3 y range, fixed values available in Valentin (2002) are used. A limitation of these correlations is that they only depend on age, whereas TBW or BSA

should definitely play a role in computing the bones, muscles, and skin weights. This limitation is related to the available data in the scientific literature and should be addressed in future work, when additional and more complete datasets are available, to increase model accuracy and degree of individualization. In any case, it is also worth mentioning that these parameters are lumped together within the compartment of Poorly perfused Tissues, along with the adipose tissue.

Figure 16 shows CO and blood volume predictions (left and right panel, respectively) against experimental data. For CO, a correlation depending on TBW was also considered, but the one proposed in Table 17 provided a better fitting, despite the data dispersion from Williams (1994) (blue and pink stars in Figure 16 (left panel)). It is also worth noticing that no gender differences were evident below 7 y (indeed, we show a continuous gender-neutral black line in Figure 16). Actually, for both CO and blood volume, gender-differences are mainly evident after 12 y (puberty). The correlation for estimation of blood volume depends on BSA (see Table 17). Similarly, blood volume correlations as a function of age and TBW were also tested on the same datasets, as complete demographic data, *i.e.* TBW, height, age, and gender were all available (see Brines et al. (1941)). The proposed one produced better results in terms of R-squared value. Blood volume prediction is validated with data from Williams (1994) (blue and pink stars in Figure 16, right panel). The dependence on BSA is the reason for the "broken" trend of the model-simulated blood volume. Indeed, blood volume is displayed as a function of age in Figure 16, but calculated basing on BSA, with body mass and height from charts referred to "standard" pediatric patients (available at https://www.disabled-world.com/calculators-charts/height-weight-teens.php). BSA was calculated via DuBois and DuBois formula (Du Bois and Du Bois, 1916).

Table 17 – Derived correlations for estimation of the individualized parameters in pediatric patients (SE = standard error associated to the regressed coefficients).

Parameter [un. of measure]	**Model**	**Coefficients (SE)**	**R^2**
Cardiac output [L/min]	$a + b\,age + c\,age^2$	$a_M = 1.12\,(0.55)$ $a_F = 1.66\,(0.52)$ $b_M = 0.508\,(0.08)$ $b_F = 0.42\,(0.09)$ $c_M = -0.0112\,(0.0028)$ $c_F = -0.0102\,(0.0035)$	M: 0.48 F: 0.43

Blood volume [L]	$a\exp(bBSA)$	$a_M = 0.530(0.061)\ a_F = 0.421(0.045)$ $b_M = 1.286(0.076)\ b_F = 1.408(0.077)$	M: 0.95 F: 0.95
Liver volume [L]	$a_1\exp(-b_1 age)TBW \quad age < 12y$ $a_2 BSA^{1.176} \quad age \geq 12y$	$a_1 = 0.399(2.26e{-}3)\ a_2 = 0.722(-)$ $b_1 = 0.032(0.007)$	0.57
Kidneys weight [kg]	$a + b\,age$	$a_M = 5.707e{-}2(4.97e{-}3)\ a_F = 5.570e{-}2(5.35e{-}3)$ $b_M = 1.227e{-}2(0.40e{-}3)\ b_F = 1.179e{-}2(0.42e{-}3)$	M: 0.97 F: 0.97
Spleen weight [kg]	$a + b\,age$	$a = 2.417e{-}2(5.12e{-}3)\ b = 6.63e{-}3(0.41e{-}3)$	0.84
Heart weight [kg]	$a + b\,age$	$a = 0.056(2.45e{-}2)\ b = 1.147e{-}2(1.89e{-}3)$	0.60
Brain weight [kg]	$a\exp\left(\frac{b}{age}\right)$	$a_M = 1.492(1.52e{-}2)\ a_F = 1.362(1.543e{-}2)$ $b_M = -0.42(0.053)\ b_F = -0.36(0.040)$	M: 0.79 F: 0.82
Muscles weight [kg]	$ref.\ from\ Valentin\ et\ al.(2002) \quad age \leq 3y$ $a\exp\left(\frac{b}{age}\right) \quad age > 3y$	$a_M = 43.444(6.892)\ a_F = 23.210(2.979)$ $b_M = -11.169(2.595)\ b_F = -6.723(1.699)$	M: 0.95 F: 0.95
Bones weight [kg]	$ref.\ from\ Valentin\ et\ al.(2002) \quad age \leq 3y$ $a\exp\left(\frac{b}{age}\right) \quad age > 3y$	$a_M = 14.819(1.964)\ a_F = 10.304(1.484)$ $b_M = -10.265(2.091)\ b_F = -7.194(1.957)$	M: 0.96 F: 0.93
Skin weight [kg]	$ref.\ from\ Valentin\ et\ al.(2002) \quad age \leq 3y$ $a\exp\left(\frac{b}{age}\right) \quad age > 3y$	$a_M = 5.744(1.129)\ a_F = 3.331(0.671)$ $b_M = -16.655(3.822)\ b_F = -11.211(3.299)$	M: 0.94 F: 0.91
Adipose tissue weight [kg]	$(a + b\,age + c age^2)TBW$	$a_M = 0.28(0.12)\ b_M = -0.05(0.088)$ $c_M = 3.5e{-}3(0.014) \quad age \leq 5y$ $a_M = 0.017(0.048)\ b_M = 0.023(8.2e{-}3)$ $c_M = 9.1e{-}4(3.2e{-}4) \quad 5 < age < 19y$ $a_F = 0.25(0.12)\ b_F = -0.018(0.087)$ $c_F = 4e{-}4(0.014) \quad age \leq 5y$ $a_F = 0.097(0.28)\ b_F = 0.02(0.077)$ $c_F = -9.6e{-}4(5.2e{-}3) \quad 5 < age \leq 10y$ $a_F = 0.067(0.2)\ b_F = 0.017(0.03)$ $c_F = -4e{-}4(9e{-}4) \quad 10 < age < 19y$	M: 0.31, 0.04 F: 0.19, 0.02, 0.04

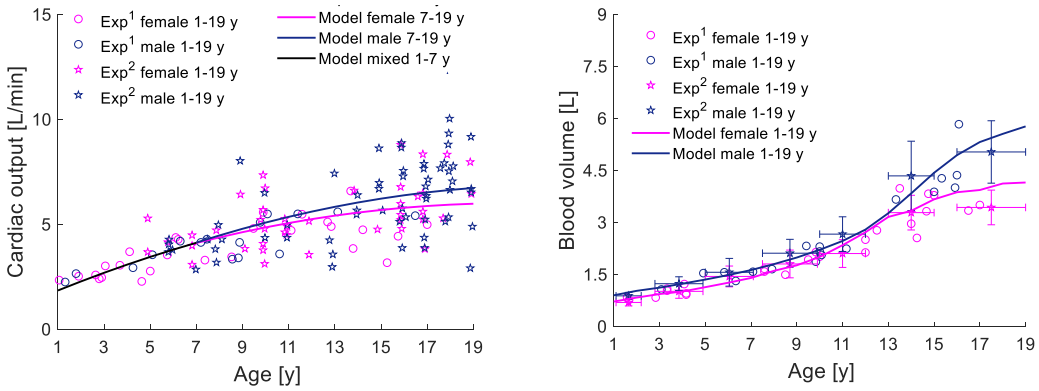

Figure 16 – Estimated (continuous line) vs measured (circles, stars) CO (left panel) and blood volume (right panel) as a function of age in the range 1-19 y. Correlations and data are in blue for males and in pink for females, while black color (see cardiac output) indicates a gender-neutral correlation. Different numbers in the legend refer to different data sources.

Figure 17 shows some of the regressed correlations against experimental data used for identification, specifically for brain weight and liver volume (top panel) and kidneys weight and adipose tissue fraction (bottom panel). For consistency with the trend of the experimental data, two different correlations are reported to calculate the liver volume (see also Table 17). The correlation in the age range 12-19 y is from Johnson et al. (2005). This correlation was tested with data in the lower age range, evidencing poor predictive performance. Thus, data from Rylance et al. (1982) were used to identify a different correlation, as a function of age and TBW. The advantage of implementing a correlation with BSA (Johnson et al., 2005) in the age interval spanning from puberty to young adulthood is that adolescents can be characterized by important inter-individual differences in TBW and height values.

R-squared values shown in Table 17 are quite satisfactory in most cases, except for the adipose tissue weight correlation (see also Figure 17 (bottom panel)). Different sources were used for the data, also including both lean and overweight individuals from different countries (see Table 11 for references). It is evident that a remarkable variability can be found in the adipose tissue fractional weight with age, and, for this reason, the correlation does not provide a higher R-squared value. In addition, it was necessary to separate the range 1-19 y in sub-ranges to obtain an acceptable fitting of data. It is also worth noticing that, differently from all the other anatomical parameters, the adipose tissue fractional weight is higher for female than male patients across the 1-19 y age range, and that males exhibit a peak during adolescence (12-15 y).

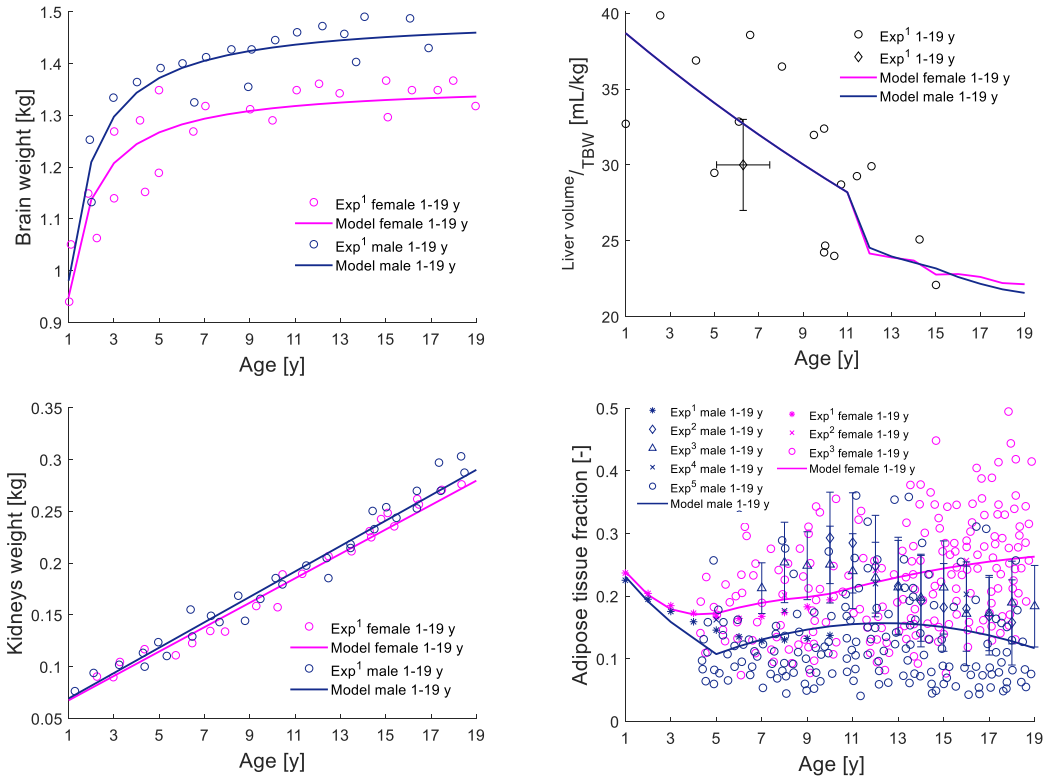

Figure 17 – Estimated (continuous line) vs measured (circles, diamonds, asterisks, and crosses) brain weight and liver volume (top panel) and kidneys weight and adipose tissue fractional weight (bottom panel) as a function of age in the 1-19 y range. Correlations and data are in blue for males and in pink for females. Different numbers in the legend refer to different data sources.

4B.7.2 Prediction of pharmacokinetics

In Figures 18, 19, 20, and 21, A panels refer to elderly patients, B panels to obese patients, and C panels to pediatric patients. Figures 18, 19, and 20 show the diagnostic plots associated to the identification (cyan dashed lines, pink diamonds) and validation (blue lines, red diamonds) of the adapted PBPK model referred to elderly, obese, and pediatric patients, respectively. Figure 21 shows the best, median, and worst validation cases associated to the three investigated categories. Table 18 reports MDPE and MDAPE values associated to validation cases of the PBPK, Schnider, and Marsh models.

Figure 18 (top panel, Schnider dataset) shows an overall satisfactory identification result, although there is space for improvement of the early concentration dynamics. Being an IV drug, propofol is directly administered into the systemic circulation. Thus, blood volume and protein binding fraction are major determinants of the earliest phase of the concentration – time curve. The employed correlation for estimation of blood volume is from Stader et al. (2019) and accounts for the whole age range 20-99 y. It is likely that the introduction of a specific correlation for the age range of elderly

patients (> 55-60 y) could improve the results. In addition, as propofol is highly bound to plasma proteins (albumin), age-related changes in protein binding, may be a contributing factor that would allow adjusting the model prediction in the early phase (*e.g.*, albumin levels decrease with age (Grandison and Boudinot, 2000)). In fact, at this stage, protein binding fraction is an assigned parameter and this aspect should be further investigated to improve the model prediction. In Figure 18 (bottom panel, Dyck dataset) the model shows both positive and negative bias in the early concentration-time curve, while overestimation in the distribution/elimination phase of propofol can be observed. It is worth underlining that some peculiarities in the pharmacokinetic data of Dyck dataset were underlined by Coetzee et al. (1995), *i.e.* inconsistencies with other PK data from similar studies. Indeed, in Dyck and Shafer (1992) most blood samples were obtained up to 19 h after a 10-min IV propofol infusion. This means that most values refer to propofol sub-anesthetic concentrations. Despite this peculiarity, the MDPE and MDAPE values and PBPK predictive performance in the three cases displayed in Figure 21 (A panel) are acceptable, although they would likely be superior if propofol concentrations were evaluated only during the maintenance and early elimination phases of the infusion. Not only MDPE and MDAPE values are within the acceptable range, but also comparable to or better than those obtained from simulation of the patients with the most used classical PK models (see Table 18). Marsh model shows the worst accuracy, since it does not include age as covariate.

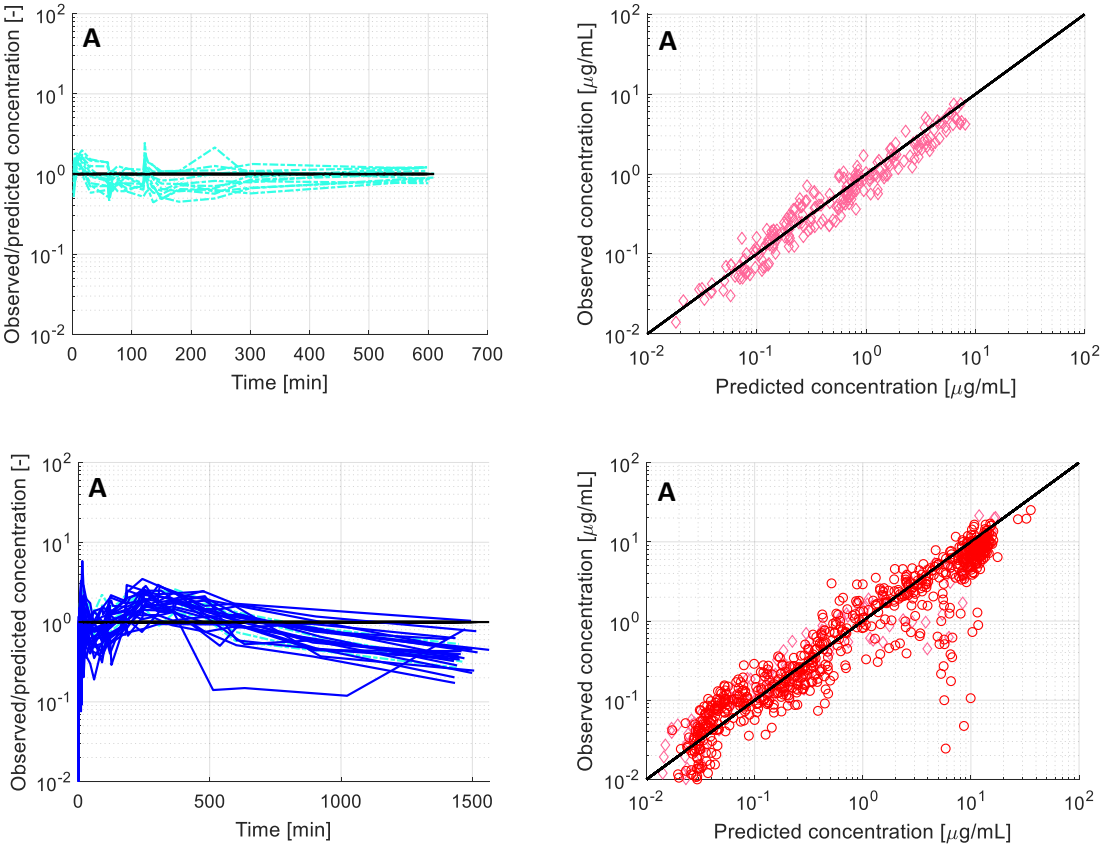

Figure 18 – Individual PBPK model predictions for elderly patients vs time (left panel) and measured propofol concentrations (right panel). Cyan dashed lines and pink diamonds are associated to data used for identification, while continuous blue lines and red circles are associated to the validation cases. Observed concentrations are from Schnider et al. (1998) (top panel) and Dyck and Shafer (1992) (bottom panel).

With respect to obese patients, Figure 19 (top panel) shows the identification results with data from Servin et al. (1993) and Figure 19 (bottom panel) shows identification and validation results with data from Cortinez et al. (2010). Servin dataset showed a remarkable inter-patient variability and although blood samples were frequent, measured concentrations were quite dispersed. One of the patients manifested rather low values of concentration compared to the other subjects of the group. Despite this, the identification results are quite satisfactory (see cyan dashed lines in Figure 19 (left panel) and pink diamonds (right panel)). Validation results are acceptable as well, see Figure 19 (bottom panel). In about 6 patients from Cortinez et al. (2010), the model underestimates the measured values of concentration during the elimination phase. Two of these are shown in Figure 21 (B panel) as they resulted the median and worst cases, basing on model accuracy. This behavior of the model is not manifested in the elimination phase of Servin dataset. More focus should be devoted to the hepatic blood flow in obese patients, on which propofol clearance from the body mainly

depends. In obese patients, this flow is increased because of increased CO and liver volume (hence number and size of parenchymal cells). Indeed, maintenance propofol infusion rates are usually scaled on TBW rather than Lean Body Weight (LBW), as opposed to the induction dose (Servin, 2017). The BMI range for both studies is 30-50 [kg/m^2], thus the reason for the different model behavior should not be related to differences in the obesity degree between the study groups. A potential explanation may be related to the fact that obesity is often associated with liver pathological conditions (*e.g.*, hepatic steatosis or "fatty" liver[13]) which may alter and reduce the liver function (Servin et al., 1993).

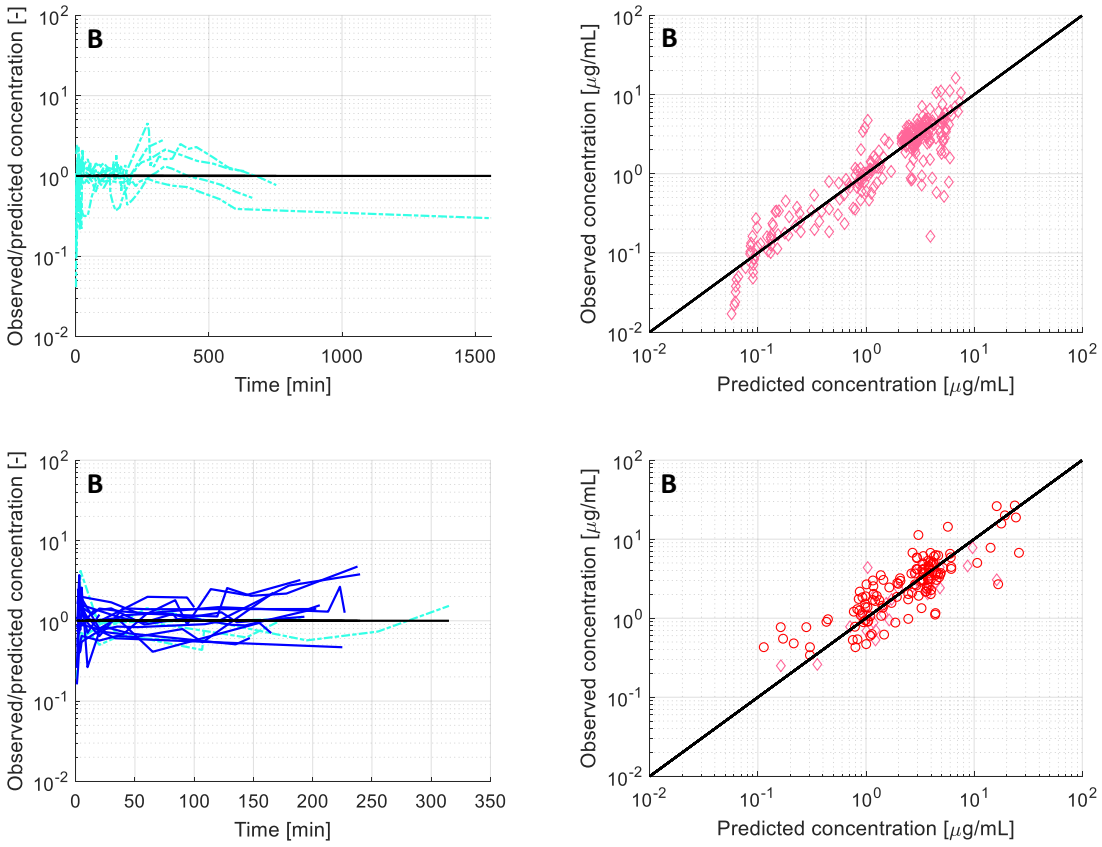

Figure 19 – Individual PBPK model predictions for obese patients vs time (left panel) and measured propofol concentrations (right panel). Cyan dashed lines and pink diamonds are associated to data used for identification, while continuous blue lines and red circles are associated to validation cases. Observed concentrations are from Servin et al. (1993) (top panel) and Cortínez et al. (2010) (bottom panel).

These pathologies may have been present in some of the patients studied by Cortinez et al. (2010), and this could explain the different model trends in the elimination phases, as absence of such diseases was not mentioned in the exclusion criteria of the study. Additional PK data corroborated with information about co-pathologies of

[13] Large droplets of fat accumulate within the liver cells, compromising the liver function in the long-term, if no treatment is applied (https://medical-dictionary.thefreedictionary.com/fatty+liver).

obese patients will be needed to verify whether the hepatic metabolism description of the proposed PBPK model should be improved. In any case, the model prediction is overall acceptable (see validation results in terms of MDPE and MDAPE in Table 18) and especially, improved compared to Schnider and Marsh models.

Figure 20 shows the diagnostic plots associated to Kataria (top panel) and Marsh dataset (bottom panel). The model prediction is quite satisfactory. A larger deviation of the model from the measured concentrations can be observed in the central part of Figure 20 (top panel) (*i.e.* concentration range 0.6-3 µg/mL), corresponding to model underestimation in the elimination phase of patients administered with either double or single infusions. In some of these cases from Kataria et al. (1994) (*e.g.*, see worst case presented in Figure 21, C panel), the trend of experimental data suggests a possible mistake in the reported duration time of the second infusion. If this is true and there is a mistake in the information associated to the PK data, this may partially cause a poor model prediction. It is worth noticing that, despite the identification dataset belongs to patients aged 3 to 11 y, the anatomical/physiological foundation of the PBPK model ensures a satisfactory prediction in patients of different age ranges, including adolescents (see bottom panel of Figure 20, in which age range is 2-17 y). Indeed, MDAPE associated to the PBPK model prediction of measured concentrations from Marsh et al. (1991) is mean 22.04 (SD = 13.72) %. It is also worth mentioning that, in this study, blood samples were obtained starting from the maintenance phase and during the early end-of-infusion phase.

In Table 18, we show the MDPE and MDAPE values compared to those obtained via Marsh pediatric model and Schnider adult model. Indeed, Marsh pediatric model showed the best predictive performance among the most used pediatric three-compartment PK models (see Coppens et al. (2011)). The PBPK model performance in terms of MDAPE is better than Marsh pediatric model and shows a similar bias (see MDPE values). Interestingly, Rigouzzo et al. (2010) proved that the best PK-PD model, identified via regression with PD data, was the one obtained by using Schnider PK model for adults. In Table 18, MDAPE associated to Schnider model is over 35%.

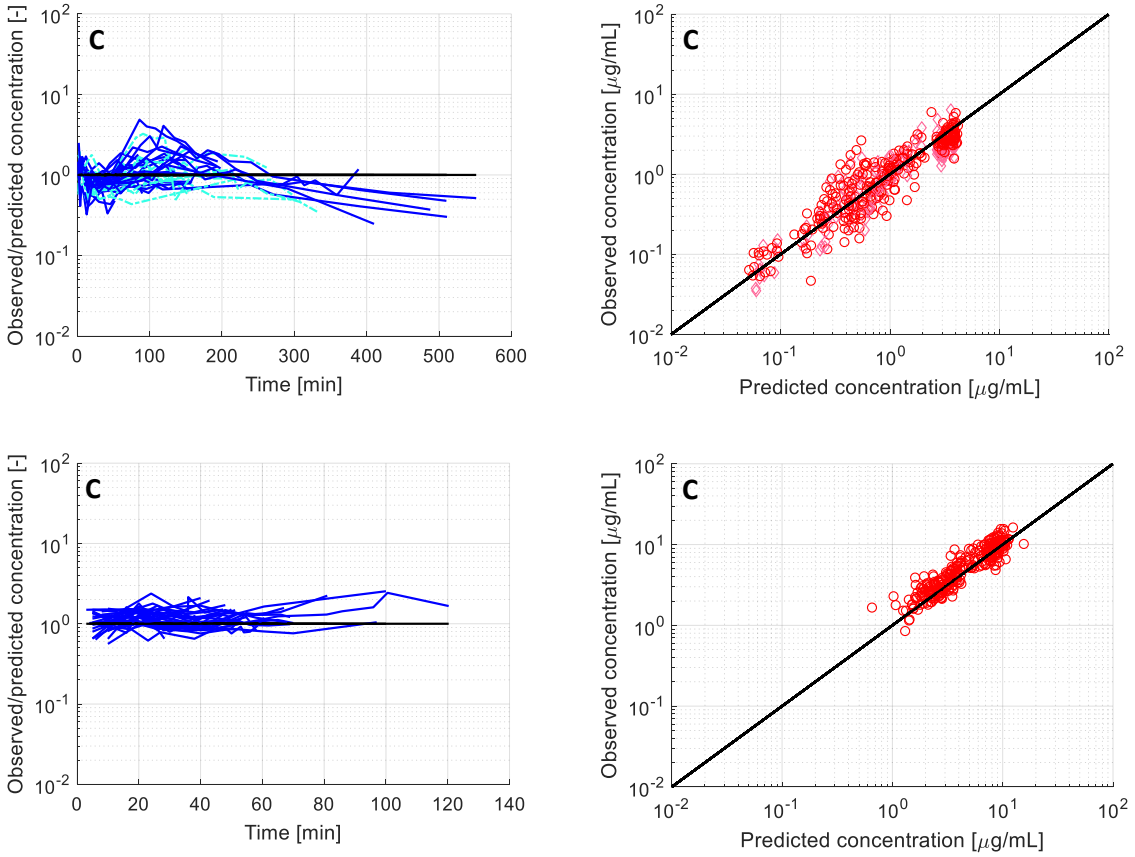

Figure 20 – Individual PBPK model predictions for pediatric patients vs time (left panel) and measured propofol concentrations (right panel). Cyan dashed lines and pink diamonds are associated to data used for identification, while continuous blue lines and red circles are associated to the validation cases. Observed concentrations are from Kataria et al. (1994) (top panel) and Marsh et al. (1991) (bottom panel).

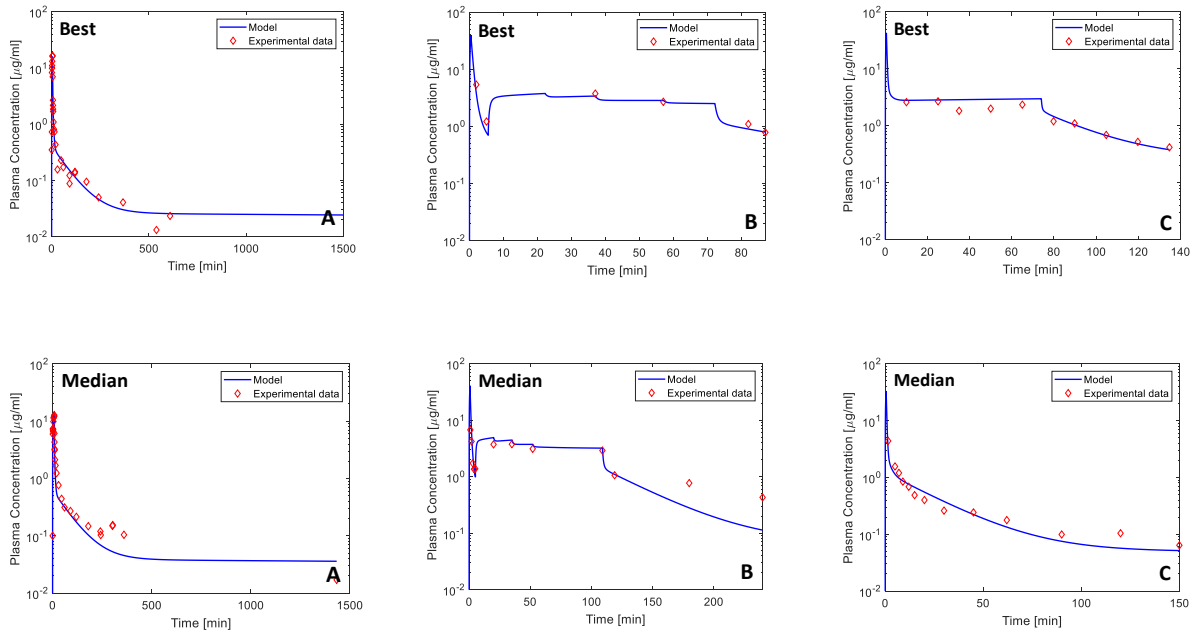

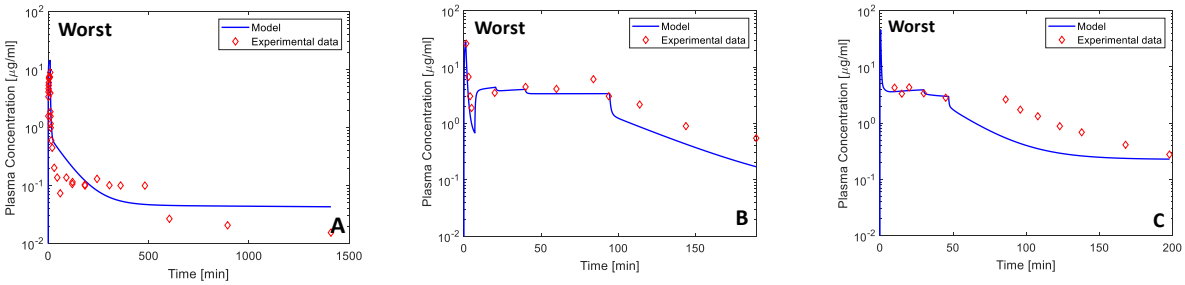

Figure 21 – Best, median, and worst validation cases according to model accuracy. The blue continuous line represents model-predicted concentration, red diamonds are individual propofol concentrations. Panel A refers to elderly patients (data from Dyck et al. 1992), panel B refers to obese patients (data from Cortinez et al. 2010), and panel C refers to pediatric patients (data from Kataria et al. (1994)).

Table 18 – MDPE and MDAPE values referred to the validation of the PBPK, Marsh, and Schnider models are provided as mean (SD) for the different populations.

CATEGORY	MDPE% PBPK	MDPE% MARSH	MDPE% SCHNIDER	MDAPE% PBPK	MDAPE% MARSH	MDAPE% SCHNIDER
Pediatric[14] (n = 21, Kataria et al. 1994)	0.33 (25.35)	15.65 (25.93)	-0.05 (29.84)	28.79 (11.67)	31.12 (10.26)	36.45 (15.47)
Elderly (n = 25, Dyck and Shafer (1992))	-13.5 (22.25)	25.75 (38.87)	-4.66 (23.58)	34.40 (8.21)	59.95 (19.81)	33.41 (11.35)
Obese (n = 14, Cortinez et al. (2010))	-11.82 (38.01)	0.72 (34.05)	-22.40 (39.56)	35.94 (22.65)	38.33 (12.87)	43.25 (20.79)

4B.7.3 Prediction of pharmacodynamics

Table 19 reports RMSE, MDPE, and MDAPE values associated to the validation of the combined PBPK-PD model in adult and pediatric patients. Figure 22 and Figure 26 show the diagnostic plots associated to the validation cases and Figure 23 reports best, median, and worst validation cases basing on model accuracy. A panels refer to adult-elderly patients, whereas C panels refer to pediatric patients.

With respect to adult patients, BIS data used to identify and validate the adult PD model are from (i) Sahinovic et al. (2014) and (ii) Hannivoort et al. (2013). In Sahinovic et al. (2014), induction was achieved via propofol IV infusion at a constant rate of 100

[14]In case of pediatric patients, Marsh pediatric model is used for comparison of predictive performance.

mL/h in 40 patients, *i.e.* 20 control patients and 20 with brain frontal tumor. We consider data of patients from both groups, because no significant differences induced by the tumor were found in the BIS profiles and general response to anesthesia. After 15 min from LOC, Sahinovic et al. (2014) induced a noxious stimulus (30 s duration) to study the patients' response to the disturbance. For the sake of clarity, since our aim was to model the dose-effect relation, we considered BIS data previous to the stimulus and related BIS changes. In Hannivoort et al. (2013), BIS was monitored in 15 patients receiving propofol at a constant rate of 40 mg/kg/h. The infusion was stopped once maximum burst-suppression was observed, and BIS was recorded until ROC. Data of 44 patients from the two studies were used for validation of the PBPK-PD model. Reported values of RMSE, MDPE, and MDAPE in Table 19 show an acceptable predictive performance.

Table 19 – RMSE, MDPE, and MDAPE values referred to the validation of the PBPK-PD adult and pediatric models.

CATEGORY	RMSE [-]	MDPE%	MDAPE%
Adults (N = 44)	12.94 (4.03)	2.68 (22.65)	24.06 (10.96)
Pediatric (N = 23)	9.62 (1.93)	1.40 (15.92)	20.98 (15.92)

However, it should be noted that data were quite noisy and more affected by disturbances than pediatric patients' BIS data. This feature is also reflected in the diagnostic plots associated to all the validation cases, shown in Figure 22. Figure 22 (bottom panel) shows the data that were clearly affected by noise and external drug-independent disturbances in green (left) and yellow (right). If data are processed by removing the parts in which they are quite clearly affected by external disturbances (see for instance median case provided in Figure 23, A panel), the RMSE and MDAPE values are reduced to mean (SD) 21.14 (9.94)% and 10.91 (3.87) [-]. In a related way, the worst case in Figure 23 (A panel) is affected by a disturbance after approximately 2.5 min from start of induction, and a constant disturbance can be observed after 5 min until the end of the data series. This kind of data trends certainly affected the quantification of the model predictive performance. It is also worth mentioning that in several cases, the first BIS measures were probably affected by the emotional state of the patients (*e.g.*, anxiety, concern, fear) and a delayed response to induction could be observed (see observed vs predicted BIS values in top right area of Figure 22, right panel). In addition, in some cases, the first BIS measure was available 30+ s after

induction of anesthesia, which made the baseline value uncertain, and affected the trend of the model-predicted curve (see for instance the median case in Figure 23, A panel). Another interesting point is that, in some cases, the model is not able to predict extremely deep levels of anesthesia (BIS < 20 [-], see observed vs predicted BIS in the bottom left area of Figure 22, right panel). For the sake of clarity, Figure 24 shows three of these cases. It is worth noticing that the model actually predicts high values in plasma (see bottom panel, red continuous lines) but the velocity of the effect-site concentration (blue continuous lines) does not allow predicting such low BIS levels. The enhanced sensitivity to propofol cannot be ascribed to age, as two of the patients in which these levels are reached are quite young (*i.e.* 31 and 43 y). A more detailed analysis of the reasons why burst suppression occurs could be made basing on hemodynamic data (*e.g.*, hypotension and CO drops might produce alterations of propofol transport to brain and low BIS values, as discussed in Chapter 4A), but such complementary bits of information were not available. However, a more physiological description of propofol brain transport corroborated by real-time data on arterial pressure and CO might lead to improvements in the prediction of this behavior. These results and those presented in Chapter 4A certainly prove the importance of focusing on these aspects in future works. Some further considerations will be discussed in Chapter 5.

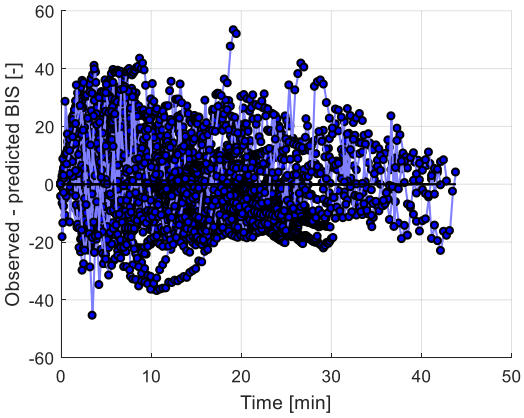

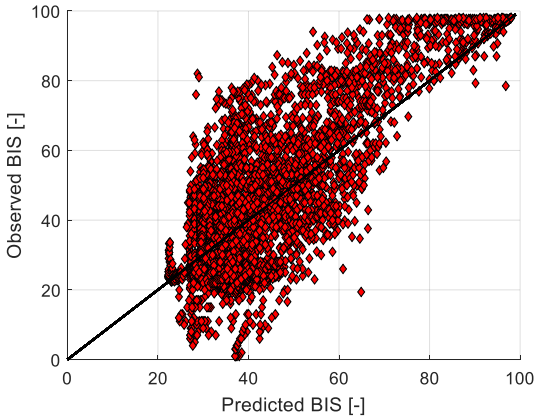

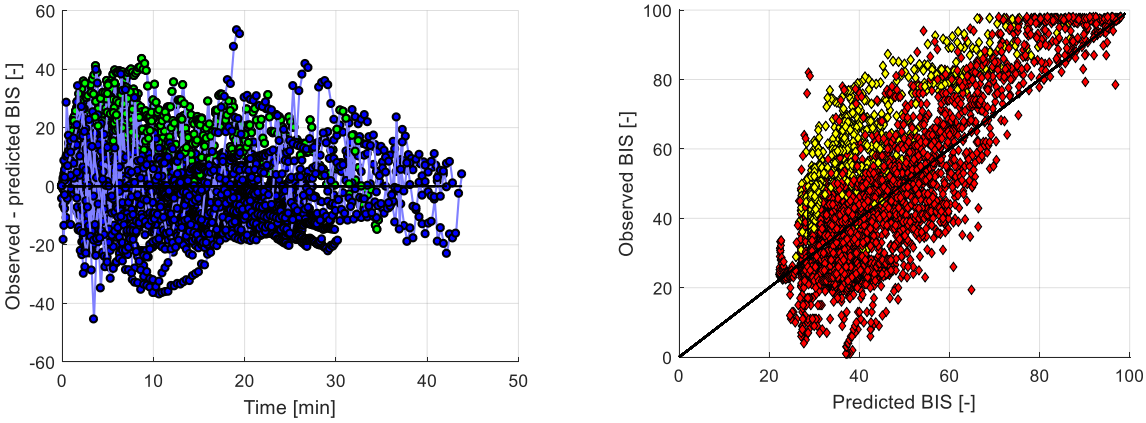

Figure 22 – Diagnostic plots associated to the validation cases of the combined PBPK-PD model in adult patients. (Left panel) Individual BIS observations – predictions vs time. (Right panel) Individual BIS observations vs predictions. In bottom panel, the presence of BIS measurements affected by external disturbances are highlighted in green (left panel) and yellow (right panel).

Regardless, the adult PD model performance is overall acceptable, also considering that data are coming from two quite different studies, in terms of infusion regimes and patients' typology. Results are also comparable to the performance of the combined PK-PD model proposed by Eleveld et al. (2018), which is the only published PD model for "broad" use in propofol anesthesia. Unfortunately, Eleveld and coauthors neither present RMSE, MDPE, and MDAPE values nor report other quantitative results associated to PD. Thus, the only possible comparison grounds on visualizing the diagnostic plots.

Figure 25 shows the identified correlation for the PD model parameter EC_{50} associated to the adult age range. The age-dependent correction factor allows accounting for the increased sensitivity manifested by elderly patients, with a reasonable decrease of EC_{50}.

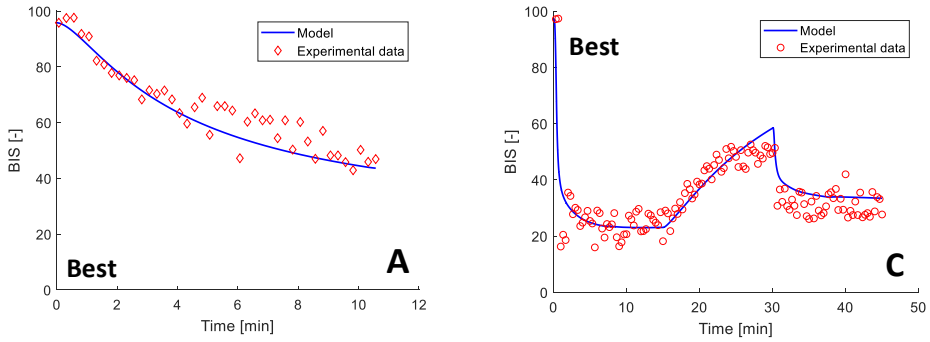

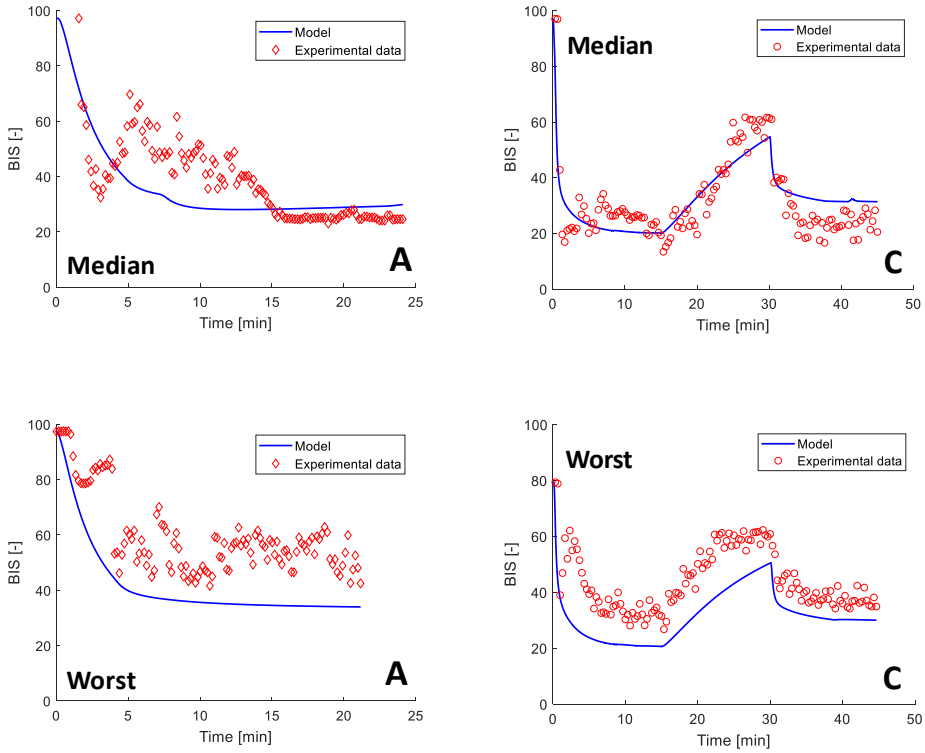

Figure 23 – Best, median, and worst validation cases of the PBPK-PD models according to model accuracy. The blue continuous line represents model predicted BIS, red diamonds and circles are measured BIS values. A panel refers to adult patients (data from Sahinovic et al. (2014) and Hannivoort et al. (2013)), C panel refers to pediatric patients (data from Coppens et al. (2011)).

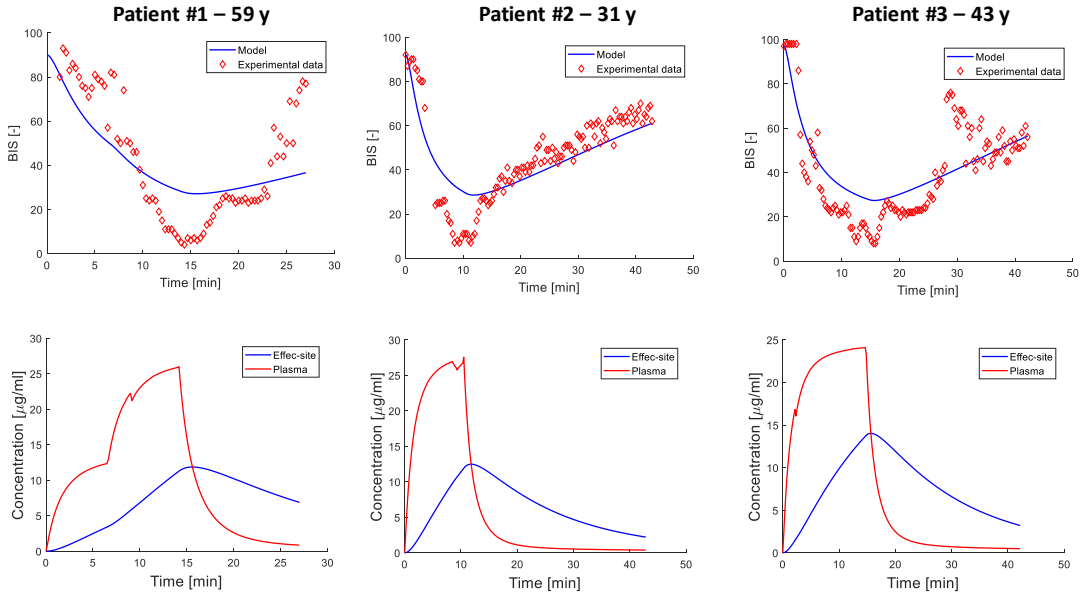

Figure 24 – (Top panel) Predicted (blue continuous line) vs observed (red diamonds) BIS dynamics in three adult patients manifesting deep hypnotic levels (BIS value < 20 [-]). (Bottom panel) Plasma (red) and effect-site (blue) concentration dynamics.

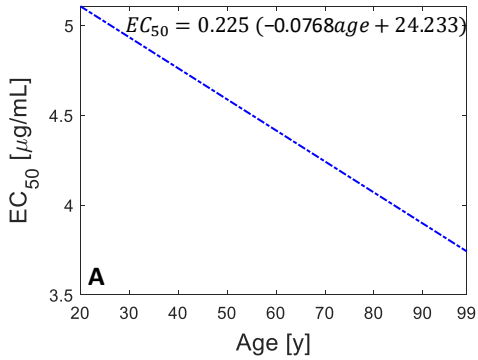

Figure 25 – Identified EC_{50} as a function of age (20-99 y age range).

As far as the identification and validation of the combined PBPK-PD model in pediatric patients is concerned, we used BIS data from Coppens et al. (2011). In their study, 28 healthy pediatric patients were given propofol anesthesia via TCI based on the pediatric Kataria PK model. Their regimen involved target plasma concentrations at (i) 7 µg/mL for 15 min, (ii) 1 µg/mL for 15 min or until awakening signs, and (iii) 5 µg/mL for the final 15 min. BIS data of 23 patients are used to validate the identified PD model. Low values of RMSE, MDPE, and MDAPE in Table 19 show a rather satisfactory predictive performance. Figure 23 (C panel) shows the best, median, and worst cases. It is worth noticing that in the worst case, the BIS signal seems to be affected by a disturbance at about 2 min after induction. This is likely the reason why the model deviates from the data and does not show a good prediction of the maintenance phase. For a better visualization of the results associated to all the validation cases, diagnostic plots are reported in Figure 26. In the early induction phase, BIS is probably affected by noise or the pre-induction anxiety level of the patient, as in some cases the first measured BIS values remain constant or increase even after induction (see deviations in the top right area of Figure 26, right panel) and we doubt that this is to be ascribed to a different velocity of drug transfer to the effect-site. In fact, we included the dependence of k_{e0} on age but we did not find a strong correlation. Indeed, the identified constant c was rather low (10^{-4} order of magnitude). However, the mentioned deviations concern the 2-3 BIS measures within 1 min after the start of propofol induction.

Another contributing factor to model deviations in the earliest phase is that for some patients a reliable pre-induction (*i.e.* baseline) value was not available, as the first BIS measure was available after more than 30 s from the start of induction. It is also worth mentioning that, similarly to the adult PD model, the pediatric PD model often overestimates BIS values lower than 20 [-].

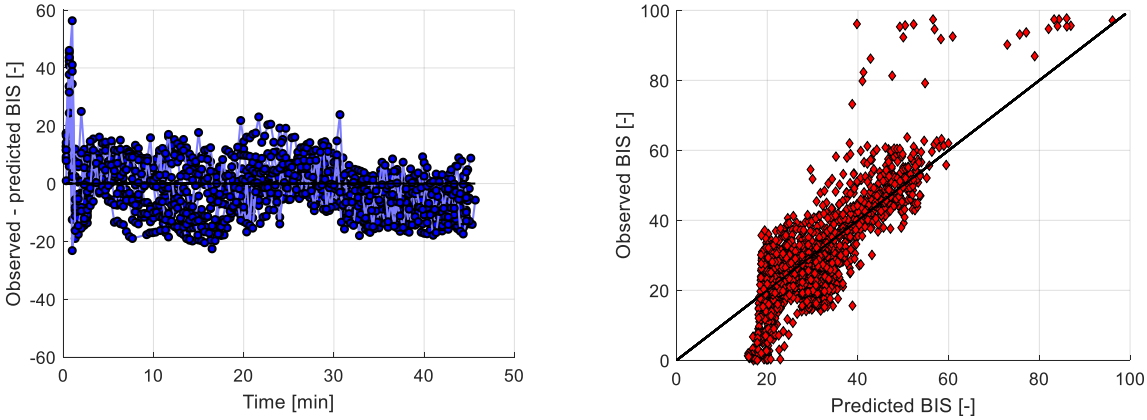

Figure 26 – Diagnostic plots associated to the validation cases of the combined PBPK-PD model in pediatric patients. (Left panel) Individual BIS observations – predictions vs time. (Right panel) Individual BIS observations vs predictions.

4B.8 Results and discussion: *in silico* experiments

4B.8.1 Effect of aging on the control action

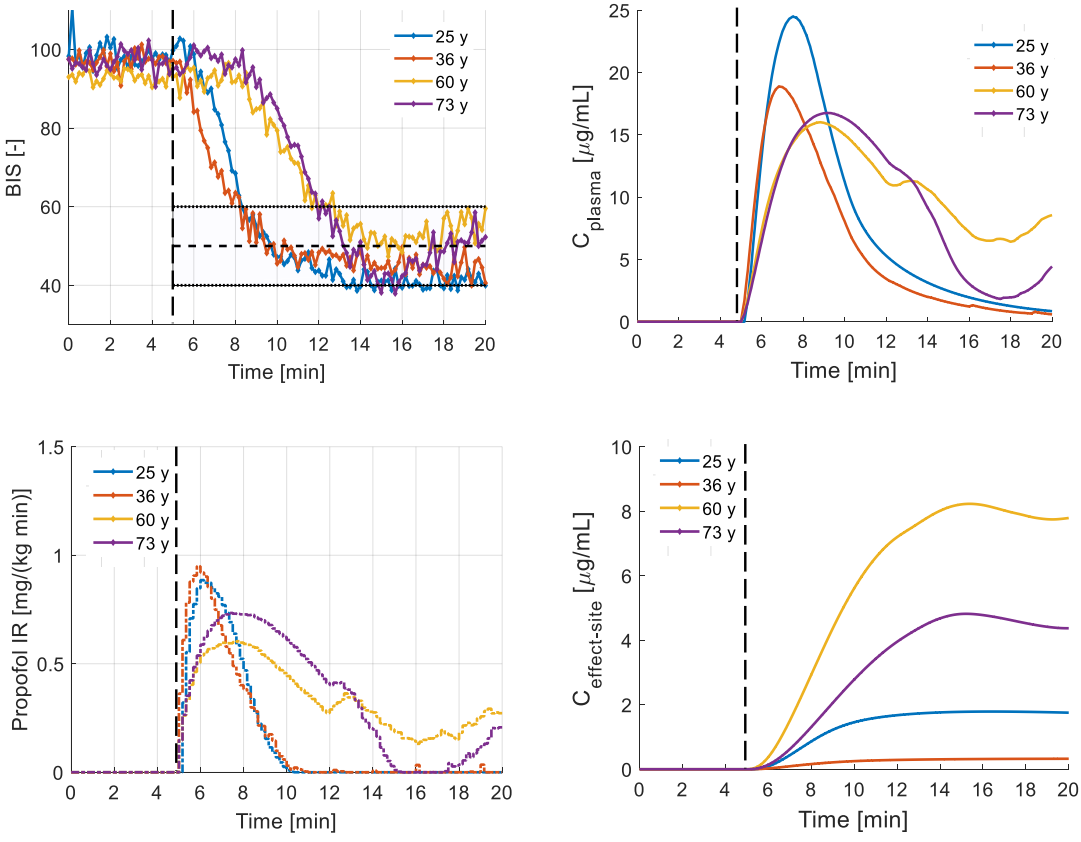

Figure 27 – Simulation of the induction phase in 4 adult healthy patients, ranging from 25 to 73 y. The black vertical dashed line marks the start of propofol infusion. (Left panel) Dynamics of controlled variable BIS and propofol infusion rate (*i.e.* manipulated variable). (Right panel) Dynamics of plasma and effect-

site concentrations. The rectangle area in the BIS graph denotes the recommended clinical range, BIS = 40-60 [-], while the black horizontal dashed line marks the setpoint, BIS = 50 [-].

In Figure 27 (left panel), the BIS dynamics and corresponding optimized propofol infusion rates are shown for 2 young and 2 elderly patients. The weights of the objective function terms associated to the (i) rate of change of propofol IR and (ii) penalty function associated to plasma concentration are fixed at slightly higher values for patients with age ≥ 60 y. Figure 27 shows that, as a result of these weights and the implemented correlations and adaptive parameters, the proposed initial infusion rates are slower for older patients, consistently with literature indications (Shafer, 2000) and standard guidelines[15]. Resulting plasma levels are lower and more sustained, which prevents dangerous plasma concentration peaks (see Figure 27, right panel). As the optimization problem features penalty functions to account for the clinical ranges, the BIS model-simulated curves are maintained within the recommended range 40-60 [-], despite the fact that the individual PD models of the elderly patients feature the Hill parameter γ > 3 [-] (see Chapter 3, Eq. (3.14)), hence a strong nonlinearity. In fact, the experimental BIS trends that we used to identify the two individual PD models of the elderly patients, feature a few burst suppression episodes of several minutes. Still, the model-predictive controller manages to tradeoff between (i) safety of the control action and (ii) distance from the setpoint value, with longer rise-times. The introduction of the MAP-remifentanil loop, and propofol-remifentanil interactions within the MAP model will be discussed in Chapter 5. These additional innovative features of the model-predictive controller allow improving the safety of the control action in elderly patients, in whom hypotension associated to propofol overdosing and combination with opioids have clinically relevant adverse effects. Figure 27 (right panel) shows the dynamics of propofol concentrations in plasma and effect-site compartments. The different BIS settling times among the patients depend on the velocity of blood-brain concentrations equilibration, and thus on the individual k_{e0} values. In *in vivo* patients, different factors affect the velocity of this process, *e.g.*, CO, cerebral perfusion, presence of co-morbidities affecting CNS/brain, and genetics. In the virtual patients, k_{e0} was identified with BIS data, along with the other individual PD parameters. The young patients feature the lowest k_{e0} values (see the lowest effect-site concentration levels, orange and blue continuous lines), therefore, the dynamics of the effect-site concentration is quite slow, which increases the resulting settling and response times.

[15] See Diprivan (propofol) dosing references available at https://reference.medscape.com/drug/diprivan-propofol-343100.

4B.8.2 Effect of obesity on the control action

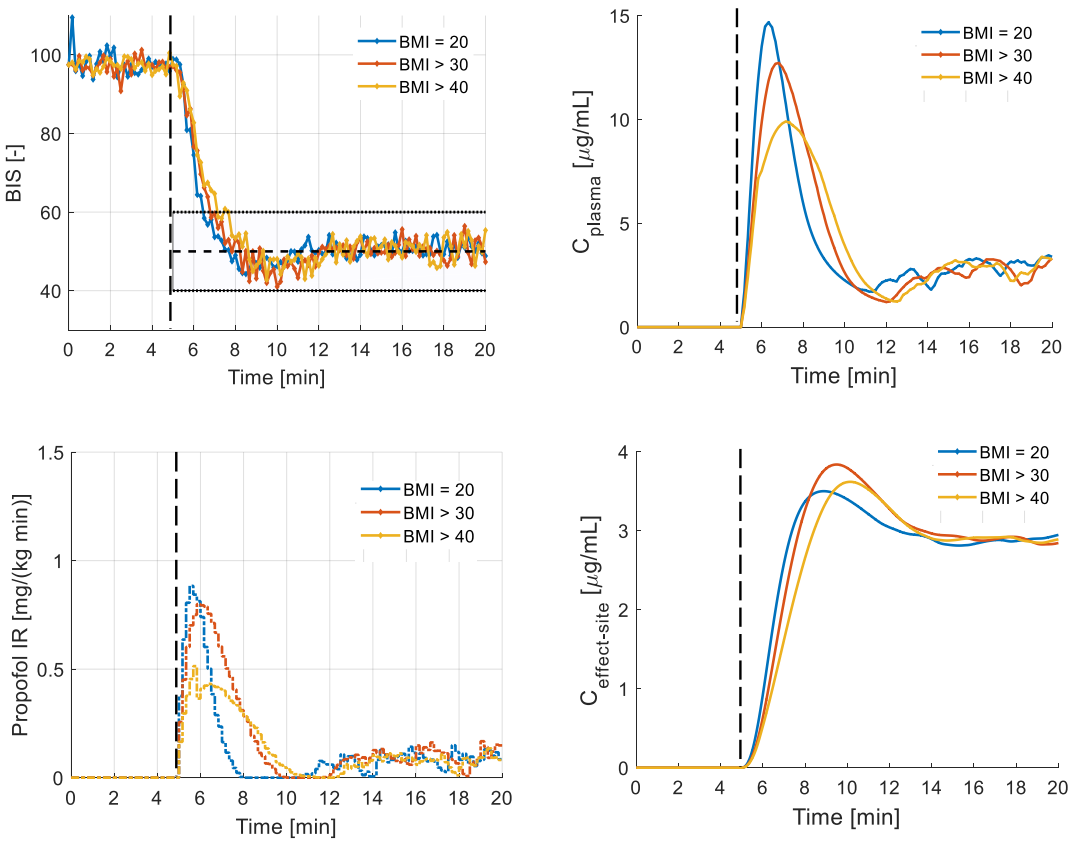

Figure 28 – Simulation of the induction phase in 3 adult patients, with BMI ranging from 20 (*i.e.* healthy) to 50 [kg/m^2] (*i.e.* morbid obese, class III). The black vertical dashed line marks the start of the control action (*i.e.* change of setpoint). (Left panel) Dynamics of controlled variable BIS and propofol infusion rate (*i.e.* manipulated variable). (Right panel) Dynamics of plasma and effect-site concentrations. The rectangle area in the BIS graph denotes the recommended clinical range, BIS = 40-60 [-], while the black horizontal dashed line marks the setpoint, BIS = 50 [-].

We compare the simulations of anesthesia induction in a 36-y-old healthy patient (BMI ~20 [kg/m^2]) and two patients with obesity class I and III, respectively. Figure 28 (left panel) shows the dynamics of BIS and corresponding propofol infusion rate. The controller proposes an increasingly slower but more sustained infusion rate with increasing BMI. This profile is also safer from the point of view of cardio-respiratory depressant effects, which is a main issue in this population (Subramani et al., 2017). According to Subramani et al. (2017), no clear clinical data exist to guide propofol dosing adjustments in the morbidly obese patients (MO, class III), while Eleveld et al. (2011) underline that conflicting results have been reported in the literature on the optimal propofol dosing in the obese. Servin et al. (1993) did not find any differences in the required maintenance infusion rates (in mg/kg/min) among obese and control subjects, which is consistent with the infusion rate levels proposed by the controller after the BIS dynamics becomes stable. In Johnson et al. (2018), obese patients in a

medical ICU required lower propofol dosages (in µg/kg/min) to reach the target RASS[16] score. These findings are consistent with the optimized infusion rates proposed by the controller during the first minutes of the simulation (*i.e.* when the objective is to reach the desired setpoint value). In the study of Subramani et al. (2017), BIS-based titration of propofol dosing during induction enhanced the stability of MO patients' anesthetic state. This result is encouraging from the point of view of additional stability and safety resulting from the use of a closed-loop controller of BIS in this "at-risk" category, since, evidently, no clear guidelines exist in the literature and thus, the clinical outcome of the procedure will heavily depend on the experience and intuition of the anesthetist, and these issues set the basis for strong variability in medical practice and may cause human errors.

4B.8.3 Effect of growth stage on the control action

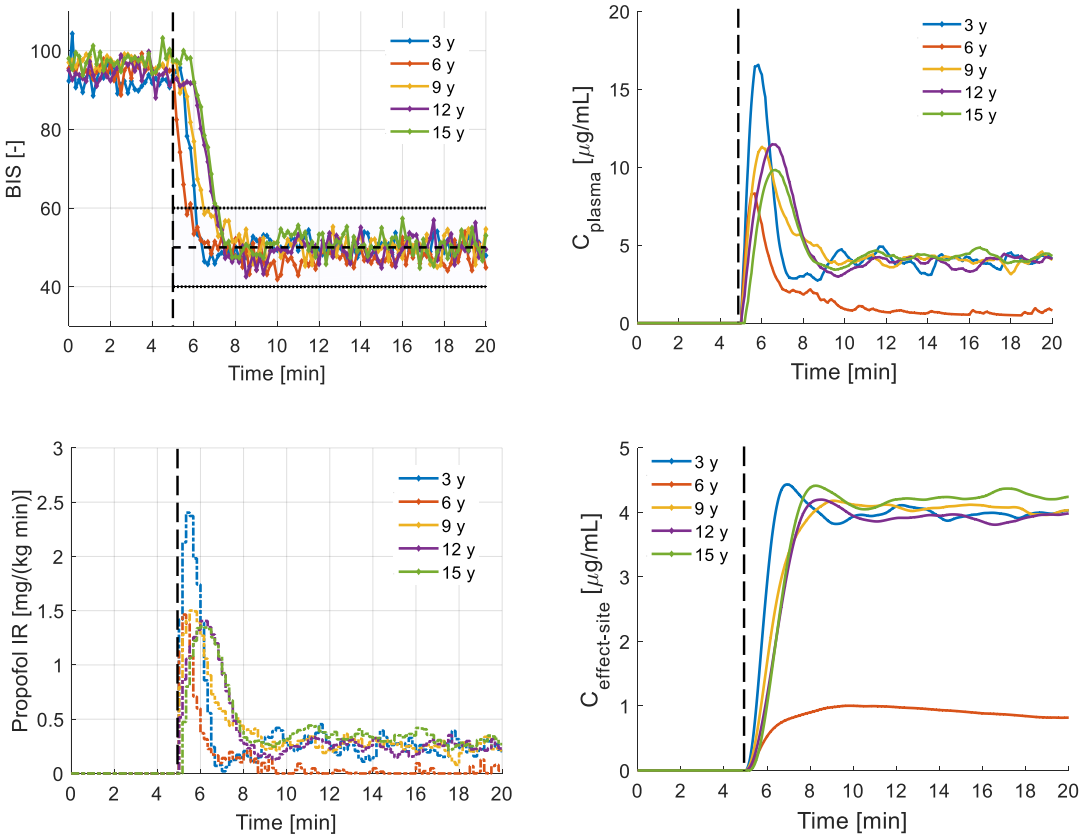

Figure 29 – Simulation of the induction phase in 5 pediatric patients, ranging from 3 to 15 y. The black vertical dashed line marks the start of the control action (*i.e.* change of setpoint). (Left panel) Dynamics of controlled variable BIS and propofol infusion rate (*i.e.* manipulated variable). (Right panel) Dynamics of plasma and effect-site concentrations. The rectangle area in the BIS graph denotes the recommended

[16] Richmond Agitation-Sedation Scale (RASS) Score is a medical scale used to measure the sedation level of a patient (Sessler et al. (2002)).

clinical range for general anesthesia, BIS = 40-60 [-], while the black horizontal dashed line marks the assigned setpoint, BIS = 50 [-].

Figure 29 shows the simulation of propofol induction in 5 virtual patients, with age ranging from 3 to 15 y. Consistently with guidelines on pediatric anesthesia (Gregory and Andropoulos, 2012), the controller simulates the highest initial infusion rate for the youngest patient, while differences are reduced after 6 y. Gregory and Andropoulos report that "[…]. *The usual doses for anesthesia induction are […] 3 – 8 years 3 – 5 mg/kg, > 8 years 3 mg/kg*" (Gregory and Andropoulos, 2012). The total dose in mg/kg proposed by the controller within the first 5 min is approximately 3 mg/kg for all patients, except for the 6-y-old patient. Figure 29 (right panel) shows the dynamics of effect-site concentrations. The PD parameters of the modified Hill equation differ among patients (as a result of individual PD parameters identification with BIS data, see Section 4B.4), and this feature results in rather different profiles of the effect-site concentration. The effect-site concentration dynamics is characterized by the transfer constant k_{e0}, which defines the delay between the profiles of plasma and effect-site concentration and represents the clinically observed delay between drug plasma concentration dynamics and manifestation of pharmacodynamic effects. In case of the 6-y-old patient, the identified k_{e0} is quite low (*i.e.* 0.0875 min^{-1}), while the other patients feature individual k_{e0} values in the 0.2-0.32 min^{-1} range. For this reason, the IR trend is rather different from the other patients. In fact, the *in vivo* observed delay between the time course of plasma concentration and the manifestation of pharmacological effect (in this case BIS) is affected by multiple factors, *e.g.*, cardiac output changes, cerebral perfusion, age (in the pediatric range), and genetics (Cortinez, 2014). These results show that the model is capable of individualizing the prediction basing on the "real" patient-specific data, which in the *in silico* framework are simulated via the individual PD models.

The pharmacokinetic differences predicted by the PBPK model, because of the implementation of proposed correlations and new adaptive parameters, result in different velocities of the infusion rate, with the one proposed for the 15-y-old patient similar to those proposed for adult patients (see Savoca and Manca, 2019). Adolescents are relatively less studied than other populations in anesthesia (Van Oud-Alblas et al., 2019). Although validation of the developed model with BIS data of adolescents should be carried out to ensure that the implemented equations to estimate the individualized parameters correctly account for the influence of maturity stage and puberty on the pharmacokinetics and resulting pharmacodynamics, we can

assume that the anatomical/physiological foundation allows extrapolating the use of the PBPK-PD model to this patients' category.

4B.8.4 Comparison with induction via manual and TCI infusion regimens

Figure 30 compares the dynamics of simulated BIS, plasma, and effect-site concentrations resulting from infusion rates obtained via (i) our MPC controller, (ii) Paedfusor TCI algorithm (Absalom and Kenny, 2005), (iii) Kataria model TCI algorithm (Kataria et al., 1994), and (iv) manual infusion regimen of McFarlan et al. (1999), to induce anesthesia in the virtual 3-y-old patient (see demographics in Table 15).

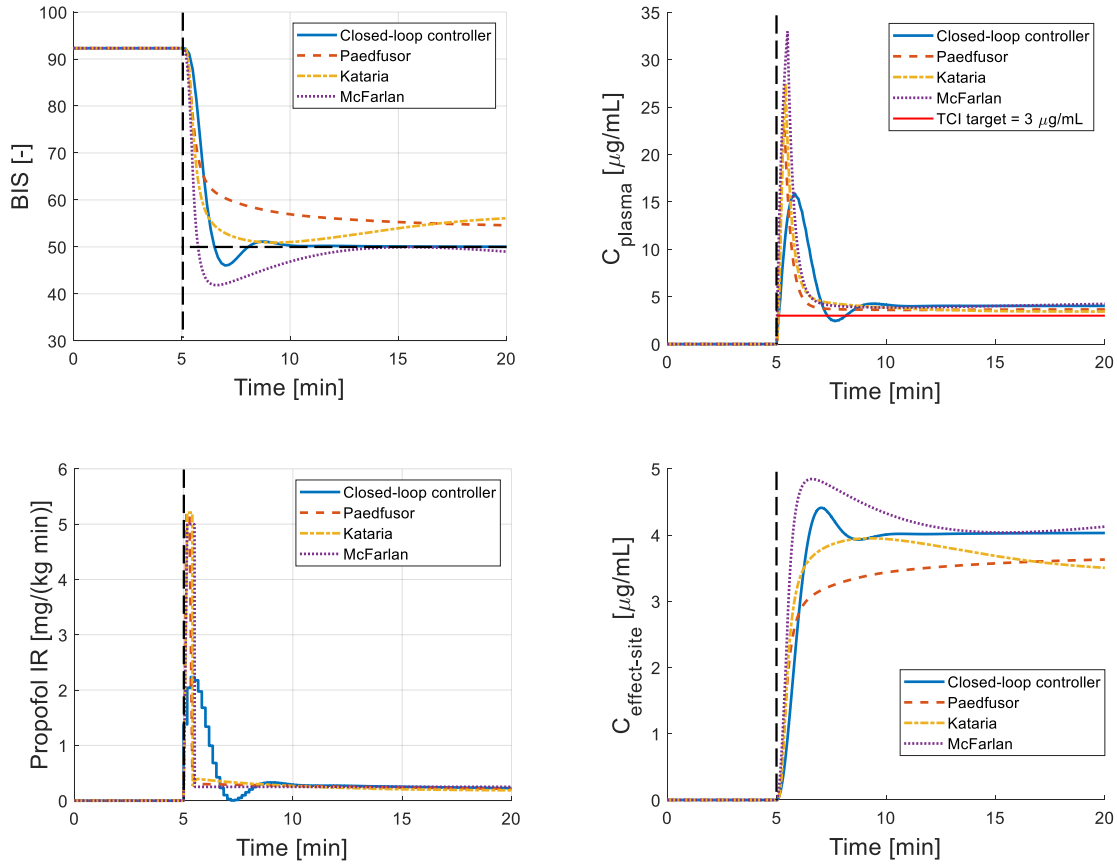

Figure 30 – Simulation of the induction phase in the 3-y-old patient via (i) closed-loop controller simulation (blue continuous line), (ii) Paedfusor TCI simulation (orange dashed line), (iii) Kataria model TCI simulation (yellow dashed-dotted line), and (iv) McFarlan manual infusion regimen (purple dotted line). (Left panel) Dynamics of controlled variable, BIS, and of manipulated variable propofol infusion rate. (Right panel) Dynamics of plasma and effect-site concentrations. The black vertical dashed line marks the start of the control action (*i.e.* change of setpoint). The black horizontal dashed line in the BIS graph marks the setpoint, BIS = 50 [-], whereas the red horizontal continuous line in the plasma concentration graph marks the target concentration in TCI simulations, *i.e.* 3 µg/mL.

Interestingly, manual induction (McFarlan) produces the most significant undershoot, although the simulated BIS value remains within the recommended clinical range 40-

60 [-]. A rather elevated plasma peak produces the minimum BIS value. Strong fluctuations of plasma concentrations are undesired, especially because propofol produces cardiovascular depressant effects (De Wit et al., 2016), due to a decrease in sympathetic activity (Marik, 2004). As the receptors of the sympathetic nervous system are distributed in different parts of the body, high plasma levels are quite dangerous, considering the fast distribution of propofol. The simulated PK profile in plasma shows that the desired target concentration (*i.e.* 3 µg/mL, see red horizontal line in plasma concentration graph in Figure 30) is reached with neither the Paedfusor nor the Kataria TCIs. This result should lead the reader to reflect upon the fact that in clinical practice, there is not any concrete verification that target concentrations implemented in TCI pumps are reached and maintained. In fact, anesthetists keep adjusting them basing on the visual feedback and personal interpretation of data from monitors of the patient's physiological variables. The proposed TCIs produce high plasma peaks that, as mentioned, may lead to dangerous adverse effects. Interestingly, BIS dynamics shows that with the Paedfusor algorithm, the target BIS value is not reached within 15 min from the start of induction. Such slow inductions may have consequences of delays and changes of the operating rooms scheduling and thus affect the operative costs of the institution (*e.g.*, hospital). Indeed, it is worth mentioning that, ideally, induction of anesthesia should be achieved within 10-15 min. The results of Figure 30 would likely lead the anesthesiologist to adjust the target concentration to accelerate the induction phase. With the Kataria TCI algorithm, BIS reaches the target value and then starts increasing, producing the need to adjust the target concentration as well, and thus setting the basis for a strong variability in the clinical practice, depending on the anesthetist's mindset, habits, experience, situational awareness, and level of attention. The closed-loop controller allows reaching and maintaining the target BIS value, and the proposed infusion rate changes gradually, to avoid dangerous plasma peaks with potential adverse effects, as a result of appropriate and careful tuning of the terms in the objective function. Similarly, the minimum BIS value is limited because of the presence of the penalty function on the controlled variable BIS. Finally, if disturbances of the anesthetic state manifested, the controller would react automatically, while both manual and TCI pump inductions would require manual adjustments of the infusion rates/target concentration values to maintain the patient anesthetic state.

All of these considerations are confirmed by the total administered dose [mg/kg], displayed in Table 20, which shows that manual and TCI induction doses are both

higher than that of our MPC controller (see % increment also reported in Table 20). Interestingly, in this simulation, TCI induction doses are the same despite the use of different three-compartment models.

Table 20 – Total propofol dose [mg//kg] over the 20 min simulation resulting from MPC closed-loop, manual, and TCI induction. The % increment respect to the MPC dose is also reported.

	MPC CONTROLLER	MANUAL REGIMEN (MCFARLAN)	TCI PAEDFUSOR	TCI KATARIA
TOTAL DOSE [mg/kg]	5.69	9.48	8.00	8.00
% INCREMENT respect to MPC dose [-]	0	+66.6	+40.6	+40.6

4B.9 Conclusions

The PBPK modeling approach allows tackling inter-individual variability of pharmacokinetics associated to the impact of age and obesity on ADME processes. The integration of age- and BMI-dependent correlations for estimation of the individualized parameters, and the identification of category-specific adaptive parameters allow applying the same model to normal and *special* patients. Not only the necessity of distinguishing among several classical PK models is eliminated, but also, it is likely that the anatomical and physiological principles beneath the model structure and parameters would enhance understanding and adoption by clinicians. Indeed, the proposed model allows predicting the PK of different categories of patients with either comparable or superior performance than the most used classical PK models for propofol, *i.e.* Marsh and Schnider models. The proposed model was combined with a suitable form of the Hill equation, whose parameters were identified with BIS data available in the scientific literature, after reformulation to account for the age-related features of propofol PD effects. The PD model proved satisfactory prediction of additional BIS data, with poor forecasts often caused by the presence of disturbances. Thus, the PBPK-PD model, corroborated with the different sets of individualized correlations and adaptive parameters, can be used to guide propofol anesthesia in normal patients and “at-risk” categories. A limitation of the study is that, in principle, for better consistency, PK and PD data used for identification of adaptive parameters should be from the same study. In addition, the PBPK-PD model performance still has to be validated in adolescents and geriatric (>80 y) patients. To our knowledge, the only PK-PD model for broad use in propofol anesthesia was

proposed by Eleveld et al. (2018) and shows similar limitations. However, the key element of distinction is that the anatomical and physiological foundation of the proposed PBPK-PD model allows reducing the risks of extrapolating the prediction to those patients' categories, whose PK-PD data were not available in the scientific literature. Indeed, individualized parameters account for the age range 1 – 99 y.

While Eleveld et al. (2018) propose an implementation of their model into a TCI pump-like system, our goal is to embed the model in a model-predictive controller for automated closed-loop anesthesia as a decision-support system for anesthetists. The main difference and advantage is that, in case of closed-loop anesthesia, the system performance does not depend solely on the model accuracy, but is continuously corrected and adjusted by real-time data that quantify the patients' hypnotic levels. Closed-loop controlled simulations of propofol anesthesia based on our PBPK-PD model take into account the pharmacokinetic and pharmacodynamic features of the elderly, pediatric, and obese patients and are in line with the recommended propofol dosing guidelines to avoid overdosing and adverse effects. The comparison with manual and TCI induction infusion rates showed improvements in both safety and stability of the overall *in silico* induction phase.

Although this Chapter focused on propofol only, the influence of propofol-remifentanil combination in high-risk patients, including elderly patients, is taken into account and discussed in Chapter 5. While tissue- and plasma-dependent remifentanil metabolism help reducing the PK and PD inter-individual variability compared to propofol, MAP and HR data are required to verify whether the adult models are suitable for prediction in pediatric patients. However, it is worth stressing that intra-operative AP changes are less concerning in children than elderly and obese patients (Shung, 2010). At this stage, we assume that the implemented correlations accounting for anatomical and physiological changes are sufficient to account for remifentanil differences in pediatric, elderly, and obese patients.

Acknowledgements: We acknowledge the "Open TCI initiative" (http://opentci.org/) due to the efforts of professors Shafer (Stanford, CA, USA), Minto (Sydney, Australia), and Schnider (St. Gallen, Switzerland), who made the use of PK data possible. For the PD data, we acknowledge Eleveld et al. (2018), who made their pharmacokinetic and pharmacodynamic datasets available.

CHAPTER 5

Anesthetic-analgesic interactions and adequate depth of anesthesia in high-risk patients

5.1 Author's Note

As discussed in Chapter 4A, patients with cardiovascular diseases and elderly are more exposed to risks of overdosing and increased cardio-respiratory depression. This chapter proposes a number of improvements of the model-predictive controller, with the aim of achieving a safer and more stable control of anesthesia in high-risk patients. Indeed, while the structure and performance of the controller proposed in Chapter 3 are quite suitable for a healthy adult patient and/or in case of minor procedures, they may result less effective in case of critical patients and major surgeries.

These modifications are of crucial importance, because physiological closed-loop control systems are meant to reduce clinicians' workload and improve their situational awareness, so that a prompter reaction to adverse events can be guaranteed. Such situations are more likely to occur in the management of intrinsically *difficult* cases, in which clinicians need to focus their attention on the patients' state to ensure a positive outcome of the procedure and reduce the risks of intra- and post-operative complications.

The work presented in this chapter was carried out during a research stay at Digital Health Innovation Laboratory, British Columbia Children's Hospital Research Institute (Vancouver, BC, Canada), headed by Profs Dumont and Ansermino.

5.2 Introduction

Anesthetists refer to several (in some cases, redundant) physiological variables to monitor the patients' anesthetic state. The minimum monitoring for anesthesia includes: pulse oximeter, non-invasive blood pressure (NIBP, at least every five minutes), continuous electrocardiogram (ECG), inspired and expired oxygen and CO_2, and temperature (ASA Standards for Basic Anesthetic Monitoring, 2015). At the discretion of the anesthetist, additional monitoring can be used. In case of TIVA, especially when combined with neuromuscular blocking drugs, use of DoH monitors is recommended, *i.e.* electroencephalogram (EEG) or some quantitative EEG monitor (*e.g.*, BISpectral Index, Spectral Entropy, and NeuroSENSE monitors) (Checketts et al., 2016). In some specific cases, *e.g.*, elderly or patients with cardiac diseases, the anesthetist will add continuous AP measurement (and possibly blood flow monitoring) to monitor circulation. In such cases, continuous AP monitoring is clinically indicated, as limiting the hemodynamic fluctuations is essential for a positive clinical outcome (see Chapter 4A for a more detailed discussion).

Optimal titration of anesthetic drugs contributes to limit hemodynamic fluctuations. As propofol is known to be a cardio-respiratory depressant, optimization of dosing is essential to avoid hypotension and extreme drops in CO, especially during induction. Indeed, such adverse effects can be detrimental in the high-risk patient. In clinical practice, intra-operative changes of the hemodynamic parameters are also employed as indicators of the adequacy of analgesia level. For the sake of completeness, it is worth mentioning that some commercialized devices are today available to monitor nociception, *e.g.*, the PMD100™ (Medasense Biometrics Ltd., Ramat Yishai, Israel) that computes a real-time NOciception Level index (NOL), based on the re-elaboration of physiological data from multiple sensors. However, they are still far from being widespread in clinical practice and their actual clinical relevance has not been demonstrated yet (Ledowski, 2019). For these reasons, the use of HR and AP to monitor intra-operative nociception is still prevalent and thus, inclusion of hemodynamic variables in closed-loop controllers of anesthesia is desirable for a safe

and stable control action on the patients' anesthetic state. Model-predictive control is the most suitable strategy to tackle such multivariable problem, with the goal of avoiding propofol overdosing with related adverse effects on the cardiovascular system and, concomitantly, rejecting the disturbances caused by noxious stimuli (*i.e.* manifested by steep increases of HR and AP). In fact, the optimization problem can be formulated by including (i) a correction of the model prediction based on real-time hemodynamic data, to detect sudden changes of the input variables, and (ii) appropriate constraints on the rate of change of the infusion rates and controlled variables, to maintain safe clinical ranges.

While the PBPK model (at this stage embedded in the controller) is substantially unchanged with respect to Chapter 4A, modifications were made to the PD component. To account for high-risk patients' sensitivity to propofol-opioids combination (Servin, 2017), AP is modeled as a function of both propofol and remifentanil concentrations by a response surface methodology to account for propofol-remifentanil synergistic interactions. HR is included as input variable to the controller and modeled as a function of remifentanil concentration. Since HR is more susceptible than AP to noxious stimuli (see the studies of Hall et al. (2000); Batra et al. (2004); Alexander et al. (1999)), a correlation with remifentanil infusion rate allows the controller adjusting the analgesic dosing if steep HR changes are detected, which manifest an inadequate analgesic level of the patient. The use of a PBPK modeling strategy within the controller also allowed investigating the effect of CO changes on the control action.

Section 5.3 details (i) the mathematical formulation of the PD models, along with their identification and validation procedures and (ii) the modified controller structure and optimization problem formulation. Section 5.4 shows the validation results of the PD models. Section 5.5 is devoted to the discussion of the results on *in silico* induction of anesthesia. Specifically, Paragraph 5.5.1 shows the *in silico* assessment of the MPC controller performance during induction of anesthesia in eight "at-risk" patients. Paragraph 5.5.2 is devoted to showing the impact of including CO data as input to the model-predictive controller.

5.3 Methods

5.3.1 PD models for prediction of MAP, HR, DoH, and CO

Propofol and remifentanil are known to display synergistic interactions. Although drug-drug interactions in anesthesia can occur at both the PK and PD levels, PD interactions are more interesting since anesthetists (and closed-loop controllers, as well) titrate dosing basing on the time course of PD effects (Van Den Berg et al., 2017). Interaction between opioids and IV anesthetics is less strong for hypnotic effects than for response to noxious stimuli, and results on remifentanil-propofol synergistic effects on EEG are controversial (Van Den Berg et al., 2017). In general, studies report that concomitant opioid-propofol administration does not seem to affect BIS (see for instance Guignard et al. (2000)). The reason may be that these classes of drugs have different site of action. Instead, there is evidence of more enhanced cardiovascular depressant effects in case of remifentanil boluses administered in combination with propofol (Guignard et al., 2000; Thompson et al., 1998). Specifically, these effects are more enhanced on AP and CO than HR, consistently with the results presented and discussed in the first section of Chapter 4A.

For these reasons, a PD model of AP accounting for propofol-remifentanil interactions was identified and validated with clinical data available from West et al. (2018) (see Chapter 4A). In the scientific literature, PD interactions of anesthetics and opioids have been modeled by response surface methodology. Minto et al. (2000) proposed the model explicated in Eqs. (5.1-8) to describe propofol interactions with midazolam and alfentanil.

$$E(t) = E_0 - (E_0 - E_{\max}) \frac{\left(\frac{C(t)}{EC_{50}} \right)^{\gamma}}{1 + \left(\frac{C(t)}{EC_{50}} \right)^{\gamma}} \tag{5.1}$$

$$U_i(t) = \frac{C_i(t)}{EC_{50,i}} \qquad i = P, R \tag{5.2}$$

$$\theta(t) = \frac{U_P(t)}{U_R(t) + U_P(t)} \tag{5.3}$$

$$E(t) = E_0 - (E_0 - E_{\max}(\theta(t))) \frac{\left(\frac{U_R(t) + U_P(t)}{U_{50}(\theta(t))} \right)^{\gamma(\theta(t))}}{1 + \left(\frac{U_R(t) + U_P(t)}{U_{50}(\theta(t))} \right)^{\gamma(\theta(t))}} \quad (5.4)$$

$$f(\theta) = \beta_0 + \beta_1 \theta + \beta_2 \theta^2 + \beta_3 \theta^3 + \beta_4 \theta^4 \quad (5.5)$$

$$E_{\max}(\theta(t)) = E_{\max,R} + (E_{\max,P} - E_{\max,R} - \beta_{2,E_{\max}} - \beta_{3,E_{\max}} - \beta_{4,E_{\max}})\theta(t) + \beta_{2,E_{\max}} \theta(t)^2 + \beta_{3,E_{\max}} \theta(t)^3 + \beta_{4,E_{\max}} \theta(t)^4 \quad (5.6)$$

$$U_{50}(\theta(t)) = 1 - \beta_{2,U_{50}} \theta(t) + \beta_{2,U_{50}} \theta^2(t) \quad (5.7)$$

$$\gamma(\theta(t)) = \gamma_R + (\gamma_P - \gamma_R - \beta_{2,\gamma} - \beta_{3,\gamma} - \beta_{4,\gamma})\theta(t) + \beta_{2,\gamma} \theta(t)^2 + \beta_{3,\gamma} \theta(t)^3 + \beta_{4,\gamma} \theta(t)^4 \quad (5.8)$$

We adapted the model to describe propofol-remifentanil effect on AP (in Eqs. (5.1-8), P stands for propofol, R for remifentanil). As in previous chapters, the virtual effect-site compartment approach is used, to account for the drugs transfer from plasma to the site of action. For the sake of clarity, the concentration $C(t)$ in Eqs. (5.1-2) refers to the effect-site. We do not report the notation "*e*" to avoid further burden on the reader.

The Hill equation can be rewritten as in Eq. (5.1). In Eq. (5.2), U_i is the normalized concentration of the drug i and is used as measure of the drug potency[17]. If θ is defined as in Eq. (5.3), Eq. (5.1) can be rewritten to represent the concentration-response relation of any ratio of the two drugs in combination. Such combination is indeed considered as a "new" drug, with concentration $U_P + U_R$. Note that this model can be applied provided that the single drugs also exhibit a sigmoid correlation with the clinical effect, which is the case of both propofol and remifentanil (and in general most IV anesthetic/analgesic drugs).

Basing on these assumptions, Eq. (5.4) becomes an "extension" of Eq. (5.1), where $E_{max}(\theta)$ is the maximum effect at ratio θ, $U_{50}(\theta)$ represents the potency of the drugs combination, and $\gamma(\theta)$ is the steepness associated to the drugs combination. To represent the dependence of these PD parameters on θ, Minto et al. (2000) propose the family of fourth-order polynomials (see Eq. (5.5)) as they are flexible functions, because limited mechanistic information is available in the literature on these relations.

[17] Note that $EC_{50,i}$ are defined from the separate propofol and remifentanil concentration-response relations.

By following this procedure, the problem of identifying the PD model parameters E_{max},EC_{50}, and γ is converted into the problem of identifying the β_j parameters. Minto et al. (2000) show how, in a two-drug combination models, some of these β_j parameters are already defined, as they are constrained by the model formulation. The remaining parameters are identified via non-linear regression with PD data. The final correlations are reported in Eqs. (5.6-8). $E_{max,P}$, $E_{max,R}$, γ_P, and γ_R in Eqs. (5.6-8) and $EC_{50,P}$ and $EC_{50,R}$ in Eq. (5.2) are derived from the separate propofol and remifentanil concentration-response relations.

As far as HR is concerned, the decrease associated to propofol induction is usually less significant or not present (see measured HR trends presented and discussed in the first section of Chapter 4A) and thus, it is not as concerning as propofol-induced hypotension. During the maintenance phase, rapid increases of HR are symptoms of inadequate level of analgesia. For these reasons, HR was modeled as a function of remifentanil effect-site concentration via modified Hill equation (as in Chapter 3, Eqs. (3.13-14)).

For reasons of consistency with the data used for hemodynamic parameters modeling, we used WAV_{CNS} data to identify and validate a PD model (*i.e.* modified Hill equation as in Chapter 3, Eqs. (3.13-14)) as a function of propofol effect-site concentration, to be applied within the controller to control the DoH component (for the sake of clarity, in this chapter the notation DoH is therefore used instead of BIS).

Finally, CO data were used to identify and validate a propofol dose-CO model that is not applied within the controller but can be used to investigate *in silico* the effect of different propofol dosing regimens on CO dynamics. In this case as well, the modified Hill equation as a function of propofol effect-site concentration is used (Eqs. (3.13-14)). Indeed, Chapter 4A showed the importance of limiting CO decrease, and because limited dedicated clinical experiments are available in the scientific literature, this PD model is provided as an investigational tool to study such effects.

The clinical data used for identification and validation of the HR, CO, and DoH models are from West et al. (2018) and have already been detailed in Paragraph 4A.4.1. The baseline pre-induction values (E_0 in the Hill equation formulation) are assigned as the values of the effect 30 s after induction (as in Van Heusden et al. (2018)). RMSE, MDPE, and MDAPE values are also provided as performance indicators of the PD models predictive performance, basing on the PD data that were not used for the parameters' identification (MDPE and MDAPE are used as measure of accuracy of

PD models in the related scientific literature (*e.g.*, Eleveld et al. (2018)).

5.3.2 Controller structure and optimization problem formulation

Figure 31 shows the *in silico* closed-loop controller framework. Input variables to the model-predictive controller are DoH, MAP, and HR. Manipulated variables are propofol and remifentanil infusion rates. Controlled variables are DoH and MAP.

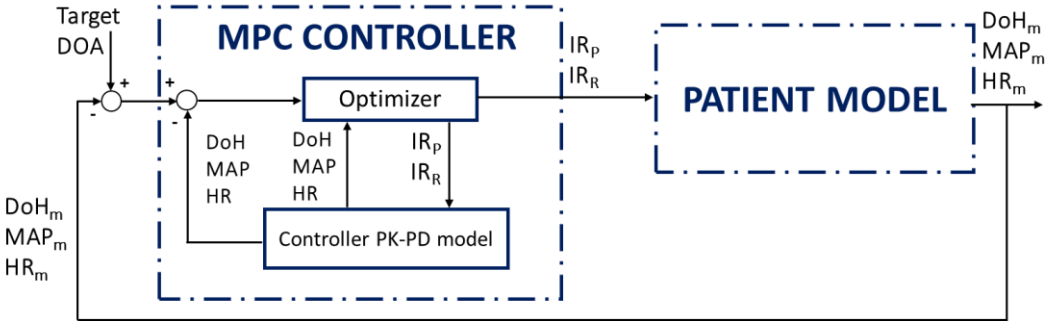

Figure 31 – *In silico* closed-loop framework for application to high-risk patients. The closed-loop elements are: (i) the control objectives (*i.e.* target DOA), (ii) the optimizer, (iii) the controller model, and (iv) the patient model.

The wave index (WAV_{CNS}) is used as measure of DoH in West et al. (2018). As for BIS, the setpoint is 50 [-], after the recommended WAV_{CNS} clinical range 40-60 [-] that suggests adequate DoH. With respect to MAP, we reformulated the control objective of Chapter 3, where MAP_{SP} was set at 70 [mmHg]. Although MAP = 70 [mmHg] is an appropriate target for healthy patients during maintenance of anesthesia, one should not assume that the same AP value can be maintained or is suitable to all sorts of patients. Depending on their characteristics and AP baseline (*i.e.* pre-induction) value, MAP = 70 mmHg may actually result too high or too low. In addition, it is not customary of anesthesiologists to assign a setpoint, *i.e.* a target desired value, for AP. Indeed, anesthesiologists rather think of clinical ranges for the hemodynamic parameters (G. Mistraletti, personal communications, Ospedale San Paolo, November 2018). The lower boundary value of the recommended range also depends on the patients' features, especially because of the discussed critical issues related to the cardiovascular response (see Chapter 4A). For instance, it is not recommendable to keep a critically ill patient at AP values below 65 mmHg for several minutes (risk of hypoperfusion), while the same values would not be problematic in a young healthy patient. For these reasons, we reformulated the MAP control objective as a maximum allowed MAP % decrease respect to the baseline value in response to propofol-remifentanil induction. From this value, which is more easily understandable for the anesthesiologist, the target value MAP_{SP} is determined by the MPC controller. For the

in silico simulations, we set an acceptable value of 20% decrease from the baseline value.

In high-risk patients, variations of the controlled variables may be faster, and it is desirable to promptly smooth those hemodynamic fluctuations. Hence, the controller operating time interval t_s was set to 10 s. Suitable values of h_p and h_c were found, respectively $40t_s$ (i.e. less than 7 min) and $4t_s$ (i.e. 4 degrees of freedom for each controlled variable, with a total of 8 degrees of freedom).

The optimization problem is formulated as in Eq. (5.9). Similarly to the optimization problem of Chapter 3, Eq. (5.9) accounts for (i) the controlled variables distance from the setpoint, e_y, where y is the vector of the controlled variables DoH and MAP, (ii) penalty function terms for the input variables, and (iii) the rate of changes of propofol and remifentanil infusion rates. HR is not a controlled variable but is included in the objective function by means of an additional term, whose purpose is to minimize positive steep changes of that specific variable (see Eq. (5.10)). This choice is made because it is more consistent with the clinical practice. Indeed, similarly to AP, there are no optimal target values of HR, but variations are more important to assess the adequacy of the patients' analgesic state. This term will be more important when disturbances of the anesthetic state due to surgical and other nociceptive stimuli (*e.g.*, intubation) manifest. We also implemented constraints for HR via a penalty function PF_{HR}. Note that a new term was included in the objective function (see also Eq. (5.11)), compared to the formulation presented in Chapter 3. This term provides the optimizer with a suitable profile of remifentanil infusion rate $IR_{R,T}$, which is based on the dosing guidelines available at https://reference.medscape.com/drug/ultiva-remifentanil-343316, and takes into account the recommended reduction of remifentanil dosing for patients aged > 60 y, who are more sensitive to opioids (Servin, 2017).

The choice of implementing this term comes from personal communications with clinicians (C. Carozzi, Istituto Neurologico Carlo Besta, December 2018). In fact, anesthesiologists accustomed to using TCI pumps usually increase preventively the target remifentanil concentration before stimulating procedures (*e.g.*, intubation, incision), without modifying the propofol infusion rate. If a quantitative measure of nociception (*e.g.*, NOL index) were clinically adopted and used within the controller as controlled variable, this action could be converted into a setpoint change (*i.e.* servo-problem). Since in clinical practice, and thus in our controller, changes in hemodynamic parameters AP and HR are used as surrogate indicators of the level of

analgesia, an alternative approach must be proposed. By introducing this term, we allow the anesthesiologist, who is the final end-user of the controller, to adapt the controller settings by modifying the $IR_{R,T}$ before the stimulating procedure, and changing it back to the preferred value afterwards, hence providing an additional degree of freedom to operate. Tuning of the weights of the objective function followed the same criteria already explained in Chapter 3.

$$\min_{IR(k),IR(k+1),\ldots,IR(k+h_c-1)} \left\{ \begin{array}{l} \sum_{j=k+1}^{k+h_p} \left[w_y {e_y}^2(j) + PF_y(j) \right] + \sum_{i=k}^{k+h_p-1} w_{IR} \Delta IR^2(i) + \\ \left[w_{HR} \Delta HR^2(k) + PF_{HR}(k) \right] + \sum_{l=k}^{k+h_p-1} w_{R,T} {\delta IR_{R,T}}^2(l) \end{array} \right\} \quad (5.9)$$

$$\Delta HR(k) = (HR_r(k) - HR(k)) \quad (5.10)$$

$$\delta IR_{R,T}(l) = IR_R(l) - IR_{R,T}(l) \quad (5.11)$$

The performance of the controller has been evaluated *in silico* for eight "at-risk" patients. The controller and the *in silico* patients feature the same individualized PBPK model, but the "mismatch" is preserved by using individualized PD models, obtained via nonlinear regression with data of individual patients from West et al. (2018).

An additional *in silico* experiment was carried out to test the behavior of the MPC controller as a result of including CO data as input information. Specifically, three different CO individual models were identified from 3 patients of West et al. (2018). The three CO models were used to simulate three different CO dynamics for the same virtual patient and compare the infusion rates proposed by the controller, as a result of the different PBPK profiles. The goal of this experiment was to verify whether the controller is able to individualize the control action basing on additional information about hemodynamics (specifically, CO data).

5.4 Pharmacodynamic modeling: results and discussion

5.4.1 Validation of the arterial pressure model

As mentioned in Chapter 4A, continuous MAP and CO measurements were available for 15 high-risk patients from West et al. (2018). For four additional patients continuous MAP measurements were available, while CO was not available. In all of these cases, AP monitoring was clinically indicated because of the patients' conditions or the type of surgical procedure (see Chapter 4A and West et al. (2018) for additional details).

Data from ten patients were used for identification of the PD model parameters, listed in Table 21. Figure 32 shows the AP model predictions resulting from simulation of MAP dynamics of the remaining patients, who were used as validation cases. Table 22 reports RMSE, MDPE, and MDAPE values for quantification of the model predictive performance.

Table 21 – Identified parameters of the response surface model for MAP.

	IDENTIFIED PARAMETERS
$k_{e0,\,R}$ [min^{-1}]	0.0083
$E_{max,R}$ [mmHg]	58.979
γ_R [-]	1.931
$EC_{50,R}$ [ng/mL]	0.145
$k_{e0,\,P}$ [min^{-1}]	0.0903
$E_{max,P}$ [mmHg]	49.727
γ_P [-]	1.066
$EC_{50,\,P}$ [µg/mL]	1.639
$\beta_{2,\,Emax}$[-]	1.324
$\beta_{3,\,Emax}$[-]	0.993
$\beta_{4,\,Emax}$[-]	0.472
$\beta_{2,\,U50}$[-]	-5.589
$\beta_{2,\,\gamma}$[-]	-2.798
$\beta_{3,\,\gamma}$[-]	0.917
$\beta_{4,\,\gamma}$[-]	0.092

In Figure 32, MAP data measured using invasive arterial line (*i.e.* continuous measurements, blue circles) and NIBP (red diamonds, sampled every 1, 2 or 3 min) are reported for comparison to the MAP model predictions (black continuous line) of nine patients (A-I panels). Small stars indicate (i) stimulation (red, *e.g.*, caused by surgical activity) or (ii) administration of vasopressors to treat mild/severe hypotension (black). The goal of our combined PBPK-PD model is to describe the functional dependency of AP on the infusion rates of propofol and remifentanil. The effects of stimulation and administration of vasopressors on AP can be assumed as external disturbances. For this reason, we did not consider these events in our model, and

thus, the effects of such disturbances provoke a deviation of the model-predicted MAP from its measured value, which increases because of either (i) the sympathoadrenal response to the stimulus or (ii) the vasopressor-induced constriction of blood vessels. For similar reasons, the time horizon for identification and validation is of the order of some minutes and differs among patients. In fact, we consider the AP dynamics before the start of the airway management[18], which was performed at different times among patients and is a stimulus, which leads to an increase of the hemodynamic values.

Indeed, modeling the relation between the drug concentrations and hemodynamic effects is not an easy task, as they are affected by such "external" factors. It is also worth noticing that the two techniques for measuring AP (*i.e.* invasive arterial line vs NIBP) sometimes produce discrepant measured values (see for instance Figure 32, B panel). Although both methods are often used intra-operatively, it is not uncommon to observe inconsistencies (Sheshadri et al., 2017). Intra-arterial line continuous measurements are usually considered more reliable, but a number of different factors may induce such discrepancies, *e.g.*, wrong cuff size or positioning, wrong cannula positioning, hypothermia, and vasoconstriction.

The significant inter-patient variability in the hemodynamic response to induction of anesthesia was already commented in Chapter 4A, and is evident from Figure 32. A systematic behavior of the model prediction cannot be detected, in some cases (*e.g.*, A and E panels) the model overestimates MAP data, in others underestimation can be observed (*e.g.*, D panel). However, considering the inter-individual variability also related to the patients' conditions and external factors (*i.e.* concomitant administration of several drugs, stimulation, and different time of the airway management) the model shows acceptable performance in prediction of AP of these high-risk patients. Table 22 shows that RMSE is lower than 20 mmHg in all cases, except for case B, and MDAPE is always lower than 25%.

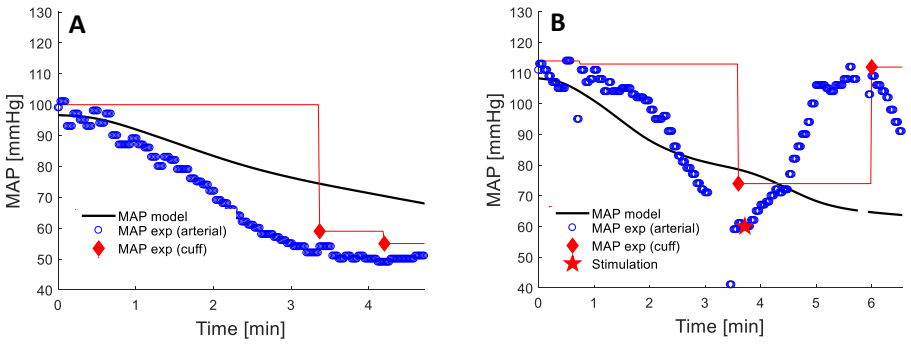

[18] Patients in West et al. (2018) are mechanically ventilated so that they can breathe while they are anesthetized.

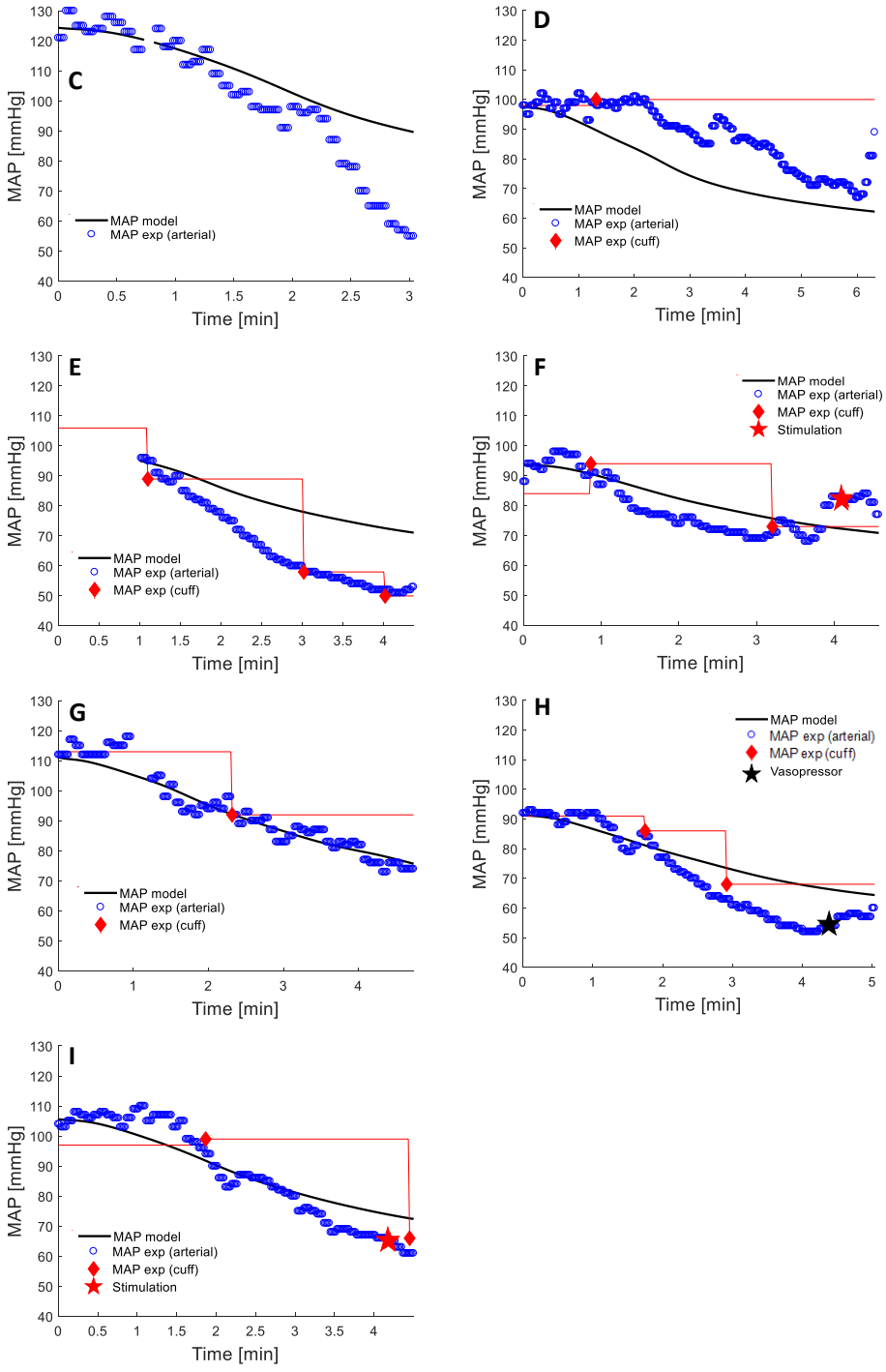

Figure 32 – Validation cases for the MAP model. Blue circles are MAP measurements from the arterial line, while red diamonds are the NIBP data (sampled every few minutes). Black continuous line is the model-predicted MAP. Red stars in B, F, and I panels indicate stimulation, while the black star in H panel marks the administration of a vasoconstrictor agent to counter hypotension.

Table 22 – RMSE, MDPE, and MDAPE values related to validation of the MAP model.

	RMSE [mmHg]	MDPE%	MDAPE%
A	15.70	21.11	21.11

B	24.81	7.55	12.42
C	13.61	4.34	4.71
D	12.59	15.35	15.35
E	15.60	22.29	22.29
F	6.48	5.44	7.94
G	3.80	1.07	2.83
H	8.73	8.7	8.7
I	6.17	0.30	5.13
Median (IQR)	10.66 (6.4-15.63)	7.55 (3.52-16.79)	8.70 (5.02-16.79)

5.4.2 Validation of the heart rate model

HR data of three patients were used to identify the PD model parameters listed in Table 23. Figure 33 shows the validation cases (*i.e.* HR data of the remaining 16 patients). HR data (blue continuous ECG signal) show remarkable inter-patient variability. Indeed, compared to AP, HR is more susceptible to stimulation, and is also more affected by the patient pre-induction state, *e.g.*, anxiety level. This complicates the definition of the pre-induction baseline value (E_0 in the sigmoidal E_{max} model). Nociceptive or other types of stimuli (*e.g.*, tactile) may have caused increases of the HR signal, evident in C, D, E, F, J, K, N, O, and P panels, and thus deviation of the model-predicted HR (black continuous line) from the measured values in Figure 33. Other factors inducing HR changes are marked with a black arrow (*i.e.* for particular events) or a red star (*i.e.* stimulation). For the sake of clarity, an increase in HR is usually observed following hypotensive episodes, because the heart will pump at a higher rate to contrast the effects of the pressure decrease, and maintain the blood flowrates to the vital organs (see G panel). In B panel, pump occlusion probably caused inadequate levels of analgesia and hypnosis, which results into a sustained increase of HR that manifests the patient stress response. As commented in Chapter 4B, the HR response to induction of anesthesia is less marked than the AP one. In fact, it is almost not present in some cases (see for instance A-C panels). The model predictive performance is similar to the AP model. RMSE, MDPE, and MDAPE values are listed in Table 24. The cases in which HR disturbances are present show the highest RMSE values.

Table 23 – Identified parameters of the modified E_{max} model for HR.

	IDENTIFIED PARAMETERS
k_{e0} [min^{-1}]	0.196
E_{max} [b/min]	0.629*$HR_{baseline}$
γ [-]	3.02
EC_{50} [ng/mL]	3.531

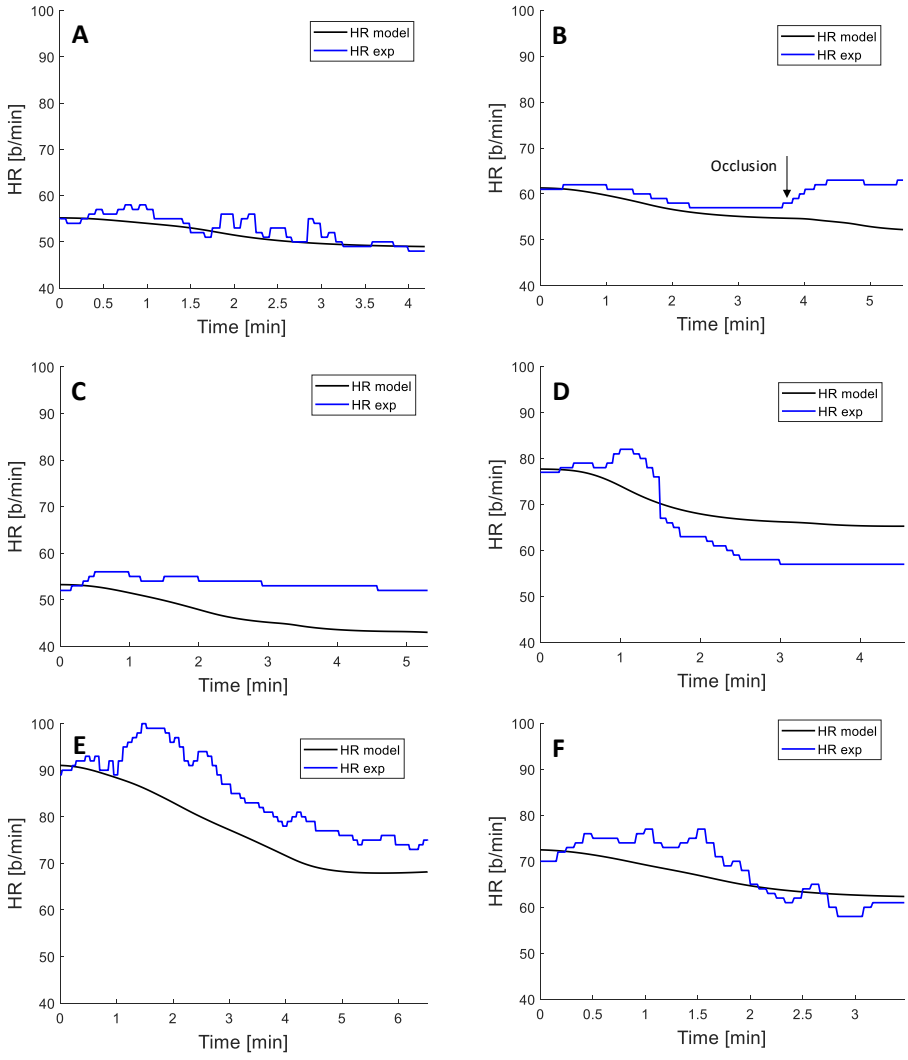

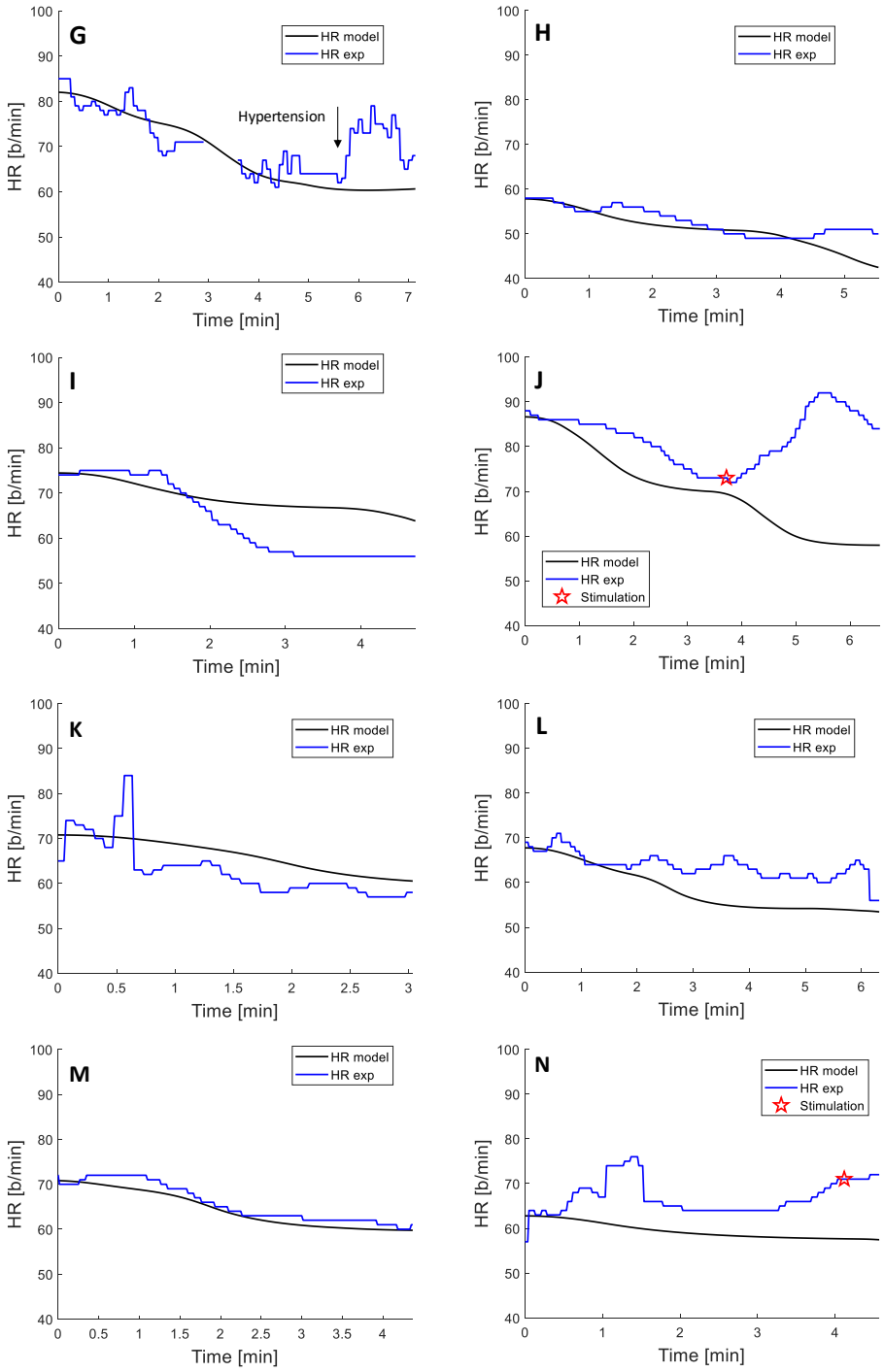
G
HR model
HR exp
Hypertension
HR [b/min]
Time [min]
H
HR model
HR exp
HR [b/min]
Time [min]
I
HR model
HR exp
HR [b/min]
Time [min]
J
HR model
HR exp
Stimulation
HR [b/min]
Time [min]
K
HR model
HR exp
HR [b/min]
Time [min]
L
HR model
HR exp
HR [b/min]
Time [min]
M
HR model
HR exp
HR [b/min]
Time [min]
N
HR model
HR exp
Stimulation
HR [b/min]
Time [min]

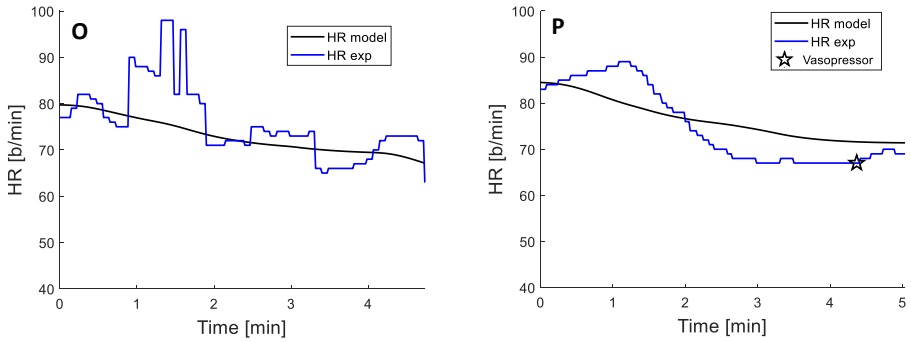

Figure 33 – Validation cases for the HR model. Blue continuous line is HR from the ECG signal, while black continuous line is the model-predicted HR. Red stars in J and N panels indicate stimulation, while the black star in P panel marks the administration of a vasoconstrictor agent to counter hypotension. A black arrow in B and G panels marks particular episodes affecting the HR signal.

Table 24 – RMSE, MDPE, and MDAPE values related to validation of the HR model.

	RMSE [b/min]	**MDPE%**	**MDAPE%**
A	2.12	-3.97	3.97
B	4.99	20.67	20.67
C	7.23	-0.48	2.36
D	6.96	-3.49	4.23
E	8.76	2.09	2.09
F	4.21	-6.31	6.31
G	6.47	-1.30	6.01
H	2.96	-4.96	4.96
I	7.22	-1.95	3.30
J	16.32	4.99	4.99
K	5.17	-9.61	12.98
L	6.21	4.02	4.76
M	1.69	1.79	1.79
N	8.63	3.49	4.47
O	6.89	-8.49	8.49
P	5.04	-3.01	3.01
Median (IQR)	6.34 (4.6-7.22)	-1.62 (-4.46-2.79)	4.61 (6.16-3.15)

5.4.3 Validation of the cardiac output model

Propofol decreases CO via a mechanism of dilation of the venous vessels, which also drives the decrease in MAP (Green, 2015). Again, the dose-effect relation can be suitably described via modified Hill equation. Data of five patients were used to identify the model parameters (listed in Table 25).

Table 25 – Identified parameters of the modified E_{max} model for CO.

	IDENTIFIED PARAMETERS
k_{e0} [min^{-1}]	0.014
E_{max} [L/min]	$CO_{baseline}$0.801
γ [-]	0.588
EC_{50} [µg/mL]	2.501

Validation cases are presented in Figure 34, with CO measurements in red (diamonds) and model predictions in black (continuous line). Missing data are either due to monitor disconnections or artifacts removal. When CO is measured by pulse pressure analysis techniques (*e.g.*, LiDCO Rapid, LiDCO Ltd, London UK, as in West et al. (2018)), CO values will be affected by AP changes. Indeed, reliability of the CO estimation is reduced during periods of hemodynamic instability (Alhashemi et al., 2011). This also means that factors affecting the accuracy of AP measurement will also affect CO measurements, *e.g.*, arterial line positioning, vasoconstriction, and hypothermia. In E and I panels, stimulation is marked with red stars. The model has an acceptable performance in most of the validation cases, despite the inter-patient variability (see also RMSE, MDPE, and MDAPE values reported in Table 26, for quantitative assessment of the model predictive performance). Worst cases are shown in A and H panels in which monitor disconnection has increased the difficulty of assessing a reliable pre-induction value. Although this model will not be used within our controller, it is reliable enough to be used for simulation of propofol effects on CO decrease and investigation of the optimal induction dose, as CO data are not abundant in the scientific literature.

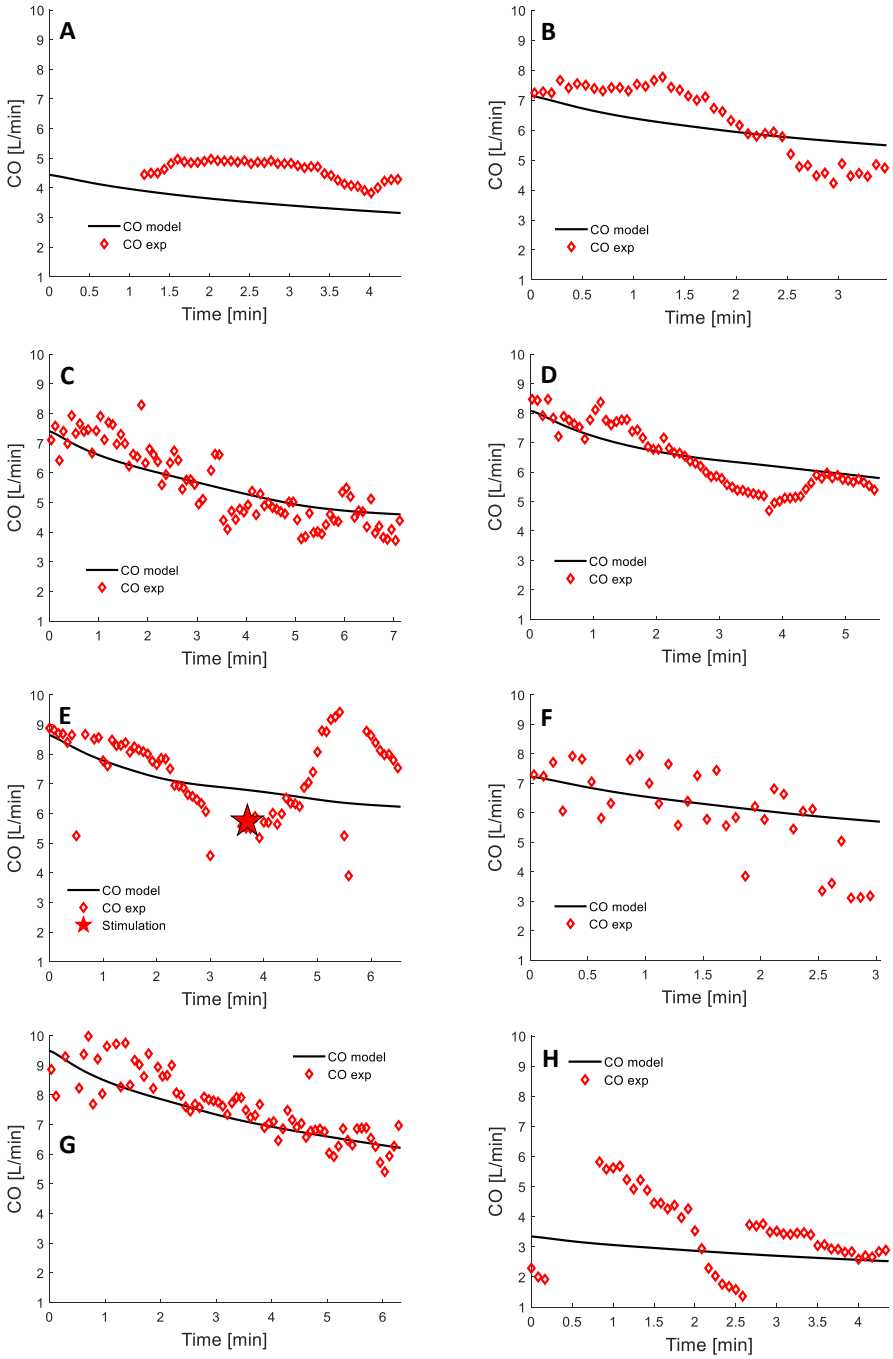
A
B
C
D
E
F
G
H
CO [L/min]
Time [min]
CO model
CO exp
Stimulation

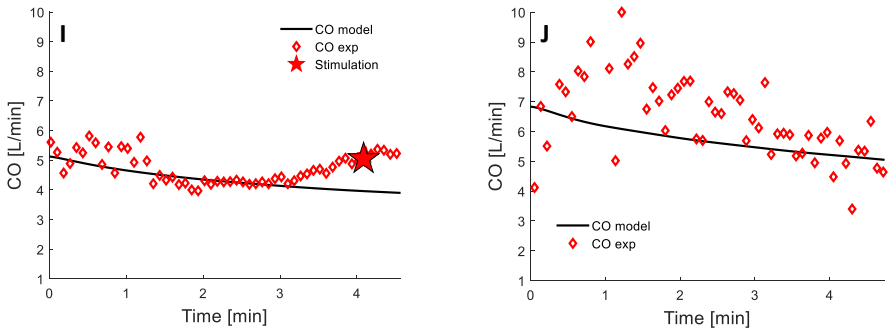

Figure 34 – Validation cases for the CO model. Red diamonds are measured CO values from LiDCO system (LiDCO Rapid, LiDCO Ltd, London UK), while black continuous line is the model-predicted CO. Red stars in E and I panels indicate stimulation.

Table 26 – RMSE, MDPE, and MDAPE values related to validation of the CO model.

	RMSE [L/min]	MDPE%	MDAPE%
A	1.265	-26.05	26.05
B	0.568	2.898	5.04
C	0.899	-1.738	7.441
D	0.597	2.456	4.88
E	1.183	-5.137	7.327
F	1.419	6.627	5.803
G	1.547	2.261	12.948
H	1.225	-12.28	27.31
I	0.828	-0.651	8.873
J	1.54	-8.728	11.574
Median (IQR)	1.204 (0.828-1.419)	-3.437 (-8.728-2.456)	7.384 (5.803-12.948)

5.4.4 Validation of depth of hypnosis model

In the study of West et al. (2018), WAV_{CNS} was used for quantitative assessment of DoH. A PD model featuring a functional dependency on propofol concentration was identified from the WAV_{CNS} data of the high-risk subgroup of the study, with PD parameters reported in Table 27. For the sake of clarity, E_{max} is fixed and equal to 0, consistently with the minimum value that WAV_{CNS} can reach in clinical practice; so it is not a degree of freedom in the identification problem. Figure 35 shows twelve validation cases. While the model performance is acceptable in “normal cases”, *e.g.*, see B, C, F, H, and N panels, strong nonlinearities (*i.e.* burst suppression) evident in

A, G, I, J, O, and P panels are not well-described. This model behavior was already highlighted in Chapter 4A and Chapter 4B, showing and commenting poor prediction of low BIS levels. It is worth mentioning that, in J panel case, hypertension was marked in concomitance with burst suppression behavior, while in all of the other cases, hypotension severe enough to be treated with vasopressors was observed. Despite the presence and robustness of the CBF autoregulation mechanism, variations of AP and CO affect the cerebral perfusion (Drummond, 2019). Indeed, according to Drummond (2019), disruption of the autoregulation and CBF reduction occur at MAP values below ~70 [mmHg]. Naturally, the efficacy of the autoregulation mechanism and this lower value of MAP differ remarkably among individuals. Studies have confirmed that burst suppression is often observed in concomitance with conditions inducing low brain perfusion (Besch et al., 2011; Diedler et al., 2009), and some authors have even investigated the use of BIS as an indicator of ischemia (*e.g.*, Hayashida et al. (2004) and Dahaba et al. (2010)). Indeed, as mentioned in Chapter 4A, the variation of CBF as a function of MAP changes will affect the mechanism of transport of propofol to brain via bloodstream. It may be speculated that the reduction of CBF causes a reduction of propofol to the brain, but at the same time a reduction in brain metabolism and, consequently, the accumulation of propofol at the effect-site. In summary, the observed burst suppression behavior may be attributed to propofol overdosing, on one hand because of its effects on MAP and CBF decrease, and on the other hand because of the potential accumulation of propofol in the body. In fact, the investigation carried out in Chapter 4A showed that part of this burst suppression behavior was observed in concomitance of predicted high plasma levels. The limitation of the currently used PD model of DoH is that the description of the effect-site is not physiologically-based, for the reasons explained in Chapter 4B. However, as explanation and prediction of this behavior remains an open problem, future research should be devoted to modeling propofol brain transport during anesthesia for a better understanding of the underlying mechanisms and the influence of CBF changes, in combination with dedicated pre-clinical and clinical studies. It is likely that such investigations would lead to an improved model for prediction of this clinically relevant phenomenon. The worst MDAPEs are obtained in D, G, and L panels (see Table 28). In D and G panels, the wave index shows an unusual delay in the response to propofol induction that may also be related to drug-independent factors, *e.g.*, problems of the monitoring device, generating inaccuracy of the measurement.

Table 27 – Identified parameters of the modified E_{max} model for DoH.

	IDENTIFIED PARAMETERS
k_{e0} [min^{-1}]	0.075
γ [-]	0.743
EC_{50} [µg/mL]	5.012

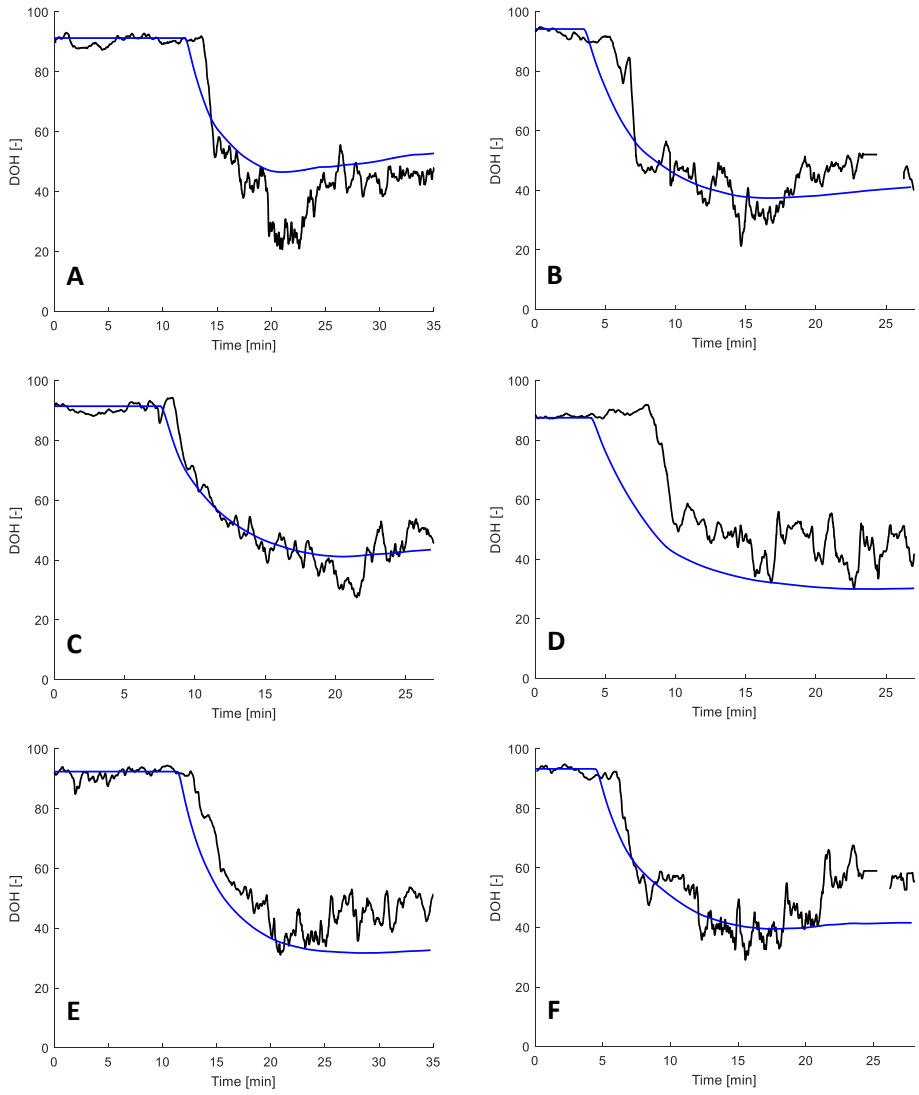

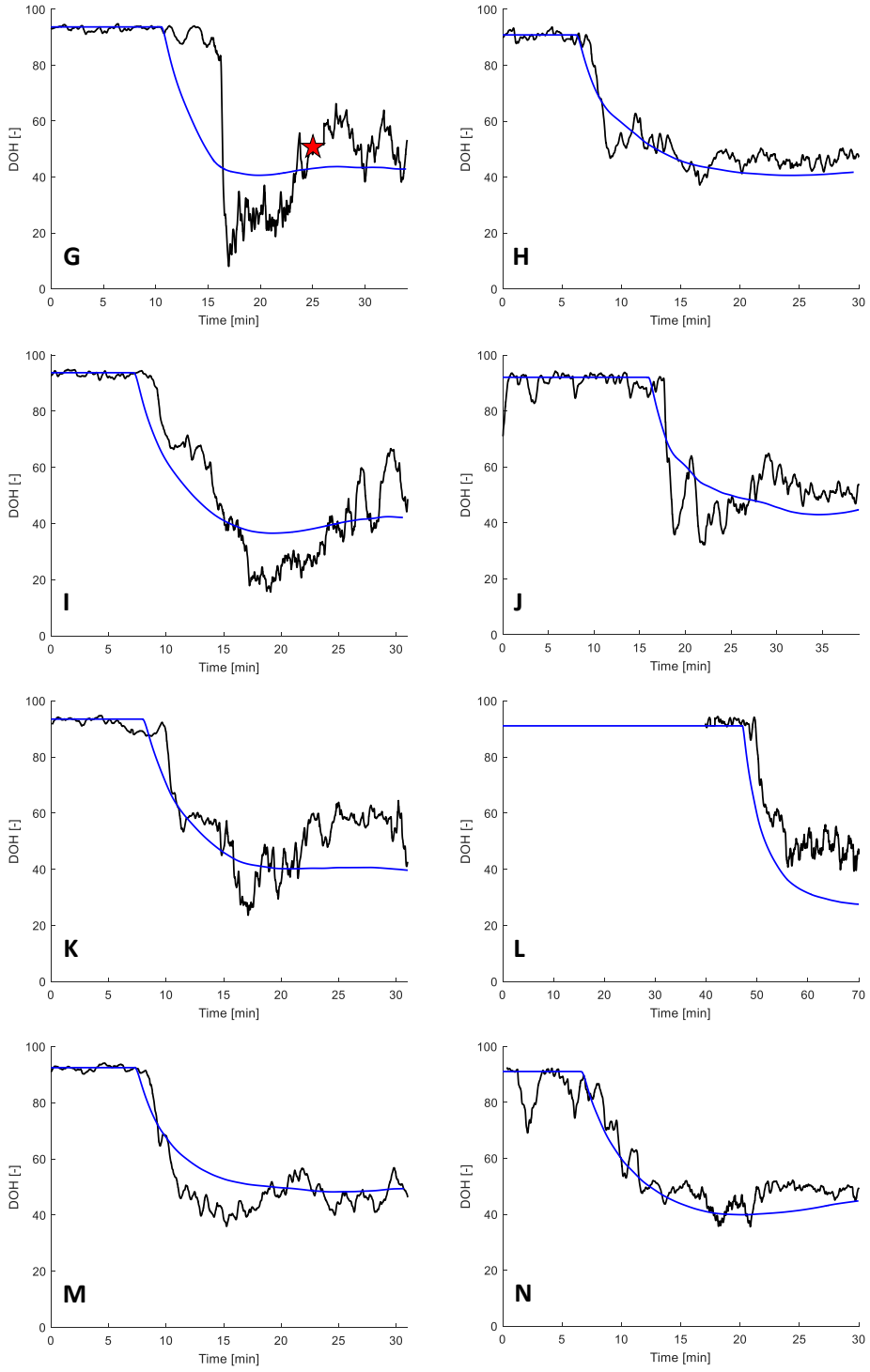
G
H
I
J
K
L
M
N
DOH [-]
Time [min]

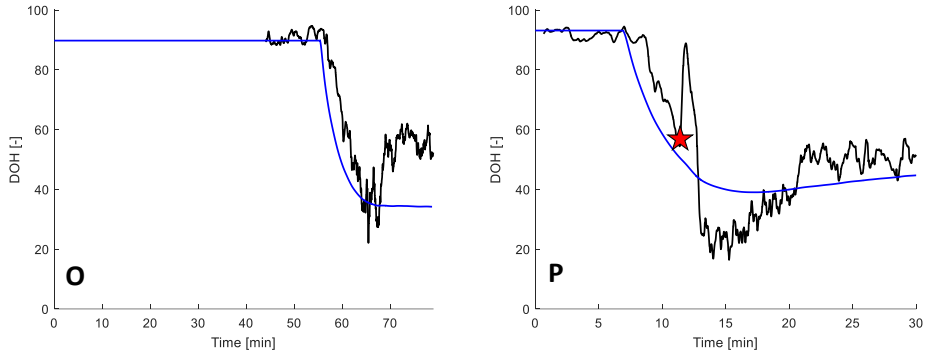

Figure 35 – Validation cases for DoH. Black continuous line is the measured DoH, while the blue continuous line is the model-predicted DoH. Red stars in G and P panels indicate stimulation.

Table 28 – RMSE, MDPE, and MDAPE values related to validation of the DoH model.

	RMSE [-]	MDPE%	MDAPE%
A	8.88	7.28	9.88
B	8.28	-5.60	12.05
C	4.76	0.86	3.67
D	16.86	-27.26	27.26
E	10.11	-14.43	14.43
F	9.53	-4.22	9.89
G	15.69	-0.11	15.38
H	5.14	-4.11	7.71
I	10.70	0.27	13.68
J	8.67	-0.38	8.42
K	10.45	-5.96	10.70
L	15.39	-28.93	28.93
M	6.58	2.13	6.02
N	6.56	-6.25	9.17
O	14.03	-16.12	17.53
P	11.09	-3.64	14.44
Median (IQR)	9.82 (7.43-12.56)	-4.16 (-10.34-0.08)	11.38 (8.80-14.91)

5.4.5 Individual PD models of DoH, MAP, and HR

To test the controller performance and simulate the “mismatch” typical of real

applications, eight PD individual models of patients were identified from the DoH, MAP, and HR data of the high-risk subgroup. We selected the patients trying to equilibrate the number of those featuring "challenging" data profiles (*i.e.* in which burst suppression and hypotension episodes were observed), and more stable cases. Unfortunately, the subgroup high-risk patients was mostly composed of male individuals, and the eight patients chosen according to these criteria are all males. The demographic characteristics of the patients are reported in Table 29. The eight models are used to simulate the dose-effect relation of *in silico* patients to evaluate the controller performance during induction of anesthesia. Identified individual PD parameters are reported in Appendix 5.A.

Table 29 – Demographics of the patients whose clinical data are used to identify the individual models of the eight *in silico* patients.

Patient #	TBW [kg]	H [cm]	Gender [-]	Age [y]
1	98	174	M	60
2	70	172	M	35
3	77	182	M	76
4	74	168	M	69
5	108	188	M	59
6	90	179	M	74
7	90	188	M	54
8	106	173	M	79

5.5 *In silico* simulations of the model-predictive controller in eight high-risk patients

5.5.1 Induction of anesthesia

Figure 36 shows the results of the simulations of closed-loop controlled induction of propofol-remifentanil anesthesia in eight high-risk patients. For a realistic simulation, noise is also simulated, based on the analysis of the clinical data (the same method as Chapter 3 was applied). Control action starts after 5 min, for a clearer visualization of the anesthesia-induced changes of the physiological parameters DoH, MAP, and HR. Figure 36 (top panel) shows the dynamics of the input variables to the controller. Figure 36 (bottom panel) shows the dynamics of the manipulated variables, *i.e.* propofol and remifentanil IRs.

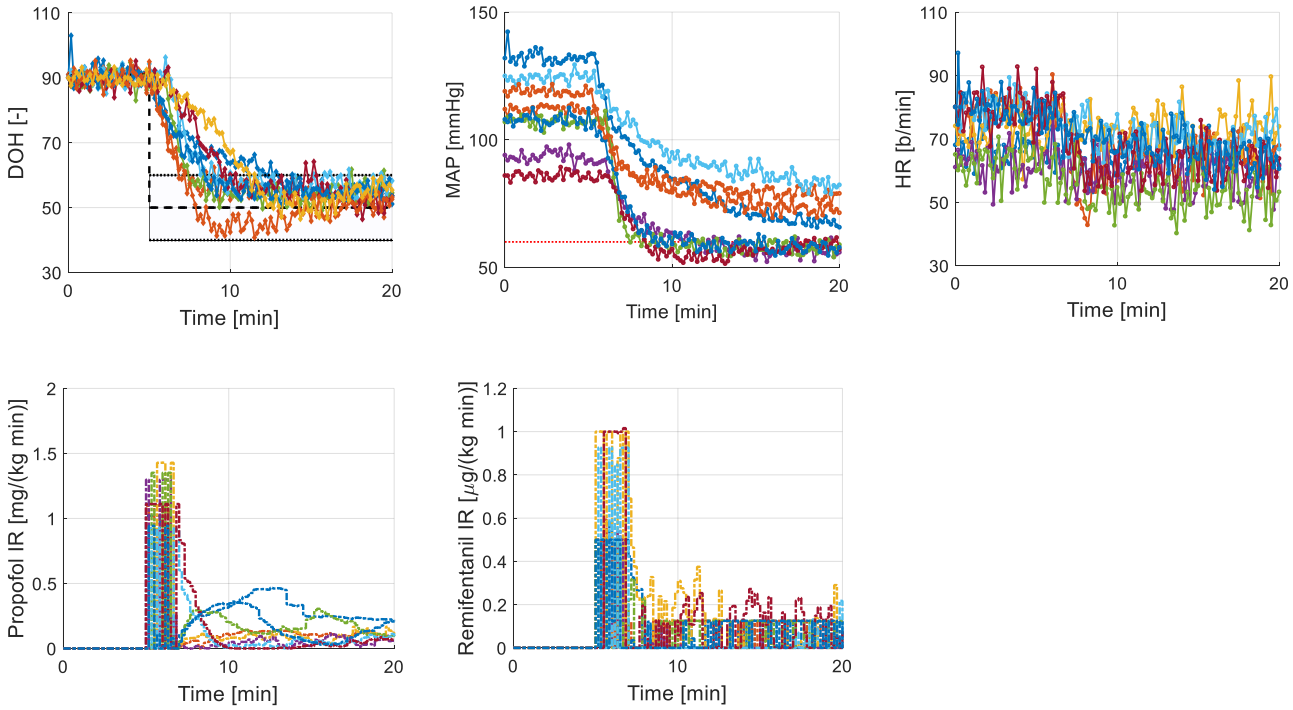

Figure 36 – Simulation of induction of propofol-remifentanil anesthesia in eight high-risk patients. (Top panel) Dynamics of controlled variables (DoH, MAP), and input variable HR. (Bottom panel) Dynamics of the manipulated variables, *i.e.* remifentanil and propofol IRs. A straight red line corresponding to MAP= 60 mmHg marks the hypotension region. The rectangle area in the DoH plot denotes the recommended clinical range, 40-60 [-], while the dashed black line marks the setpoint = 50 [-].

For the sake of clarity, it is worth underlining that while DoH setpoint is set at 50 [-] and marked with a dashed black line and a rectangle area indicating the recommended clinical range, *i.e.* 40-60 [-], no setpoint is marked in the MAP panel. Indeed, each patient has a specific setpoint, which is individualized depending on their pre-induction value (that was set basing on the patients' clinical data from West et al. (2018)). For this reason, MAP trends tend to different values after 15 min from the start of induction. As PD models are from "at-risk" patients, MAP rise-times are quite low (~2-3 min) but take longer to stabilize. Indeed, the dynamics of propofol hypnotic effects is faster than that of the cardiovascular effects (Kazama et al., 1999). DoH rise-times are higher compared to those obtained for standard adult patients (see Chapter 3), ranging from 3 to 20 min (approximately), but propofol induction infusion rates are lower and MAP and HR drops are contained within safe ranges. The performance is thus more appropriate for high-risk patients, as the controller finds a successful trade-off among inducing and maintaining a suitable level of DoH and preventing hypotension/bradycardia episodes. Indeed, the horizontal red line in MAP graph indicates the lower boundary value that is generally 60 [mmHg]. In clinical practice, the lower boundary can be higher than that, depending on the patients' conditions. In

any case, it is worth underlining that the MAP trends of the simulated patients do not actually overcome this value, except for the patient with the lowest pre-induction MAP value. Consistently with the analysis of clinical data shown in Chapter 4A, HR shows a reduced decrease compared to MAP. At this stage, neither HR nor MAP changes were implemented to test the controller reaction to disturbances caused by stimuli. For this reason, remifentanil IR shows a standard bolus-infusion trend, in accordance with the clinical practice of anesthesia induction. The remifentanil IRs shows different profiles, as they are modulated according to the patients' age.

5.5.2 Effect of CO changes on induction

In Chapter 4A, we showed how the cardiovascular changes affect the pharmacokinetics and pharmacodynamics of propofol, and thus alter the response to induction of anesthesia, contributing to inter-individual variability. In this section, we show how by feeding CO data to the controller, the optimization routine takes into account this piece of information to better individualize the infusion rate profiles.

Three individual CO models depending on the propofol infusion rate were identified with data of West et al. (2018). Results are shown in Table 30 and Figure 37, in which the black continuous line is the model-predicted CO and red diamonds are CO measurements of that specific patient. The model provides a satisfactory fitting in all cases and, interestingly, the resulting value of k_{e0} is the same in all the three cases.

Table 30 – Identified PD parameters of the three individual modified E_{max} models for CO.

	PATIENT 1	**PATIENT 2**	**PATIENT 3**
k_{e0} [min^{-1}]	0.011	0.011	0.011
E_{max} [L/min]	E_0*0.809	E_0*1.021	E_0*0.988
γ [-]	0.62	0.35	0.88
EC_{50} [µg/mL]	2.869	3.184	1.004

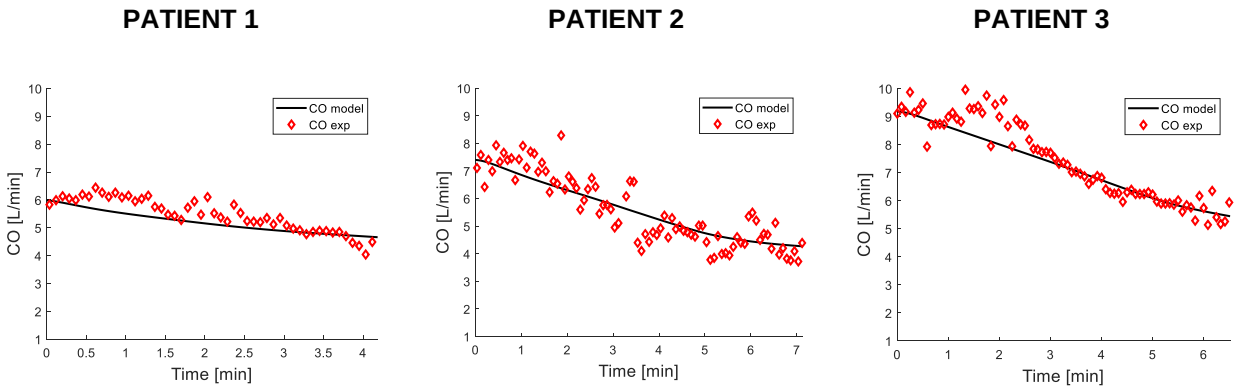

Figure 37 – Individual CO predictions (black continuous lines) vs measured CO (red diamonds) of three different patients from West et al. (2018).

The three models are used to simulate different CO dynamics for the same virtual patient (see Figure 38, A panel in which the model derived from data of patients 1, 2, and 3 are respectively represented by the blue, yellow, and orange continuous lines) and test the controller performance during induction of anesthesia following the resulting three different pharmacokinetic profiles. In Chapter 4A, we observed that more enhanced CO drops correspond to higher plasma levels. As a result, the controller proposes a total of -12% and - 15% (yellow and orange lines, respectively) propofol dosing for induction (see Figure 38, B panel), while it is able to maintain an acceptable control action on DoH and MAP (see Figure 38, C-D panels). In fact, induction is slower (as in Paragraph 5.5.1) with a DoH rise-time of ~10 min for DoH, but MAP does not overcome the lower boundary value of 60 mmHg.

These simulations confirm that the inclusion of CO data, when available, contributes to individualize the prediction and, most importantly, can help avoiding unnecessary overdosing. This feature is only possible as a result of PBPK modeling application within the controller.

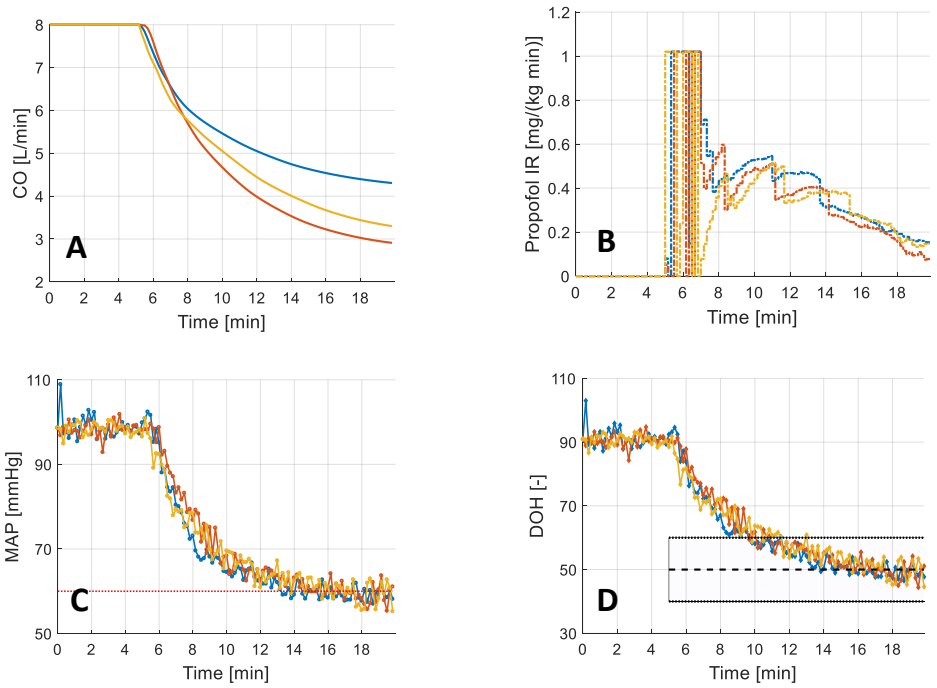

Figure 38 – (A panel) Three different CO dynamics simulating three different trends of CO for the same patient. (B panel) Dynamics of propofol infusion rate proposed by the MPC controller. (C and D panels) Dynamics of controlled variables MAP and DoH. In C panel, red horizontal dotted line indicates lower limit of MAP, *i.e.* 60 mmHg. In D panel, the black horizontal dashed line indicates the setpoint, and the black continuous horizontal lines indicate the optimal range of DoH (40-60).

5.6 Conclusions

Challenging cases from the point of view of optimal dosing represent the most appealing and promising clinical application of closed-loop controllers of anesthesia. However, to provide an actual support tool for the clinicians, it is necessary to tackle the procedure as a multivariable problem. Closed-loop studies rarely focus on hemodynamic parameters, despite their impact on the outcome of the procedure and on the patients' recovery. Inclusion of hemodynamic parameters within closed-loop controllers is indeed complicated, mainly because hemodynamic data are affected by several anesthetic/analgesic drug-independent events. We showed that, despite these intrinsic difficulties, the identified PD models exhibit acceptable predictive performance, and their inclusion in the model-predictive controller allows achieving a slower but safer induction in simulated high-risk patients. The inclusion of AP and HR within the model structure also opens to the guarantee of fast rejection of disturbances during the maintenance phase, which will be focus of further investigations.

To our knowledge, no other study on closed-loop controllers has ever tested the use of CO data within a model-predictive controller of anesthesia. We showed that

inclusion of such an additional piece of information is extremely valuable from the point of view of avoiding unnecessary overdosing, which can provoke either minor or major complications in high-risk patients, *e.g.*, it was associated to post-operative delirium. This kind of investigation was only possible because of the application of a physiologically-based approach to PK modeling.

Acknowledgements: We acknowledge Profs Guy Dumont and John Ansermino for precious discussions and suggestions and for making their datasets available for this work.

5.7 Appendix 5.A

Table A – Individual MAP models for the eight *in silico* patients.

	1	**2**	**3**	**4**	**5**	**6**	**7**	**8**
$k_{e0,R}$ **[min^{-1}]**	2.5e-2	1.4e-2	1.97e-2	2.7e-2	9.1e-2	5.3e-2	7.4e-2	7.4e-2
$E_{max,R}$ **[mmHg]**	51.31	37.72	57.53	30.54	28.66	61.09	31.53	27.78
γ_R **[-]**	1.26	1.99	2.0	1.37	1.101	1.99	1.3	1.28
$EC_{50,R}$ **[ng/mL]**	2.53	0.29	0.17	2.045	1.58	0.87	1.77	1.94
$k_{e0,P}$ **[min^{-1}]**	0.0493	0.091	0.018	0.051	0.075	0.0503	0.059	0.0586
$E_{max,P}$ **[mmHg]**	54.133	50.36	57.11	51.24	23.599	38.27	40.973	65.87
γ_P **[-]**	1.152	1.20	2.029	1.11	1.50	1.4	1.243	1.18
$EC_{50,P}$ **[µg/mL]**	1.849	1.869	0.156	1.769	2.251	1.7	1.936	1.602
$\beta_{2,Emax}$ **[-]**	1.773	1.713	1.033	1.983	1.764	1.53	1.517	1.773
$\beta_{3,Emax}$ **[-]**	1.131	0.991	0.229	0.817	1.065	1.081	1.046	1.20
$\beta_{4,Emax}$ **[-]**	0.523	0.507	0.324	0.283	0.139	0.492	0.471	0.557
$\beta_{2,U50}$**[-]**	-2.356	-6.288	-5.696	-9.433	-6.845	-4.716	-4.792	-2.226
$\beta_{2,\gamma}$ **[-]**	-2.248	0.055	-5.006	-0.613	-3.743	-2.554	-2.288	-0.890

$\beta_{3,\gamma}$ [-]	1.336	1.638	0.084	1.732	0.448	1.01	1.122	1.537
$\beta_{4,\gamma}$ [-]	0.104	0.092	0.142	0.052	0.072	0.101	0.106	0.098

Table B – Individual HR models for the eight *in silico* patients.

	1	2	3	4	5	6	7	8
$k_{e0,R}$ [min^{-1}]	4.96e-1	1.15e-1	1.75e-2	1.32e-1	4.8e-2	7.1e-2	1.39e-1	3.4e-2
$E_{max,R}/E_0$[-]	0.118	0.575	0.867	0.64	0.779	0.614	0.776	0.4
γ_R [-]	2.71	1.17	2.0	0.494	1.21	1.324	7.312	1.0
$EC_{50,R}$ [ng/mL]	12.35	1.634	0.343	1.767	1.11	2.128	2.142	2.264

Table C – Individual DoH models for the eight *in silico* patients.

	1	2	3	4	5	6	7	8
$k_{e0,P}$ [min^{-1}]	0.0566	0.148	0.078	0.287	0.0654	0.075	0.088	0.155
$E_{max,P}$ [-]	0.	0.	0.	0.	0.	0.	0.	0.
γ_P [-]	0.584	1.056	2.045	1.8	0.592	7.785	0.895	1.47
$EC_{50,P}$ [µg/mL]	15.47	4.630	3.458	10.106	5.824	6.303	5.114	12.012

CHAPTER 6

Melatonin benefits for the critically ill

6.1 Author's Note

In recent years, researchers have manifested a great enthusiasm for melatonin, as several beneficial effects on the human body have been emerging in addition to the well-known action as sleep regulator, *e.g.*, immunomodulatory, anti-oxidant, and anti-carcinogenic functions. This chapter introduces the main characteristics of critically ill patients and explains the reasons for that significant interest in applying melatonin to intensive care.

Some parts of this chapter are re-elaborated from a work produced in collaboration with Ospedale San Paolo (Milan, Italy) and published in "Clinical Endocrinology" journal:

> ***Different routes and formulations of melatonin in critically ill patients. A pharmacokinetic randomized study***
>
> *Giovanni Mistraletti, Rita Paroni, Moro Salihovic, Sara Froio, Paolo Gasco, Adriana Savoca, Davide Manca, Russel J Reiter, Gaetano Iapichino*
>
> *Clinical Endocrinology, 91(1):209-218*

DOI: 10.1111/cen.13993

6.2 The critically ill patient and melatonin

Critical illness is a life-threatening process that leads to mortality or significant morbidity, in lack of medical intervention. It is usually related to one or more patho-physiological processes that compromise cardiovascular, respiratory, and neurological functions (Robertson and Al-Haddad, 2013). Critically ill patients require intensive care, and most of them need life support and intensive monitoring. Because of the heterogeneity and critical level of their conditions, they usually manifest remarkable variability in the response to drugs.

In recent years, there has been a remarkable hype for melatonin, as testified by the increasing trend of the number of scientific publications on melatonin since the year 2000 (see Figure 39). Melatonin is an endogenous substance produced by the mammalian pineal gland. In healthy individuals, the production process is entrained with the circadian (*i.e.* day-night) rhythm (Brzezinski, 1997). Indeed, melatonin endogenous production onsets with darkness, when the retinal photoreceptors release norepinephrine to the gland, provoking the increase of the number of α-1 and β-1 adrenergic receptors. Such receptors activate the enzymes involved in melatonin bio-synthesis from serotonin. Thus, melatonin levels are low during the day, peak between 2-4 AM, and return to low baseline values in the early morning (see Figure 40). Endogenous melatonin levels also decline gradually with advancing age (see Figure 40).

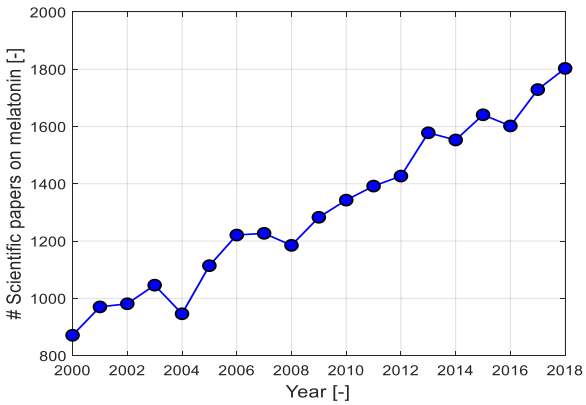

Figure 39 – Number of published scientific papers on melatonin over the years 2000-2018. *Source*: Scopus database research.

Alterations of the circadian rhythms are associated with sleep disturbances, *e.g.*,

night-shift workers and people suffering from jet-lag are among the patients presenting disruption of such secretion rhythm. Exogenous melatonin can be administered to restore the endogenous rhythm and its use as cure for sleep disorders is quite spread (Auld et al., 2017; Fares, 2011; Medeiros et al., 2007). However, several other functions are emerging when supraphysiological levels are reached, associated to melatonin action as an anti-oxidant and a scavenger of free radicals, among which anti-carcinogenic, immunomodulatory, and anti-aging effects (Karbownik et al., 2001; Kleszczynski and Fischer, 2012; Mehta and Kaur, 2014; Reiter et al., 2014; Srinivasan et al., 2006).

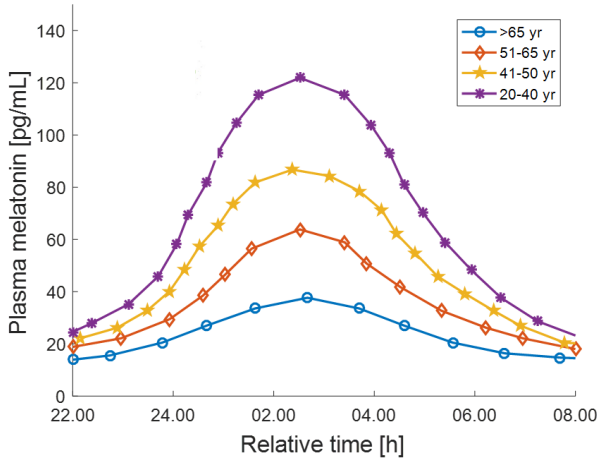

Figure 40 – Typical endogenous melatonin levels in healthy patients as a function of age (Adapted from Karasek and Winczyk (2006))

Sleep disruption is a common problem in intensive care unit (ICU) patients and has adverse short- and long-term effects on their health. In fact, it is associated with emotional distress and mood disorders, alterations in metabolism, impairment of immune, hormonal and cardiovascular system, and gastrointestinal disorders (Mistraletti et al., 2019). Andersen et al. (2014) emphasize that the appeal of melatonin use in clinical practice is related not only to the beneficial clinical effects, but especially to the safety profile, because most used analgesics and sedatives have clinically relevant side-effects, *i.e.* respiratory depression, post-operative delirium, post-operative nausea and vomiting (PONV), and would thus introduce risks of further compromising the health status of critically ill patients. In fact, in an interesting and complete review investigating melatonin administration to different categories of individuals (including the critically ills), Andersen et al. (2016a) show that exogenous melatonin administration to humans is safe, even at high doses (*e.g.*, Andersen et al. (2016b)) and only mild adverse effects have been reported *e.g.*, sleepiness, dizziness,

nausea, and headache, but in levels corresponding to placebo treatments.

Altered patterns of circadian melatonin secretion and/or low endogenous levels have been found in a number of studies on critically ills (Mundigler et al., 2002; Paul and Lemmer, 2007; Shilo et al., 1999). Whether this phenomenon is to be attributed to lower endogenous production or enhanced elimination is still unclear (Mistraletti et al., 2019). Advanced age is a typical feature of ICU patients and is likely a contributing factor. In the scientific literature, different approaches have been proposed to analyze circadian rhythms (Refinetti et al., 2007). The cosinor method is one of the simplest and most well-established approaches. A model of cosine curves with 24 h period is fitted to the data, so that the periodicity of the circadian pattern can be analyzed, basing on the goodness-of-fit. In Mistraletti et al. (2019), we used this method to investigate the periodicity of endogenous melatonin secretion in 21 critically ill patients (see Figure 41). Figure 41 shows the resulting cosine curves (orange continuous lines) against the experimental data of endogenous melatonin concentration (blue diamonds) in the studied patients. Despite inter-individual variability of melatonin PK, the analysis confirmed a 24h-periodicity of endogenous melatonin concentration profile. As expected, significant inter-individual differences were found. Specifically, three of the patients manifested abnormal values of C_{max} (> 100 pg/mL, see asterisks in Figure 41). Interestingly, Mistraletti et al. (2019) underline that high endogenous concentrations have been associated with mortality in septic patients (Lorente et al., 2015). Interactions with other drugs, organs failure, septic state, and mechanical ventilation are all factors potentially contributing to such variability, which has already been described by other authors in the critically ills. Zero-amplitude testing revealed that the circadian rhythm was not significant in 85% of the patients. These results are consistent with literature findings on similar patients (Paul and Lemmer, 2007; Perras et al., 2007). However, it is worth mentioning that a limitation of this study is the limited number of blood samples and especially the sampling period (*i.e.* over 24 h) (Mistraletti et al., 2019).

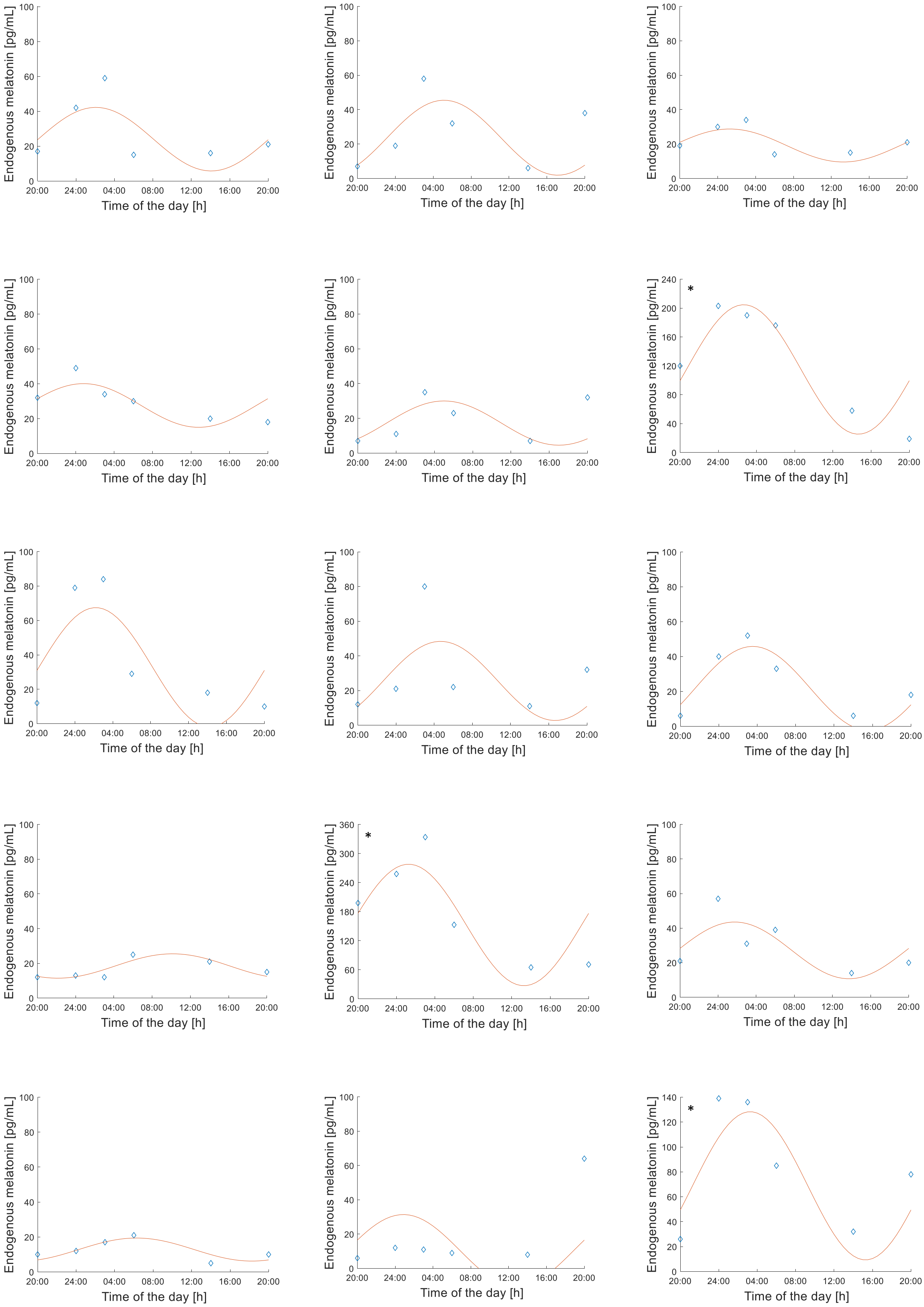

Endogenous melatonin [pg/mL]
Time of the day [h]
20:00 24:00 04:00 08:00 12:00 16:00 20:00
*

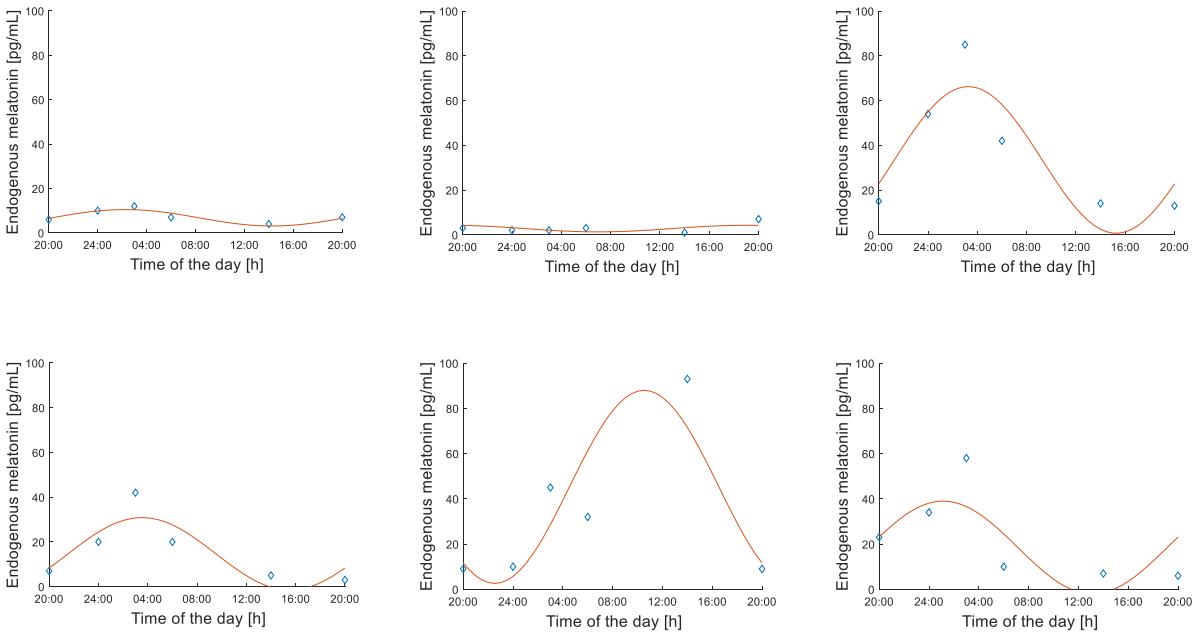

Figure 41 – Regressed cosinusoidal functions (orange continuous line) against the experimental data of endogenous melatonin (blue diamonds) in 21 critically-ill patients. Small black asterisks indicate three patients whose levels are abnormally high (*i.e.* C_{max} >100 pg/mL).

In critically ill patients, exogenous melatonin has been proved to have hypnotic, anti-oxidant, analgesic, and anti-septic effects, other than being a sleep regulator (Bellapart and Boots, 2012; Galley et al., 2014; Gitto et al., 2001; Mistraletti et al., 2017; Mistraletti et al., 2015; Wilhelmsen et al., 2011). A number of recent PK studies have investigated different dosing and routes of administration with the goal of restoring healthy endogenous levels in these patients (Bellapart et al., 2016; Bourne et al., 2008; Gögenur et al., 2014; Mistraletti et al., 2019; Mistraletti et al., 2010; Shilo et al., 2000).

Indeed, because of its physiochemical characteristics (*i.e.* high lipophilicity and small molecular weight), melatonin can be administered via at least three different routes: IV, oral (*per os*, PO), and transdermal (TD). The selection of the optimal route should take into account the features (and limitations) of each route along with the characteristics of the PK curve resulting from the route-specific ADME processes and the patients' conditions (see Table 31). For instance, IV route may not meet compliance in a healthy patient, while it is more feasible in an ICU patient, who is often subject to enteral and parenteral nutrition and continuous administration of fluids/drugs. A healthy patient may prefer painless routes such as PO and TD, which also allow self-administration. PO and TD routes are characterized by slow absorption processes, because the drug has to be absorbed through gastrointestinal walls and

skin layers, respectively, before reaching the systemic circulation and being distributed to the organs and tissues, and thus the site of action. Differently, the IV route features the administration of the total dose to the systemic circulation and also avoids the so-called “first-pass” hepatic effect. As a consequence, higher levels in plasma are to be expected with the same dose administered via IV rather than PO or TD pathways. Indeed, the IV route can induce higher peaks and concentration oscillations that may result in a faster response to the drug but also potential adverse effects. The processes of (i) absorption through the intestinal walls and skin layers and (i) metabolism within the liver and skin, introduce remarkable inter- and intra-individual variability (*e.g.*, related to the digestion state, pH, and temperature in the gastrointestinal environment, skin characteristics, genetics, and interactions with concomitant medications).

Table 31 – Some features of the three main routes of administration for melatonin.

ORAL	**TRANSDERMAL**	**INTRAVENOUS**
Easy, patient-compliant, not always feasible	Easy, patient-compliant	Distressing for many patients and expensive
Slow absorption, “first-pass” hepatic effect	Very slow absorption, no “first-pass” hepatic effect	Directly administered to the systemic circulation
High inter-individual variability (pH, body temperature, genetics)	High-inter-individual variability (skin characteristics, peripheral perfusion, body temperature, genetics, location of the drug delivery system)	Reduced inter-individual variability compared to other routes

These qualitative knowledge can be supported by quantitative PK simulations to assess the *optimal* route of administration and dosing for a better design and outcome of the clinical experiment. In fact, Andersen et al. (2014), who discuss the perioperative use of melatonin, highlight that the correct time of administration in relation to the desired effect is still under investigation, as well as the effective dosage. Indeed, they report “*The correct dosage of melatonin in humans seems largely unknown and should be investigated further, documenting dose–response curves for the individual indications* “. PBPK simulations can thus offer support in this sense, as they can be used as tool for investigation of optimal dosing and time of administration to obtain the desired PK profile. The following chapters are thus devoted to the development of a PBPK model to simulate resulting pharmacokinetics of melatonin from the three mentioned routes, and to show a methodology for assessment of optimal dosing and timing of administration for critically ill subjects.

CHAPTER 7

Physiologically-based pharmacokinetic modeling for transdermal delivery

7.1 Author's Note

TD administration of drugs has the advantages of meeting patients' compliance and producing sustained drug levels within the blood. This chapter focuses on the adaptation of a reference PBPK model to include TD administration route. Indeed, the typical homogenous compartmental description of PBPK modeling is combined with a more detailed description of the drug evolution along the skin depth coordinate to account for the drug absorption through skin. The model can be suitably adapted to any drug that is appropriate for TD administration (*e.g.*, depending on solubility and molecular weight). The specific case of melatonin is used here for identification and validation of the model.

This work was published in "Computers and Chemical Engineering" journal:

A physiologically-based diffusion-compartment model for transdermal administration – The melatonin case study

Adriana Savoca, Giovanni Mistraletti, Davide Manca

Computers and Chemical Engineering 113, 115–124, (2018)
DOI: 10.1016/j.compchemeng.2018.03.008

7.2 Abstract

There is a significant hype in the medical sector for the transdermal administration of drugs as it allows achieving a combination of multiple advantages: non-invasive procedure, pain avoidance, no first-pass hepatic metabolism, and induction of sustained plasma levels. This paper proposes a model for the study and prediction of drug transport through skin and the following distribution to human body. This is achieved by an innovative combination of the physiologically-based compartmental approach with Fick's laws of diffusion. The skin model features three strata: stratum corneum, viable epidermis, and dermis, which have a major impact on the absorption, distribution, and metabolism of transdermal drugs. The combined model accounts for skin transport via diffusion equations, and absorption and distribution in the rest of the body (*i.e.* organs/tissues) via material balances on homogeneous compartments. Experimental data of transdermal melatonin allow validation. Main applications are optimization of the dosage and study of skin transport.

7.3 Introduction

Recent years have seen a rising interest in transdermal (TD) delivery as an efficient route for drug administration. Figure 42 shows the number of transdermal drugs approved by Food and Drug Administration (FDA, USA) since 1996 (FDA Orange Book, 2017).

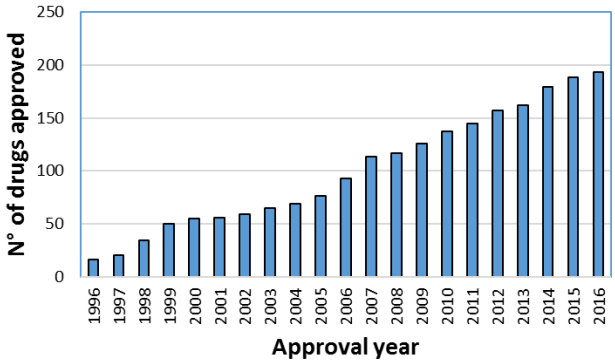

Figure 42 – Cumulative amount of transdermal drugs approved by Food and Drug Administration (FDA) since 1996 (FDA Orange Book, 2017).

This interest arises from some advantages that transdermal delivery exhibits if

compared to other routes of administration (*e.g.*, enteral and parenteral). From a practical point of view, the most evident appeal of percutaneous (*i.e.* TD) delivery consists of combining a positive patient compliance with ease of administration. In fact, TD delivery does not necessarily require specialized medical staff and is noninvasive.

From the pharmacokinetic point of view, the main advantage is that the drug is directly administered to the systemic circulation. This means avoiding the first-pass hepatic metabolism, which is the main cause for the characteristic low bioavailability resulting from oral route, although some minor metabolism or binding to cellular components may occur in the skin (Prausnitz and Langer, 2008).

Therefore, skin permeation is an attractive alternative whenever factors such as gastrointestinal pH, drug interaction with food, and liver diseases prevent oral administration (Mali, 2015). Furthermore, TD delivery ensures no risks of sudden fluctuations or peaks of the drug concentration in plasma, which translates into sustained levels and reduced side effects.

On the other hand, TD application comes with high inter-patient variability related to age, gender, physical characteristics, genetic factors, and living habits (Sandby-Moller et al., 2003), and is not suitable for all drugs. In fact, some physicochemical characteristics such as molecular weight and solubility may have a significant impact on the pharmacokinetics, and therefore must be taken into account when selecting the route of administration. In addition, slow absorption is another undesired pharmacokinetic trait that is intrinsic to TD administration.

In order to simulate the transdermal administration route of drugs and their distribution, metabolism, and excretion (*i.e.* ADME processes) within the human body, we developed a physiologically-based diffusion-compartment pharmacokinetic (PBDCPK) model. This dynamic model can be useful for the assessment of the optimal dosage, and in general for the development of drugs/substances for TD delivery, evaluation of toxicity/positive effects, and analysis of skin transport mechanisms.

Some authors describe skin transport by assuming stationary conditions, as their only goal is to either analyze or explain specific experimental data (Anissimov et al., 2013). Higaki et al. (2002), and Singh and Roberts (1994) developed compartment models that allow describing drugs pharmacokinetics in the skin layers, in the systemic circulation, and in some tissues of the body, *e.g.*, muscles, adipose tissue. However,

they only focused on some specific tissues and did not consider the parameters governing skin transport as depending on skin depth. In fact, skin was described as a bi-layer homogenous concentration compartment.

Furthermore, they did not consider the possibility of any occurring metabolism or binding.

The idea of describing skin transport as a function of both time and space is not new. In fact, Marquez-Lago et al. (2010) proposed a noteworthy 3D porous media model of the stratum corneum (*i.e.* the most superficial layer of the skin epidermis) but did not investigate the distribution in the whole human body. Kretsos et al. (2004) employed diffusion equations focused exclusively on skin penetration. This manuscript attempts to combine two aspects investigated in the literature: (i) the physiologically oriented approach towards skin transport and (ii) the attention to ADME processes within the rest of the body. The proposed model is applied to the simulation and prediction of TD melatonin pharmacokinetics. Melatonin is a biogenic amine that is commonly found in animals, plants, and microbes. In mammals, melatonin is the main substance produced by the pineal gland (Brzezinski, 1997). In humans the endogenous production follows the day-night cycle (*aka* “circadian rhythm”), with a baseline level of about 10 pg/mL during the day. Melatonin concentration starts increasing with the onset of darkness and peaks (60-100 pg/mL) at 2-4 AM. Afterwards, the concentration gradually decreases and stabilizes on the daily baseline value. Several researchers are nowadays interested in melatonin numerous benefits on the human body. In humans, melatonin is regularly employed as a treatment for sleep disturbances (*e.g.*, jet lag, nightshift workers, people suffering from insomnia) (Brzezinski, 1997). Melatonin proved to benefit patients suffering from mood disorders (*e.g.*, depression, seasonal affective disorder), and neurological pathologies (*e.g.*, Alzheimer’s disease) (Hickie and Rogers, 2011; Srinivasan et al., 2006). There is some evidence of anti-proliferative effects in cancer and anti-aging effects through anti-oxidant and free-radical scavenging mechanisms (Karbownik et al., 2001; Kleszczynski and Fischer, 2012; Mehta and Kaur, 2014; Srinivasan et al., 2008). A disruption of the circadian rhythm of melatonin can be observed in intensive care unit (ICU) patients (Mistraletti et al., 2010). ICU stay is thought to have a series of negative effects on patients’ sleep and, in general, on their health status. As ICU patients’ conditions can be improved by the melatonin anti-oxidant, immune-regulatory, and sleep regulatory properties, it is possible to administer exogenous melatonin in order to restore the endogenous production rhythm. Indeed, it is desirable that the pharmacokinetics of exogenous

melatonin mimics the sustained endogenous profile. Therefore, for this specific case, the previously reported advantages of the transdermal administration are convenient, and the slow absorption becomes actually a useful characteristic, despite being a drawback for most drugs.

Furthermore, melatonin physicochemical characteristics (*i.e.* low molecular weight and lipophilicity) increase the probability of crossing the skin barrier.

7.4 Methods

7.4.1 Skin histology and transdermal devices

An in-depth understanding of human anatomy and physiology allows driving the engineers' modeling activity of the transdermal administration route and correlated PBDCPK. Skin is the means for transdermal release of drugs and deserves a comprehensive insight to recognize the main mass transfer phenomena that rule their percutaneous delivery to the systemic blood flow. Human skin is the largest organ of the body and consists of three main layers: epidermis, dermis, and hypodermis (*i.e.* subcutaneous tissue). Epidermis is the thinnest and most superficial layer, and the most important for its protective function. Dermis (thickness 1.5-4 mm, Anissimov et al. (2013)) is thicker and consists of connective tissue. It contains nerves, sweat glands, hair follicles, and blood and lymphatic vessels. Hypodermis mainly consists of adipose tissue and sweat glands. Its main function is to support epidermis and dermis.

From the modeling point of view and according to the skin physiology, it is more consistent to separately consider two sublayers of the epidermis: stratum corneum (SC) (average thickness of fore-arms, face, abdomen 10-30 µm, Anissimov et al. (2013)) and viable epidermis (VE) (average thickness of fore-arms, face, and abdomen 50-100 µm, Anissimov et al. (2013)). In fact, SC is the outermost stratum and consists of a keratinized tissue, which comprises low hydrated and highly dense cell layers. For this reason, it is the most difficult to penetrate. VE is a more aqueous phase, and can be site of metabolism, binding, and active transport. In some models, it is merged with dermis, which is an aqueous medium as well (Jepps et al., 2013).

Differently from topical delivery, the goal of transdermal (or percutaneous) delivery is to pass the skin barrier and enter systemic circulation. In this case, drugs are directly applied on the skin in gel or transdermal devices (TDDs), *i.e.* patches. Hence, the amount of drug and the surface of the skin area on which the drug is applied are key

parameters. Patches contain therapeutic amounts of drugs, and mainly consist of a backing for protection from the external environment and a polymeric matrix that controls the drug release. Patches often contain some penetration enhancement agents (*e.g.*, alcohols) to improve skin penetration of the drug, and other excipients (*e.g.*, adhesive). Depending on the patch, they are usually applied from one to seven days (Mali, 2015).

7.4.2 Skin transport equations

Our model accounts for three main layers to describe the drug concentration evolution in the skin: SC, VE, and dermis (DE). Hypodermis is neglected as the drug enters the systemic blood flow as soon as it reaches the dermis. Diffusion is the main phenomenon involved in drug transport across skin. For this reason, we consider the drug concentration as a function of both time and skin depth x (Eqs. (7.1-4)).

$$\frac{\partial C_{SC}}{\partial t} = \mathfrak{D}_{SC}\ \frac{\partial^2 C_{SC}}{\partial x^2} \qquad 0 \le x < h_{SC} \quad (7.1)$$

$$\frac{\partial C_{VE}{}'}{\partial t} = \left(\mathfrak{D}_{VE}\ \frac{\partial^2 C_{VE}{}'}{\partial x^2}\right) - \frac{k_{EL}\, C_{VE}{}'}{k_M + C_{VE}{}'} \quad C'_{VE} = C_{VE}(1 - f_b) \qquad h_{SC} \le x < h_{VE} \quad (7.2)$$

$$\frac{\partial C_{DE}}{\partial t} = \mathfrak{D}_{DE}\ \frac{\partial^2 C_{DE}}{\partial x^2} \qquad h_{VE} \le x \le h_{DE} \quad (7.3)$$

$$\frac{\partial Q}{\partial t} = -\ \left(\mathfrak{D}_{DE}\ \frac{\partial C_{DE}}{\partial x}\right)_{x=H} \qquad H = h_{SC} + h_{VE} + h_{DE} \quad (7.4)$$

Where $\mathfrak{D}\ [\frac{cm^2}{min}]$ is the drug diffusivity, $C\ [\frac{ng}{mL}]$ the drug concentration, and $x\ [cm]$ the axial coordinate across skin h_{SC}, h_{VE}, h_{DE} represent the thicknesses of the three skin layers respectively, and k_{EL} and k_M are metabolism constants. $Q\ [\frac{ng}{cm^2}]$ refers to the specific amount permeated across skin. $f_b\ [-]$ quantifies the drug sequestration by viable epidermis cellular components.

The basic assumptions of the model are that (i) drug diffusion coefficients only depend on the skin depth coordinate (x), (ii) diffusion in SC is slower than diffusion in VE and DE, and (iii) diffusion velocities in VE and DE are of the same order of magnitude (Scheuplein, 1967). We accounted for metabolism in VE by introducing the Michaelis-Menten equation, that can be simplified to a first order kinetics in case $k_{EL} \gg k_M$.

The following boundary conditions complete the previous set of equations:

$$C_{DONOR} = C_{SC} \qquad t \le t_{rel} \qquad x = 0 \qquad (7.5)$$

$$\frac{\partial C_{SC}}{\partial x} = 0 \qquad x = 0 \qquad (7.6)$$

$$C_{SC} = k_{part1} C_{VE} \qquad \mathfrak{D}_{SC} \left.\frac{\partial C_{SC}}{\partial x}\right|_{h_{SC}^-} = \mathfrak{D}_{VE} \left.\frac{\partial C_{VE}}{\partial x}\right|_{h_{SC}^+} \qquad x = h_{SC} \tag{7.7}$$

$$C_{VE} = k_{part2} C_{DE} \qquad \mathfrak{D}_{VE} \left.\frac{\partial C_{VE}}{\partial x}\right|_{h_{VE}^-} = \mathfrak{D}_{DE} \left.\frac{\partial C_{DE}}{\partial x}\right|_{h_{VE}^+} \qquad x = h_{VE} \tag{7.8}$$

$$C_{DE} = 0 \qquad x = h_{SC} + h_{VE} + h_{DE} \tag{7.9}$$

Where C_{DONOR} $[\frac{ng}{mL}]$ is the TDD concentration (depending on the drug amount and the skin surface area covered) and t_{rel} $[h]$ is the duration of the drug release from the patch. k_{part1} and k_{part2} $[-]$ account for the phase change between layers and respectively represent the partition coefficients between SC and VE, and between VE and DE. k_{part2} is assumed 1, since there should be no discontinuity between VE and DE (Scheuplein, 1967). At t = 0 (*i.e.* initial conditions) the drug concentration is null in the three skin layers.

Eq. (7.9) is the so-called “sink condition” and accounts for the drug clearance in the innermost stratum DE for uptake of the systemic circulation. The diffusion process is in fact supported by convective transport once the drug reaches DE, which contains blood and lymphatic vessels. Eq. (7.4) allows calculating the specific flux of drug permeated across skin. This flux consists of the input term R_{TD} in the plasma concentration equation:

$$R_{TD} = S_{patch} \frac{\partial Q}{\partial t} \tag{7.10}$$

R_{TD} $[\frac{ng}{min}]$ is the drug input rate entering the systemic circulation, and S_{patch} $[cm^2]$ the surface area of the TDD.

7.4.3 Numerical methods

The remaining organs and tissues of the human body, including the cardiovascular system (*i.e.* plasma compartment), are described with a physiologically-based pharmacokinetic (PBPK) approach: they are assimilated to perfectly stirred vessels in which the drug concentration can be considered homogenous. Thus, the mathematical model consists of material balances on these compartments (*i.e.* ordinary differential equations (ODEs)), and their numerical integration allows determining the drug pharmacokinetic evolution in the body and assessing the effect of ADME processes. The structure of the PBPK model is the same as the one proposed in Abbiati et al. (2016). However, some modifications and enhancements were added to adapt the model to different drugs and delivery routes. Indeed, Section 7.5 provides details on the compartments added for the sake of the case-study on

melatonin. As skin pharmacokinetics depends on both time and axial coordinate, the partial derivative equations (PDEs) (Eqs. (7.1-4)) are discretized respect to the spatial coordinate by means of the finite differences method. The method chosen for the discretization is the central difference scheme for second-order derivatives and forward difference for first-order derivatives. The optimal number of discretization layers is 23 for each skin stratum, which results from a compromise between computational time and numerical consistency as well as precision of the solution (*i.e.* asymptotic spatial profile of the drug concentration as a function of time). This means that the final number of equations and variables (*i.e.* the concentration profile in the different strata) related to skin is 69. The complete model includes the ODEs of the PBPK model, whose number depends on the physical and chemical characteristics of the drug (*e.g.*, 18 for melatonin, as commented in Abbiati et al. (2016)). The number of parameters does not change as a consequence of the discretization, because we assume that the diffusivity is constant for each discretization layer of the same skin stratum (Eq. (7.11)). Similarly, the elimination constants $k_{EL}(j)$ and $k_M(j)$ are not subject to variations throughout the discretization layers of the VE (Eqs. (7.12-13)).

$$\mathfrak{D}_i(j) = \mathfrak{D}_i(j+1) \qquad i = SC, VE, DE \qquad j = 1, 2, \dots N_{layers,i} \tag{7.11}$$

$$k_{EL}(j) = k_{EL}(j+1) \tag{7.12}$$

$$k_M(j) = k_M(j+1) \tag{7.13}$$

As coordinate x in Eqs. (7.1-9) goes from 0 to the total skin thickness, H, the spatial discretization step is:

$$\Delta x_i = \frac{h_i}{N_{layers,i}} \qquad i = SC, VE, DE \tag{7.14}$$

The finite differences method allows converting the mathematical skin model into a system of ODEs that can be combined with the ODEs of the PBPK model. As extensively discussed in Abbiati et al. (2016), Abbiati and Manca (2016), and Abbiati and Manca (2017), the parameters of the combined PBDCPK model are grouped into three categories: (i) individualized, (ii) assigned, and (iii) regressed. Individualized parameters can be calculated depending on some specific physical features of the patient, according to empirical correlations that can be found in the literature (*e.g.*, the volumes of organs/compartments and flowrates between them). We considered as specific features the sex, body weight, and height. Assigned parameters are some drug physicochemical properties whose value can be determined from available scientific and literature data (*e.g.*, protein binding). Some parameters can be neither found in the literature nor calculated by empirical correlations (*e.g.*, diffusivity, transfer

coefficients, metabolic constants), thus they are computed via a non-linear regression procedure respect to experimental data. In particular, the objective function of the non-linear regression procedure is the squared difference between the experimental (Benes et al., 1997 for the proposed case-study) and predicted values of the concentrations. For the sake of correctness, we acknowledge that the value of some transfer coefficients might be determined from *in vitro* studies. However, *in vitro* experiments do not take into account the interactions among organs and tissues in the full living organism, which dramatically affect the resulting values.

7.4.4 Sensitivity analysis

We performed a local sensitivity analysis to assess the influence of the model adaptive parameters on the concentration of the most representative compartments. We calculated the normalized sensitivity matrix $\boldsymbol{S}$ whose elements consist of the normalized derivatives of the concentrations $C(t)$ respect to the regressed parameters p of the model:

$$\boldsymbol{S} = \frac{\boldsymbol{p}}{\boldsymbol{C}(t)} \frac{\partial \boldsymbol{C}(t)}{\partial \boldsymbol{p}} \tag{7.15}$$

Since the model is dynamic we carried out the sensitivity analysis at the most critical time points from the pharmacokinetic point of view, *i.e.* (i) immediately after drug administration, (ii) at $t = t_{max}$ (time corresponding to the experimental maximum concentration, C_{max}), and (iii) immediately after the end of the patch release time. Section 7.5 (see also Figure 48) discusses the most significant results at $t = t_{max}$. The derivatives in Eq. (7.15) are approximated by means of the finite differences method. The perturbation on the parameters is:

$$\Delta \boldsymbol{p} = |\boldsymbol{p}| \cdot \varepsilon_r + \varepsilon_a \tag{7.16}$$

Where ε_r, the relative tolerance, is optimally set to the square root of the macheps constant, and ε_a, the absolute tolerance, is suitably chosen as the macheps constant.

7.5 Case study: melatonin

Several melatonin applications (*e.g.*, ICU patients, jetlag, and insomnia) call for reaching sustained and physiological plasma levels of such a substance. These goals can be achieved by transdermal delivery. In fact, orally administered melatonin is characterized by short half-life of elimination (40-60 min, (DeMuro et al., 2000; Gooneratne et al., 2012)) and low bioavailability because of the first-pass hepatic

metabolism. Furthermore, because of its lipophilic characteristics, melatonin can cross the SC hydrophobic barrier. Its low molecular weight (232.278 g/mol) contributes to ensuring fast diffusion. The skin transport equations reported above can therefore be adapted to melatonin. We accounted for melatonin metabolism in VE with a first-order elimination constant. In fact, although skin metabolism certainly occurs via an enzymatic mechanism, we chose not to use the Michaelis-Menten equation. Indeed, the Michaelis-Menten parameters are related to specific enzymes involved in the metabolic process, but the tissue contribution to melatonin metabolism is still not fully assessed and clarified. Therefore, we decided upon avoiding the introduction of an additional adaptive parameter that should be identified via the non-linear regression procedure. Furthermore, the assumption of first-order kinetics is not unrealistic, as in many applications $k_{EL} \gg k_M$. Likewise, the scientific literature (Slominski et al., 2012) reports the presence of melatonin receptors in skin, which are involved in some skin-related physiological (*e.g.*, regulation of skin pigmentation, hair growth) and pathophysiological processes (*e.g.*, melanoma growth).

However, there are no literature findings that quantify the melatonin binding in the skin. For this reason, we neglected the binding fraction f_b. If further details become available in the literature, the model will be re-adapted accordingly. As we explain in Paragraph 7.4.3, ADME processes in the body are described via ODEs according to Abbiati et al. (2016). In particular, the PBPK model features 8 compartments: Plasma, Gastric Lumen (GL), Small Intestinal Lumen (SIL), Large Intestinal Lumen (LIL), Liver, Gastro-Intestinal Circulatory System (GICS), Poorly perfused Tissues (PT), and Highly perfused Organs (HO). We added two more compartments to adapt to melatonin pharmacokinetic properties, *i.e.* the salivary glands and the pineal gland (Eq. (7.17) and Eq. (7.18), respectively). It is known that a non-negligible amount of melatonin diffuses from plasma to saliva. Indeed, several experimental studies assess the melatonin amount in the human body by measuring both plasma and saliva concentrations or, in some cases, only saliva (Benloucif et al., 2008; Laakso et al., 1993; Voultsios et al., 1997). The pineal gland is added because it is the source of endogenous melatonin in mammals (Brzezinski, 1997). Eq. (7.19) describes the dynamic evolution of melatonin's main metabolite 6-sulfatoxymelatonin (aMT6s) concentration in plasma.

$$\frac{dC_{PG}}{dt} = \frac{1}{V_{PG}} \left(Qin_{PG} C_P - Qout_{PG} C_{PG} + r_{prod}(T)\right) \tag{7.17}$$

$$\frac{dC_{SA}}{dt} = \frac{1}{V_{SA}} Q_{sal} C_P \ - k_{sal} C_{SA} \tag{7.18}$$

$$\frac{dC_{aMT6s}}{dt} = \frac{1}{V_P} (0.9 \cdot CL_H C_L \ - CL_K C_{aMT6s}) \tag{7.19}$$

Where V_{PG}, V_{SA}, and V_P $[mL]$ are the volumes of the pineal gland, salivary glands, and plasma compartments, respectively, Qin_{PG}, $Qout_{PG}$, Q_{sal} $[\frac{mL}{min}]$ are the blood flowrates entering/exiting the corresponding compartments, k_{sal} $[min^{-1}]$ is the saliva-plasma transfer coefficient. CL_H and CL_K $[\frac{mL}{min}]$ are the hepatic and renal clearances, where 90% is the average percentage of melatonin that the liver converts into aMT6s (Karasek and Winczyk, 2006), which is eventually eliminated by kidneys. For the sake of simplicity, and for the lack of quantitative information in the literature, we consider only the hepatic metabolism, although we are aware that some aMT6s is produced in skin and other tissues (Pandi-Perumal et al., 2006). $r_{prod}(T)$ is the production rate of endogenous melatonin in the pineal gland, which is entrained with the day-night cycle ($T = 24\ h$). This term consists of a Fourier series truncated to the second term to account for the periodicity of secretion. The Fourier coefficients are determined via a separate nonlinear regression respect to suitable experimental data of the endogenous melatonin concentration (Voultsios et al., 1997). It is possible to employ this strategy for any endogenous substance that follows the circadian rhythm, *e.g.*, corticosteroids.

We employed experimental data of plasma melatonin and aMT6s concentration from Benes et al. (1997) to identify the parameters of the diffusion-compartment model. They used a $20\ cm^2$ patch loaded with $8\ mg$ of melatonin and administered to 12 healthy volunteers. Averaged demographic and experimental data of the group of patients are available in that article.

7.6 Results and discussion

Preliminary to the regression with experimental data, we investigated the influence of some key parameters on the amount of permeated drug across skin and the plasma concentration profile. In particular, we focused our attention on the variation of the SC diffusivity $\mathfrak{D}_{SC}$ and the SC/VE partition coefficient k_{part1}. Figure 43 shows the results of this analysis in terms of specific drug amount (A), melatonin and aMT6s plasma concentration (B, C), and SC layers concentration (D, E, and F) trends.

In Figure 43 (top panel) SC diffusivity $\mathfrak{D}_{SC}$ varies from10^{-6} to 10^{-3} $[\frac{cm^2}{min}]$ while the

partition coefficient k_{part1} is kept constant at 2 [-]. As expected, if the diffusivity value is too low, no drug can permeate and reach the systemic circulation. In particular, the lowest value of the SC diffusivity $\mathfrak{D}_{SC}$ (blue curve) results in such a slow absorption in skin that the resulting plasma concentration (Figure 43 B and C, top panels) and permeated drug amount (Figure 43 A, top panels) are practically null. For higher values, the skin absorption (Figure 43 D, E, and F, top panels) increases significantly and this leads to higher plasma concentration and permeated drug amount.

Afterwards, we studied the influence of the SC/VE partition coefficient k_{part1} (values from 1.5 to 3 [-]) at $\mathfrak{D}_{SC} = 10^{-5}[\frac{cm^2}{min}]$ (see Figure 43 bottom panels). The increase of the SC/VE partition coefficient lowers VE (and DE) concentrations and, consequently lowers the plasma levels (Figure 43 B and C, bottom panels), while having smaller influence on the SC concentration.

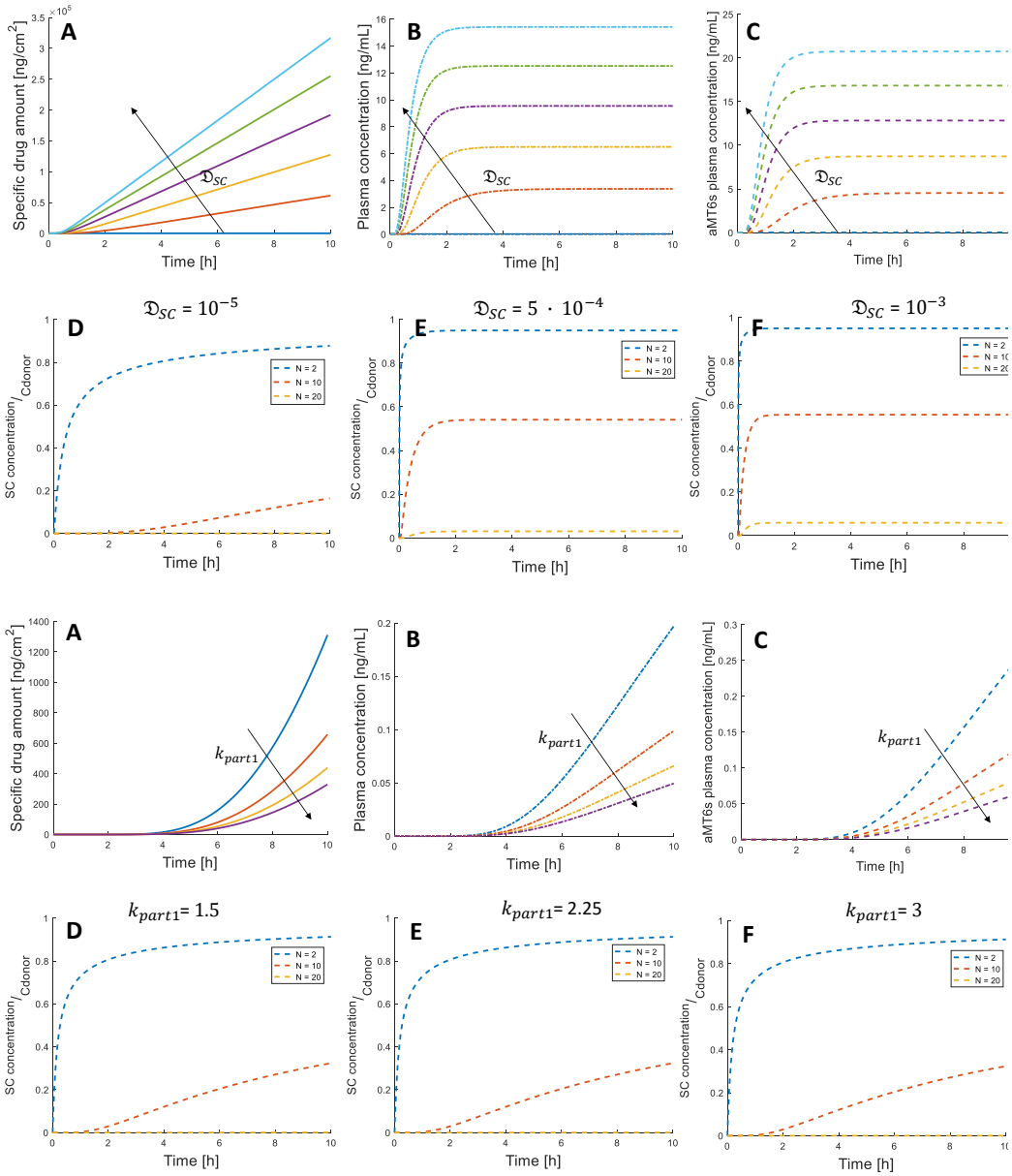

Figure 43 – Trends of (A) amount of drug permeated, and (B, C) resulting plasma concentration for increasing values of $\mathfrak{D}_{SC}$ (top panels) and k_{part1} (bottom panels).Graphs D, E, F show the trends of the concentration in specific SC layers for different values of $\mathfrak{D}_{SC}$ (top panels) and k_{part1} (bottom panels). $\mathfrak{D}_{SC}$ varies in the 10^{-6} to 10^{-3}[$^{cm^2}/_{min}$] interval, while k_{part1} varies in the 1.5 to 3 [-] interval.

As far as the parameters identification is concerned, the nonlinear regression procedure achieves acceptable results (see Figure 44), as the simulated melatonin plasma curve is near to the central values of the experimental measures (left panel). On the other hand, the model simulation underestimates the experimental metabolite aMT6s plasma concentration (right panel) before the experimental concentration peak. This result can be attributed to some simplifying assumptions that we made about the melatonin metabolism. In fact, we considered aMT6s as the only metabolite, and we did not consider the intermediate reactions and products in the metabolic

scheme of melatonin. The metabolite equation, Eq. (7.19), accounts for the metabolism in the liver, although we are aware that metabolism occurs also in skin and other tissues. As it is not clear which tissues play a role in melatonin metabolism, and to what extent, we chose to make a compromise between real physiology and model complexity, and consider only the liver.

The experimental trend of Figure 44 shows that the velocity of the distribution-elimination phase (after the experimental concentration peak C_{max} the 13th hour) is slower compared to the velocity of the uptake in the systemic circulation (preceding the experimental concentration peak C_{max} at the 13th hour). This occurs also because of the onset of melatonin endogenous secretion from the pineal gland (note the "Real time of day", on the top x axis and the black vertical dashed line), which our model can take into account. The wide error bars in the experimental data confirm high inter-individual variability.

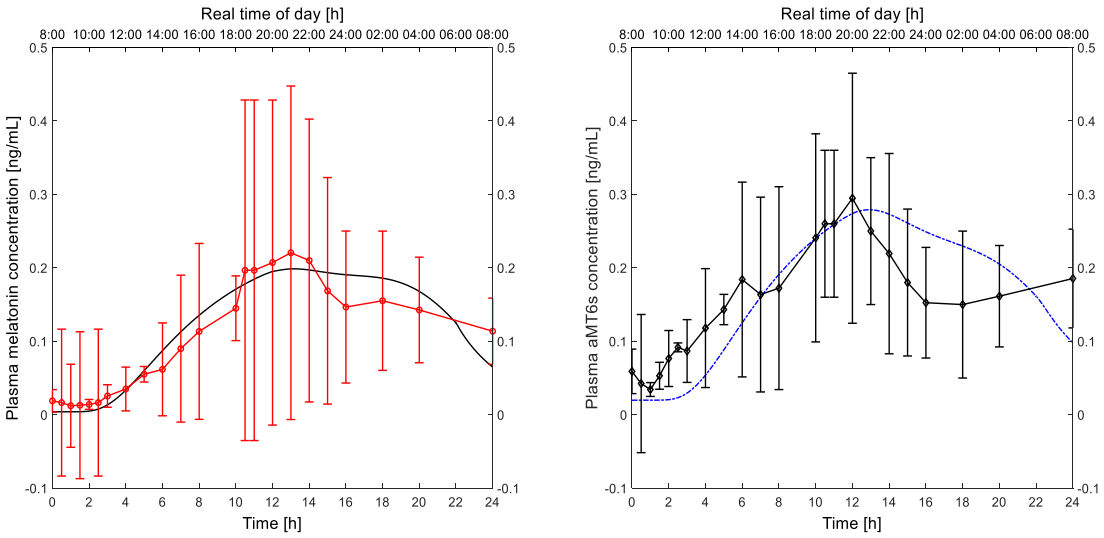

Figure 44 – Results of the regression procedure for identification of PBDCPK model parameters. Experimental data (Benes et al., 1997) show the evolution of melatonin concentration (left panel, red circles) and aMT6s concentration (right panel, black diamonds) in plasma. The continuous smooth curves represent the corresponding simulated results. The model curve is quite near to the central values of the error bands for most of the experimental sampled values of melatonin plasma concentration. The experimental aMT6s concentration is underestimated, consistently with the simplifying mechanistic assumptions on the metabolism. The black vertical dashed line shows the time of onset of endogenous melatonin production.

Figure 45 shows the single and total contributions of plasma melatonin as predicted by the proposed model: blue dash-dotted line shows the exogenous melatonin contribution while dashed red line shows the endogenous contribution. The black continuous curve comes from the combination of the two. Three black dotted vertical lines show (i) the end of application time of the TDD, (ii) the onset of melatonin

endogenous secretion by pineal gland, and (iii) the endogenous predicted peak (at 4 AM). It is interesting to notice that after the end of the time of application of the patch the exogenous curve keeps increasing for a while (*i.e.* about 3 h) as skin behaves as a reservoir. The fact that we are considering the pineal gland as the only organ capable of secreting melatonin can contribute explaining the underestimation of the experimental data observable after the 20th hour (Figure 44, left panel). In fact, although it is acknowledged in the literature that other tissues have a smaller contribution to melatonin secretion (Conti et al., 2000; Huether, 1993; Kleszczynski and Fischer, 2012), their extent is not yet quantified. It is worth observing that the values of the regressed parameters are consistent with the preliminary hypotheses and with both the skin anatomy and physiology, as the SC diffusivity is indeed lower than VE and DE diffusivities, which instead assume the same order of magnitude (see also Table 32).

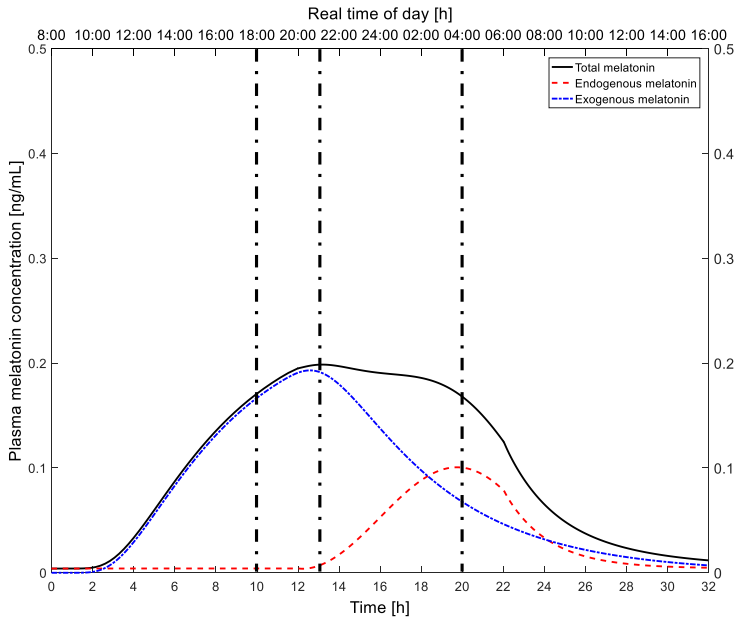

Figure 45 – Trends of the single and total contributions of plasma melatonin pharmacokinetics. Dashed red line curve shows the endogenous melatonin pharmacokinetic profile, with onset indicated by a dash-dotted black line. Dash-dotted blue line shows the pharmacokinetic profile of TD exogenous melatonin. Black vertical lines indicate respectively (i) the end of application of the TDD, (ii) the onset of endogenous production, and (iii) the peak of endogenous melatonin.

Figure 46 shows the simulation of the pharmacokinetic profile resulting from administration of melatonin 5 mg by a 10 cm^2 patch, which is removed after 8 h. The simulated patient does not exhibit endogenous melatonin production. The resulting model plasma concentration (Figure 46 right panel, blue continuous curve) is comparable to the endogenous profile of melatonin in healthy human beings

(experimental data in black circles from Voultsios et al. (1997)). The model can in fact be employed to study and simulate the resulting pharmacokinetic profile of transdermal melatonin for administration to patients who manifest endogenous production disruption, *i.e.* ICU patients, people suffering from insomnia or jet-lag, and night-shift workers. This result can be achieved by dose optimization.

On the left panel, we show the evolution of melatonin concentration along the skin depth (x axis) and in time (y axis). The pharmacokinetic profile exhibits melatonin accumulation within SC, and very low levels in DE. The reservoir function of SC produces a small increase towards the end of administration, even after the end of release from the transdermal device. Unfortunately, it is not possible to validate the results of the permeated drug amount and the concentration in the skin layers (see Figure 46, left panel), as it is not feasible to obtain this piece of information during *in vivo* experiments in humans. However, the order of magnitude of the permeated drug amount is consistent with the experimental results of Dubey et al. (2007) on melatonin permeation across human cadaver skin (*ex vivo*). Consistent with expectations, we observed that SC is the main resistance to skin transport, while the concentration levels in DE are very low compared to those of the other two strata, because of the continuous clearance of the blood supply. Lower concentration in VE respect to adjacent SC is explained by the presence of metabolism.

Table 32 – Values of the skin equations parameters identified by the regression procedure. They denote consistency with the basic model hypotheses and the anatomy/physiology of the human patients. Last two columns list the 90% bootstrap confidence intervals (CI) of the skin equations parameters.

Parameters	**Description**	**Regressed values**	**90% CI_{lb}**	**90% CI_{ub}**
$\mathfrak{D}_{SC}[cm^2/min]$	SC Diffusivity	3.352e-5	1.269e-5	5.431e-5
$\mathfrak{D}_{VE}[cm^2/min]$	VE Diffusivity	5.943e-3	2.122e-3	9.763e-3
$\mathfrak{D}_{DE}[cm^2/min]$	DE Diffusivity	2.776e-3	1.395e-3	6.946e-3
$k_{part1}[-]$	SC/VE Partition coefficient	1.763	1.209	2.317

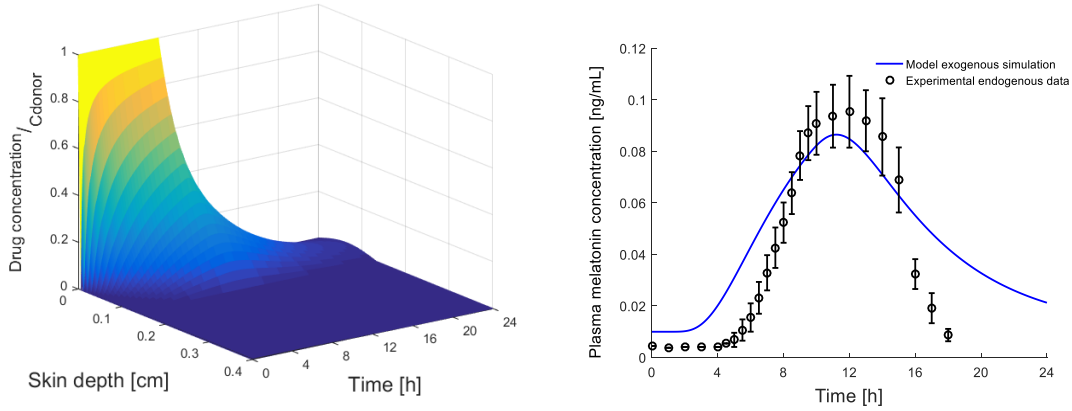

Figure 46 – (Left panel) Skin concentration profiles. x-axis represents skin depth [cm], while y-axis represents time [h]. z-axis shows the ratio between the drug concentration in skin strata and the donor concentration, *i.e.* TDD concentration. As expected, SC exhibits drug accumulation, while DE concentration is very low. We can observe the effect of SC that plays the role of reservoir towards the end of the simulation. (Right panel) Simulated profile of plasma concentration (blue continuous curve) after TD administration in a patient with no endogenous production, compared with experimental data (black circles) of endogenous levels in healthy human beings (Voultsios et al., 1997). It is evident that TD administration is a valid option to reproduce melatonin endogenous profile.

Figure 47 shows a distinct experimental case-study for validation purposes. Aeschbach et al. (2009) administered melatonin 2.1 mg/1.2 cm^2 as patch. The purpose of the study was to show that TD administration of melatonin can reduce awakening after sleep onset and therefore improve sleep maintenance. The reported demographic data consist only of averaged measures of the subjects' group, thus the black continuous curve is the pharmacokinetics of an averaged individual simulated by the model, while the circles are the experimental values of melatonin concentration of the individuals who took part to the study. It is worth observing that the model curve is consistently near to three out of four individual trends. The most distant individual trend (orange circles) shows abnormal pharmacological levels, probably related to differences in the skin characteristics.

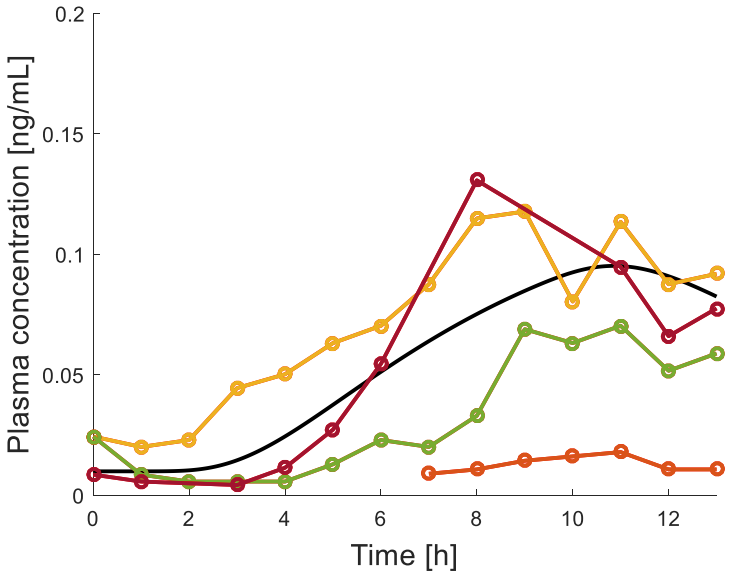

Figure 47 – The colored circles and trends represent the plasma pharmacokinetics of transdermal melatonin in four healthy individuals (Aeschbach et al., 2009). The black continuous curve depicts the simulated melatonin pharmacokinetics of an averaged in-silico individual.

The sensitivity analysis provided some insights on the influence of the most representative parameters on the model variables. Figure 48 (top panel) shows the sensitivity of skin diffusivities $\mathfrak{D}_{SC}, \mathfrak{D}_{VE}$, and $\mathfrak{D}_{DE}$ on (i) melatonin (M) concentration (at $t = t_{max}$) in intermediate layers of SC, VE, DE, and in plasma and liver, and (ii) aMT6s concentration (at $t = t_{max}$) in plasma. $\mathfrak{D}_{VE}$ seems to be the most sensitive parameter for the concentration in skin layers, while the effect of $\mathfrak{D}_{DE}$ is less evident. This particular point allows remarking that the sensitivity indexes calculation depends considerably on the punctual ($t = t_{max}$) value of the concentration (see Eq. (7.15)).

Figure 48 (medium panel) shows the results of the sensitivity analysis of the same variables at same time ($t = t_{max}$) respect to the parameters that characterize the liver, hepatic, and skin metabolism. Consistently with the model structure and hypotheses, Eff_K is the most sensitive parameter for plasma aMT6s concentration, as it is the parameter governing renal clearance of the metabolized drug. Similarly, Eff_H variation significantly affects liver concentration, while the skin metabolic constant k_{EL} sensitivity index is smaller compared to the renal and kidneys efficiencies. In fact, the tissue contribution to melatonin metabolism/elimination process is less significant than the contribution exerted by the liver and kidneys. It is worth remarking that although VE is the stratum where skin metabolism occurs, the concentration in VE is not the most affected one by k_{EL} variation.

Figure 48 (bottom panel) shows sensitivity indexes values of the partition coefficients

k_{part1} and k_{part2}. Both are sensitive respect to all the key model variables, especially plasma and liver concentration. This result may be seen as a warning, considering that we have assigned k_{part2} equal to 1. Despite this result, we think that it is more sensible to try and reduce the degrees of freedom of the nonlinear regression by assigning some of the unknown parameter values based on hypotheses resting on physiology. Therefore, we stand by our decision of assigning k_{part2}.

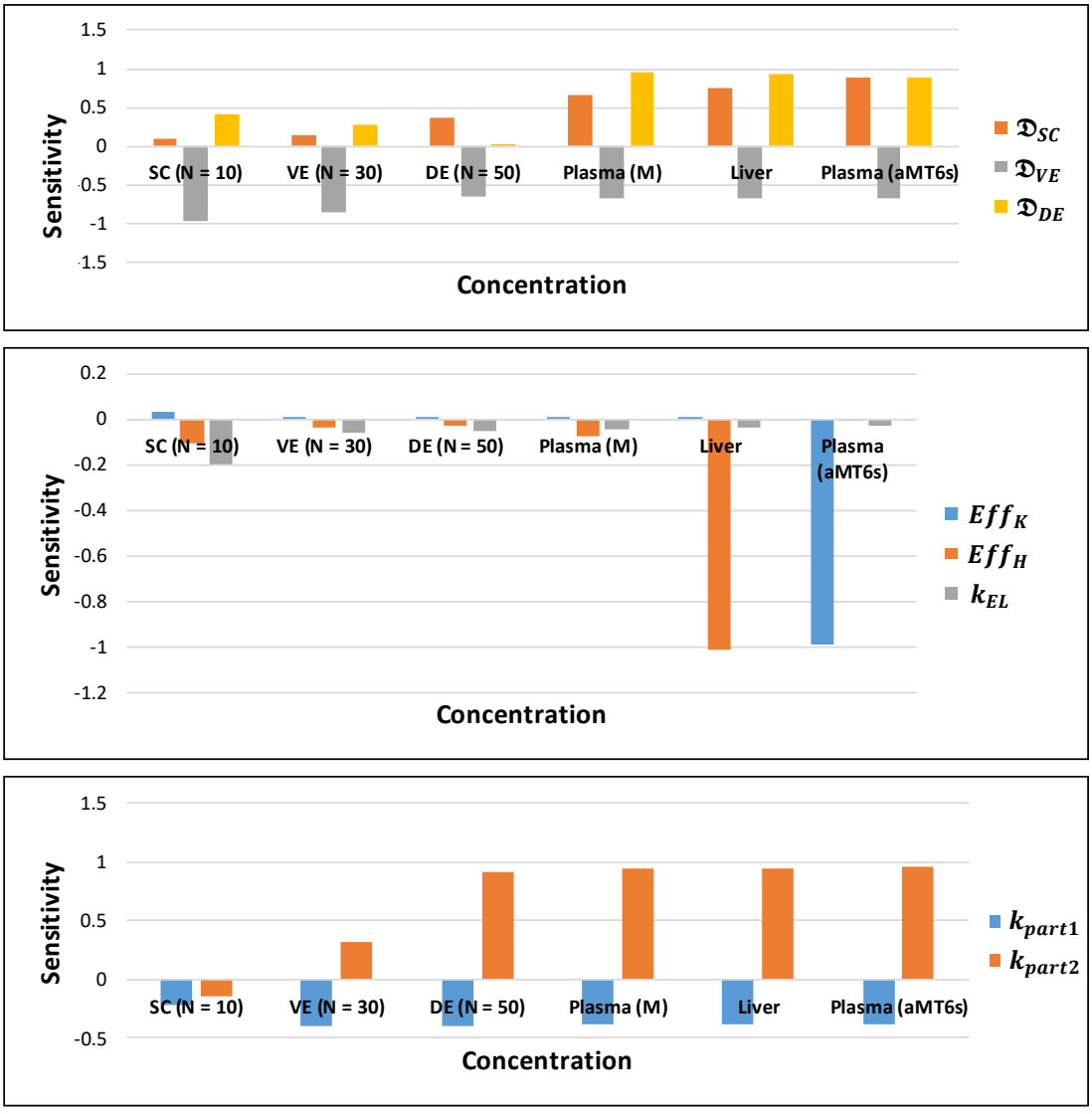

Figure 48 – Local sensitivity analysis of skin strata diffusivities (top panel), elimination/metabolic constants (medium panel), and partition coefficients (bottom panel). Model variables considered are the melatonin (M) concentration in SC, VE, DE, plasma, and liver, and the metabolite (aMT6s) concentration in plasma. The analysis is carried out at $t = t_{max}$.

The method employed for the sensitivity analysis allows observing the influence of variation of only one parameter at a time. A more in-depth future investigation would require a global sensitivity analysis implying that all the parameters vary at the same

time, which may be a more likely situation in a biological system such as the human body subject to some clinical treatment.

7.7 Conclusions

The proposed PBDCPK model can be employed for the simulation and prediction of the pharmacokinetics resulting from percutaneous administration of drugs and specifically of melatonin. The model identification procedure based on nonlinear parametric regression provided results consistent with the physiology of human body. In spite of high inter-individual variability, the validation shows that the model can be used to predict averaged patient transdermal melatonin pharmacokinetics. *In silico* simulations are an effective and costless tool for studies on skin transport, dose optimization, and route of administration selection. In fact, compared to other models describing percutaneous absorption, this work overcomes some simplifying assumptions *e.g.*, one- or two-layer approximation, not physiologically-based pharmacokinetic model (Cevc and Vierl, 2007), stationary (*i.e.* steady-state) assumptions (Anissimov et al., 2013), and homogeneous concentration in skin (Higaki et al., 2002). As a final remark, it would be interesting to include a release kinetics in our model dependent on the type of transdermal device employed.

As a consequence of the increased interest in melatonin in several medical fields, such as treatment of ICU patients, it would be interesting to focus on some recurring features of those subjects (*e.g.*, hypoperfusion, hepatic diseases, renal failure, gastro-intestinal disturbs, inflammation). Indeed, the capability of the model to describe ICU patients for TD administration and the resulting PK would strengthen the versatility attribute of the proposed model and its predictive reliability.

The main challenge is represented by inter- and intra-patient variability of the pharmacokinetics. Future work will see the model as a tool for the selection of the optimal dose/formulation. Inter-individual variability may in fact be tackled with a scenario-based approach for optimization. Artificially generated scenarios of virtual patients would help account for the stochastic uncertainty that comes from different physical characteristics, genetics, gender, race, and the resulting impact on pharmacokinetics.

CHAPTER 8

Physiologically-based pharmacokinetic simulations for selection of the optimal administration route

8.1 Author's Note

Because of its physiochemical characteristics, exogenous melatonin can be administered via at least three different pathways: IV, PO, and TD. PO route provides an additional degree of freedom with the possible choice between immediate and controlled release formulations. Depending on the desired target of clinical treatment (*e.g.*, restoring the healthy secretion rhythm or providing anti-oxidant action) and the patients' characteristics and conditions, an optimal route can be identified. This chapter investigates and compares the pharmacokinetics resulting from those administration routes, showing the value of PBPK simulations as a tool for *a priori* design of successful clinical treatments.

This work was published in "ADMET & DMPK" journal, in a special issue on PBPK modeling:

Physiologically-based pharmacokinetic simulations in pharmacotherapy: selection of the optimal administration route for exogenous melatonin

Adriana Savoca, Davide Manca

ADMET & DMPK 7(1) (2019) 44-59
DOI: 10.5599/admet.62544

8.2 Abstract

The benefits of melatonin on human body are drawing increasing attention from several researchers in different fields. While its role as cure for sleep disturbances (*e.g.*, jet lag, insomnia) is well documented and established, new functions in physiological and pathophysiological processes are emerging. To investigate these effects, there is need for the characterization of melatonin transport processes in the body and resulting pharmacokinetics. Although recent works propose physiologically-based pharmacokinetic modelling of melatonin, no work has yet highlighted the potential of physiologically-based pharmacokinetic simulations to shed light on melatonin pharmacokinetic aspects and discrimination among administration routes. This paper presents, validates, and discusses a versatile physiologically-based pharmacokinetic model featuring different ways of administration and compares the resulting pharmacokinetic profiles of intravenous, oral, and transdermal administration, with the goal of understanding which is the optimal route to achieve either physiological and/or supraphysiological melatonin levels.

8.3 Introduction

In recent years, physiologically-based pharmacokinetic (PBPK) models have become widely used and accepted tools to study, simulate, and predict drugs concentration in the body as well as provide insight on their pharmacological effects via combination with pharmacodynamic models. PBPK models are currently applied throughout the phases of drug discovery and development with various goals, *e.g.*, inter-species extrapolation, analysis of chemical toxicity or efficiency, investigation of different routes of administration, and study of inter-individual variability (Bois et al., 2010; Hall et al., 2012; Jones et al., 2011; Lin et al., 2016; Savoca et al., 2018). Indeed, PBPK simulations are extremely useful to study the pharmacokinetic differences among

individuals, from pediatric patients (Abduljalil et al., 2014) to healthy adults to special subjects, with particular conditions (*e.g.*, pregnancy (Ke et al., 2012)) or specific diseases with high probability of affecting drugs pharmacokinetics (*e.g.*, renal insufficiency or liver diseases). The reason is that PBPK models (first theorized in 1937 by Teorell (Teorell, 1937)) incorporate the anatomy and physiology of the patients' body into the mathematical description of drugs absorption, distribution, metabolism, and elimination (ADME) processes. Their recent success is also related to the current availability of modern tools to solve complex mathematical problems, such as systems of ordinary differential equations (ODEs) with a large number of parameters. *In silico* simulations are appealing because of the possibility to carry out "free" and fast experiments (Sager et al., 2015), compared to the actual clinical trials, whose costs and duration have increased over the past 20 years (Abbiati et al., 2018).

Not only drug discovery and development (Del Cont et al., 2014), but also the clinical practice may take advantage from simulation via PBPK models, as it tackles the problem of selecting the optimal dose that maximizes therapeutic efficacy while minimizing adverse effects. On one hand, inter-individual variability and medication errors are significant obstacles in this decision, on the other hand, the choice of the optimal administration route and dosing regimen are crucial degrees of freedom of this problem.

In this respect, melatonin is a useful and interesting case-study. The pleiotropic functions of melatonin in the human body are catalyzing the attention of several researchers in different fields, and its exogenous administration can follow different pathways. Although melatonin is particularly popular as a cure for sleep disturbances (*i.e.* jet-lag, insomnia), a number of other physiological and pathophysiological functions have been investigated and are still emerging. For instance, receptor-mediated actions include regulatory functions, *e.g.*, immune response, homeostasis, and blood pressure regulation (Calvo et al., 2013; Celinski et al., 2011; Pandi-Perumal et al., 2008; Slominski et al., 2012; Tan et al., 2002). Indeed, melatonin receptors are distributed in the whole body. Besides, non-receptor mediated actions are of great interest, especially the potency of its anti-oxidant, anti-proliferative, and anti-inflammatory action via radical scavenging (Reiter et al., 2014). The application in chemotherapy in combination with other substances improves both the chances of survival and quality of the patients' life (Innominato et al., 2016).

In healthy people, melatonin is endogenously produced by the pineal gland. The

production rhythm is entrained with the day-night cycle, with darkness causing the onset around 9-10 PM, peak between 2-4 AM (with C_{max} range 60-100 pg/mL), and baseline low values during the day at about 5-10 pg/mL (Brzezinski, 1997). However, this endogenous rhythm may be subject to either disruption or levels reduction, and medical doctors think that this has negative impact on the patients' health status, especially in critically ills (Damasceno et al., 2015; Dauchy et al., 2014; Mistraletti et al., 2010).

In order to identify the optimal melatonin dosage, a detailed characterization of exogenous melatonin ADME processes within the human body is recommended. Through the years, several authors have carried out pharmacokinetic studies to identify the most suitable dosage and route of administration to produce physiological and supraphysiological melatonin levels in different populations (Galley et al., 2014; Gooneratne et al., 2012; Markantonis et al., 2008; Mistraletti et al., 2017). Although some recent works exist on the PBPK modelling of melatonin in the human body (*e.g.*, Peng et al. (2013)), our aim is not only to provide a valuable PBPK model but also to compare melatonin levels that result from different routes of administration, *i.e.* intravenous (IV), oral (*per os*, PO), and transdermal (TD). The first goal is to understand which route has the highest potential to reproduce the endogenous profile of healthy patients, with the purpose of restoring melatonin physiological roles. The second goal is to identify the routes that allow achieving higher levels, with the purpose of producing pharmacological effects (for instance strong anti-oxidative action for ICU, intensive care unit, patients). Despite high inter-individual variability that is typical of melatonin pharmacokinetics (*e.g.*, related to different physical characteristics, genetic factors, and presence of impairments/diseases), we intend to show that *in silico* simulations can provide guidance and advice in selecting the optimal routes of administration and dosage, once the reliability of the employed model is verified. Indeed, model simulations constitute a powerful tool for optimal pharmacotherapy, especially in combination with experimental studies.

8.4 Methods

In general, the PBPK approach combines anatomical and physiological aspects with mathematical modeling, by assuming that the organs and tissues of the human body can be represented by compartments with homogeneous concentration. The reference model of this work (from Abbiati et al. (2016)) considers 8 compartments in

the description of the human body: Plasma, Gastric Lumen (GL), Small Intestinal Lumen (SIL), Large Intestinal Lumen (LIL), Liver, Gastro-Intestinal Circulatory System (GICS), Poorly perfused Tissues (PT), and Highly perfused Organs (HO). Actually, some compartments represent single organs while other compartments represent lumped parts so to reduce the number of model parameters. In fact, a too high number of parameters may lead to mathematical predicaments of over-parameterization and model identification (see Abbiati et al. (2018) for an exhaustive discussion on this topic). The HO compartment stands for organs that are highly perfused by blood, *i.e.* kidneys, brain, lungs, spleen, and heart. The PT compartment lumps tissues that are poorly reached by blood vessels, *e.g.*, adipose tissue, skin, and muscles (specifically in ill/treated patients). The GICS compartment lumps the portal vein, the mesenteric artery, and the microcirculatory blood vessels of the gastrointestinal system.

We applied some modifications to this basic structure of the model to adapt it to melatonin pharmacokinetic features. Particularly, we added (i) the pineal gland, and (ii) the salivary glands. Pineal gland is the source of endogenous melatonin. Within our PBPK model, the material balance on the pineal gland accounts for the production of endogenous melatonin with a term that exhibits a 24-h periodicity (see Savoca et al. (2018)). Several authors evaluate melatonin endogenous and exogenous amount by measuring either saliva and plasma or only saliva concentrations (Benloucif et al., 2008; Laakso et al., 1993; Shirakawa et al., 1998; Voultsios et al., 1997). Thus, we found more correct (from a physiological point of view) to add the salivary glands to the model compartments. The drug material balances, in the form of an ODE system, describe the concentration dynamics of melatonin in each compartment. Finally, an additional equation allows accounting for the dynamics of melatonin main metabolite 6-sulfatoxymelatonin (aMT6s).

In case of IV route, the drug directly inputs the Plasma compartment. Conversely, in case of PO administration, the drug enters the GL and moves through SIL and LIL to be absorbed through the intestinal walls and conveyed to Liver via the portal vein. This results into the so called “first-pass metabolism effect”. After that, it is drained from the Liver to reach the systemic circulation and distributes to the other organs and tissues via the bloodstream. It is worth stressing that the model structure takes into consideration GL, SIL, and LIL only in case of PO administration. In fact, in other cases, we assume that the drug counter-diffusion from GICS to SIL and LIL is negligible, and therefore it is possible to neglect such compartments, along with GL and reduce significantly the number of ODEs. We do not report here the complete

mathematical description of the model, as it is extensively detailed in Abbiati et al. (2016) and Abbiati et al. (2018).

While in case of IV and PO routes, the skin is incorporated into the PT compartment, in case of TD administration the skin becomes the mean for drug absorption and therefore calls for a specific and detailed description. In particular, melatonin evolution has to be considered not only in time but also along the skin depth coordinate. Thus, the homogenous approach (based on the perfectly mixed hypothesis) to compartment modeling is replaced and the resulting skin mathematical description involves partial differential equations (PDEs) with suitable boundary conditions (Savoca et al., 2018). Particularly, three skin layers are considered: (i) stratum corneum that is the most external and thinnest but also the main barrier, (ii) viable epidermis that may constitute a metabolism site, and (iii) dermis, from which the drug is supposed to reach the systemic circulation via the contained blood vessels, and then distribute to the rest of the body.

In case of TD administration, the PDEs describing the skin and the ODEs describing the rest of the body are combined via the finite differences method. In fact, the PDEs are discretized respect to the spatial coordinate (*i.e.* skin depth) and therefore converted to ODEs (Savoca et al., 2018).

Independently of the administration pathway, the model parameters can be divided into three categories: (i) individualized, (ii) assigned, and (iii) regressed. Individualized parameters (*e.g.*, volumes of compartments and flowrates among them) are calculated according to empirical correlations that are available in the literature and depend on the patients' physical characteristics. We consider as specific features the sex, body weight, and height. Assigned parameters are some drug physicochemical properties whose value can be determined from the scientific literature (*e.g.*, protein binding). Some parameters, strictly related to the transport properties, can be neither found in the literature nor calculated by empirical correlations (*e.g.*, diffusivity, transfer coefficients, metabolic constants), thus they are obtained via a nonlinear regression procedure respect to experimental data from the literature. Indeed, although the value of some transfer coefficients might be determined from *in vitro* studies, such experiments would not account for the interactions among organs and tissues in the living organism, and therefore would affect the reliability of the mathematical model and consistency/validity of the simulated results.

Once the model transfer coefficients and metabolic constants are identified (with data

from DeMuro et al. (2000) for IV route, Andersen et al. (2016c) and Shirakawa et al. (1998) for PO, and Benes et al. (1997) for TD), a model validation with additional experimental pharmacokinetic data allows assessing its prediction capability. To do so, we chose (i) the median squared error (MeSE) (Eq. (8.1)) over the mean squared error (MSE) (Peng et al., 2013) for robustness reasons, (ii) the difference between the experimental area under the curve AUC_{exp} and the model predicted AUC_{mod} (Abbiati et al. (2016), Eq. (8.2)), and (iii) the difference between the observed and predicted values of C_{max}. Comments on the difference between the observed and predicted values of T_{max} are also present. The AUC is calculated via trapezoidal rule over the NM measured concentration values. We consider satisfactory MeSE values below 0.1 [ng/mL] and %ΔAUC values below 30%.

$$MeSE = median\left\{\left(C_i^{exp} - C_i^{mod}\right)^2\right\} \qquad i = 1,\ldots,NM \tag{8.1}$$

$$\%\Delta_{AUC} = 100 \cdot \frac{\left|AUC_{exp} - AUC_{mod}\right|}{AUC_{exp}} \tag{8.2}$$

Once the prediction capability of the PBPK model is evaluated, it is interesting to assess *in silico* the optimal administration route. In particular, we investigated three distinct administration routes: (i) IV continuous infusion over 7 h, (ii) PO in both the immediate and controlled release (CR) formulations (the last one with a release time of 7 h), and (iii) TD with a standard patch of 10 cm^2. The PO (CR) tablet release is modeled according to the dissolution characteristics elucidated in Lee et al. (1996) and employed in Lee et al. (1995). Results from all the administration routes are compared for an assigned dose range between 0.75-12 mg, grounding on the state-of-art pharmacokinetic studies on exogenous melatonin administration. For this preliminary study, we do not consider high doses (Andersen et al., 2016b). Our virtual subject is a healthy adult male of 80 kg and 185 cm. To provide a quantitative comparison of the pharmacokinetics resulting from the three administration routes, we calculate and compare the AUC and the maximum concentration C_{max}. Finally, we comment on the concentration dynamics in the different compartments of the body that result by simulating the administration of melatonin 3 mg via IV, PO, and TD routes to the same *in silico* patient. For an unbiased comparison of melatonin ADME, we intentionally neglected the endogenous melatonin production.

8.5 Results and Discussion

We computed the prediction performance with data coming from melatonin pharmacokinetic studies. The validation cases for each route of administration are proposed and discussed.

8.5.1 IV validation case

Figure 49 shows the model curve resulting from the simulation of 20 µg IV infusion over 5 h to 6 healthy subjects (A-F panels) and 1 individual subjected to pinealectomy 2 years earlier (G panel), as in Mallo et al. (1990). Experimental data (red diamonds) show the individual pharmacokinetic profiles. The model performance (*i.e.* the blue line) is acceptable, but for A panel of Figure 49. Nevertheless, the values of the performance indexes (see Table 33) remain quite satisfactory, as even the AUC value of that patient (A panel) is only slightly higher than 30%. It is worth observing that the experimental inter-individual variability of melatonin levels is reduced in case of IV administration if compared to other routes (see also Figure 50 and Figure 51). As a result, also confidence intervals of the IV model parameters are narrower (see values Tables A-C reported in Appendix 8.A). Figure 49 (G panel) shows the experimental trend for the pinealectomized patient where the model performance is as good as for the others. The IV model was further tested with experimental results of additional patients from the same study (subjected to bolus injection) and supplementary validation cases (Andersen et al., 2016b; Fourtillan et al., 2000), for which the results of the $\%\Delta AUC$, $\%\Delta C_{max}$, and MeSE (not reported) are adequate as well. In this case, we do not calculate the experimental/predicted T_{max} and the relative error, because in case of IV constant rate of infusion the T_{max} corresponds to the infusion duration (*i.e.* in this case study, equal to 5 h).

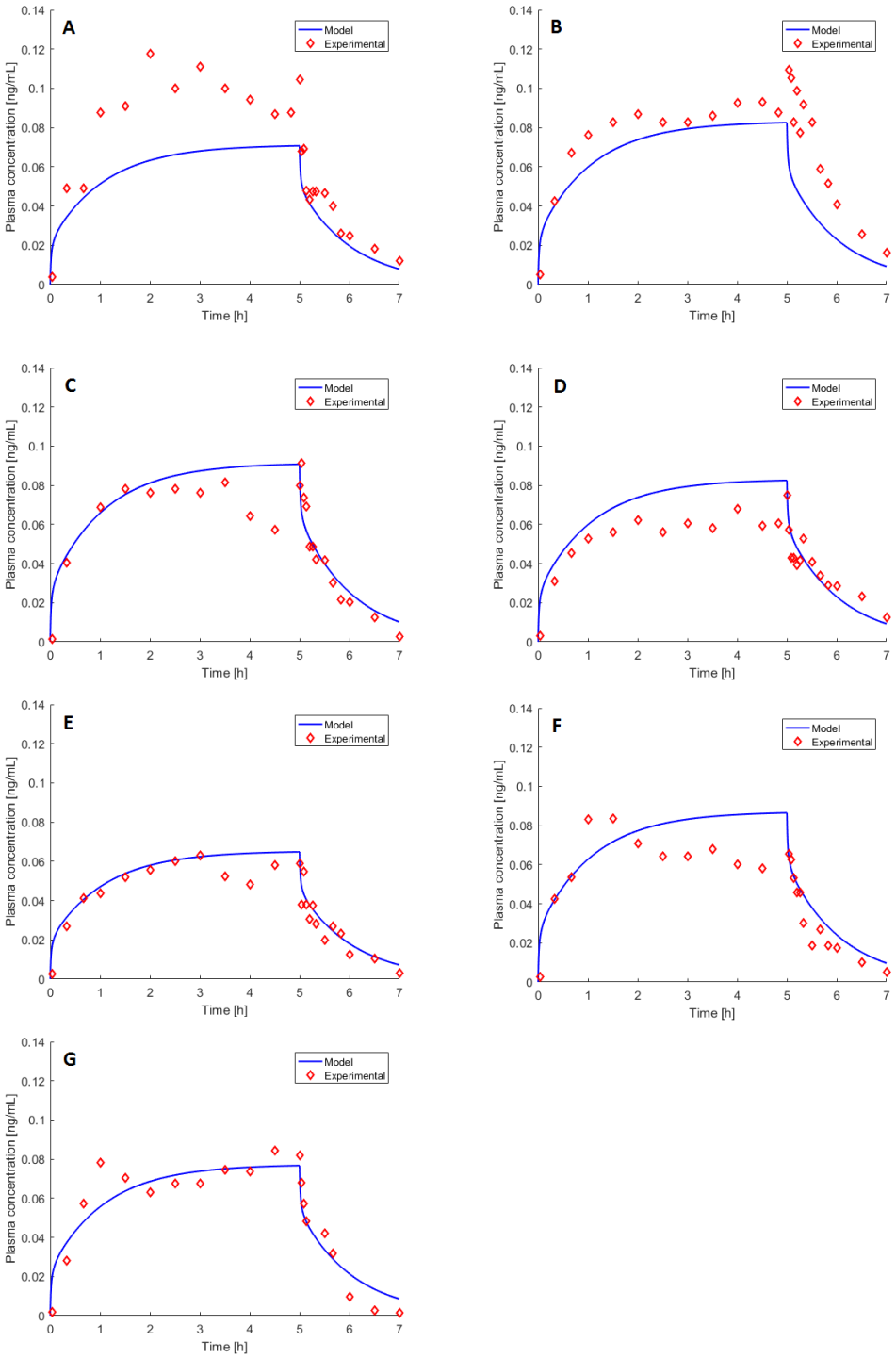

Figure 49 – Experimental data (red diamonds, (Mallo et al., 1990)) represent the pharmacokinetics of 6 healthy subjects (A-F panels) and 1 pinealectomized patient (G panel) who received IV 20 µg infused over 5 h. The blue continuous line is the model-simulated pharmacokinetic profile.

Table 33 – Performance indexes $\%\Delta_{AUC}$, $\%\Delta C_{max}$, and MeSE values for the IV validation case.

Patient	$\%\Delta_{AUC}$	$\%\Delta C_{max}$	*MeSE*
A	31.2	32.1	2.4e-4

B	18.8	24.5	2.6e-4
C	14.2	13.4	4.6e-5
D	20.6	10.1	8.3e-5
E	10.5	10.4	2.0e-5
F	16.3	31.8	4.5e-5
G	0.7	6.4	5.1e-5

8.5.2 PO validation case

Figure 50 shows experimental results on melatonin concentration in case of PO administration. The blue line in Figure 50 (A and B panels) simulates the pharmacokinetics after administration of 2 and 4 mg respectively, to 12 healthy volunteers (DeMuro et al., 2000). The experimental data (red diamonds) show mean concentration values of the volunteers group. Figure 50 (C panel) shows both individual (red circles) and median (black diamonds) concentration profiles of 5 subjects administered with 50 mg (Galley et al., 2014). Finally, Figure 50 (D panel) shows the simulation (blue line) of the averaged profile of 5 healthy subjects administered with 2 mg (Aldhous et al., 1985). In all these cases, only a single curve is displayed, because the literature data report only averaged demographic and/or pharmacokinetic data. Despite the literature differences in features and dosages, the model performance is acceptable as the simulation curve is near to the average experimental profile in all the cases. In fact, Table 34 lists low values of MeSE, except for Figure 50 (C panel). It is worth observing that the simulated profile (*i.e.* blue line) anticipates the experimental data (see Figure 50 (A, B, and C panels)). The difference between the observed and predicted T_{max} is about 30 min. This may be related to digestion features and to the patients' condition (*e.g.*, fed or fasting). Future work should adapt the PO model to such issues. However, the observed T_{max} depends also on the experimental protocol, and in particular, on the blood sampling time. In addition, this parameter is affected by a certain degree of experimental error. The %ΔAUC in Table 34 is always below 15% while the relative error between the observed and predicted C_{max} is below 15% except for case A. It is fair to acknowledge that the pharmacokinetics resulting from the PO route features a higher degree of inter- and intra-individual variability compared to the IV route, because of several interacting factors that affect absorption (*e.g.*, pH, stomach emptying time, intestinal transit times, and variation of blood supply to stomach and intestine) and metabolism (*e.g.*, genetic

factors and presence of diseases). In fact, MeSE results for the IV validation cases are at least one order of magnitude lower and, consistently, confidence intervals of the model parameters are larger (Table B in Appendix 8.A). Additional case studies are employed for validation, with similar results in terms of performance assessment (Fourtillan et al., 2000).

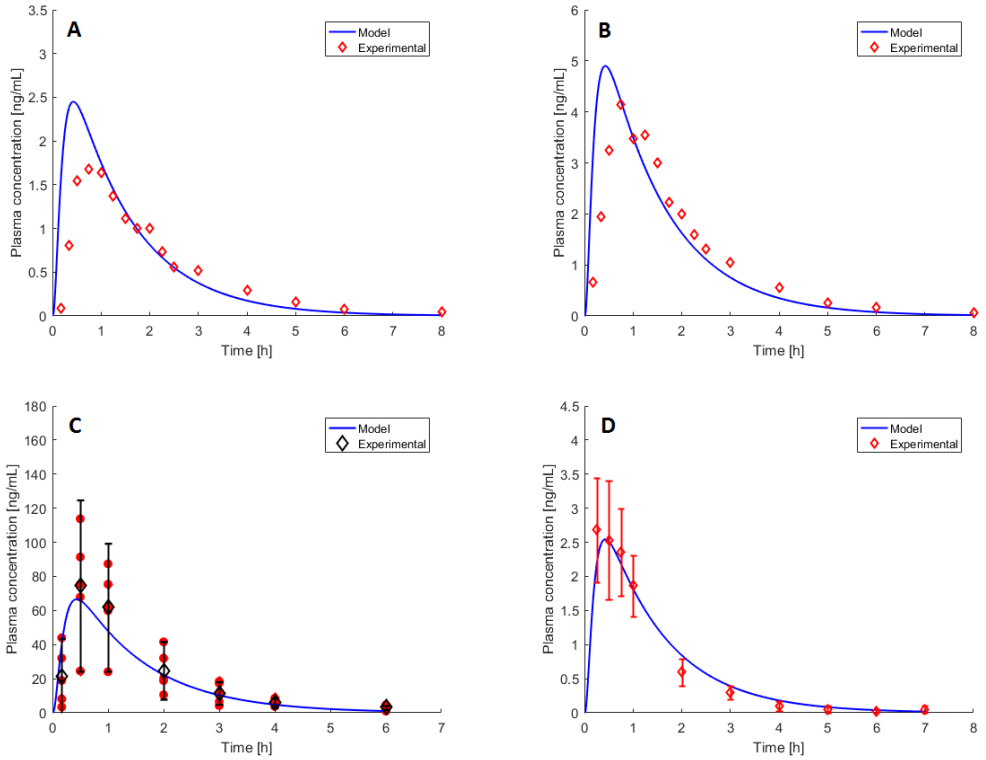

Figure 50 – A-B panels: experimental data (red diamonds, (DeMuro et al., 2000)), represent the average pharmacokinetics of 12 subjects administered with melatonin PO 2 and 4 mg. C panel: experimental individual (red circles) and median (black diamonds) pharmacokinetics after melatonin PO 50 mg (Galley et al., 2014). D panel: experimental data (red diamonds) averaged over 5 healthy subjects from Aldhous et al. (1985) (melatonin PO 2 mg). The blue continuous line is the model-simulated pharmacokinetic profile.

Table 34 – Performance indexes $\%\Delta_{AUC}$, $\%\Delta C_{max}$, and MeSE values for the PO validation case.

Panel	$\%\Delta_{AUC}$	$\%\Delta C_{max}$	*MeSE*
A	2.6	40.1	0.009
B	7.3	13.5	0.103
C	14.3	10.7	5.68
D	8.4	5.0	0.004

8.5.3 TD validation case

Figure 51 shows a validation case from Aeschbach et al. (2009) for the TD route. In

the study, melatonin was administered 2.1 mg/12 cm^2 as TD patch. Since the reported demographic data consist only of averaged measures over the subjects' group, the model curve (blue line) is the pharmacokinetics of an averaged individual, while red diamonds represent the experimental values of melatonin concentration of the individuals who took part to the study, connected with red lines for the sake of clarity. The model prediction is quite near to three out of four individual trends. The most distant individual trend shows atypical pharmacological levels, which may be related to either differences in the skin features of that specific subject and/or melatonin dermal deposition (Aeschbach et al., 2009). This results into a nonsensical value of %ΔAUC (Table 35). In general, TD pharmacokinetic data show high inter-individual variability having to do with the process of transdermal absorption (Aeschbach et al., 2009). This aspect is also reflected in the confidence intervals of the model parameters (Table C in Appendix 8.A) and in the variability of observed C_{max} and T_{max} values, although it should be remarked that blood sampling occurred every hour. Thus, it is not guaranteed that the real experimental maximum value corresponds to the observed C_{max}. In any case, the $\%\Delta C_{max}$ is around 25-30% for the first three individuals. As far as the T_{max} is concerned, it is worth observing that the model seems to predict a slower absorption compared to the experimental trend.

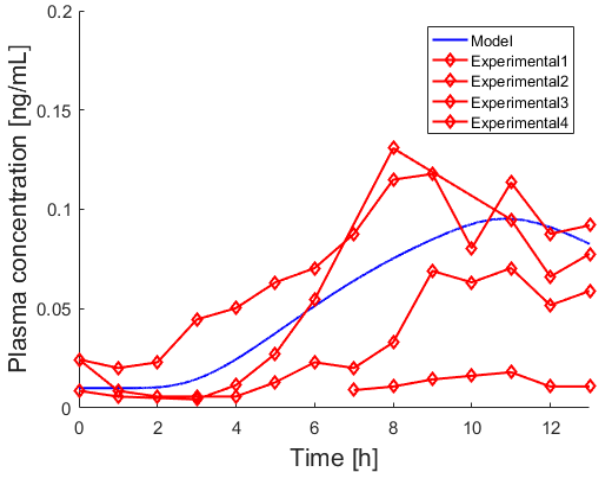

Figure 51 – Experimental data (red diamonds, (Aeschbach et al., 2009)) are the individual pharmacokinetic trends, resulting from melatonin TD 2.1 mg over 12 cm2 patch administration. The blue continuous line is the model-simulated pharmacokinetic profile of the averaged subject.

Table 35 – Performance indexes $\%\Delta_{AUC}$, $\%\Delta C_{max}$, and MeSE values for the TD validation case.

Patient	$\%\Delta_{AUC}$	$\%\Delta C_{max}$	*MeSE*
1	39.1	34.9	8.2e-4

2	38.1	27.7	2.1e-4
3	26.2	23.6	5.4e-5
4	>100	>100	4.0e-3

Despite the high values of %ΔAUC, it is likely that the reliability of the model for this route might further improve by relying on a higher number of experimental data sets for the identification of the parameters. For all the considered routes (*i.e.* IV, PO, and TD), the results are acceptable enough to continue with the analysis of melatonin ADME in the body as a function of the different administration pathways.

8.5.4 *In silico* simulations for optimal dose selection

A number of pharmacokinetic studies focus on selecting the optimal dose that produces either physiological (*e.g.*, Mallo et al. (1990)) or supraphysiological levels. In fact, while physiological levels can improve sleep maintenance and resynchronize circadian rhythms (Reiter et al., 2014), supraphysiological levels may produce strong anti-oxidant action (Galley et al., 2014) and analgesic effects (Andersen et al., 2016b). To investigate melatonin pharmacokinetic properties, a few studies compare the *in vivo* results of different routes of administration (Andersen et al., 2016c), and/or specific populations (*e.g.*, elderly (Gooneratne et al., 2012), critically ills (Mistraletti et al., 2010), and patients suffering from severe oxidative stress (Galley et al., 2014)). To prove the efficiency of *in silico* simulations within this context, we compare the pharmacokinetic profile resulting from three different routes, with doses ranging from 0.75 to 12 mg. The selected range is considered safe as it has been covered by a number of pharmacokinetic studies. Figure 52 shows the results of the simulations, along with comparison to experimental data of endogenous profile in healthy adult volunteers from Voultsios et al. (1997).

As expected, smoother and more sustained levels are achieved via TD and PO (CR) formulations. The slow absorption phase, which is characteristic of TD release, proves particularly suitable for mimicking the endogenous levels produced by the pineal gland. Equally, the PO (CR) solution provides sustained levels as well (T_{max} about 4 h), coupled with a steeper absorption (see especially the case of 0.75 mg). This difference in the velocity of absorption has to be considered in the choice of the administration time, as this will affect the onset time of melatonin effects. In case of PO (CR) 0.75 mg administration, shifting the time of administration would allow quite

a close imitation of the endogenous profile. The same consideration holds for the case of TD 6 mg administration. Thus, not only dosing, but also the time of administration is a key degree of freedom in the problem of melatonin delivery optimization to restore/produce physiological levels. Failing in considering this aspect would likely result into unsatisfactory outcomes in terms of pharmacodynamic effects. In this sense, PBPK simulations can be used as a tool for therapy design, to determine the time of administration that more likely leads to the desired effects. It should also be noted that, although the TD route produces sustained levels over 24 h, it is unlikely that the subject will manifest adverse effects, for instance related to sleep. Firstly, levels are quite similar to the endogenous pattern (see the black circles), and after about 10 h, they start decreasing towards the daily baseline (black dotted line). Secondly, doses up to 3500 mg (PO) have been administered without any acute adverse effects and the scientific literature does not report any toxic threshold for melatonin dose (Andersen et al., 2016b). For instance, in Andersen et al. (2016b) there is no evidence of sedative effects for doses up to 100 mg (IV), which would produce more than 3-order-of-magnitude higher levels than those shown in Figure 52, case 12 mg via TD route (according to our simulations and consistently with experimental results reported in the study). Predictably, even low doses of continuous IV infusion produce the highest levels and bioavailability, thus it is probably the most appropriate mean to reach prompt pharmacological (*i.e.* supraphysiological) levels. In fact, even for the lowest dose considered (*i.e.* 0.75 mg), the resulting plasma concentration is an order of magnitude higher than the endogenous one (see black circles compared to the blue line). On the contrary, TD administration should be excluded for the purpose of producing pharmacological levels (see highest doses 12 mg in Figure 52 and C_{max} value in Figure 53). Figure 52 also shows that in case of melatonin, PO immediate release formulation is not able to produce sustained levels. However, for doses higher than 5 mg, this administration route can be considered to reach pharmacological levels, alternatively to IV infusion. All of these considerations are confirmed by the values of the pharmacokinetic parameters AUC and C_{max}, compared in Figure 53. The highest AUC is in fact associated with the IV continuous infusion route, whereas the other routes of administration produce lower values. Another possibility to be explored is the combination of oral immediate release and CR formulations.

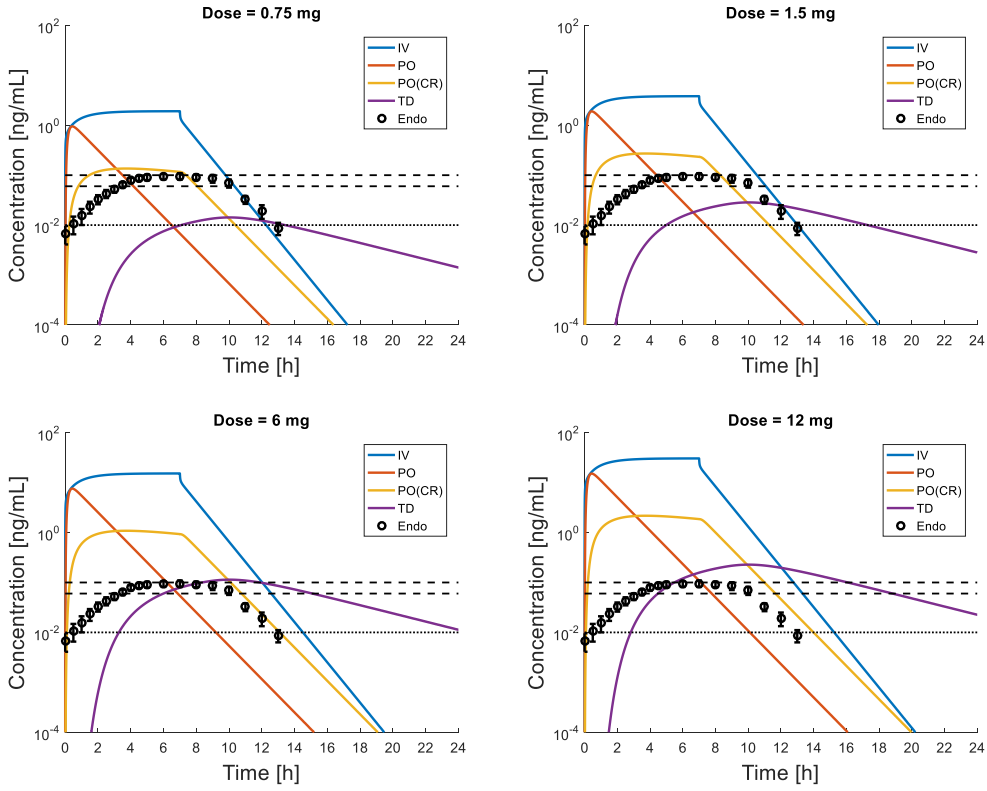

Figure 52 – Dynamics of the melatonin plasma concentration over 24 h after IV, PO, PO (CR), and TD administration of 1.5 to 12 mg to a virtual subject (male, adult, 80 kg, 185 cm). Black circles describe the endogenous profile in healthy adult volunteers (Voultsios et al., 1997). Black horizontal dashed lines indicate the range of endogenous C_{max} in healthy subjects (60-100 pg/mL). Black dotted line marks the average value of daily melatonin baseline in plasma.

Depending on the treatment goal, for instance the attainment of either endogenous or pharmacological levels, it is possible to explore additional contributing factors, other than the route, dose, and time of administration. In fact, different dissolution curves can be employed in the PO (CR) formulations and can be combined with the PBPK model to study the resulting ADME processes. The same approach can be applied in case of TD route, since both the features, position, and application extent of the patch are degrees of freedom for the medical doctor. The main degree of freedom of the IV infusion route is its duration. Once the main goal is assigned (in terms of ideal pharmacokinetic profile for a specific application), an optimization can be carried out to identify the optimal dose and dosing regimen by considering those additional degrees of freedom.

Since melatonin roles affect several organs and tissues, with cerebral, immune, gastrointestinal, cardiovascular, renal, and endocrine functions (Calvo et al., 2013), and melatonin receptors are distributed in the whole body, model compartment levels should be visualized and discussed, as well. Figure 54 shows the simulation in

different compartments for 3 mg administered IV, PO, PO (CR), and TD. The slow drug absorption, typical of TD administration, is reflected in the slow distribution to the organs/tissues of the body. Conversely, IV infusion induces higher levels in all the compartments (see Highly perfused Organs and Liver compartments in Figure 54). Thus, in case the goal of melatonin administration is a diffused anti-oxidant action in the patient body via radicals scavenging, this route should be preferred. The same can be stated in case of immune system enhancement (hence with potential beneficial effects in terms of cancer cells detection and elimination). In addition, when target organs are the highly perfused ones (*e.g.*, pancreas, liver, and kidneys), this route should be definitely considered. When a more localized target action is required, it should be considered that in case of PO administration, higher levels are expected in the liver and gastrointestinal tract, as confirmed by the model simulation. According to Celinski et al. (2011), melatonin is gastro-protective at endogenous levels, whereas pharmacological levels of melatonin (in combination with other drugs) contribute to healing of gastroduodenal ulcers. The difference of goal (*i.e.* gastro-protection vs healing of local ulcer) will be the discriminating factor for selecting the most suitable dose to produce either endogenous or higher levels. The velocity of excretion via the kidneys is comparable for both the IV and PO routes, and is faster for these routes when compared to TD. Concluding, anatomical and physiological considerations can be converted into quantitative data to be carefully assessed, analyzed, and visualized via PBPK model simulations. This kind of information is not only useful when several routes of administration are viable, but also especially important when the drug target site is not plasma.

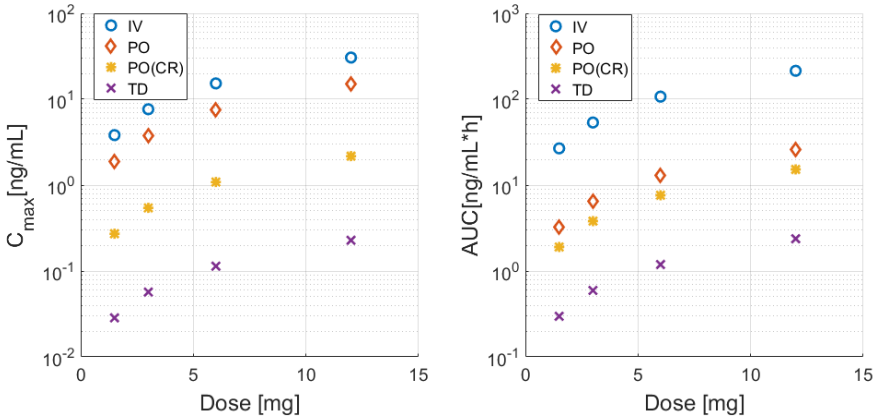

Figure 53 – Comparison of pharmacokinetic parameters C_{max} (left panel) and AUC (right panel) resulting from the three routes of administration. The x-axis reports the simulated dose range, *i.e.* 0.75 to 12 mg.

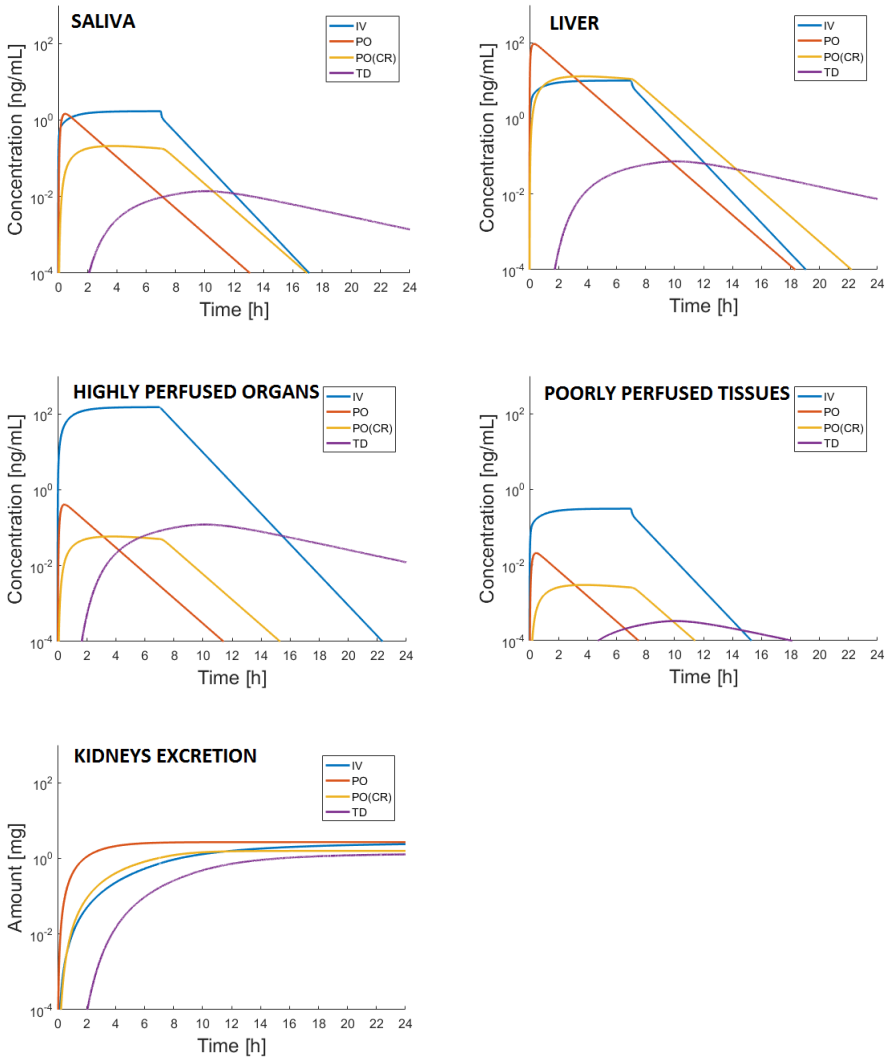

Figure 54 - Simulation of the melatonin concentration dynamics in the compartments Saliva, Liver, Highly and Poorly perfused Organs/Tissues, and the Kidneys-excreted amount after administration of 3 mg via

IV, PO, PO (CR), and TD.

8.6 Conclusions

While PBPK simulators allow evaluating melatonin levels in plasma and the rest of the body, further practical considerations should support the pharmacokinetic investigation with the aim of achieving optimal clinical efficacy. In fact, while IV route may hold the advantage of the highest bioavailability and fastest distribution to organs and tissues, most of the patients may find it distressing. Therefore, this route is viable only in case of specific categories such as critically ill patients, who usually receive continuous infusion of different drugs and enteral nutrition for quite long periods. On one hand, PO route is easy and simple but it is subject to first-pass hepatic metabolism, which implies a certain degree of inter-individual variability related to different metabolism characteristics, and different patients' features (*e.g.*, gastrointestinal pH, temperature, and other previously mentioned factors). As well as PO (CR) option, TD route allows obtaining sustained levels and avoids first-pass hepatic metabolism. On the other hand, it is subject to slow absorption through skin, possible metabolism within viable epidermis, and high inter- and intra-individual variability related to different skin features.

In this work, we introduced and discussed a case-study to compare pharmacokinetic levels resulting from different doses and three administration routes, *i.e.* IV, PO, and TD, also considering both oral immediate release and CR formulations. PBPK simulations are particularly interesting for their intrinsic nature and structure, because they provide quantitative information on the drug ADME processes in the body. Besides, coupling with intelligent drug design and *in vitro* experiments enhances the potential to maximize their efficacy. As far as melatonin is concerned and with reference to both practical and pharmacokinetic aspects, it is possible to conclude that PO (CR) and TD routes represent the best options in case of disruption of the endogenous rhythm (*e.g.*, in people suffering from either insomnia or jet-lag and critically ills). Equally, PO (with doses significantly higher than 3 mg) and IV infusion are preferable when higher concentration levels are required for other goals, for instance to contrast severe oxidative stress and possibly cancer, and target specific organs as sites of pharmacological action. This work can be extended and improved by focusing on one administration route and running a numerical optimization of the

melatonin dose respect to a target trajectory, also considering a number of degrees of freedom depending on the selected route. It is also worth stressing the transferability of the presented approach to any other drugs that are versatile from the point of view of the administration routes. Such investigations may become especially interesting in case of drugs with narrow therapeutic windows, such as chemotherapy drugs whose pharmacokinetics quantification is essential and critical.

Acknowledgements: The authors acknowledge the precious discussions and suggestions provided by Dr. Giovanni Mistraletti and prof. Franco Fraschini.

8.7 Appendix 8.A

Table A – Key model parameters in case of the PO route, correlated by 90% confidence intervals.

Parameters	Description	Regressed values	90% CI_{lb}	90% CI_{ub}
$k_{A,SIL}$ $[min^{-1}]$	SIL absorption constant	2.205	0.245	5.655
$k_{CA,SIL}$ $[min^{-1}]$	SIL counter-diffusion constant	2.920	0.158	5.683
$k_{A,LIL}$ $[min^{-1}]$	LIL absorption constant	0.167	0.003	0.337
$k_{CA,LIL}$ $[min^{-1}]$	LIL counter-diffusion constant	0.455	0.059	0.851
Eff_H $[-]$	Hepatic metabolism efficiency	0.467	0.235	0.699
Eff_K $[-]$	Kidneys excretion efficiency	0.053	0.007	0.113

Table B – Key model parameters in case of the IV route, correlated by 90% confidence intervals.

Parameters	Description	Regressed values	90% CI_{lb}	90%CI_{ub}
k_{T-P} $[min^{-1}]$	Plasma- Poorly perfused tissues transfer coefficient	0.3955	0.373	0.418
k_{P-T} $[min^{-1}]$	Poorly perfused-tissues plasma transfer coefficient	0.8	0.774	0.826

k_{HP-P} $[min^{-1}]$	Highly perfused organs-plasma transfer coefficient	0.047	0.045	0.05
k_{P-HP} $[min^{-1}]$	Plasma-highly perfused organs transfer coefficient	1.48	1.416	1.544

Table C – Key model parameters in case of the TD route, correlated by 90% confidence intervals.

Parameters	**Description**	**Regressed values**	**90% CI_{lb}**	**90% CI_{ub}**
$\mathfrak{D}_{SC}[cm^2/min]$	SC Diffusivity	3.352e-5	1.269e-5	5.431e-5
$\mathfrak{D}_{VE}[cm^2/min]$	VE Diffusivity	5.943e-3	2.122e-3	9.763e-3
$\mathfrak{D}_{DE}[cm^2/min]$	DE Diffusivity	2.776e-3	1.395e-3	6.946e-3
$k_{part1}[-]$	SC/VE Partition coefficient	1.763	1.209	2.317

CHAPTER 9

Optimal dosing for endogenous levels in ICU patients

9.1 Author's Note

Chapter 8 showed how PBPK simulations suggest that the most suitable routes for producing sustained levels that mimic healthy melatonin endogenous levels are PO (CR formulation) and TD. This chapter focuses on PO (CR) route and compares the results of dosing optimization for critically ill and healthy patients. Specifically, three CR formulations from the scientific literature are used as inputs to the model. The remarkable inter-individual variability typical of critically ill patients' pharmacokinetics is considered within the optimization problem formulation via a Monte Carlo approach applied to the model parameters.

This work was published in "Computer Aided Chemical Engineering" book series and presented at the "European Symposium on Computer-Aided Process Engineering (ESCAPE-29)" conference:

Optimization under uncertainty of melatonin dosing for critically ill patients

Adriana Savoca, Giuseppe Pesenti, Davide Manca

Computer Aided Chemical Engineering (46) (2019) 565-570
DOI: 10.1016/B978-0-12-818634-3.50095-3

9.2 Abstract

Computer-aided modelling and simulation are effective tools to provide guidance in the design of clinical experiments and treatments. Simulations with physiologically-based pharmacokinetic (PBPK) models combine the drug material balances within the body to its real physiological and anatomical features and can be used to optimize drugs dosing and administration timing. We focus on melatonin administration to critically ill patients, a challenging population because of their high inter-individual variability in the pharmacokinetics (due to their heterogeneous and severe conditions). We show how the optimization problem can be suitably formulated to tackle this uncertainty, and compare the results obtained for critically ill patients and healthy individuals. The approach can be easily transferred to any other drug routinely administered in intensive care units whenever a desired pharmacokinetic profile is available.

Keywords: optimization, modelling, simulation, uncertainty, pharmacokinetics.

9.3 Introduction

Recent years have seen an increasing interest in melatonin. Although it is particularly well-known as a cure for sleep disturbances and restoration of circadian rhythms, researchers are investigating additional physiological and pathophysiological functions. Indeed, there is evidence of anti-cancer, anti-oxidative, anti-inflammatory, and analgesic properties (Brzezinski, 1997). Healthy individuals produce melatonin endogenously by means of the pineal gland according to the day-night rhythm. Melatonin production onsets with darkness (around 9-10 PM) and peaks at 2-4 AM. Healthy plasma peak levels are in between 60-100 pg/mL. After the peak, melatonin levels settle to the low daily baseline (5-10 pg/mL). Collaboration with Intensive Care

Unit (ICU) of Ospedale San Paolo di Milano (Italy) allowed focusing on critically ill patients. Such patients exhibit disorders in melatonin secretion rhythm and/or lower levels compared to healthy individuals. This phenomenon is correlated to the lack of sleep, which likely increases both patients' morbidity and probability of mortality. There is evidence that exogenous melatonin has beneficial effects on these patients, mainly for treatment of sleep disorder, delirium, and oxidative stress (Bourne and Mills, 2006; Mistraletti et al., 2010). Several studies investigated the optimal dose with the purpose of reproducing the desired physiological levels of melatonin and proposed different doses (regimens) to restore the healthy endogenous rhythm. While physiological levels are desirable to restore circadian rhythms, pharmacological levels (*i.e.* supraphysiological levels, for instance about 3 orders of magnitude higher) are more suitable for anti-oxidant or anti-cancer purposes (Reiter et al., 2014). We show that computer simulation is an efficient tool to design and/or integrate such pharmacokinetic (PK) studies, with the advantage of reducing times and costs of the experiments. In addition, simulations using physiologically-based pharmacokinetic (PBPK) models allow comparing and evaluating the pharmacokinetics from not only different doses but also routes of administration. In fact, our first goal is to select the administration route that best mimics human physiological levels. Subsequently, we focus on that route and optimize dosing, also by comparing results for healthy individuals (by neglecting the endogenous contribution for the sake of clarity) and critically ill patients. The main issue with critically ill patients is that they are intrinsically rather heterogeneous, because of their different conditions (*e.g.*, age, dysfunctions, organs failure) (Mistraletti et al., 2010). This feature enhances inter-individual variability of melatonin pharmacokinetics. To deal with this problem, we propose a prospective approach to drug dosing optimization.

9.4 Methods

Figure 55 shows the structure of a multi-route compartmental PBPK model. The reference model for this work is Abbiati et al. (2016), where organs and tissues of the human body are represented by homogenous compartments. We complemented those compartments number and model structure to melatonin features and administration routes, by adding (i) the pineal gland, which is the source of endogenous melatonin, and (ii) the salivary glands (Savoca et al., 2018). A further equation accounts for the dynamics of main melatonin metabolite: 6-sulfatoxymelatonin (aMT6s) both in plasma and in urine. In case of oral administration

(PO, *per os*, see also Figure 55), the model consists of material balances on either single or lumped homogenous compartments.

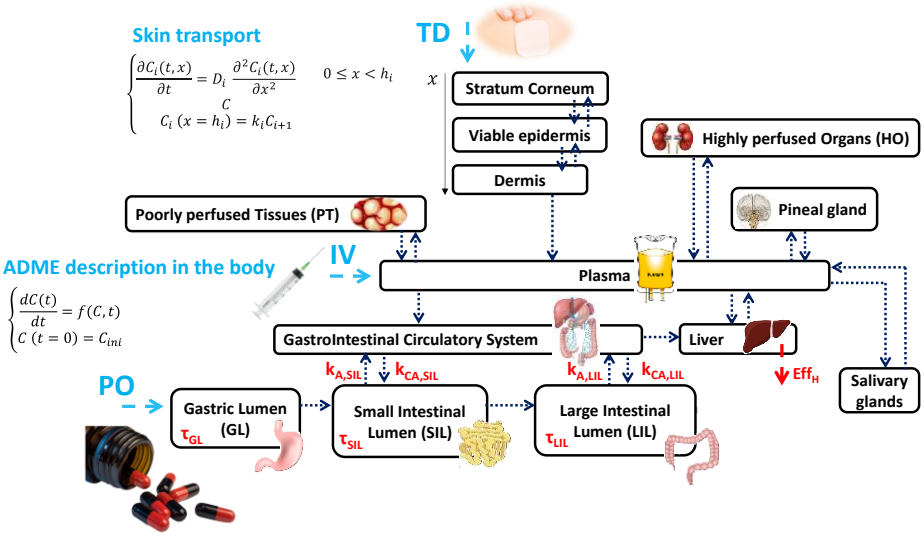

Figure 55 – Scheme of the PBPK model for description of melatonin ADME processes. Parameters in red are associated to the main processes responsible for inter-patient variability. While skin transport is described via PDEs discretized with respect to skin depth x, the other body compartments feature melatonin material balances in the form of ODEs.

These are the gastric lumen (GL), the small and large intestinal lumina (SIL and LIL), the gastrointestinal circulatory system (GICS), the plasma, the liver, the poorly perfused tissues (PT, lumping adipose tissue, skin, and muscles), and the highly perfused organs (HO, lumping brain, lungs, and spleen). In case of intravenous (IV) route, the gastrointestinal compartments are neglected. Finally, in case of transdermal (TD) administration, skin is assumed as a separate compartment from PT and described by a set of partial differential equations (PDEs) with proper boundary conditions for skin TD absorption. The model features three skin layers: (i) stratum corneum, (ii) viable epidermis (also a metabolism site), and (iii) dermis, from which the drug is supposed to reach the systemic circulation. These PDEs are discretized with respect to the spatial coordinate (*i.e.* skin depth) and converted to ODEs and merged to those of the other compartments (Savoca et al., 2018). Model parameters include (i) individualized and assigned parameters that are either calculated as a function of patient's characteristics or found in the literature, and (ii) adaptive parameters (*e.g.*, diffusivities, transfer coefficients, metabolic constants) that are obtained via a nonlinear regression of experimental data from the literature. Firstly, we use the multi-route PBPK simulations to compare levels resulting from PO, IV, and TD administration routes. Secondly, we perform an optimization based only on PO controlled release (CR), as it resulted the most suitable to mimic endogenous

pharmacokinetics. Based on experimental release curves from the scientific literature, the optimal melatonin amount and time of administration are identified for three *in silico* individuals, (i) a healthy male, (ii) a healthy female, and (iii) an ICU patient. The PBPK model parameters for healthy individuals are identified with melatonin PK experimental data of healthy volunteers. Equally, the parameters that describe the PK of ICU patients are identified via regression with experimental data of the critically ill.

To account for considerable inter-individual variability, the optimization problem considers the uncertainty related to the (patho-) physiological differences of such patients. The processes that most likely produce inter-subject variability are (i) absorption from the intestinal walls into gastrointestinal circulation (characterized by absorption constants $k_{A,SIL}$, $k_{A,LIL}$, $k_{CA,SIL}$, and $k_{CA,LIL}$ and residence times in gastrointestinal region τ_{GL}, τ_{SIL}, and τ_{LIL}) and (ii) hepatic metabolism (described by hepatic efficiency Eff_H). These model parameters are randomized within a proper range, which is chosen referring to physiology for the transit times, and model uncertainty for the others, to produce different PK profiles for the ICU virtual patient, VP. These additional NS "scenarios" embody the structure of the optimization problem in Eq. (9.1), where NM is the number of experimental data C_i^{ideal} that describe the healthy endogenous plasma concentration profile (Voultsios et al., 1997). The degrees of freedom are: dose and t_{adm} (*i.e.* timing of administration).

$$\min_{dose,\, t_{adm}} \sum_{k=1}^{NS} \left(\frac{\sum_{i=1}^{NM} \left(C_i^{ideal} - C_i^{VP,k} \right)^2}{NM} \right) \tag{9.1}$$

9.5 Results

9.5.1 Comparison of administration routes

The physiochemical properties of melatonin (*e.g.*, lipophilicity and low molecular weight) make it suitable for at least three administration routes, *i.e.* PO, IV, and TD. As far as the PO route is concerned, we consider both immediate and controlled release (CR) formulations. Figure 56 allows comparing the pharmacokinetics of these different routes under the same melatonin dose (1.5 mg in the left panel, 12 mg in the right panel). The characteristic slowness of TD absorption is particularly appropriate to mimic the sustained endogenous levels produced by the pineal gland. Equally, the PO (CR) formulation provides continued levels (T_{max} about 4 h), coupled with a steeper absorption.

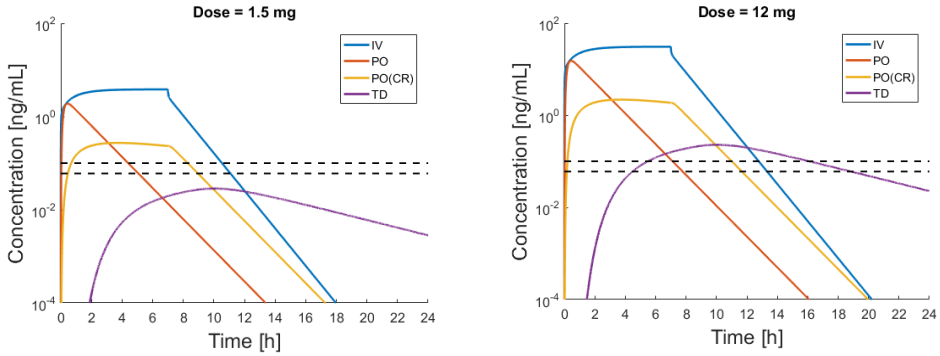

Figure 56 – PK simulations of a healthy individual with IV, PO (immediate release and controlled release (CR) formulations), and TD administrations of melatonin. Black dashed horizontal lines show the range of concentration peak after healthy endogenous production (60-100 pg/mL).

The difference in the velocity of early absorption affects the selection of the optimal administration timing as it affects the onset time of the pharmacological and physiological effects. Predictably, even low doses of continuous IV infusion produce the highest levels, thus it is probably the most appropriate to achieve prompt pharmacological (*i.e.* supraphysiological) levels. On the contrary, TD administration should be excluded for that purpose, even in case of higher doses. In case of PO immediate-release formulation, the melatonin concentration decreases rapidly after administration. However, even for low doses, this administration formulation allows reaching pharmacological levels, alternatively to IV infusion. This conclusion is in line with experimental studies where oral doses higher than 0.3 mg produce supra-physiological levels.

9.5.2 Optimization for PO CR route

Panel A of Figure 57 compares three PO (CR) formulations with different percentages of polymer coating (5-10-20%) that generate three different release curves as in Lee et al. (1995). Panel B of Figure 57 shows experimental data of the endogenous profile of an healthy individual (red squares, from Voultsios et al. (1997)), while continuous, dotted, and dashed lines are the optimized pharmacokinetics of an ICU patient who receives tablets featuring the three different release curves. The most suitable release curve corresponds to the 10% coating tablet that best approaches the PK endogenous profile.

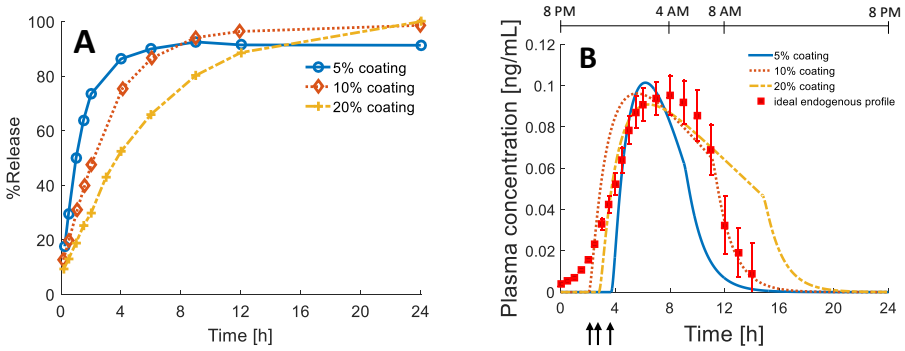

Figure 57 – (A) Experimental release curves for different formulations, as in Lee et al. (1995). (B) Optimized PK levels (continuous, dashed, and dotted lines) in ICU and ideal (experimental) healthy endogenous data (red squares). Black arrows indicate optimal timing of administration.

Figure 58 shows the melatonin optimal doses and timing of administration. On the x-axis, HM and HF stand for the male and female healthy individuals, while ICU stands for the critically ill patient. It is worth noticing that the lowest dose is associated to the ICU patient. Indeed, for the same dose, PK studies show higher melatonin concentrations in critically ill patients, compared to healthy individuals. Probably, the continuous enteral nutrition of ICU patients facilitates melatonin absorption. Notably, PBPK model simulations are consistent with this behavior. In addition, optimal dose values for the healthy individuals are in line with the results of experimental studies (as already mentioned, oral doses higher than 0.3 mg produce supraphysiological levels). Our results are not so far from this approximate value.

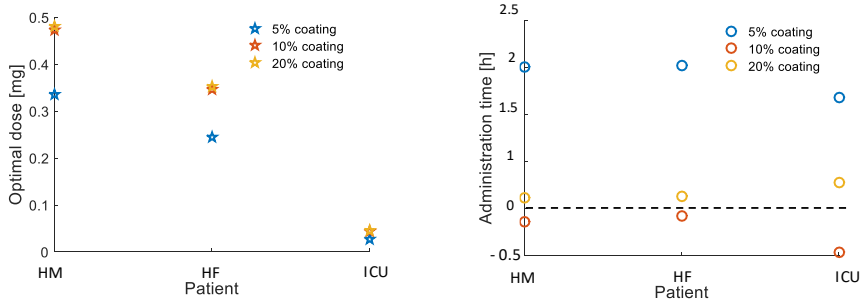

Figure 58 – Optimal melatonin dose (left panel) and timing of administration (right panel) for HM and HF (healthy male and female individuals) and ICU (critically ill patient). Dashed horizontal line (right panel) indicates the desired time of onset of melatonin effects.

Figure 59 (right panel) shows the optimal timing of administration in relation to the desired onset time for melatonin effects (see the horizontal dashed line at 0). In case of 10% coating, the optimal administration timing for the ICU patient is about 30 min before the desired onset, while it is shorter for healthy individuals. This is consistent with the fact that critically ill patients exhibit higher levels of melatonin after exogenous administration. In all the other cases, to mimic the endogenous profile optimally, the administration timing should occur after the desired onset time, which evidently makes

no sense. This confirms that the 10% coating formulation is the most appropriate to deliver physiological levels of melatonin. Finally, Figure 59 shows melatonin PK simulations in different compartments (*i.e.* Gastric Lumen, Liver, and HO, Highly perfused Organs) and the eliminated amount of melatonin metabolite, aMT6s, after the optimal administration of PO (CR) formulation to the ICU patient. Low levels in HO are consistent with the typical tissue hypoperfusion of critically ill patients. Experimentally, the eliminated melatonin is usually higher than 85%, while this threshold is not reached in our simulations. This may be related to two different reasons: (i) from the modeling point of view, our model underestimates aMT6s metabolic production as we consider (for simplicity) the liver contribution only, (ii) from the physical point of view, ICU patients may exhibit lower metabolism compared to healthy patients.

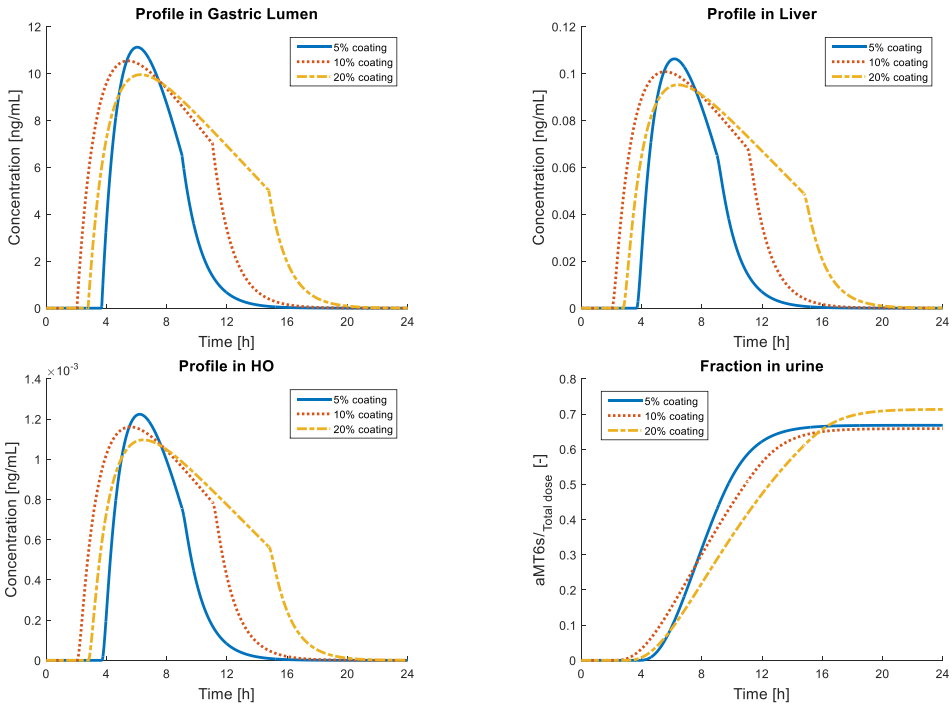

Figure 59 – PBPK model simulations for the critically ill patient in Gastric Lumen, Liver, HO (Highly perfused Organs), and aMT6s fraction in urine.

9.6 Conclusions

PBPK model simulations are an effective tool in melatonin optimal pharmacotherapy. We optimized melatonin dosing by comparing healthy individuals and critically ill patients. As the latter ones represent an extremely heterogeneous population, we proposed an approach that allows accounting for inter-subject variability generated by

the gastrointestinal absorption and metabolic processes. Results are in line with conclusions from past experimental PK studies and can provide aid in future study for the challenging identification of melatonin optimal dose regimens in critically ill patients.

CHAPTER 10

Conclusions and future perspectives

10.1 Closed-loop control of anesthesia

Closed-loop controllers of IV anesthesia delivery are useful to answer two main needs of anesthesiologists with respect to the problem of selecting the optimal anesthetic and analgesic drugs dose, *i.e.* (i) a more robust and rigorous approach to tackle inter-individual variability of the response to drugs, and (ii) a support system capable of accounting for both the several variables involved and the drug-drug interactions that affect and describe the anesthetic state of the patient.

The few studies on PBPK modeling applied to anesthesia have not yet focused on the actual use of such methodology in clinical practice. We showed how this modeling approach allows accounting for the anatomical and physiological differences across the lifespan and different conditions of individuals. Specifically, we focused on three populations, *i.e.* (i) elderly, (ii) obese, and (iii) pediatric patients, who represent a challenge from the point of view of optimal dosing because they are especially susceptible to propofol adverse effects. PK prediction via classical three-compartment models is often poor in these *special* patients, as they were mostly identified with data of healthy young adults. Regardless, these models feature remarkable variability of the PK prediction, potentially creating ambiguity and confusion among clinicians. As the approach *one-size-fits-all* is likely to fail, we proposed an individualization strategy for adaptation of the PBPK model, which allows overcoming the limitations of the most

commonly used three-compartment PK models and, in some cases, outperforming their predictive capability. The proposed closed-loop controller, based on the individualized model, proved to take into account the differences of these populations, providing infusion rates for induction of anesthesia in *in silico* patients that were consistent with clinical guidelines.

The PBPK-PD model also allowed investigating the effects of hemodynamic changes on the response to anesthesia. These effects can indeed lead to clinically relevant adverse reactions in high-risk patients. This is a problem that, at the current stage, entirely relies on the anesthetists' experience and intuition, as few studies are available on the topic. In addition, no studies have investigated the impact of hemodynamic changes on the alterations of pharmacokinetics and pharmacodynamics within the context of closed-loop anesthesia. We showed how inclusion of CO data helps the controller individualizing the proposed infusion rate and avoiding unnecessary overdosing.

Thus, it is fair to acknowledge and underline that application of PBPK modeling has produced several points of innovation compared to the current methods of clinical practice and the state-of-art work on closed-loop anesthesia.

Additional changes to the model-predictive controller algorithm and structure were made for application to high-risk patients, by considering propofol-remifentanil synergistic interactions on arterial pressure and including heart rate as input variable, to account for their sensitivity to propofol-remifentanil-induced hypotension and faster changes of the hemodynamic parameters.

The introduction of both a quantitative measure of DoH and hemodynamic parameters within the controller structure is another key point of innovation compared to several published works on propofol-remifentanil closed-loop administration, and is essential to provide a more complete control of the anesthetic and analgesic state of the patient. However, this issue comes with complications from the practical point of view. In clinical practice, anesthesiologists in some cases administer vasopressors (*e.g.*, epinephrine, phenylephrine) to treat mild to severe intra-operative hypotension. Therefore, in some occasions, hemodynamic parameters may increase independently of the patients' analgesic level. In this case, using such parameters to monitor the analgesic level may be misleading as the controller would modify accordingly the analgesic infusion rate. On the other hand, intraoperative hypotension can have different interpretations, for instance it can be a result of overdosing but also a sign of

a blood loss, depending on the extent of the decrease. Similarly, with respect to the use of BIS as controlled variable, personal communications with clinicians warned us from overtrusting BIS to assess the patients' DoH (C. Carozzi and D. Caldiroli, Istituto Neurologico Carlo Besta, December 2018). Indeed, monitoring of the EEG trace characteristics (*e.g*, frequency and amplitude of the waves) and additional parameters (*e.g.*, Signal Quality Index (SQI) and electromyographic (EMG) activity) help skilled anesthesiologists to identify "false" BIS variations (Bennett et al., 2009; Carozzi and Caldiroli, 2018).

Hence, to increase the controller robustness against those episodes, some rules based on the anesthesiologists' expertise and experience may be implemented within the controller logic (*i.e.* expert system), so that the control action can be suspended by providing a stable infusion rate in an "open-loop" configuration, at the discretion of the anesthesiologist, leaving them free to operate. An example of such rules is represented in the decision tree of Figure 60.

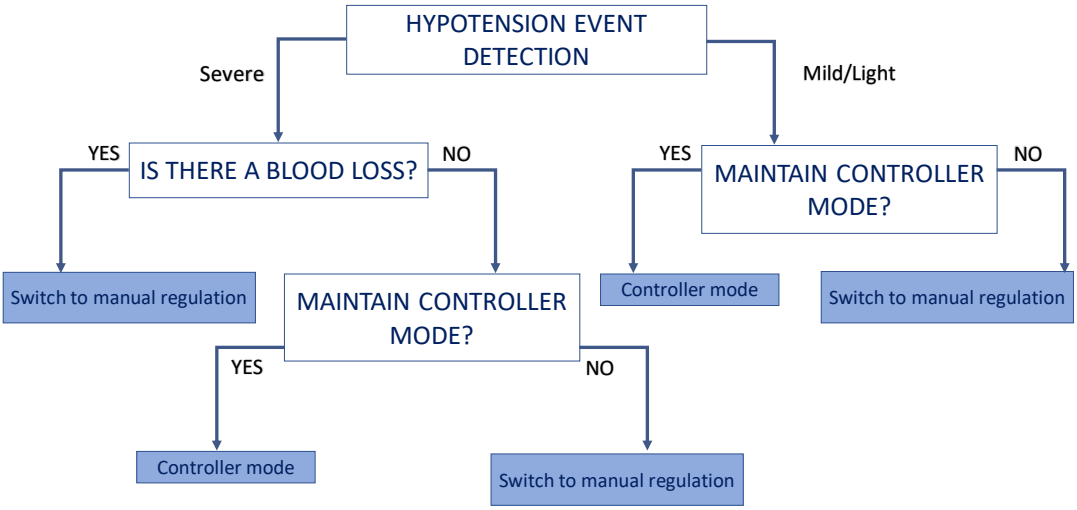

Figure 60 – Decision-tree to respond to hypotensive events.

After implementation of this combined rule-based and MPC logic, the software should be integrated with routinely-used monitoring instruments and infusion pumps, for *in vivo* testing.

At this stage, the controller can be used *in silico* to study and investigate the patients' response via simulations. In the anesthesia fields, where human factors play a key role, the adoption of *in silico* investigational tools for study of the optimal dose and education of trainees in anesthesiology would be extremely beneficial, especially considering that the model we developed and validated is suitable for "at-risk"

categories of patients, for which standard dosing guidelines are lacking/insufficient and TCI pumps risk providing non-optimal infusion rates because of model inaccuracies.

10.2 Optimization of melatonin dosing

The combination of anatomical and physiological principles with the mathematical description of ADME processes allowed building a PBPK model for melatonin, considering administration via three main routes, *i.e.* IV, PO, and TD. Few changes can be applied to account for other less common but interesting routes, *e.g.*, buccal (*i.e.* via the cheek oral mucosa) and sublingual (*i.e.* via the mucous membrane beneath the tongue). Oral mucosa is indeed rather vascularized, and these routes allow administering the drug directly into the systemic circulation, thus avoiding the "first-pass" hepatic metabolism. Indeed, they have the potential to induce faster drug onset and higher blood levels, compared to PO route. PBPK modeling of these routes can help designing new melatonin formulations by evaluating and quantifying their effectiveness via simulations of *in silico* patients and identifying optimal dosing ranges. In fact, we showed how PBPK simulations can be used to select the optimal route of administration, considering IV, PO (immediate and controlled release formulations), and TD. Melatonin treatments can have the purpose of either (i) restoring physiological levels, *e.g.*, to cure sleep disorders, or (ii) inducing supra-physiological levels, *e.g.*, to produce anti-oxidant or anti-proliferative effects. The safety of melatonin use, even at high doses, makes it extremely appealing for use in fragile individuals, such as cancer patients or critically ills, since most drugs used in these fields feature narrow therapeutic windows, which makes the identification and personalization of the dosing extremely difficult. The proposed use of PBPK simulations to predict and optimize melatonin dosing can transform pharmacotherapy, leading to the reduction of ineffective clinical treatments. Indeed, it is worth noticing that although this work focused on melatonin, the proposed approach is transferable to any other drugs for which (i) several routes are possible and/or (ii) a desired target level/profile of plasma concentration is to be achieved or maintained. This is the case of some drugs for ICU patients (*e.g.*, the antibiotic vancomycin) and anti-cancer drugs with narrow therapeutic windows.

From the PBPK simulations, we found that PO (CR) formulation was suitable for administration to critically ills with the purpose of restoring the healthy endogenous

levels and cure their sleep disorders. An innovative approach was also proposed to account for remarkable inter-individual variability of these patients, which is a main issue in optimal pharmacotherapy. In this work, optimal dosing and time of administration were identified using CR trajectories available in the scientific literature on melatonin. However, it is worth noticing that the methodology can be “reversed” into the problem of designing the ideal delivery system, *i.e.* the optimal “release” trajectory that is able to produce the desired healthy endogenous profile in either the generic patient or a special category (via model individualization). Coupling of the design of drug delivery systems (*i.e.* for PO and TD formulations) with PBPK simulations opens promising perspectives to improve efficacy, and identify faults and weaknesses before commercialization.

In summary, implications of this section of the work span from improved design of drug delivery systems to enhancement of clinical treatments, as the methodology and results are easy to generalize, provided that PK data for reliable identification and validation of the model are available.

10.3 Future perspectives

This thesis focused on the development of PBPK model-based tools for support to clinical decision in optimal drug dosing in the fields of anesthesia and intensive care. Such fields present significant difficulties related to the inter-individual variability and critical conditions of patients, quantity and type of variables to consider in the definition of the dose-response relation, and other factors that increase the probability of administration errors. Several points of innovations compared to the current approaches and state-of-the-art research have been presented to tackle such issues. The developed approaches can further be improved and extended with the collaboration of clinicians to evolve to actual biomedical systems by integration with monitoring instruments and drug infusion systems (anesthesia) and development of dedicated user interfaces (melatonin/other drugs dosing optimization for critically ills).

Healthcare requires new approaches and tools to face future challenges. The success of technological innovation and digital transformation of healthcare calls for robust understanding and clear visions of both the technological and medical sectors. The fact that by 2020, medical information about the body and health will double every 73 d, compared to the 3.5-y doubling-time estimated in 2010 (Densen, 2011), creates a major obstacle. For this reason, the formation of multidisciplinary teams with mixed

scientific backgrounds is essential to guarantee the highest possibilities of success. The current hype for innovative solutions applied to the biomedical sector confirms the relevance and timing of the presented work, which could not have been developed without the support of collaborations with clinicians and gives hope for future improvements of clinical practice via fruitful “contamination” among clinicians and engineers.

References

1. Abbiati, R.A., Lamberti, G., Grassi, M., Trotta, F., Manca, D. (2016). Definition and validation of a patient-individualized physiologically-based pharmacokinetic model. Computers & Chemical Engineering, 84, 394-408.
2. Abbiati, R.A., Manca, D. (2016). A modeling tool for the personalization of pharmacokinetic predictions. Computers & Chemical Engineering, 91, 28-37.
3. Abbiati, R.A., Manca, D. (2017). Innovations and improvements in pharmacokinetic models based on physiology. Curr Drug Deliv, 14, 190-202.
4. Abbiati, R.A., Savoca, A., Manca, D. (2018). Chapter 2 - An engineering oriented approach to physiologically based pharmacokinetic and pharmacodynamic modeling. In D. Manca (Ed.), Computer Aided Chemical Engineering (Vol. 42, pp. 37-63): Elsevier.
5. Abduljalil, K., Jamei, M., Rostami-Hodjegan, A., Johnson, T.N. (2014). Changes in Individual Drug-Independent System Parameters during Virtual Paediatric Pharmacokinetic Trials: Introducing Time-Varying Physiology into a Paediatric PBPK Model. The AAPS Journal, 16, 568-576.
6. Absalom, A., Kenny, G. (2005). 'Paedfusor' pharmacokinetic data set. BJA: British Journal of Anaesthesia, 95, 110-110.
7. Absalom, A., Struys, M. (2007). An Overview of TCI and TIVA. Academia Press.
8. Absalom, A.R., De Keyser, R., Struys, M.M. (2011). Closed loop anesthesia: are we getting close to finding the holy grail? Anesthesia & Analgesia, 112, 516-518.
9. Absalom, A.R., Glen, J.I., Zwart, G.J., Schnider, T.W., Struys, M.M. (2016). Target-Controlled Infusion: A Mature Technology. Anesthesia & Analgesia, 122, 70-78.
10. Absalom, A.R., Mani, V., De Smet, T., Struys, M.M.R.F. (2009). Pharmacokinetic models for propofol—defining and illuminating the devil in the detail. BJA: British Journal of Anaesthesia, 103, 26-37.
11. Adachi, Y.U., Watanabe, K., Higuchi, H., Satoh, T. (2001). The determinants of propofol induction of anesthesia dose. Anesthesia & Analgesia, 92, 656-661.
12. Adams, K.F., Schatzkin, A., Harris, T.B., Kipnis, V., Mouw, T., Ballard-Barbash, R., Hollenbeck, A., Leitzmann, M.F. (2006). Overweight, obesity, and mortality in a large prospective cohort of persons 50 to 71 years old. New England Journal of Medicine, 355, 763-778.
13. Aeschbach, D., Lockyer, B.J., Dijk, D.J., Lockley, S.W., Nuwayser, E.S., Nichols, L.D., Czeisler, C.A. (2009). Use of transdermal melatonin delivery to improve sleep maintenance during daytime. Clin Pharmacol Ther, 86, 378-382.
14. Aldhous, M., Franey, C., Wright, J., Arendt, J. (1985). Plasma concentrations of melatonin in man following oral absorption of different preparations. Br J Clin Pharmacol, 19, 517-521.
15. Alexander, J.K., Dennis, E.W., Smith, W.G., Amad, K.H., Duncan, W.C., Austin, R.C. (1962). Blood volume, cardiac output, and distribution of systemic blood flow in extreme obesity. Cardiovasc Res Cent Bull, 1, 39-44.

16. Alexander, R., Olufolabi, A.J., Booth, J., El-Moalem, H.E., Glass, P.S. (1999). Dosing study of remifentanil and propofol for tracheal intubation without the use of muscle relaxants. Anaesthesia, 54, 1037-1040.
17. Alhashemi, J.A., Cecconi, M., Hofer, C.K. (2011). Cardiac output monitoring: an integrative perspective. Critical Care, 15, 214.
18. American Society of Anesthesiologists. Standards for Basic Anesthetic Monitoring. Committee of Origin: Standards and Practice Parameters. (Available at: https://www.asahq.org/standards-and-guidelines/standards-for-basic-anesthetic-monitoring).
19. Andersen, L., Rosenberg, J., Gögenur, I. (2014). III. Perioperative melatonin: not ready for prime time. In: Oxford University Press.
20. Andersen, L.P., Gogenur, I., Rosenberg, J., Reiter, R.J. (2016a). The Safety of Melatonin in Humans. Clin Drug Investig, 36, 169-175.
21. Andersen, L.P., Werner, M.U., Rosenkilde, M.M., Fenger, A.Q., Petersen, M.C., Rosenberg, J., Gogenur, I. (2016b). Pharmacokinetics of high-dose intravenous melatonin in humans. J Clin Pharmacol, 56, 324-329.
22. Andersen, L.P.H., Werner, M.U., Rosenkilde, M.M., Harpsøe, N.G., Fuglsang, H., Rosenberg, J., Gögenur, I. (2016c). Pharmacokinetics of oral and intravenous melatonin in healthy volunteers. BMC Pharmacology & Toxicology, 17, 8.
23. Anderson, B.J. (2012). Pharmacology in the very young: anaesthetic implications. European Journal of Anaesthesiology (EJA), 29, 261-270.
24. Anderson, B.J., Meakin, G.H. (2002). Scaling for size: some implications for paediatric anaesthesia dosing. Pediatric Anesthesia, 12, 205-219.
25. Andresen, J.M., Girard, T.D., Pandharipande, P.P., Davidson, M.A., Ely, E.W., Watson, P.L. (2014). Burst suppression on processed electroencephalography as a predictor of post-coma delirium in mechanically ventilated ICU patients. Crit Care Med, 42, 2244.
26. Anissimov, Y.G., Jepps, O.G., Dancik, Y., Roberts, M.S. (2013). Mathematical and pharmacokinetic modelling of epidermal and dermal transport processes. Adv Drug Deliv Rev, 65, 169-190.
27. Auld, F., Maschauer, E.L., Morrison, I., Skene, D.J., Riha, R.L. (2017). Evidence for the efficacy of melatonin in the treatment of primary adult sleep disorders. Sleep Medicine Reviews, 34, 10-22.
28. Batra, Y.K., Al Qattan, A.R., Ali, S.S., Qureshi, M.I., Kuriakose, D., Migahed, A. (2004). Assessment of tracheal intubating conditions in children using remifentanil and propofol without muscle relaxant. Paediatr Anaesth, 14, 452-456.
29. Bellapart, J., Boots, R. (2012). Potential use of melatonin in sleep and delirium in the critically ill. BJA: British Journal of Anaesthesia, 108, 572-580.
30. Bellapart, J., Roberts, J.A., Appadurai, V., Wallis, S.C., Nunez-Nunez, M., Boots, R.J. (2016). Pharmacokinetics of a novel dosing regimen of oral melatonin in critically ill patients. Clin Chem Lab Med, 54, 467-472.
31. Bendel, S., Ruokonen, E., Polonen, P., Uusaro, A. (2007). Propofol causes more hypotension than etomidate in patients with severe aortic stenosis: a double-blind, randomized study comparing propofol and etomidate. Acta Anaesthesiol Scand, 51, 284-289.
32. Benes, L., Claustrat, B., Horriere, F., Geoffriau, M., Konsil, J., Parrott, K.A., DeGrande, G., McQuinn, R.L., Ayres, J.W. (1997). Transmucosal, oral controlled-release, and transdermal drug administration in human subjects: a crossover study with melatonin. J Pharm Sci, 86, 1115-1119.

33. Benloucif, S., Burgess, H.J., Klerman, E.B., Lewy, A.J., Middleton, B., Murphy, P.J., Parry, B.L., Revell, V.L. (2008). Measuring Melatonin in Humans. Journal of Clinical Sleep Medicine : JCSM : official publication of the American Academy of Sleep Medicine*,* 4, 66-69.
34. Bennett, C., Voss, L.J., Barnard, J.P., Sleigh, J.W. (2009). Practical use of the raw electroencephalogram waveform during general anesthesia: the art and science. Anesthesia & Analgesia*,* 109, 539-550.
35. Besch, G., Liu, N., Samain, E., Pericard, C., Boichut, N., Mercier, M., Chazot, T., Pili-Floury, S. (2011). Occurrence of and risk factors for electroencephalogram burst suppression during propofol–remifentanil anaesthesia. BJA: British Journal of Anaesthesia*,* 107, 749-756.
36. Bois, F.Y., Jamei, M., Clewell, H.J. (2010). PBPK modelling of inter-individual variability in the pharmacokinetics of environmental chemicals. Toxicology*,* 278, 256-267.
37. Boneva-Asiova, Z., Boyanov, M. (2008). Body composition analysis by leg-to-leg bioelectrical impedance and dual-energy X–ray absorptiometry in non-obese and obese individuals. Diabetes, Obesity and Metabolism, 10, 1012-1018.
38. Botney, R. (2008). Improving patient safety in anesthesia: a success story? International Journal of Radiation Oncology* Biology* Physics*,* 71, S182-S186.
39. Bourne, R.S., Mills, G.H. (2006). Melatonin: possible implications for the postoperative and critically ill patient. Intensive Care Med*,* 32, 371-379.
40. Bourne, R.S., Mills, G.H., Minelli, C. (2008). Melatonin therapy to improve nocturnal sleep in critically ill patients: encouraging results from a small randomised controlled trial. Crit Care*,* 12, R52.
41. Brines, J.K., Gibson, J.G., Kunkel, P. (1941). The blood volume in normal infants and children. The Journal of Pediatrics*,* 18, 447-457.
42. Brodie, S.M., Gorges, M., Ansermino, J.M., Dumont, G.A., Merchant, R.N. (2017). Closed-Loop Control of Total Intravenous Anesthesia During Significant Intraoperative Blood Loss: A Case Report. A A Case Rep*,* 9, 239-243.
43. Brzezinski, A. (1997). Melatonin in humans. N Engl J Med*,* 336, 186-195.
44. Buil-Bruna, N., López-Picazo, J.-M., Martín-Algarra, S., Trocóniz, I.F. (2016). Bringing model-based prediction to oncology clinical practice: A review of pharmacometrics principles and applications. The oncologist*,* 21, 220-232.
45. Buzzi-Ferraris, G. (1993). Scientific C++: Building Numerical Libraries the Object-oriented Way: Addison-Wesley Publishing Company.
46. Calvo, J.R., González-Yanes, C., Maldonado, M.D. (2013). The role of melatonin in the cells of the innate immunity: a review. Journal of Pineal Research*,* 55, 103-120.
47. Carozzi, C., Caldiroli, D. (2018). The Subjective and Objective Monitoring of Sedation. In A. R. De Gaudio & S. Romagnoli (Eds.), Critical Care Sedation (pp. 47-67). Cham: Springer International Publishing.
48. Celinski, K., Konturek, S.J., Konturek, P.C., Brzozowski, T., Cichoz-Lach, H., Slomka, M., Malgorzata, P., Bielanski, W., Reiter, R.J. (2011). Melatonin or l-tryptophan accelerates healing of gastroduodenal ulcers in patients treated with omeprazole. Journal of Pineal Research*,* 50, 389-394.
49. Cevc, G., Vierl, U. (2007). Spatial distribution of cutaneous microvasculature and local drug clearance after drug application on the skin. J Control Release*,* 118, 18-26.
50. Checketts, M., Alladi, R., Ferguson, K., Gemmell, L., Handy, J., Klein, A., Love, N., Misra, U., Morris, C., Nathanson, M. (2016). Recommendations for standards of monitoring during anaesthesia and recovery 2015: Association of Anaesthetists of Great Britain and Ireland. Anaesthesia*,* 71, 85-93.

51. Chidambaran, V., Costandi, A., D'Mello, A. (2015). Propofol: a review of its role in pediatric anesthesia and sedation. CNS Drugs, 29, 543-563.
52. Claeys, M.A., Gepts, E., Camu, F. (1988). Haemodynamic changes during anaesthesia induced and maintained with propofol. BJA: British Journal of Anaesthesia, 60, 3-9.
53. Coetzee, J.F., Glen, J.B., Wium, C. A., Boshoff, L. (1995). Pharmacokinetic Model Selection for Target Controlled Infusions of Propofol: Assessment of Three Parameter Sets. Anesthesiology, 82, 1328-1345.
54. Coleman, R.M., Tousignant-Laflamme, Y., Ouellet, P., Parenteau-Goudreault, É., Cogan, J., Bourgault, P. (2015). The use of the bispectral index in the detection of pain in mechanically ventilated adults in the intensive care unit: A review of the literature. Pain Research & Management : The Journal of the Canadian Pain Society, 20, e33-e37.
55. Constant, I. (2004). BIS use in pediatric anesthesia: where are we? Can J Anaesth, 51, 411-416.
56. Constant, I., Rigouzzo, A. (2010). Which model for propofol TCI in children. Paediatr Anaesth, 20, 233-239.
57. Conti, A., Conconi, S., Hertens, E., Skwarlo-Sonta, K., Markowska, M., Maestroni, G.J.M. (2000). Evidence for melatonin synthesis in mouse and human bone marrow cells. Journal of Pineal Research, 28, 193-202.
58. Cooper, L., DiGiovanni, N., Schultz, L., Taylor, R., Nossaman, B. (2009). Human factors contributing to medication errors in anaesthesia practice. ASA, 2009, A614.
59. Coppens, M.J., Eleveld, D.J., Proost, J.H., Marks, L.A., Van Bocxlaer, J.F., Vereecke, H., Absalom, A.R., Struys, M.M. (2011). An evaluation of using population pharmacokinetic models to estimate pharmacodynamic parameters for propofol and bispectral index in children. Anesthesiology, 115, 83-93.
60. Cortinez, L.I. (2014). What is the ke0 and what does it tell me about propofol? Anaesthesia, 69, 399-402.
61. Cortinez, L.I., Anderson, B.J., Penna, A., Olivares, L., Munoz, H.R., Holford, N.H., Struys, M.M., Sepulveda, P. (2010). Influence of obesity on propofol pharmacokinetics: derivation of a pharmacokinetic model. BJA: British Journal of Anaesthesia, 105, 448-456.
62. Cortinez, L.I., De la Fuente, N., Eleveld, D.J., Oliveros, A., Crovari, F., Sepulveda, P., Ibacache, M., Solari, S. (2014). Performance of propofol target-controlled infusion models in the obese: pharmacokinetic and pharmacodynamic analysis. Anesthesia & Analgesia, 119, 302-310.
63. Cortínez, L.I., Fuentealba, A., Montalván, C., Vega, R., Sepúlveda, P. (2011). Derivation and prospective validation of four pharmacokinetic-pharmacodynamic models in elderly patients. Rev Chil Anest, 40, 122-137.
64. Cravero, J.P., Beach, M.L., Blike, G.T., Gallagher, S.M., Hertzog, J.H. (2009). The incidence and nature of adverse events during pediatric sedation/anesthesia with propofol for procedures outside the operating room: a report from the Pediatric Sedation Research Consortium. Anesthesia & Analgesia, 108, 795-804.
65. Daabiss, M. (2011). American Society of Anaesthesiologists physical status classification. Indian journal of anaesthesia, 55, 111.
66. Dahaba, A.A., Xue, J.X., Hua, Y., Liu, Q.H., Xu, G.X., Liu, Y.M., Meng, X.F., Zhao, G.G., Rehak, P.H., Metzler, H. (2010). The utility of using the bispectral index-Vista for detecting cross-clamping decline in cerebral blood flow velocity. Neurosurgery, 67, ons102-107; discussion ons107.
67. Damasceno, A., Moraes, A.S., Farias, A., Damasceno, B.P., dos Santos, L.M., Cendes, F. (2015). Disruption of melatonin circadian rhythm production is related to multiple sclerosis severity: A preliminary study. J Neurol Sci, 353, 166-168.

68. Danias, P.G., Tritos, N.A., Stuber, M., Kissinger, K.V., Salton, C.J., Manning, W.J. (2003). Cardiac Structure and Function in the Obese: A Cardiovascular Magnetic Resonance Imaging Study: STRUCTURE AND FUNCTION. Journal of Cardiovascular Magnetic Resonance, 5, 431-438.
69. Dar, A.Q., Shah, Z.A. (2010). Anesthesia and sedation in pediatric gastrointestinal endoscopic procedures: a review. World journal of gastrointestinal endoscopy, 2, 257.
70. Das, S.K., Roberts, S.B., Kehayias, J.J., Wang, J., Hsu, L.K.G., Shikora, S.A., Saltzman, E., McCrory, M.A. (2003). Body composition assessment in extreme obesity and after massive weight loss induced by gastric bypass surgery. American Journal of Physiology-Endocrinology and Metabolism, 284, E1080-E1088.
71. Dauchy, R.T., Xiang, S., Mao, L., Brimer, S., Wren, M.A., Yuan, L., Anbalagan, M., Hauch, A., Frasch, T., Rowan, B.G., Blask, D.E., Hill, S.M. (2014). Circadian and melatonin disruption by exposure to light at night drives intrinsic resistance to tamoxifen therapy in breast cancer. Cancer Res, 74, 4099-4110.
72. De Divitiis, O., Fazio, S., Petitto, M., Maddalena, G., Contaldo, F., Mancini, M. (1981). Obesity and cardiac function. Circulation, 64, 477-482.
73. De Wit, F., Van Vliet, A.L., De Wilde, R.B., Jansen, J.R., Vuyk, J., Aarts, L.P., de Jonge, E., Veelo, D.P., Geerts, B.F. (2016). The effect of propofol on haemodynamics: cardiac output, venous return, mean systemic filling pressure, and vascular resistances †. BJA: British Journal of Anaesthesia, 116, 784-789.
74. Del Cont, R., Abrami, M., Hasa, D., Perissutti, B., Voinovich, D., Barba, A., Lamberti, G., Grassi, G., Colombo, I., Manca, D. (2014). A physiologically-oriented mathematical model for the description of in vivo drug release and absorption. ADMET and DMPK, 2, 80-97.
75. DeMuro, R.L., Nafziger, A.N., Blask, D.E., Menhinick, A.M., Bertino, J.S., Jr. (2000). The absolute bioavailability of oral melatonin. J Clin Pharmacol, 40, 781-784.
76. Densen, P. (2011). Challenges and opportunities facing medical education. Trans Am Clin Climatol Assoc, 122, 48-58.
77. Devinney, M.J., Sanders, R.D., Bauer, R.M. (2015). Climbing the delirium mountain: is alpine anaesthesia the perioperative cause? BJA: British Journal of Anaesthesia, 115, 342-344.
78. Diedler, J., Sykora, M., Bast, T., Poli, S., Veltkamp, R., Mellado, P., Steiner, T., Rupp, A. (2009). Quantitative EEG correlates of low cerebral perfusion in severe stroke. Neurocritical care, 11, 210-216.
79. Doufas, A.G., Bakhshandeh, M., Bjorksten, A.R., Shafer, S.L., Sessler, D.I. (2004). Induction speed is not a determinant of propofol pharmacodynamics. Anesthesiology, 101, 1112-1121.
80. Drenick, E.J., Fisler, J.S. (1992). Myocardial Mass in Morbidly Obese Patients and Changes with Weight Reduction. Obes Surg, 2, 19-27.
81. Drummond, J.C. (2019). Blood Pressure and the Brain: How Low Can You Go? Anesthesia & Analgesia, 128, 759-771.
82. Du Bois, D., Du Bois, E.F. (1916). Clinical calorimetry: tenth paper a formula to estimate the approximate surface area if height and weight be known. Arch Intern Med, 17, 863-871.
83. Dubey, V., Mishra, D., Jain, N.K. (2007). Melatonin loaded ethanolic liposomes: Physicochemical characterization and enhanced transdermal delivery. European Journal of Pharmaceutics and Biopharmaceutics, 67, 398-405.
84. Dumont, G.A. (2014). Feedback control for clinicians. J Clin Monit Comput, 28, 5-11.
85. Dyck, J., Shafer, S L. (1992). Effects of age on propofol pharmacokinetics. Seminars in Anesthesia, 11, 2-4.

86. El-Nagar, A.M., El-Bardini, M. (2014). Interval type-2 fuzzy neural network controller for a multivariable anesthesia system based on a hardware-in-the-loop simulation. Artificial Intelligence in Medicine, 61, 1-10.
87. Eleveld, D.J., Colin, P., Absalom, A.R., Struys, M. (2018). Pharmacokinetic-pharmacodynamic model for propofol for broad application in anaesthesia and sedation. BJA: British Journal of Anaesthesia, 120, 942-959.
88. Eleveld, D.J., Proost, J.H., Absalom, A.R., Struys, M.M. (2011). Obesity and allometric scaling of pharmacokinetics. Clin Pharmacokinet, 50, 751-753; discussion 755-756.
89. Fairfield, J.E., Dritsas, A., Beale, R.J. (1991). Haemodynamic effects of propofol: induction with 2.5 mg kg-1. BJA: British Journal of Anaesthesia, 67, 618-620.
90. Fares, A. (2011). Night-time exogenous melatonin administration may be a beneficial treatment for sleeping disorders in beta blocker patients. Journal of cardiovascular disease research, 2, 153-155.
91. Fernandez, E., Perez, R., Hernandez, A., Tejada, P., Arteta, M., Ramos, J.T. (2011). Factors and Mechanisms for Pharmacokinetic Differences between Pediatric Population and Adults. Pharmaceutics, 3, 53-72.
92. Flaishon, R., Windsor, A., Sigl, J., Sebel, P.S. (1997). Recovery of consciousness after thiopental or propofol. Bispectral index and isolated forearm technique. Anesthesiology, 86, 613-619.
93. Fomon, S.J., Haschke, F., Ziegler, E.E., Nelson, S.E. (1982). Body composition of reference children from birth to age 10 years. Am J Clin Nutr, 35, 1169-1175.
94. Forbes, M.G., Patwardhan, R.S., Hamadah, H., Gopaluni, R.B. (2015). Model Predictive Control in Industry: Challenges and Opportunities. IFAC-PapersOnLine, 48, 531-538.
95. Fourtillan, J.B., Brisson, A.M., Gobin, P., Ingrand, I., Decourt, J.P., Girault, J. (2000). Bioavailability of melatonin in humans after day-time administration of D(7) melatonin. Biopharm Drug Dispos, 21, 15-22.
96. Frost, E.A. (2014). Differential diagnosis of delayed awakening from general anesthesia: a review. Middle East J Anaesthesiol, 22, 537-548.
97. Fuster, J.J., Ouchi, N., Gokce, N., Walsh, K. (2016). Obesity-Induced Changes in Adipose Tissue Microenvironment and Their Impact on Cardiovascular Disease. Circ Res, 118, 1786-1807.
98. Galley, H.F., Lowes, D.A., Allen, L., Cameron, G., Aucott, L.S., Webster, N.R. (2014). Melatonin as a potential therapy for sepsis: a phase I dose escalation study and an ex vivo whole blood model under conditions of sepsis. J Pineal Res, 56, 427-438.
99. Gaynor, J., Ansermino, J. (2016). Paediatric total intravenous anaesthesia. Bja Education, 16, 369-373.
100. Geliebter, A., Atalayer, D., Flancbaum, L., Gibson, C.D. (2013). Comparison of body adiposity index (BAI) and BMI with estimations of % body fat in clinically severe obese women. Obesity (Silver Spring), 21, 493-498.
101. Gentilini, A., Schaniel, C., Morari, M., Bieniok, C., Wymann, R., Schnider, T. (2002). A new paradigm for the closed-loop intraoperative administration of analgesics in humans. IEEE Trans Biomed Eng, 49, 289-299.
102. Gepts, E., Camu, F., Cockshott, I.D., Douglas, E.J. (1987). Disposition of propofol administered as constant rate intravenous infusions in humans. Anesthesia & Analgesia, 66, 1256-1263.
103. Gholamzadeh, S., Zarenezhad, M., Montazeri, M., Zareikordshooli, M., Sadeghi, G., Malekpour, A., Hoseni, S., Bahrani, M., Hajatmand, R. (2017). Statistical Analysis of Organ Morphometric Parameters and Weights in South Iranian Adult Autopsies. Medicine (Baltimore), 96, e6447.

104. Gitto, E., Karbownik, M., Reiter, R.J., Tan, D.X., Cuzzocrea, S., Chiurazzi, P., Cordaro, S., Corona, G., Trimarchi, G., Barberi, I. (2001). Effects of melatonin treatment in septic newborns. Pediatric research*,* 50, 756.

105. Gögenur, I., Kücükakin, B., Panduro Jensen, L., Reiter, R.J., Rosenberg, J. (2014). Melatonin reduces cardiac morbidity and markers of myocardial ischemia after elective abdominal aortic aneurism repair: a randomized, placebo-controlled, clinical trial. Journal of Pineal Research*,* 57, 10-15.

106. Gooneratne, N.S., Edwards, A.Y., Zhou, C., Cuellar, N., Grandner, M.A., Barrett, J.S. (2012). Melatonin pharmacokinetics following two different oral surge-sustained release doses in older adults. J Pineal Res*,* 52, 437-445.

107. Grandison, M.K., Boudinot, F.D. (2000). Age-related changes in protein binding of drugs. Clinical Pharmacokinetics*,* 38, 271-290.

108. Gray, P.A., Park, G.R., Cockshott, I.D., Douglas, E.J., Shuker, B., Simons, P.J. (1992). Propofol metabolism in man during the anhepatic and reperfusion phases of liver transplantation. Xenobiotica*,* 22, 105-114.

109. Green, D., Bidd, H., Rashid, H. (2014). Multimodal intraoperative monitoring: an observational case series in high risk patients undergoing major peripheral vascular surgery. International journal of surgery*,* 12, 231-236.

110. Green, D.W. (2015). Cardiac output decrease and propofol: what is the mechanism? BJA: British Journal of Anaesthesia*,* 114, 163.

111. Gregory, G.A., Andropoulos, D.B. (2012). Gregory's pediatric anesthesia: John Wiley & Sons.

112. Groenendaal, W., von Basum, G., Schmidt, K.A., Hilbers, P.A., Van Riel, N.A. (2010). Quantifying the composition of human skin for glucose sensor development. J Diabetes Sci Technol*,* 4, 1032-1040.

113. Guignard, B., Menigaux, C., Dupont, X., Fletcher, D., Chauvin, M. (2000). The effect of remifentanil on the bispectral index change and hemodynamic responses after orotracheal intubation. Anesthesia & Analgesia*,* 90, 161-167.

114. Hall, A.P., Thompson, J.P., Leslie, N.A., Fox, A.J., Kumar, N., Rowbotham, D.J. (2000). Comparison of different doses of remifentanil on the cardiovascular response to laryngoscopy and tracheal intubation. BJA: British Journal of Anaesthesia*,* 84, 100-102.

115. Hall, C., Lueshen, E., Linninger, A.A. (2012). Interspecies scaling in pharmacokinetics: A novel whole-body physiologically based modeling framework to discover drug biodistribution mechanisms in vivo. J Pharm Sci*,* 101, 1221-1241.

116. Hannivoort, L.N., Wyler, B., Eleveld, D.J., Absalom, A.R., VEREECKE, H., Struys, M. (2013). Influence of the method of PK and PD modeling on the objective function and the PD parameters. In 22nd Annual meeting of the International Society for Anaesthetic Pharmacology (ISAP 2013).

117. Hara, M., Masui, K., Eleveld, D.J., Struys, M., Uchida, O. (2017). Predictive performance of eleven pharmacokinetic models for propofol infusion in children for long-duration anaesthesia. BJA: British Journal of Anaesthesia*,* 118, 415-423.

118. Hartmanshenn, C., Scherholz, M., Androulakis, I.P. (2016). Physiologically-based pharmacokinetic models: approaches for enabling personalized medicine. Journal of pharmacokinetics and pharmacodynamics*,* 43, 481-504.

119. Hayashida, M., Kin, N., Tomioka, T., Orii, R., Sekiyama, H., Usui, H., Chinzei, M., Hanaoka, K. (2004). Cerebral ischaemia during cardiac surgery in children detected by combined monitoring of BIS and near-infrared spectroscopy. BJA: British Journal of Anaesthesia*,* 92, 662-669.

120. Hickie, I.B., Rogers, N.L. (2011). Novel melatonin-based therapies: potential advances in the treatment of major depression. The Lancet, 378, 621-631.

121. Higaki, K., Asai, M., Suyama, T., Nakayama, K., Ogawara, K., Kimura, T. (2002). Estimation of intradermal disposition kinetics of drugs: II. Factors determining penetration of drugs from viable skin to muscular layer. Int J Pharm, 239, 129-141.

122. Higgins, J.P. (2002). Nonlinear systems in medicine. The Yale journal of biology and medicine, 75, 247.

123. Hinderliter, P.M., Price, P.S., Bartels, M.J., Timchalk, C., Poet, T.S. (2011). Development of a source-to-outcome model for dietary exposures to insecticide residues: an example using chlorpyrifos. Regulatory Toxicology and Pharmacology, 61, 82-92.

124. Hiraoka, H., Yamamoto, K., Miyoshi, S., Morita, T., Nakamura, K., Kadoi, Y., Kunimoto, F., Horiuchi, R. (2005). Kidneys contribute to the extrahepatic clearance of propofol in humans, but not lungs and brain. Br J Clin Pharmacol, 60, 176-182.

125. Hsia, S.-H., Wu, C.-T., Wang, H.-S., Yan, D.-C., Chen, S.-C. (2004). The use of bispectral index to monitor unconscious children. Pediatric neurology, 31, 20-23.

126. Huether, G. (1993). The contribution of extrapineal sites of melatonin synthesis to circulating melatonin levels in higher vertebrates. Experientia, 49, 665-670.

127. Innominato, P.F., Lim, A.S., Palesh, O., Clemons, M., Trudeau, M., Eisen, A., Wang, C., Kiss, A., Pritchard, K.I., Bjarnason, G.A. (2016). The effect of melatonin on sleep and quality of life in patients with advanced breast cancer. Support Care Cancer, 24, 1097-1105.

128. James, W. (1976). Research on Obesity. Group Report. In: London: Her Majesty's Stationery Office.

129. Janda, M., Simanski, O., Bajorat, J., Pohl, B., Noeldge-Schomburg, G.F., Hofmockel, R. (2011). Clinical evaluation of a simultaneous closed-loop anaesthesia control system for depth of anaesthesia and neuromuscular blockade*. Anaesthesia, 66, 1112-1120.

130. Janssen, I., Heymsfield, S.B., Wang, Z., Ross, R. (2000). Skeletal muscle mass and distribution in 468 men and women aged 18–88 yr. J Appl Physiol (1985), 89, 81-88.

131. Jeleazcov, C., Ihmsen, H., Schmidt, J., Ammon, C., Schwilden, H., Schuttler, J., Fechner, J. (2008). Pharmacodynamic modelling of the bispectral index response to propofol-based anaesthesia during general surgery in children. BJA: British Journal of Anaesthesia, 100, 509-516.

132. Jepps, O.G., Dancik, Y., Anissimov, Y.G., Roberts, M.S. (2013). Modeling the human skin barrier—Towards a better understanding of dermal absorption. Adv Drug Deliv Rev, 65, 152-168.

133. Johnson, A.L., Altshuler, D., Schwartz, D.R., Papadopoulos, J. (2018). Effect of obesity on propofol dosing requirements in mechanically ventilated patients in a medical intensive care unit. Journal of Emergency and Critical Care Medicine, 2.

134. Johnson, T.N., Tucker, G.T., Tanner, M.S., Rostami-Hodjegan, A. (2005). Changes in liver volume from birth to adulthood: A meta-analysis. Liver Transplantation, 11, 1481-1493.

135. Jones, H.M., Gardner, I.B., Collard, W.T., Stanley, P.J., Oxley, P., Hosea, N.A., Plowchalk, D., Gernhardt, S., Lin, J., Dickins, M., Rahavendran, S.R., Jones, B.C., Watson, K.J., Pertinez, H., Kumar, V., Cole, S. (2011). Simulation of human intravenous and oral pharmacokinetics of 21 diverse compounds using physiologically based pharmacokinetic modelling. Clin Pharmacokinet, 50, 331-347.

136. Karasek, M., Winczyk, K. (2006). Melatonin in humans. J Physiol Pharmacol, 57 Suppl 5, 19-39.

137. Karbownik, M., Lewinski, A., Reiter, R.J. (2001). Anticarcinogenic actions of melatonin which involve antioxidative processes: comparison with other antioxidants. Int J Biochem Cell Biol, 33, 735-753.

138. Kataria, B.K., Ved, S.A., Nicodemus, H.F., Hoy, G.R., Lea, D., Dubois, M.Y., Mandema, J.W., Shafer, S.L. (1994). The pharmacokinetics of propofol in children using three different data analysis approaches. Anesthesiology*,* 80, 104-122.

139. Kazama, T., Ikeda, K., Morita, K., Kikura, M., Doi, M., Ikeda, T., Kurita, T., Nakajima, Y. (1999). Comparison of the effect-site k(eO)s of propofol for blood pressure and EEG bispectral index in elderly and younger patients. Anesthesiology*,* 90, 1517-1527.

140. Ke, A., Nallani, S., Zhao, P., Rostami-Hodjegan, A., Unadkat, J. (2012). A PBPK model to predict disposition of CYP3A-metabolized drugs in pregnant women: verification and discerning the site of CYP3A induction. CPT: pharmacometrics & systems pharmacology*,* 1, 1-10.

141. Kertai, M.D., Pal, N., Palanca, B.J., Lin, N., Searleman, S.A., Zhang, L., Burnside, B.A., Finkel, K.J., Avidan, M.S. (2010). Association of perioperative risk factors and cumulative duration of low bispectral index with intermediate-term mortality after cardiac surgery in the B-Unaware Trial. Anesthesiology*,* 112, 1116-1127.

142. Kiekkas, P., Karga, M., Lemonidou, C., Aretha, D., Karanikolas, M. (2011). Medication errors in critically ill adults: a review of direct observation evidence. American Journal of Critical Care*,* 20, 36-44.

143. Kirkpatrick, T., Cockshott, I.D., Douglas, E.J., Nimmo, W.S. (1988). Pharmacokinetics of propofol (diprivan) in elderly patients. BJA: British Journal of Anaesthesia*,* 60, 146-150.

144. Kleszczynski, K., Fischer, T.W. (2012). Melatonin and human skin aging. Dermatoendocrinol*,* 4, 245-252.

145. Kortelainen, J., Koskinen, M., Mustola, S., Seppanen, T. (2009). Effects of remifentanil on the spectrum and quantitative parameters of electroencephalogram in propofol anesthesia. Anesthesiology*,* 111, 574-583.

146. Kothari, D., Gupta, S., Sharma, C., Kothari, S. (2010). Medication error in anaesthesia and critical care: A cause for concern. Indian journal of anaesthesia*,* 54, 187.

147. Kretsos, K., Kasting, G.B., Nitsche, J.M. (2004). Distributed diffusion–clearance model for transient drug distribution within the skin. J Pharm Sci*,* 93, 2820-2835.

148. Kreuer, S., Schreiber, J.U., Bruhn, J., Wilhelm, W. (2005). Impact of patient age on propofol consumption during propofol-remifentanil anaesthesia. Eur J Anaesthesiol*,* 22, 123-128.

149. Kumar, N.T., Liestol, K., Loberg, E.M., Reims, H.M., Maehlen, J. (2014). Postmortem heart weight: relation to body size and effects of cardiovascular disease and cancer. Cardiovasc Pathol*,* 23, 5-11.

150. Kurita, T., Morita, K., Kazama, T., Sato, S. (2002). Influence of cardiac output on plasma propofol concentrations during constant infusion in swine. Anesthesiology*,* 96, 1498-1503.

151. Laakso, M.-L., Hätönen, T., Stenberg, D., Alila, A., Smith, S. (1993). One-hour exposure to moderate illuminance (500 lux) shifts the human melatonin rhythm. Journal of Pineal Research*,* 15, 21-26.

152. Larsen, R., Rathgeber, J., Bagdahn, A., Lange, H., Rieke, H. (1988). Effects of propofol on cardiovascular dynamics and coronary blood flow in geriatric patients. A comparison with etomidate. Anaesthesia*,* 43 Suppl, 25-31.

153. Laso, L.F., López-Picado, A., de La Fuente, E.O., Murua, A.M., Sánchez-Castro, C., Ruilope, L.P., Valero-Martínez, C. (2016). Manual vs. target-controlled infusion induction with propofol: An observational study. Colombian Journal of Anesthesiology*,* 44, 272-277.

154. Ledowski, T. (2019). Objective monitoring of nociception: a review of current commercial solutions. BJA: British Journal of Anaesthesia*,* 123, e312-e321.

155. Lee, B.J., Parrott, K.A., Ayres, J.W., Sack, R.L. (1996). Development and Characterization of an Oral Controlled-Release Delivery System for Melatonin. Drug Development and Industrial Pharmacy, 22, 269-274.

156. Lee, B.J., Parrott, K.A., Ayres, J.W., Sack, R.L. (1995). Design and evaluation of an oral controlled release delivery system for melatonin in human subjects. Int J Pharm, 124, 119-127.

157. Leil, T.A., Bertz, R. (2014). Quantitative Systems Pharmacology can reduce attrition and improve productivity in pharmaceutical research and development. Frontiers in Pharmacology, 5, 247.

158. Leil, T.A., Ermakov, S. (2015). The emerging discipline of quantitative systems pharmacology. Frontiers in Pharmacology, 6, 129.

159. Lemmens, H.J., Bernstein, D.P., Brodsky, J.B. (2006). Estimating blood volume in obese and morbidly obese patients. Obes Surg, 16, 773-776.

160. Levy, G. (1998). Impact of pharmacodynamic variability on drug delivery(1). Adv Drug Deliv Rev, 33, 201-206.

161. Lin, Z., Monteiro-Riviere, N.A., Kannan, R., Riviere, J.E. (2016). A computational framework for interspecies pharmacokinetics, exposure and toxicity assessment of gold nanoparticles. Nanomedicine, 11, 107-119.

162. Liu, J.S., Zhang, J.M., Yue, Y. (2008). Variation of bispectral index monitoring in paediatric patients undergoing propofol-remifentanil anaesthesia. Eur J Anaesthesiol, 25, 821-825.

163. Liu, N., Chazot, T., Hamada, S., Landais, A., Boichut, N., Dussaussoy, C., Trillat, B., Beydon, L., Samain, E., Sessler, D.I., Fischler, M. (2011). Closed-Loop Coadministration of Propofol and Remifentanil Guided by Bispectral Index: A Randomized Multicenter Study. Anesthesia & Analgesia, 112, 546-557.

164. Liu, N., Lory, C., Assenzo, V., Cocard, V., Chazot, T., Le Guen, M., Sessler, D.I., Journois, D., Fischler, M. (2015). Feasibility of closed-loop co-administration of propofol and remifentanil guided by the bispectral index in obese patients: a prospective cohort comparison. BJA: British Journal of Anaesthesia, 114, 605-614.

165. López Sánchez, G.F., Sgroi, M., D'Ottavio, S., Díaz-Suárez, A., González-Víllora, S., Veronese, N., Smith, L. (2019). Body Composition in children and adolescents residing in Southern Europe: Prevalence of overweight and obesity according to different international references. Frontiers in physiology, 10, 130.

166. Lorente, L., Martín, M.M., Abreu-González, P., de la Cruz, T., Ferreres, J., Solé-Violán, J., Labarta, L., Díaz, C., Jiménez, A., Borreguero-León, J.M. (2015). Serum melatonin levels are associated with mortality in severe septic patients. J Crit Care, 30, 860. e861-860. e866.

167. Louvet, N., Rigouzzo, A., Sabourdin, N., Constant, I. (2016). Bispectral index under propofol anesthesia in children: a comparative randomized study between TIVA and TCI. Pediatric Anesthesia, 26, 899-908.

168. Lu, H., Rosenbaum, S. (2014). Developmental pharmacokinetics in pediatric populations. The Journal of Pediatric Pharmacology and Therapeutics, 19, 262-276.

169. Ludbrook, G.L., Upton, R.N., Grant, C., Martinez, A. (1998). The effect of rate of administration on brain concentrations of propofol in sheep. Anesthesia & Analgesia, 86, 1301-1306.

170. Mackey, D.C. (2012). Can we finally conquer the problem of medical quality? The systems-based opportunities of data registries and medical teamwork. Anesthesiology, 117, 225-226.

171. Mali, A.D. (2015). An updated review on transdermal drug delivery systems. skin, 8, 9.

172. Mallo, C., Zaidan, R., Galy, G., Vermeulen, E., Brun, J., Chazot, G., Claustrat, B. (1990). Pharmacokinetics of melatonin in man after intravenous infusion and bolus injection. Eur J Clin Pharmacol, 38, 297-301.

173. Mandal, R., Loeffler, A.G., Salamat, S., Fritsch, M.K. (2012). Organ Weight Changes Associated With Body Mass Index Determined From a Medical Autopsy Population. The American Journal of Forensic Medicine and Pathology, 33, 382-389.

174. Marik, P.E. (2004). Propofol: therapeutic indications and side-effects. Current pharmaceutical design, 10, 3639-3649.

175. Markantonis, S.L., Tsakalozou, E., Paraskeva, A., Staikou, C., Fassoulaki, A. (2008). Melatonin pharmacokinetics in premenopausal and postmenopausal healthy female volunteers. J Clin Pharmacol, 48, 240-245.

176. Marques-Vidal, P., Marcelino, G., Ravasco, P., Camilo, M.E., Oliveira, J.M. (2008). Body fat levels in children and adolescents: effects on the prevalence of obesity. e-SPEN, the European e-Journal of Clinical Nutrition and Metabolism, 3, e321-e327.

177. Marquez-Lago, T.T., Allen, D.M., Thewalt, J. (2010). A novel approach to modelling water transport and drug diffusion through the stratum corneum. Theoretical Biology and Medical Modelling, 7, 33.

178. Marsh, B., White, M., Morton, N., Kenny, G.N.C. (1991). Pharmacokinetic model driven infusion of propofol in children. BJA: British Journal of Anaesthesia, 67, 41-48.

179. Masui, K., Upton, R.N., Doufas, A.G., Coetzee, J.F., Kazama, T., Mortier, E.P., Struys, M.M. (2010). The performance of compartmental and physiologically based recirculatory pharmacokinetic models for propofol: a comparison using bolus, continuous, and target-controlled infusion data. Anesthesia & Analgesia, 111, 368-379.

180. Mayo, C.W., Bickford, R.G., Faulconer, A., Jr. (1950). Electroencephalographically controlled anesthesia in abdominal surgery. J Am Med Assoc, 144, 1081-1083.

181. Mazoit, J.X., Samii, K. (1999). Binding of propofol to blood components: implications for pharmacokinetics and for pharmacodynamics. Br J Clin Pharmacol, 47, 35-42.

182. McFarlan, C.S., Anderson, B.J., Short, T.G. (1999). The use of propofol infusions in paediatric anaesthesia: a practical guide. Paediatr Anaesth, 9, 209-216.

183. McLeod, H., Relling, M., Crom, W., Silverstein, K., Groom, S., Rodman, J., Rivera, G., Crist, W., Evans, W. (1992). Disposition of antineoplastic agents in the very young child. The British journal of cancer. Supplement, 18, S23.

184. Medeiros, C.A.M., Carvalhedo de Bruin, P.F., Lopes, L.A., Magalhães, M.C., de Lourdes Seabra, M., Sales de Bruin, V.M. (2007). Effect of exogenous melatonin on sleep and motor dysfunction in Parkinson's disease. J Neurol, 254, 459-464.

185. Mehta, A., Kaur, G. (2014). Potential role of melatonin in prevention and treatment of oral carcinoma. Indian Journal of Dentistry, 5, 86-91.

186. Merigo, L., Padula, F., Pawlowski, A., Dormido, S., Guzmán Sánchez, J.L., Latronico, N., Paltenghi, M., Visioli, A. (2018). A model-based control scheme for depth of hypnosis in anesthesia. Biomedical Signal Processing and Control, 42, 216-229.

187. Messerli, F.H., Christie, B., DeCarvalho, J.G., Aristimuno, G.G., Suarez, D.H., Dreslinski, G.R., Frohlich, E.D. (1981). Obesity and essential hypertension: hemodynamics, intravascular volume, sodium excretion, and plasma renin activity. Arch Intern Med, 141, 81-85.

188. Messerli, F.H., Ventura, H.O., Reisin, E.D., Dreslinski, G.R., Dunn, F.G., Frohlich, E.D. (1982). Obesity and essential hypertension. In Stress and Hypertension (Vol. 30, pp. 116-123): Karger Publishers.

189. Minto, C.F., Schnider, T.W., Egan, T.D., Youngs, E., Lemmens, H.J., Gambus, P.L., Billard, V., Hoke, J.F., Moore, K.H., Hermann, D.J., Muir, K.T., Mandema, J.W., Shafer, S.L. (1997). Influence of age and gender on the pharmacokinetics and pharmacodynamics of remifentanil. I. Model development. Anesthesiology, 86, 10-23.

190. Minto, C.F., Schnider, T.W., Short, T.G., Gregg, K.M., Gentilini, A., Shafer, S.L. (2000). Response surface model for anesthetic drug interactions. Anesthesiology, 92, 1603-1616.

191. Mistraletti, G., Paroni, R., Umbrello, M., D'Amato, L., Sabbatini, G., Taverna, M., Formenti, P., Finati, E., Favero, G., Bonomini, F., Rezzani, R., Reiter, R.J., Iapichino, G. (2017). Melatonin Pharmacological Blood Levels Increase Total Antioxidant Capacity in Critically Ill Patients. Int J Mol Sci, 18.

192. Mistraletti, G., Paroni, R., Umbrello, M., Moro Salihovic, B., Coppola, S., Froio, S., Finati, E., Gasco, P., Savoca, A., Manca, D., Chiumello, D., Reiter, R.J., Iapichino, G. (2019). Different routes and formulations of melatonin in critically ill patients. A pharmacokinetic randomized study. Clinical Endocrinology, 91, 209-218.

193. Mistraletti, G., Sabbatini, G., Taverna, M., Figini, M.A., Umbrello, M., Magni, P., Ruscica, M., Dozio, E., Esposti, R., DeMartini, G., Fraschini, F., Rezzani, R., Reiter, R.J., Iapichino, G. (2010). Pharmacokinetics of orally administered melatonin in critically ill patients. J Pineal Res, 48, 142-147.

194. Mistraletti, G., Umbrello, M., Sabbatini, G., Miori, S., Taverna, M., Cerri, B., Mantovani, E.S., Formenti, P., Spanu, P., D'Agostino, A., Salini, S., Morabito, A., Fraschini, F., Reiter, R.J., Iapichino, G. (2015). Melatonin reduces the need for sedation in ICU patients: a randomized controlled trial. Minerva Anestesiol, 81, 1298-1310.

195. Mundigler, G., Delle-Karth, G., Koreny, M., Zehetgruber, M., Steindl-Munda, P., Marktl, W., Ferti, L., Siostrzonek, P. (2002). Impaired circadian rhythm of melatonin secretion in sedated critically ill patients with severe sepsis. Crit Care Med, 30, 536-540.

196. Munoz, H., Cortinez, L., Ibacache, M., Leon, P. (2006). Effect site concentrations of propofol producing hypnosis in children and adults: comparison using the bispectral index. Acta Anaesthesiol Scand, 50, 882-887.

197. Munoz, H.R., Cortinez, L.I., Ibacache, M.E., Altermatt, F.R. (2004). Estimation of the plasma effect site equilibration rate constant (ke0) of propofol in children using the time to peak effect: comparison with adults. Anesthesiology, 101, 1269-1274.

198. Nakayama, M., Kanaya, N., Edanaga, M., Namiki, A. (2003). Hemodynamic and bispectral index responses to tracheal intubation during isoflurane or sevoflurane anesthesia. J Anesth, 17, 223-226.

199. Nascu, I., Krieger, A., Ionescu, C.M., Pistikopoulos, E.N. (2015). Advanced model-based control studies for the induction and maintenance of intravenous anaesthesia. IEEE Trans Biomed Eng, 62, 832-841.

200. Nogueira, F.N., Mendonça, T., Rocha, P. (2014). Controlling the depth of anesthesia by a novel positive control strategy. Computer Methods and Programs in Biomedicine, 114, e87-e97.

201. O'Hare, R., McAtamney, D., Mirakhur, R.K., Hughes, D., Carabine, U. (1999). Bolus dose remifentanil for control of haemodynamic response to tracheal intubation during rapid sequence induction of anaesthesia. BJA: British Journal of Anaesthesia, 82, 283-285.

202. Olmos, M., Ballester, J.A., Vidarte, M.A., Elizalde, J.L., Escobar, A. (2000). The combined effect of age and premedication on the propofol requirements for induction by target-controlled infusion. Anesthesia & Analgesia, 90, 1157-1161.

203. Organisation for Economic Co-operation and Development (OECD). “Fiscal sustainability of health systems: bridging health and finance perspectives” (2015). (Available at: https://read.oecd-ilibrary.org/social-issues-migration-health/fiscal-sustainability-of-health-systems_9789264233386-en#page1)

204. Organisation for Economic Co-operation and Development (OECD). “Obesity Update 2017” (2017). (Available at: https://www.oecd.org/els/health-systems/Obesity-Update-2017.pdf)

205. Padmanabhan, R., Meskin, N., Haddad, W.M. (2015). Closed-loop control of anesthesia and mean arterial pressure using reinforcement learning. Biomedical Signal Processing and Control, 22, 54-64.

206. Padula, F., Ionescu, C., Latronico, N., Paltenghi, M., Visioli, A., Vivacqua, G. (2017). Optimized PID control of depth of hypnosis in anesthesia. Computer Methods and Programs in Biomedicine, 144, 21-35.

207. Pandi-Perumal, S.R., Srinivasan, V., Maestroni, G.J., Cardinali, D.P., Poeggeler, B., Hardeland, R. (2006). Melatonin: Nature's most versatile biological signal? FEBS J, 273, 2813-2838.

208. Pandi-Perumal, S.R., Trakht, I., Srinivasan, V., Spence, D.W., Maestroni, G.J., Zisapel, N., Cardinali, D.P. (2008). Physiological effects of melatonin: role of melatonin receptors and signal transduction pathways. Progress in neurobiology, 85, 335-353.

209. Parvinian, B., Scully, C., Wiyor, H., Kumar, A., Weininger, S. (2018). Regulatory Considerations for Physiological Closed-Loop Controlled Medical Devices Used for Automated Critical Care: Food and Drug Administration Workshop Discussion Topics. Anesthesia & Analgesia, 126, 1916-1925.

210. Paul, T., Lemmer, B. (2007). Disturbance of circadian rhythms in analgosedated intensive care unit patients with and without craniocerebral injury. Chronobiol Int, 24, 45-61.

211. Peacock, J.E., Blackburn, A., Sherry, K.M., Reilly, C.S. (1995). Arterial and Jugular Venous Bulb Blood Propofol Concentrations During Induction of Anesthesia. Anesthesia & Analgesia, 80, 1002-1006.

212. Peng, H.T., Bouak, F., Vartanian, O., Cheung, B. (2013). A physiologically based pharmacokinetics model for melatonin--effects of light and routes of administration. Int J Pharm, 458, 156-168.

213. Perras, B., Meier, M., Dodt, C. (2007). Light and darkness fail to regulate melatonin release in critically ill humans. Intensive Care Med, 33, 1954-1958.

214. Petroni, M., Bertoli, S., Maggioni, M., Morini, P., Battezzati, A., Tagliaferri, M., Liuzzi, A., Testolin, G. (2003). Feasibility of air plethysmography (BOD POD) in morbid obesity: a pilot study. Acta diabetologica, 40, s59-s62.

215. Potočnik, I., NOVAK JANKOVIĆ, V., Štupnik, T., Kremžar, B. (2011). Haemodynamic changes after induction of anaesthesia with sevoflurane vs. propofol. Signa vitae: journal for intesive care and emergency medicine, 6, 52-57.

216. Prausnitz, M.R., Langer, R. (2008). Transdermal drug delivery. Nature biotechnology, 26, 1261-1268.

217. Press, W.H., Teukolsky, S.A., Vetterling, W.T., Flannery, B.P. (1996). Numerical recipes in Fortran 90 (2nd ed.): the art of parallel scientific computing: Cambridge University Press.

218. Reason, J. (2005). Safety in the operating theatre–Part 2: Human error and organisational failure. BMJ Qual Saf, 14, 56-60.

219. Reekers, M. (2012). Recirculatory modeling in man using Indocyanine green.

220. Refinetti, R., Lissen, G.C., Halberg, F. (2007). Procedures for numerical analysis of circadian rhythms. Biol Rhythm Res, 38, 275-325.

221. Reich, D.L., Hossain, S., Krol, M., Baez, B., Patel, P., Bernstein, A., Bodian, C.A. (2005). Predictors of hypotension after induction of general anesthesia. Anesthesia & Analgesia, 101, 622-628.

222. Reiter, R.J., Tan, D.X., Galano, A. (2014). Melatonin: exceeding expectations. Physiology (Bethesda), 29, 325-333.

223. Rhodes, A., Ferdinande, P., Flaatten, H., Guidet, B., Metnitz, P. G., & Moreno, R. P. (2012). The variability of critical care bed numbers in Europe. Intensive care medicine, 38(10), 1647-1653.

224. Rigouzzo, A., Girault, L., Louvet, N., Servin, F., De-Smet, T., Piat, V., Seeman, R., Murat, I., Constant, I. (2008). The relationship between bispectral index and propofol during target-controlled infusion anesthesia: a comparative study between children and young adults. Anesthesia & Analgesia, 106, 1109-1116, table of contents.

225. Rigouzzo, A., M.D., Servin, F., M.D., Ph.D., Constant, I., M.D., Ph.D. (2010). Pharmacokinetic-Pharmacodynamic Modeling of Propofol in Children. Anesthesiology, 113, 343-352.

226. Roberts, F., Dixon, J., Lewis, G., Tackley, R., Prys-Roberts, C. (1988). Induction and maintenance of propofol anaesthesia: a manual infusion scheme. Anaesthesia, 43, 14-17.

227. Robertson, L.C., Al-Haddad, M. (2013). Recognizing the critically ill patient. Anaesthesia & Intensive Care Medicine, 14, 11-14.

228. Rylance, G.W., Moreland, T.A., Cowan, M.D., Clark, D.C. (1982). Liver volume estimation using ultrasound scanning. Arch Dis Child, 57, 283-286.

229. Sachdeva, A.K., Russell, T.R. (2007). Safe introduction of new procedures and emerging technologies in surgery: education, credentialing, and privileging. Surg Clin North Am, 87, 853-866, vi-vii.

230. Sager, J.E., Yu, J., Raguenau-Majlessi, I., Isoherranen, N. (2015). Physiologically Based Pharmacokinetic (PBPK) Modeling and Simulation Approaches: A systematic review of published models, applications and model verification. Drug Metabolism and Disposition.

231. Sahinovic, M.M., Beese, U., Heeremans, E.H., Kalmar, A., Van Amsterdam, K., Steenbakkers, R.J., Kuiper, H., Spanjersberg, R., Groen, R.J., Struys, M.M., Absalom, A.R. (2014). Bispectral index values and propofol concentrations at loss and return of consciousness in patients with frontal brain tumours and control patients. BJA: British Journal of Anaesthesia, 112, 110-117.

232. Sandby-Moller, J., Poulsen, T., Wulf, H.C. (2003). Epidermal thickness at different body sites: relationship to age, gender, pigmentation, blood content, skin type and smoking habits. Acta Derm Venereol, 83, 410-413.

233. Saroj, P., Satyanarayana, A., Suhasini, P.S., Chaitanya, B.K., J., K. (2016). Comparative study of effect of intravenous magnesium sulphate and intravenous fentanyl in attenuating the haemodynamic responses to laryngoscopy and intubation. J. Evid. Based Med. Healthc., 3, 1360-1367.

234. Savoca, A., Abbiati, R.A., Manca, D. (2017). Performance of classical and physiologically-based PK-PD modelling for prediction of remifentanil hemodynamic effects. In A. Espuña, M. Graells & L. Puigjaner (Eds.), Computer Aided Chemical Engineering (Vol. 40, pp. 2755-2760): Elsevier.

235. Savoca, A., Manca, D. (2019). A physiologically-based approach to model-predictive control of anesthesia and analgesia. Biomedical Signal Processing and Control, 53, 101553.

236. Savoca, A., Mistraletti, G., Manca, D. (2018). A physiologically-based diffusion-compartment model for transdermal administration – The melatonin case study. Computers & Chemical Engineering, 113, 115-124.

237. Scheuplein, R.J. (1967). Mechanism of Percutaneous Absorption: II. Transient Diffusion and the Relative Importance of Various Routes of Skin Penetration**From the Research Laboratories of the Department of Dermatology of the Harvard Medical School at the Massachusetts General Hospital, Boston, Massachusetts 02114. Journal of Investigative Dermatology, 48, 79-88.

238. Schiff, J.H., Wagner, S. (2016). Anesthesia related mortality? A national and international overview. Trends in Anaesthesia and Critical Care, 9, 43-48.

239. Schmidt, S.C., Bosy-Westphal, A., Niessner, C., Woll, A. (2019). Representative body composition percentiles from bioelectrical impedance analyses among children and adolescents. The MoMo study. Clinical Nutrition, 38, 2712-2720.

240. Schnider, T.W., Minto, C.F., Gambus, P.L., Andresen, C., Goodale, D.B., Shafer, S.L., Youngs, E.J. (1998). The influence of method of administration and covariates on the pharmacokinetics of propofol in adult volunteers. Anesthesiology, 88, 1170-1182.

241. Sebel, P.S. (2001). Can We Monitor Depth of Anesthesia? Anesthesia & Analgesia, 92, 94-98.

242. Sepulveda, P., Cortinez, L.I., Saez, C., Penna, A., Solari, S., Guerra, I., Absalom, A.R. (2011). Performance evaluation of paediatric propofol pharmacokinetic models in healthy young children. BJA: British Journal of Anaesthesia, 107, 593-600.

243. Servin, F., Farinotti, R., Haberer, J.P., Desmonts, J.M. (1993). Propofol infusion for maintenance of anesthesia in morbidly obese patients receiving nitrous oxide. A clinical and pharmacokinetic study. Anesthesiology, 78, 657-665.

244. Servin, F.S. (2017). TCI in Special Patients Groups: The Elderly and Obese. In Total Intravenous Anesthesia and Target Controlled Infusions (pp. 571-578): Springer.

245. Servin, F.S., Marchand-Maillet, F., Desmonts, J.M. (1998). Influence of analgesic supplementation on the target propofol concentrations for anaesthesia with 'Diprifusor' TCI. Anaesthesia, 53 Suppl 1, 72-76.

246. Sessler, C.N., Gosnell, M.S., Grap, M.J., Brophy, G.M., O'Neal, P.V., Keane, K.A., Tesoro, E.P., Elswick, R.K. (2002). The Richmond Agitation-Sedation Scale: validity and reliability in adult intensive care unit patients. Am J Respir Crit Care Med, 166, 1338-1344.

247. Sha'aban, Y.A., Lennox, B., Laurí, D. (2013). PID versus MPC Performance for SISO Dead-time Dominant Processes. IFAC Proceedings Volumes, 46, 241-246.

248. Shafer, S.L. (2000). The pharmacology of anesthetic drugs in elderly patients. Anesthesiology clinics of North america, 18, 1-29.

249. Sheshadri, V., Tiwari, A., Nagappa, M., Venkatraghavan, L. (2017). Accuracy in blood pressure monitoring: The effect of noninvasive blood pressure cuff inflation on intra-arterial blood pressure values. Anesthesia: Essays and Researches, 11, 169-173.

250. Shilo, L., Dagan, Y., Smorjik, Y., Weinberg, U., Dolev, S., Komptel, B., Balaum, H., Shenkman, L. (1999). Patients in the intensive care unit suffer from severe lack of sleep associated with loss of normal melatonin secretion pattern. Am J Med Sci, 317, 278-281.

251. Shilo, L., Dagan, Y., Smorjik, Y., Weinberg, U., Dolev, S., Komptel, B., Shenkman, L. (2000). Effect of melatonin on sleep quality of COPD intensive care patients: a pilot study. Chronobiol Int, 17, 71-76.

252. Shirakawa, S.-I., Tsuchiya, S., Tsutsumi, Y., Kotorii, T., Uchimura, N., Sakamoto, T., Yamada, S. (1998). Time course of saliva and serum melatonin levels after ingestion of melatonin. Psychiatry and Clinical Neurosciences, 52, 266-267.

253. Shung, J. (2010). Intra-operative hypotension in children: does it matter? Southern African Journal of Anaesthesia and Analgesia, 16.

254. Singh, P., Roberts, M.S. (1994). Skin permeability and local tissue concentrations of nonsteroidal anti-inflammatory drugs after topical application. J Pharmacol Exp Ther, 268, 144-151.

255. Singh, R., Choudhury, M., Kapoor, P.M., Kiran, U. (2010). A randomized trial of anesthetic induction agents in patients with coronary artery disease and left ventricular dysfunction. Ann Card Anaesth, 13, 217-223.

256. Slominski, R.M., Reiter, R.J., Schlabritz-Loutsevitch, N., Ostrom, R.S., Slominski, A.T. (2012). Melatonin membrane receptors in peripheral tissues: Distribution and functions. Mol Cell Endocrinol*,* 351, 152-166.

257. Smuszkiewicz, P., Wiczling, P., Przybylowski, K., Borsuk, A., Trojanowska, I., Paterska, M., Matysiak, J., Kokot, Z., Grzeskowiak, E., Bienert, A. (2016). The pharmacokinetics of propofol in ICU patients undergoing long-term sedation. Biopharm Drug Dispos*,* 37, 456-466.

258. Soehle, M., Dittmann, A., Ellerkmann, R.K., Baumgarten, G., Putensen, C., Guenther, U. (2015). Intraoperative burst suppression is associated with postoperative delirium following cardiac surgery: a prospective, observational study. BMC Anesthesiol*,* 15, 61.

259. Soltesz, K., Hahn, J.-O., Hägglund, T., Dumont, G.A., Ansermino, J.M. (2013). Individualized closed-loop control of propofol anesthesia: A preliminary study. Biomedical Signal Processing and Control*,* 8, 500-508.

260. Song, D., Whitten, C.W., White, P.F. (1999). Use of remifentanil during anesthetic induction: a comparison with fentanyl in the ambulatory setting. Anesthesia & Analgesia*,* 88, 734-736.

261. Srinivasan, V., Pandi-Perumal, S.R., Cardinali, D.P., Poeggeler, B., Hardeland, R. (2006). Melatonin in Alzheimer's disease and other neurodegenerative disorders. Behavioral and Brain Functions*,* 2, 15-15.

262. Srinivasan, V., Spence, D.W., Pandi-Perumal, S.R., Trakht, I., Cardinali, D.P. (2008). Therapeutic actions of melatonin in cancer: possible mechanisms. Integr Cancer Ther*,* 7, 189-203.

263. Stader, F., Siccardi, M., Battegay, M., Kinvig, H., Penny, M.A., Marzolini, C. (2019). Repository Describing an Aging Population to Inform Physiologically Based Pharmacokinetic Models Considering Anatomical, Physiological, and Biological Age-Dependent Changes. Clin Pharmacokinet*,* 58, 483-501.

264. Steib, A., Freys, G., Beller, J.P., Curzola, U., Otteni, J.C. (1988). Propofol in elderly high risk patients. A comparison of haemodynamic effects with thiopentone during induction of anaesthesia. Anaesthesia*,* 43, 111-114.

265. Strong, V.E., Forde, K.A., MacFadyen, B.V., Mellinger, J.D., Crookes, P.F., Sillin, L.F., Shadduck, P.P. (2014). Ethical considerations regarding the implementation of new technologies and techniques in surgery. Surg Endosc*,* 28, 2272-2276.

266. Struys, M., Versichelen, L., Rolly, G. (1998). Influence of pre-anaesthetic medication on target propofol concentration using a 'Diprifusor' TCI system during ambulatory surgery. Anaesthesia*,* 53 Suppl 1, 68-71.

267. Struys, M.M., Coppens, M.J., De Neve, N., Mortier, E.P., Doufas, A.G., Van Bocxlaer, J.F., Shafer, S.L. (2007). Influence of administration rate on propofol plasma-effect site equilibration. Anesthesiology*,* 107, 386-396.

268. Struys, M.M., Vereecke, H., Moerman, A., Jensen, E.W., Verhaeghen, D., De Neve, N., Dumortier, F.J., Mortier, E.P. (2003). Ability of the bispectral index, autoregressive modelling with exogenous input-derived auditory evoked potentials, and predicted propofol concentrations to measure patient responsiveness during anesthesia with propofol and remifentanil. Anesthesiology*,* 99, 802-812.

269. Subramani, Y., Riad, W., Chung, F., Wong, J. (2017). Optimal propofol induction dose in morbidly obese patients: A randomized controlled trial comparing the bispectral index and lean body weight scalar. Canadian Journal of Anesthesia/Journal canadien d'anesthésie*,* 64, 471-479.

270. Tan, D., Reiter, R.J., Manchester, L.C., Yan, M., El-Sawi, M., Sainz, R.M., Mayo, J.C., Kohen, R., Allegra, M., Hardeland, R. (2002). Chemical and physical properties and potential

mechanisms: melatonin as a broad spectrum antioxidant and free radical scavenger. Curr Top Med Chem, 2, 181-197.

271. Teorell, T. (1937). Kinetics of distribution of substances administered to the body, I : The extravascular modes of administration. Archives internationales de pharmacodynamie et de therapie, 57, 205-225.

272. Thompson, J., Hall, A., Russell, J., Cagney, B., Rowbotham, D. (1998). Effect of remifentanil on the haemodynamic response to orotracheal intubation. BJA: British Journal of Anaesthesia, 80, 467-469.

273. United Nations, Department of Economic and Social Affairs. “World Population Ageing 2017 Report” (2017). (Available at: https://www.un.org/en/development/desa/population/publications/pdf/ageing/WPA2017_Report.pdf)

274. Upton, R.N., Ludbrook, G. (2005). A physiologically based, recirculatory model of the kinetics and dynamics of propofol in man. Anesthesiology, 103, 344-352.

275. Upton, R.N., Ludbrook, G.L., Grant, C., Martinez, A.M. (1999). Cardiac output is a determinant of the initial concentrations of propofol after short-infusion administration. Anesthesia & Analgesia, 89, 545-552.

276. US Food and Drug Administration (FDA). Physiological Closed-Loop Controlled (PCLC) Medical Devices Workshop (FDA-2015-N-2734). (2015).

277. US Food and Drug Administration (FDA) Orange Book (2017). Approved Drug Products with Therapeutic Equivalence Evaluations. Silver Spring, MD 20993.

278. Valentin, J. (2002). Basic anatomical and physiological data for use in radiological protection: reference values: ICRP Publication 89. Annals of the ICRP, 32, 1-277.

279. Van Den Berg, J., Vereecke, H., Proost, J., Eleveld, D., Wietasch, J., Absalom, A., Struys, M. (2017). Pharmacokinetic and pharmacodynamic interactions in anaesthesia. A review of current knowledge and how it can be used to optimize anaesthetic drug administration. BJA: British Journal of Anaesthesia, 118, 44-57.

280. Van der Sluis, I.M., de Ridder, M.A., Boot, A.M., Krenning, E.P., de Muinck Keizer-Schrama, S.M. (2002). Reference data for bone density and body composition measured with dual energy x ray absorptiometry in white children and young adults. Arch Dis Child, 87, 341-347; discussion 341-347.

281. Van Heusden, K., Yousefi, M., Ansermino, J.M., Dumont, G.A. (2018). Closed-loop MISO identification of propofol effect on blood pressure and depth of hypnosis. IEEE Transactions on Control Systems Technology.

282. Van Kralingen, S., Diepstraten, J., Peeters, M.Y., Deneer, V.H., Van Ramshorst, B., Wiezer, R.J., Van Dongen, E.P., Danhof, M., Knibbe, C.A. (2011). Population pharmacokinetics and pharmacodynamics of propofol in morbidly obese patients. Clin Pharmacokinet, 50, 739-750.

283. Van Norman, G.A. (2016). Drugs and Devices: Comparison of European and U.S. Approval Processes. JACC: Basic to Translational Science, 1, 399-412.

284. Van Oud-Alblas, H.J.B., Brill, M.J., Peeters, M.Y., Tibboel, D., Danhof, M., Knibbe, C.A. (2019). Population pharmacokinetic-pharmacodynamic model of propofol in adolescents undergoing scoliosis surgery with intraoperative wake-up test: a study using Bispectral index and composite auditory evoked potentials as pharmacodynamic endpoints. BMC Anesthesiol, 19, 15.

285. Varvel, J.R., Donoho, D.L., Shafer, S.L. (1992). Measuring the Predictive Performance of Computer-Controlled Infusion Pumps. Journal of Pharmacokinetics and Biopharmaceutics, 20, 63-94.

286. Vincent, J.L., Fagnoul, D. (2012). Do We Need to Monitor Cardiac Output during Major Surgery? Anesthesiology, 117, 1151-1152.

287. Vos, J.J., Poterman, M., Hannivoort, L.N., Renardel De Lavalette, V.W., Struys, M.M., Scheeren, T.W., Kalmar, A.F. (2014). Hemodynamics and tissue oxygenation during balanced anesthesia with a high antinociceptive contribution: an observational study. Perioper Med (Lond), 3, 9.

288. Voultsios, A., Kennaway, D.J., Dawson, D. (1997). Salivary melatonin as a circadian phase marker: validation and comparison to plasma melatonin. J Biol Rhythms, 12, 457-466.

289. Vuyk, J., Oostwouder, C.J., Vletter, A.A., Burm, A.G.L., Bovill, J.G. (2001). Gender differences in the pharmacokinetics of propofol in elderly patients during and after continuous infusion. BJA: British Journal of Anaesthesia, 86, 183-188.

290. Watson, P.L., Shintani, A.K., Tyson, R., Pandharipande, P.P., Pun, B.T., Ely, E.W. (2008). Presence of electroencephalogram burst suppression in sedated, critically ill patients is associated with increased mortality. Crit Care Med, 36, 3171.

291. West, N., Dumont, G.A., Van Heusden, K., Petersen, C.L., Khosravi, S., Soltesz, K., Umedaly, A., Reimer, E., Ansermino, J.M. (2013). Robust closed-loop control of induction and maintenance of propofol anesthesia in children. Pediatric Anesthesia, 23, 712-719.

292. West, N., Van Heusden, K., Gorges, M., Brodie, S., Rollinson, A., Petersen, C.L., Dumont, G.A., Ansermino, J.M., Merchant, R.N. (2018). Design and Evaluation of a Closed-Loop Anesthesia System With Robust Control and Safety System. Anesthesia & Analgesia, 127, 883-894.

293. Wiczling, P., Bieda, K., Przybylowski, K., Hartmann-Sobczynska, R., Borsuk, A., Matysiak, J., Kokot, Z.J., Sobczynski, P., Grzeskowiak, E., Bienert, A. (2016). Pharmacokinetics and pharmacodynamics of propofol and fentanyl in patients undergoing abdominal aortic surgery - a study of pharmacodynamic drug-drug interactions. Biopharm Drug Dispos, 37, 252-263.

294. Wilhelmsen, M., Amirian, I., Reiter, R.J., Rosenberg, J., Gögenur, I. (2011). Analgesic effects of melatonin: a review of current evidence from experimental and clinical studies. Journal of Pineal Research, 51, 270-277.

295. Williams, L.R. (1994). Reference values for total blood volume and cardiac output in humans. In: Oak Ridge National Lab., TN (United States).

296. World Medical Association. World Medical Association Declaration of Helsinki. Ethical principles for medical research involving human subjects. (2013). JAMA, 310, 2191-2194. (Available at: https://www.wma.net/wp-content/uploads/2016/11/DoH-Oct2013-JAMA.pdf)

297. Wu, C., Honarmand, A.R., Schnell, S., Kuhn, R., Schoeneman, S.E., Ansari, S.A., Carr, J., Markl, M., Shaibani, A. (2016). Age-related changes of normal cerebral and cardiac blood flow in children and adults aged 7 months to 61 years. Journal of the American Heart Association, 5, e002657.

298. Yang, N., Yue, Y., Pan, J.Z., Zuo, M.-Z., Shi, Y., Zhou, S.-Z., Peng, W.-P., Gao, J.-D. (2016). Changes in the Bispectral Index in Response to Loss of Consciousness and No Somatic Movement to Nociceptive Stimuli in Elderly Patients. Chin Med J (Engl), 129, 410-416.

299. Young, J.F., Luecke, R.H., Pearce, B.A., Lee, T., Ahn, H., Baek, S., Moon, H., Dye, D.W., Davis, T.M., Taylor, S.J. (2009). Human organ/tissue growth algorithms that include obese individuals and black/white population organ weight similarities from autopsy data. Journal of Toxicology and Environmental Health, Part A, 72, 527-540.

300. Zhang, J., Wang, F., Xin, Z., Zi, T., Lv, H. (2015). Treatment of different-aged children under bispectral index monitoring with intravenous anesthesia with propofol and remifentanil. Eur Rev Med Pharmacol Sci, 19, 64-69.

301. Zhusubaliyev, Z.T., Medvedev, A., Silva, M.M. (2015). Bifurcation analysis of PID-controlled neuromuscular blockade in closed-loop anesthesia. Journal of Process Control, 25, 152-163.

List of publications of the Author

Journal Articles

1. **Savoca, A.**, Manca, D. Optimal dosing of anesthesia in pediatric patients: a physiologically-based model predictive control study. (Under review for “The Canadian Journal of Chemical Engineering” – invitation to Special issue GRICU 2019, March 2020)
2. **Savoca, A.**, van Heusden, K., Manca, D., Ansermino, J., Dumont, G. (2020). The effect of cardiac output on the pharmacokinetics and pharmacodynamics of propofol during closed-loop induction of anesthesia. Computer Methods and Programs in Biomedicine, 105406 (*In press*).
3. **Savoca, A.**, Manca, D. (2019). A physiologically-based approach to model-predictive control of anesthesia and analgesia. Biomedical Signal Processing and Control, 53, 101553.
4. Mistraletti, G., Paroni, R., Umbrello, M., Moro Salihovic, B., Coppola, S., Froio, S., Finati, E., Gasco, P., **Savoca, A.**, Manca, D., Chiumello, D., Reiter, RJ., Iapichino, G. (2019). Different routes and formulations of melatonin in critically ill patients. A pharmacokinetic randomized study. Clinical Endocrinology, 91, 209-218.
5. **Savoca, A.**, Manca, D. (2019). Physiologically-based pharmacokinetic simulations in pharmacotherapy: selection of the optimal administration route for exogenous melatonin. ADMET & DMPK, 7, 44-59.
6. **Savoca, A.**, Mistraletti, G., Manca, D. (2018). A physiologically-based diffusion-compartment model for transdermal administration -The melatonin case study. Computers & Chemical Engineering, 113, 115-124.

Book chapters

1. **Savoca, A.**, Manca, D. (2020). Control strategies in general anesthesia administration. In A. T. Azar (Ed.), Control Applications for Biomedical Engineering Systems: Elsevier.
2. Abbiati, R.A., **Savoca, A.**, Manca, D. (2018). An engineering oriented approach to physiologically based pharmacokinetic and pharmacodynamic modeling. In Computer Aided Chemical Engineering (Vol. 42, pp. 37-63): Elsevier.

Conference proceedings

1. **Savoca, A.**, Pesenti, G., Manca, D. (2019). Optimization under uncertainty of melatonin dosing for critically ill patients. In Computer Aided Chemical Engineering (Vol. 46, pp. 565-570): Elsevier.
2. Pesenti, G., **Savoca, A.**, Manca, D. (2019). Optimal dose administration of renally excreted drugs. In Computer Aided Chemical Engineering (Vol. 46, pp. 547-552): Elsevier.

3. **Savoca, A.**, Barazzetta, J., Pesenti, G., Manca, D. (2018). Model predictive control for automated anesthesia. In Computer Aided Chemical Engineering (Vol. 43, pp. 1631-1636): Elsevier.
4. **Savoca, A.**, Abbiati, R.A., Manca, D. (2017). Performance of classical and physiologically-based PK-PD modelling for prediction of remifentanil hemodynamic effects. In Computer Aided Chemical Engineering (Vol. 40, pp. 2755-2760): Elsevier.

Acknowledgements

A conclusione di questo elaborato, desidero menzionare e ringraziare le persone che, nel corso dei tre anni di attività di ricerca, hanno contribuito alla realizzazione dello stesso.

Prima di tutto un ringraziamento speciale va' al mio supervisore, il prof. Davide Manca, per la sua pazienza, per i suoi indispensabili consigli, per le conoscenze che mi ha trasmesso durante il percorso. La sua creatività, il suo entusiasmo, la sua passione, e la sua dedizione per la ricerca sono state e saranno sempre per me fonte di ispirazione, sia dal punto di vista professionale che personale.

Desidero poi ringraziare il professor Dumont per avermi dato la possibilità di lavorare per sei mesi nel gruppo di ricerca suo e del prof. Mark Ansermino al British Columbia Children's Hospital Research Institute a Vancouver, per la sua gentilezza e per i suoi apprezzamenti e consigli sul mio lavoro. L'esperienza è stata per me estremamente formativa, in quanto mi ha permesso di apprezzare l'effetto di un ambiente di lavoro multidisciplinare e fortemente volto ad introdurre soluzioni innovative nella pratica clinica. Ringrazio anche il prof. Ansermino per i preziosi consigli, commenti e suggerimenti. Desidero ringraziare anche l'Ing. Klaske van Heusden che durante i 6 mesi mi ha supportato con preziosi consigli e ispirato con il suo profondo senso critico e la sua esperienza, aiutandomi a rendere il mio lavoro sempre più robusto e rigoroso.

Ringrazio il Dr. Giovanni Mistraletti dell'Ospedale San Paolo di Milano per la sua infinita disponibilità e gentilezza, e per averci proposto di lavorare sulla melatonina nell' ambito della terapia intensiva, introducendomi ad un tema interessante e stimolante.

Desidero ringraziare inoltre la Dr. ssa Orena ed il Dr. Caldiroli dell'Istituto Carlo Besta per la loro incredibile disponibilità, la loro fiducia ed il loro entusiasmo nei confronti delle nostre attività di ricerca. Sento che l'interazione con loro mi ha davvero permesso di far fare un salto di qualità del mio lavoro, di capirne meglio le implicazioni nella pratica clinica, i limiti e le potenzialità. L' interazione con voi, con il Dr. Mistraletti

e con il Dr. Ansermino mi ha fatto apprezzare l'arricchimento che deriva dall' integrazione di background scientifici diversi e dallo sforzo di comunicare con le menti aperte per amore della conoscenza, della ricerca, e del voler apportare un contributo concreto al miglioramento della pratica clinica.

Grazie a tutti voi; forse una delle cose più importanti che questo percorso di Dottorato mi lascia è la conferma di quanto sia bello "contaminarsi" (come dice il prof. Manca) per cercare insieme nuove soluzioni ai problemi.

In conclusion, I would like to mention and thank the people who contributed to the development and finalization of this work throughout my three (and more) years of research activity.

First of all, I would like to give special thanks to my supervisor, prof. Davide Manca, for his patience, his indispensable advice, and for the knowledge that he has provided me over the years. His creativity, enthusiasm, passion, and even devotion for science and research have been and will always be a source of admiration and inspiration, in both my personal and professional lives.

I wish to thank prof. Dumont for hosting me in his research group at British Columbia Children's Hospital Research Institute in Vancouver for six months and for his suggestions and kind words on my work. The experience was highly educational, as I had the chance to interact with a multidisciplinary group focused on the introduction of innovative solutions in the clinical practice. I also wish to thank the co-head of the group, prof. Ansermino, for his advice, comments, and suggestions, and Ing. Klaske van Heusden who supported me with precious suggestions throughout the six months and helped me improve my work in robustness and rigor of methods with her critical thinking and experience.

I would like to thank Dr. Giovanni Mistraletti for his availability and kindness, and for introducing me to the work on melatonin administration to critically ill patients, an interesting and stimulating part of my research activity.

I would like to thank Dr. Orena and Dr. Caldiroli for their incredible availability, trust, and enthusiasm for our research activities. I feel that the interactions with them led me to improve my work and better understand clinical implications, limitations, and potentialities. Interactions with them, Dr. Mistraletti, and Dr. Ansermino made me

appreciate the benefits that come from the integration of different scientific backgrounds in an effort to communicate with open minds for the sake of science, research, and desire of giving an actual contribution to the improvement of clinical practice.

Thanks to all of you. I guess the most important thing that I learned over these years is that, in order to find new solutions to problems, one must “contaminate” oneself (as prof. Manca always says).